

Lawrence Berkeley National Laboratory
Lawrence Berkeley National Laboratory

Title

EFFECT OF NUCLEAR SPIN ON CHEMICAL REACTIONS AND INTERNAL MOLECULAR ROTATION

Permalink

<https://escholarship.org/uc/item/6g68w3fc>

Author

Sterna, L.L.

Publication Date

2008-09-18



Lawrence Berkeley Laboratory

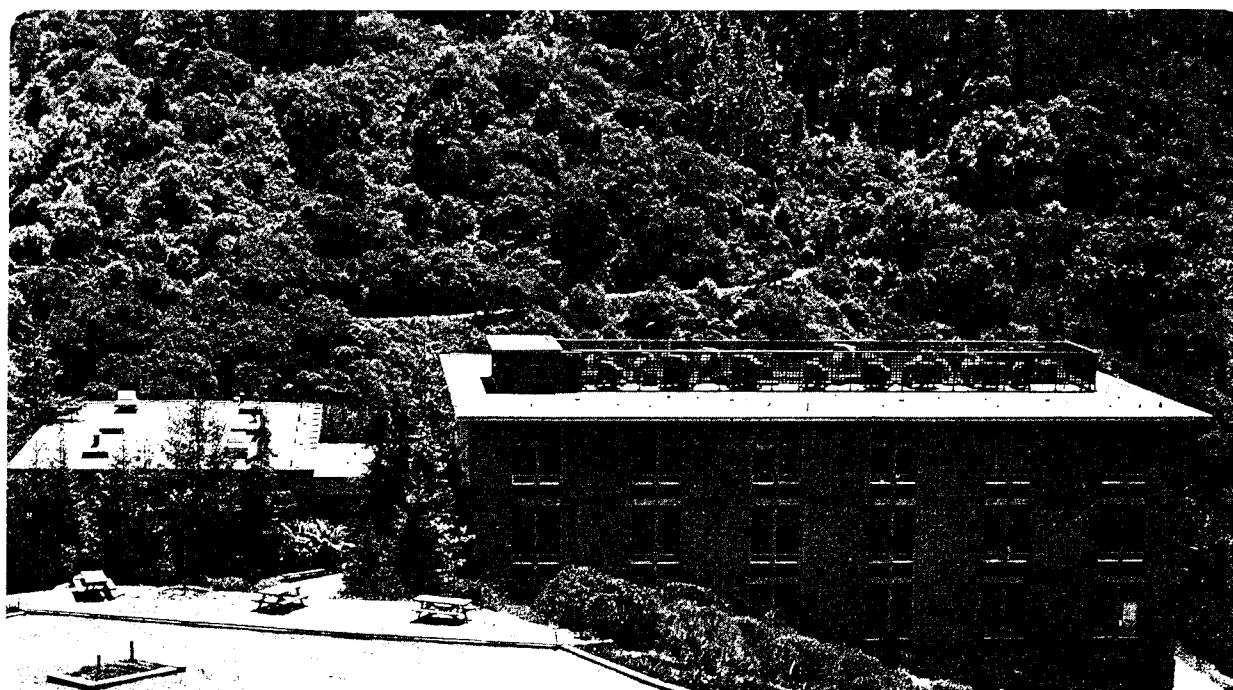
UNIVERSITY OF CALIFORNIA

Materials & Chemical Sciences Division

Effect of Nuclear Spin on Chemical Reactions and Internal Molecular Rotation

L.L. Sterna
(Ph.D. Thesis)

December 1980



EF

EFFECT OF NUCLEAR SPIN ON CHEMICAL
REACTIONS AND INTERNAL MOLECULAR ROTATION

le

Larry Lee Sterna

7
ey

Materials and Molecular Research Division
Lawrence Berkeley Laboratory
University of California
Berkeley, CA 94720

Ph.D. Thesis

December 1980

em

a

n

es

ar

r

at

This work was supported by the Director, Office of Energy Research, Office of Basic Energy Sciences, Materials Sciences Division of the U.S. Department of Energy under Contract Number W-7405-ENG-48.

include more than three collisions of the radical pair, a closed-form solution, accounting for all possible collisions, is obtained when the singlet state radical pairs have unit probability of bonding during a collision.

In the second model the intersystem crossing is treated via first-order rate constants which are average values of the hyperfine couplings. Using these rate constants and hydrodynamic diffusion equations, an analytical solution, which accounts for all collisions, is obtained for the geminate recombination. This model was extended to treat the case of recombination within a spherical reflecting boundary, such as a micelle. Both models contain terms which account for loss of radicals due to competitive chemical reactions.

The two reactions studied are photolysis of benzophenone and toluene and the photolytic decomposition of dibenzylketone (1,3-diphenyl-2-propanone). No magnetic isotope effect was observed in the benzophenone reaction, and this is shown to be consistent with the operation of spin-orbit coupling (which is estimated) in the radical pair. ^{13}C enrichment was observed for the dibenzylketone reaction, and this enrichment was substantially enhanced at intermediate viscosities and low temperatures.

Part II of this dissertation is a presentation of theory and results for the use of Zeeman spin-lattice relaxation as a probe of methyl group rotation in the solid state. The coupling between spin and spatial degrees of freedom is a result of the

Pauli principle and is analogous to the behavior of ortho and para hydrogen. This coupling is associated with a spin degree of freedom termed rotational polarization, and its size is related to the non-exponentiality of the Zeeman relaxation. The theory is presented for the relaxation of methyl groups coupled by fast spin diffusion and it is extended to treat the case of adjacent methyl groups which are geared together.

Experimental results are presented for the time and angular dependences of rotational polarization, the methyl group magnetic moment, and methyl-methyl steric interactions. The compounds studied are 2,6-dimethylphenol, methyl iodide, 1,4,5,8-tetramethylanthracene, 1,4,5,8-tetramethylnaphthalene, 1,2,4,5-tetramethylbenzene, and 2,3-dimethylmaleicanhydride. Calculations are presented to show the relationship between the tunneling frequency and rotation rate of a hindered methyl group.

ACKNOWLEDGEMENTS

Several years of work have gone into producing this dissertation, and I hope to express some measure of my gratitude here to those who have had a part in it. Professor Alex Pines has been most generous in his support and encouragement throughout this work. His ideas and inspiration were an essential part in the success of any experiment.

I am grateful to Dr. Soemi Emid who was my mentor in the understanding of methyl groups and rotational polarization and who participated, as did Dr. Shan Hsi, in the methyl iodide experiments. The work on the magnetic isotope effect greatly benefited from Dr. David Ronis' help in developing the Continuous Diffusion Model. For many discussions and arguments on NMR and help with experiments, I am grateful to my fellow graduate students Gary Drobny, Dick Eckman, Joel Garbow, Jim Murdoch, Steve Sinton, George Wolf, and Yu-Sze Yen as well as to Drs. Dave Wemmer, Warren Warren, and Luciano Mueller. Special thanks are due to Dan Weitekamp and Jau Tang for their willingness to devote much of their time to resolving problems related to my research.

Sidney Wolfe and Herbert Zimmerman contributed a tremendous amount in the synthesis of compounds and growing of single crystals, as did the people of the departmental shops who either constructed or repaired much of the equipment used in the experiments. Sanford Bustamente, Jon Sessler, Harry Weeks, and Paul Mayeda helped with the magnetic isotope experiments. Dione Carmichael and Carol Hacker

are to be thanked for their excellent typing abilities in producing the first and final drafts of this manuscript. Marshall Tuttle did an outstanding job in turning my sketches into flawless drawings. My parents Hugo and Dorothy Sterna deserve a wealth of gratitude for their support of me during all my years of study. To all of my friends and colleagues, including those I have neglected to mention, this work is dedicated.

This research was supported in part by the Director, Office of Energy Research, Office of Basic Energy Sciences, Materials Sciences Division of the U.S. Department of Energy under Contract Number W-7405-ENG-48 and by a grant from the Dreyfus Foundation.

Berkeley

March 1981

L.L. Sterna

INTRODUCTORY NOTE

Parts I and II of this dissertation contain very different subject matter, and with the exception of Appendix F, they were designed to be read independently of one another. Consequently, the reader is forewarned that there are instances where the same symbols are used in the two parts but with different meanings. The references are marked with square brackets [], and the reference lists contain only publications, no footnotes.

*And whatsoever ye do, in word or
deed, do all in the name of the
Lord Jesus, giving thanks to God
the Father through him.*

Colossians 3.17

CONTENTS

PART I

INTERACTION BETWEEN NUCLEAR SPIN AND
CHEMICAL REACTIONS

MAGNETIC ISOTOPE EFFECT	2
1. INTRODUCTION	4
1.1. Free Radical Reaction Scheme	5
1.2. Geminate Recombination	7
1.3. Diffusion	11
1.4. Electron Spin States	14
1.5. Electron Spin State Interconversion	17
2. FIRST COLLISION MODEL	19
2.1. Recombination Yield	19
2.2. First Collision Probability Function	22
2.3. Chemical Reactivity	26
2.4. Spin Hamiltonian	28
2.4.1. Two-Electron Hamiltonian Terms	31
2.4.2. One-Electron Hamiltonian Terms	35
2.4.3. Spin-Orbit Coupling	37
2.5. Time Evolution of the Spin States	43
2.5.1. Basis Functions	43
2.5.2. Initial Conditions	46
2.5.3. Time Evolution up to the First Collision	47
2.5.4. Time-Dependent Singlet Character	53
2.5.5. First Collision and Thereafter	57

2.5.6.	Spin-Orbit Coupling	61
2.6.	Competitive Channels and Radical Lifetimes	70
2.7.	Special Case of High Singlet Reactivity	73
3.	CONTINUOUS DIFFUSION MODEL	76
3.1.	Diffusion	77
3.2.	Classical Treatment of Intersystem Crossing	78
3.3.	Chemical Loss	81
3.4.	Time Evolution Equations and Boundary Conditions	82
3.5.	Recombination Yield	84
3.6.	Restricted Volume and Micelles	88
4.	PHOTOCHEMISTRY	91
4.1.	Benzophenone and Toluene	91
4.2.	Dibenzylketone	99
5.	EXPERIMENTAL DETAILS	104
5.1.	Benzophenone and Toluene	104
5.2.	Dibenzylketone	109
5.3.	Benzaldehyde	122
6.	CALCULATIONS AND EXPERIMENTAL RESULTS	124
6.1.	Benzophenone and Toluene	125
6.1.1.	Geminate Recombination	125
6.1.2.	Isotope Enhancement Factor	135
6.2.	Dibenzylketone	144
6.2.1.	Geminate Recombination	144
6.2.2.	Isotope Enrichment Factor	147
7.	SUMMARY AND DISCUSSION	162
	REFERENCES	165

PART II

INTERACTIONS BETWEEN NUCLEAR SPIN AND METHYL GROUP ROTATIONAL
AND TORSIONAL DEGREES OF FREEDOM

8.	INTRODUCTION	171
8.1.	Partitioning of States in Space and Spin	172
9.	SPIN THERMODYNAMICS	175
9.1.	Grand Canonical Ensemble	177
9.2.	Quasi-Equilibrium	180
9.3.	Number Operators	183
10.	METHYL GROUP DESCRIPTION	187
10.1.	Spatial Hamiltonian	187
10.2.	Spin Hamiltonian	194
10.2.1.	Zeeman Hamiltonian	194
10.2.2.	Dipolar Hamiltonian	197
10.3.	The Pauli Principle and the Tunneling System	201
11.	SPIN DIFFUSION AND SPIN-LATTICE RELAXATION	204
11.1.	Symmetry Restricted Spin Diffusion	204
11.2.	Rotational Polarization	207
11.3.	Spin-Lattice Relaxation	211
11.3.1.	Independent Methyl Groups	211
11.3.2.	Coupled Methyl Groups	217
12.	EXPERIMENTAL DETAILS	226
12.1.	Samples	226
12.2.	Signal to Noise	228

12.3.	106 MHz Spectrometer	230
12.3.1.	Magnet	230
12.3.2.	Pulse Generation	230
12.3.3.	Probe	230
12.3.4.	Receiver	231
12.3.5.	Digitizer	234
12.4.	185 MHz Spectrometer	235
12.4.1.	Magnet	235
12.4.2.	Pulse Generation	235
12.4.3.	Probe	235
12.4.4.	Receiver	238
12.4.5.	Digitizers	238
13.	EXPERIMENTAL RESULTS AND CALCULATIONS	240
13.1.	Bi-exponential Relaxation	240
13.2.	Time Dependence of Rotational Polarization	245
13.3.	Angular Dependence of Rotational Polarization	249
13.4.	Equilibrium Rotational Polarization	255
13.5.	Methyl-methyl Steric Interaction	265
13.5.1.	Strong and Weak Coupling	265
13.5.2.	Intermediate Coupling	271
13.6.	Temperature Dependent Tunneling Frequency	290
14.	SUMMARY AND DISCUSSION	298
	REFERENCES	301
	APPENDIX A: Program "sing5.f4p"	305
	APPENDIX B: Program "diffus.f4p"	318


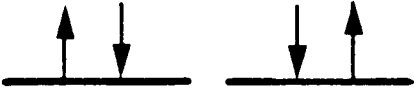

APPENDIX C: Program "methyl.f4p"	324
APPENDIX D: Reduction of $(N + 1) \times (N + 1)$ Set of Relaxation Equations to 2×2 System	331
APPENDIX E: Program "couple.c"	334
APPENDIX F: Synthesis and Crystal Growing	340
REFERENCES	342

PART I: INTERACTION BETWEEN NUCLEAR SPIN AND CHEMICAL
REACTIONS

MAGNETIC ISOTOPE EFFECT

The phenomenon which provided the motivation for work on the magnetic isotope effect is that of Chemically Induced Dynamic Nuclear Polarization (CIDNP) [1,2,3]. CIDNP refers to the non-equilibrium nuclear spin polarizations which are observed in reaction products during the course of free radical reactions. Contrary to the implication of its name, the process is not one where nuclear spin state populations are dynamically pumped as in microwave pumped Dynamic Nuclear Polarization experiments, but rather one where different nuclear spin states follow different paths of chemical reaction (see Figure I.1). The different reaction products are thereby formed with certain nuclear spin states preferentially populated and hence with non-equilibrium nuclear spin polarizations. The principles behind nuclear spin state selective chemistry apply also to nuclear spin isotopes. Thus, it is possible to design chemical reaction schemes where different nuclear isotopes end up in different chemical products thereby achieving isotope separation [4,5,6,7]. We term this the Magnetic Isotope Effect.

The purpose of this work has been to find chemical reactions in which appropriate conditions apply for the magnetic isotope effect to manifest itself and to understand the physics and chemistry of the process so as to modify the reaction conditions and optimize isotope separation.

Spin	State	Product
-1		A
0		B
+1		A

XBL 8010-12461

Figure I.1 In Chemically Induced Dynamic Nuclear Polarization different nuclear spin states end up in different reaction products. The nuclear spin state determines the hyperfine coupling which the unpaired electrons experience, and the hyperfine coupling influences the chemistry by causing intersystem crossing.

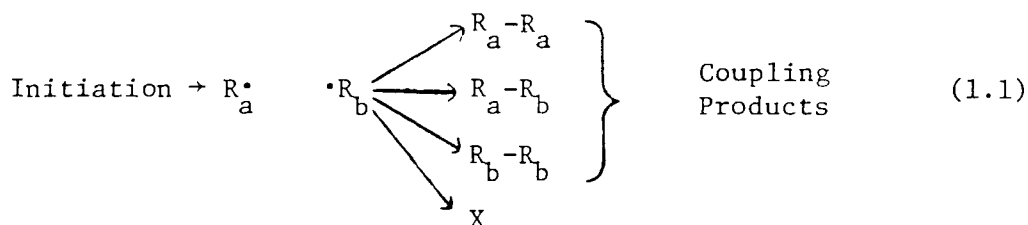
1. INTRODUCTION

In addition to knowing the chemical reactivity of the free radicals, the explanation of the magnetic isotope effect requires a detailed description of free radical diffusion and the electron-nuclear hyperfine interactions within each radical. Such a description will be presented in this chapter and in the following two chapters. In this chapter a phenomenological picture is given for the radical pair theory [1,8,9] of free radical reactions, and the roles of diffusion and electronic spin states on chemical reactivity are discussed. In Chapters 2 and 3 two different models are presented which take into account all of the features of radical pair chemistry and which are readily amenable to computer calculations.

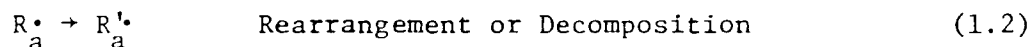
In Chapter 4 the two radical pairs which have been studied and the photochemistry of the reactions for preparing them are described. The experimental arrangement and methods of product analysis are described in Chapter 5. Chapter 6 contains experimental results on geminate yield and isotopic enrichment for the two reactions studied along with the predictions of the two models. Chapter 7 contains a brief summary of the experimental and theoretical results and a discussion of the magnetic isotope effect and its suitability for isotope separation under various circumstances. There is also a discussion of the validity and applicability of the two models from Chapters 2 and 3.

1.1 Free Radical Reaction Scheme

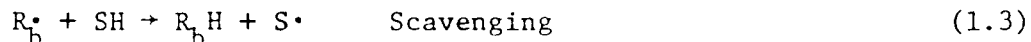
A generalized scheme for the generation (through thermolysis or photolysis) and reaction of free radicals is as follows:



where X indicates all other processes resulting in the disappearance of R_a^\bullet and R_b^\bullet such as:

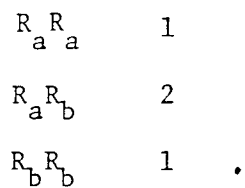


or



where SH is a free radical scavenger. Since all starting materials used in this study are diamagnetic, the radicals are always formed in pairs.

To determine the products formed and their relative amounts, it is necessary to know the detailed chemical processes and the rate of each for the reaction under consideration. However, in practice the reactivity of organic free radicals is often so great that the kinetics are diffusion-controlled. In the absence of all but radical-radical coupling processes, then, for the diffusion controlled reaction of two species R_a^\bullet and R_b^\bullet of equal diffusivity, the following binomial distribution of products results:



If one radical, say R_a^\bullet , is more reactive than the other (i.e., it either diffuses faster or has less stabilization of the unpaired-electron center), then $R_a R_a$ will be formed faster than $R_b R_b$. Since by mass balance the yield of $R_a R_a$ must equal that of $R_b R_b$, the result is that the yield of the asymmetric coupling product $R_a R_b$ drops as the difference in the reactivities of R_a^\bullet and R_b^\bullet increases.

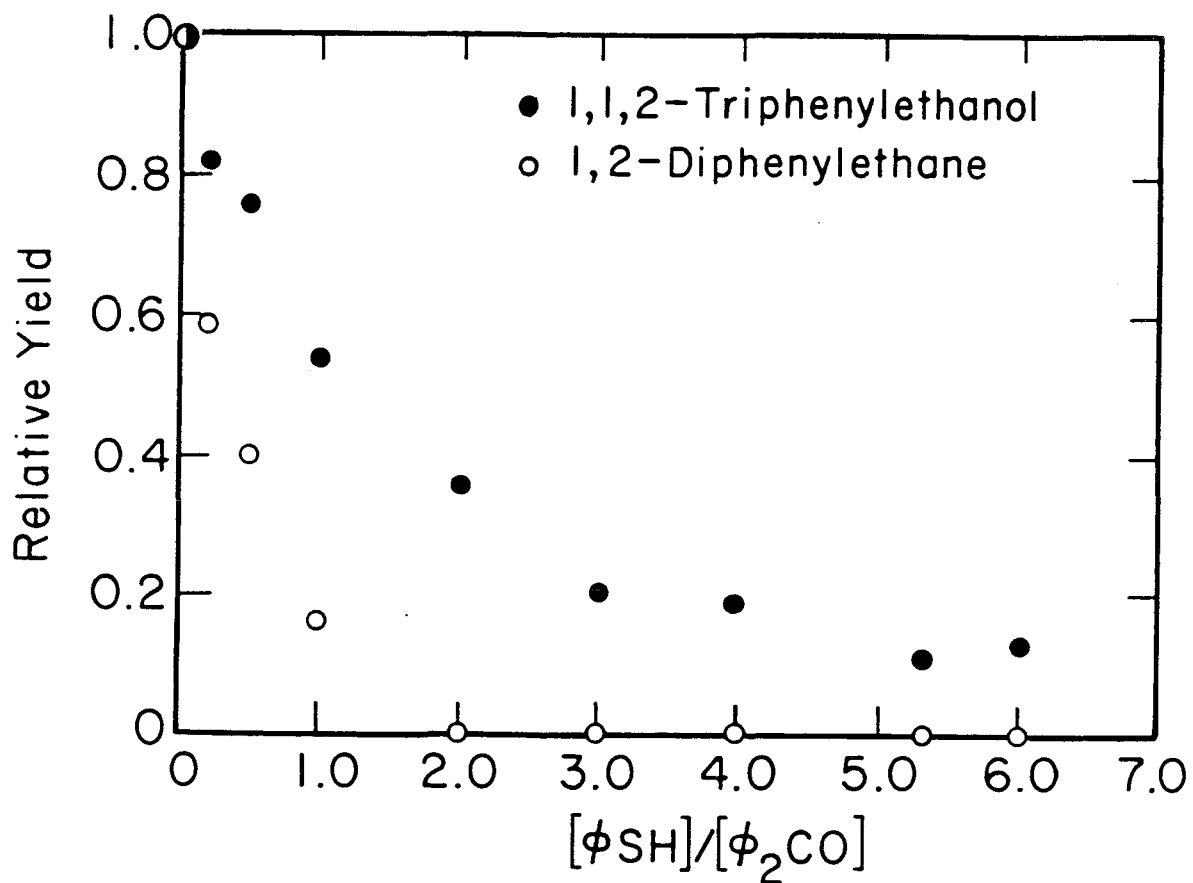
1.2 Geminate Recombination

If a scavenger SH is added to a free radical reaction, either the overall yield of coupling products will fall, or if one radical, say R_a^\bullet , is selectively scavenged, the yields of R_aR_a and R_aR_b will drop and that of R_bR_b will increase. If the initiation step of the reaction is the formation of an asymmetric radical pair, it is found experimentally [10] that upon increasing addition of scavenger, the yields of the symmetric coupling products R_aR_a and R_bR_b go to zero (if both radicals are scavenged) while the yield of R_aR_b asymptotically approaches a non-zero value as shown in Figure I.2. This asymptotic yield of R_aR_b is attributed to those initially formed radical pairs which react too quickly either to be scavenged or to encounter other radicals in solution. In effect, the reaction takes place in isolation from all other radicals in solution, and since it involves a single pair of radicals, it is termed "geminate", or "radical pair", recombination [8].

The explanation for the inability of scavenging to compete with geminate recombination is as follows. The rate of chemical reaction between two species is equal to the frequency of collision of the two species times the probability of reaction upon collision. For the reaction of homogeneously distributed particles the rates take the form:

$$\text{Scavenging rate} = k_S [\text{SH}][R_a^\bullet] \quad (1.4)$$

$$\text{Coupling rate} = k_R [R_a^\bullet][R_b^\bullet] \quad (1.5)$$



XBL 8010-12618

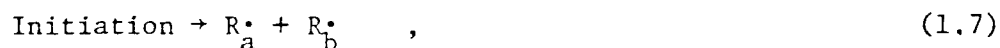
Figure I.2. Influence of scavenger on homogeneous and geminate reaction products in the benzophenone plus toluene photolysis (see Section 6.1.1). As the thiophenol concentration is increased, all of the 1,2-diphenylethane and most of the 1,1,2-triphenylethanol, which are formed homogeneously, are removed; the fraction of the triphenylethanol which is formed geminately cannot be scavenged. The yields are relative to the unscavenged reaction; the solvent is toluene; the thiophenol to benzophenone ratio is for the beginning of the photolysis when $[\phi_2 CO] \approx 0.003$ M.

where k_S and k_R are the appropriate rate constants. Since the concentration of radicals is typically very low ($<10^{-6}$ M) due to their high reactivity, the condition is easily obtained where:

$$k_S[\text{SH}] \gg k_R [\text{R}_a^\bullet] \quad , \quad k_R [\text{R}_b^\bullet] \quad , \quad (1.6)$$

and the scavenger quenches all homogeneous coupling reactions.

In contrast, in geminate recombination the radicals are initially formed with a separation of a few angstroms:



and it is inappropriate to use the homogeneous concentrations $[\text{R}_a^\bullet]$, $[\text{R}_b^\bullet]$ as a measure of the frequency of collisions between R_a^\bullet and R_b^\bullet [8a]. Rather it is necessary to construct a model of particle motion which gives the collision frequency of two particles which start at a given microscopic separation from one another (see sections 1.3, 2.2, 3.1). With such a model it is found that the rate of geminate reaction is orders of magnitude faster than homogeneous reaction, and for the scavenger to compete with it, the scavenger must be used as solvent [8b].

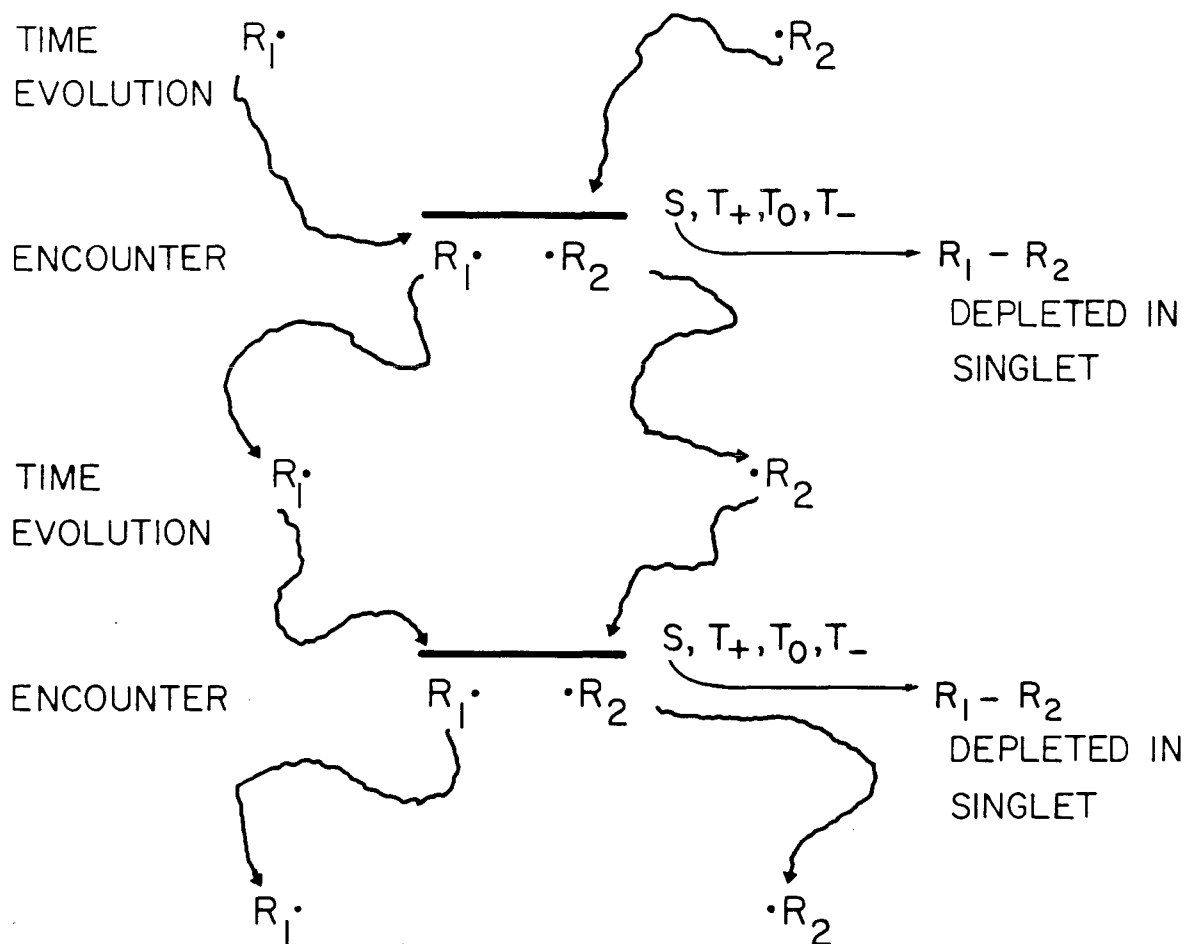
In this work advantage is taken of those chemical systems where the geminate recombination product R_aR_b can be isolated from all other products. This means that the homogeneous production of R_aR_b is quenched either by use of intermediate scavenger concentrations or by exploiting other mechanisms of free radical removal, such as decomposition, which occur on a time scale intermediate to geminate recombination and homogeneous reaction.

When only geminate recombination is considered, one can study the evolution of an isolated pair of radicals prepared in a well-defined electronic spin state. Under these conditions the magnetic isotope effect can be observed and optimized simply.

1.3 Diffusion

For the light intensities used in this work radical concentrations are $\sim 10^{-8}$ M so that homogeneously distributed radicals would be $\sim 6000 \text{ \AA}$ apart. Since this separation is much larger than molecular dimensions, the diffusion of the radicals would be accurately described by macroscopic diffusion equations. When a radical pair is formed, however, the initial separation is $\sim 10 \text{ \AA}$, which is comparable to the particle size (i.e., the "graining" of the solvent), and the diffusive behavior is dependent on the microscopic structure of the solvent [11] (see Figure I.6, section 2.4). Two models have been predominantly used to describe radical pair diffusion at short times. One model [8c,9] treats the two radicals as occupying sites on a three-dimensional lattice, and by assuming a particular jump length and jump frequency, the frequency of collisions is calculated. The other model [12] simply assumes that the diffusion can always be described by macroscopic diffusion equations. The latter model is used in this work (see sections 2.2 and 3.1) and is found to be a sufficient approximation.

The diffusive behavior of a pair of radicals is indicated schematically in Figure I.3. The radicals undergo random diffusive displacements in solution except when they reach the collision radius r_c defined as the separation of centers for a hard sphere collision. At each encounter there is a certain probability (see sections 1.4 and 1.5) of product formation. It may take several collisions before bonding occurs or else



XBL 802-8352-A

Figure I.3. Collisions of two freely diffusing radicals. The overbar indicates a collision; if two radicals are in the singlet state during collision, they may bond, otherwise they separate. During separation the spin states interconvert. This representation of radical pair reactivity is from a lecture given by P. W. Atkins at the NATO Advanced Study Institute on "Chemically Induced Magnetic Polarization", Urbino, Italy, 1977.

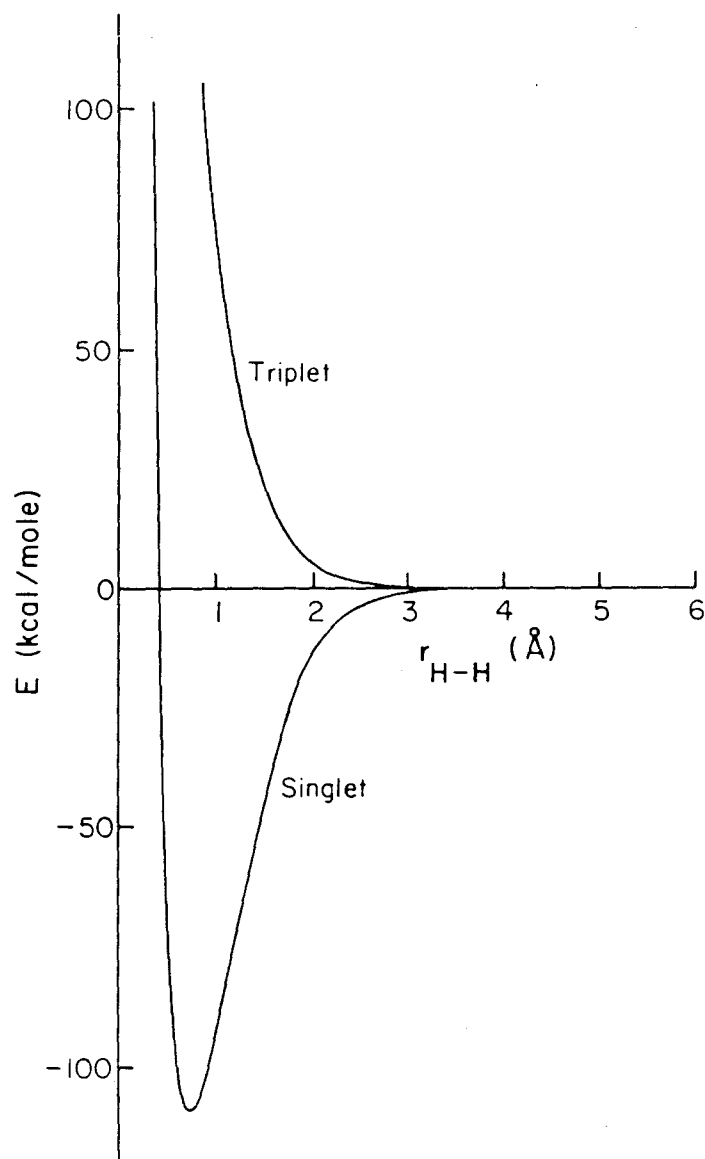
the radicals diffuse apart and/or are consumed by some other mechanism.

1.4 Electronic Spin States

At large interrational separations where radical-radical interactions become vanishingly small, it is accurate to treat each radical as having a doublet spin. That is, the spin multiplicity of a single unpaired electron of spin $1/2$ is two. At small interrational separations where the electron-electron exchange interaction $J(\underline{r})$ becomes dominant, it is no longer appropriate to treat the electrons individually; they must be considered a pair. In the two-electron basis the two doublets form three triplet states and one singlet. The singlet potential energy surface is attractive and is the ground electronic state; the triplet states are repulsive and correspond to an unbound excited electronic state made up of three substates (see Figure I.4). Using this picture of potential energy surfaces, it is convenient to refer in the adiabatic approximation to radical pairs as singlets or triplets even at very large radical separations where the two energy surfaces become degenerate.

If higher electronic states are considered, there may be attractive triplet potential energy surfaces. However, since the energy of the first excited bound state is generally much greater than kT for organic molecules, the assumption is made that the ground electronic state is the only accessible bound state. With this restriction, bond formation is limited to those radical pairs which lie on the singlet potential energy surface.

If the electron-electron exchange interaction $J(\underline{r})$ is the



XBL 8010-12623

Figure I.4. Singlet and Triplet Potential energy surfaces for two hydrogen atoms. The triplet surface is made up of three sublevels T_{+1} , T_0 , T_{-1} . The energy difference between the singlet and triplet surfaces is $2 J(r)$ where $J(r)$ is the exchange interaction. The data for this figure are taken from the work of Kolos and Wolniewicz [13a].

only interaction present, a radical pair starting on a given potential energy surface will remain on that surface indefinitely. Consequently, a pair of radicals starting on the triplet surface cannot bond, and they constitute an "inert" radical pair. For these radicals to react, there must be a mechanism for converting the triplet electron spin correlation into singlet.

1.5 Electron Spin State Interconversion

The crux of the magnetic isotope effect is that the predominant mechanism for electron spin state interconversion (intersystem crossing) in the radical pair is the electron-nuclear hyperfine interaction. By coupling to the electron spin angular momenta, the nuclei can direct the radical pair from an unreactive potential energy surface to a reactive one (or vice versa) and thereby have a substantial effect on the fate of the radicals. That is, whereas a singlet radical pair can form geminate product, a triplet radical pair can only undergo homogeneous reaction in which the reaction products may be different (see section 1.2). The dependence of the intersystem crossing rate on hyperfine coupling provides the basis for the differential chemical reactivity of different nuclear spin states (CIDNP) and isotopes (magnetic isotope effect). The explicit relationship between hyperfine coupling and intersystem crossing is described in detail in sections 2.4, 2.5, and 3.2.

The importance of the diffusive behavior of the radicals is evident when one considers the effect of the singlet-triplet energy spacing on intersystem crossing. In first-order perturbation theory the mixing of two levels $|\ell\rangle$ and $|m\rangle$ due to a perturbation \mathcal{H}' is given by:

$$\text{Mixing coefficient} \approx \frac{\langle \ell | \mathcal{H}' | m \rangle}{E_m - E_\ell} \quad (1.9)$$

where E_ℓ and E_m are the energies of the respective states. If $|\ell\rangle$ and $|m\rangle$ are taken to be a singlet and a triplet state, respectively, and if \mathcal{H}' is the hyperfine interaction, then for typical organic radicals (i.e., ^1H or ^{13}C coupled to an unpaired electron):

$$\text{Mixing coefficient} \approx \frac{10^8}{2 J(\underline{r})} \text{ Hz} \quad . \quad (1.10)$$

For two carbon-centered radicals within bonding distance the exchange interaction $J(\underline{r})$ is $\sim 10^{15}$ Hz, and the mixing coefficient is $\sim 10^{-7}$. As the radicals separate, $J(\underline{r})$ falls rapidly to zero ($J(\underline{r})$ is strongly dependent upon the orbital overlap of the two unpaired electrons [13b]), and the mixing coefficient becomes quite large. In fact, it is no longer valid to use perturbation theory; the singlet and triplet states interconvert on the time scale of the hyperfine interaction (i.e., $1/\langle\ell|\mathcal{H}'|m\rangle$).

Thus, if a radical pair is prepared in one electron spin state, the radicals may diffuse apart where the hyperfine couplings mix the spin states, and then diffusively re-encounter in a new spin state. If diffusion is very fast, the rate limiting step in intersystem crossing is the strength of the hyperfine interaction. Conversely, if the time scale for diffusion is slower than that of the hyperfine interaction, then diffusion will be rate limiting. Consequently, diffusion plays a crucial role in the magnetic isotope effect.

2. FIRST COLLISION MODEL

2.1 Recombination Yield

Restricting bond formation to those radical pairs with singlet electron spin correlation, geminate recombination may be pictured as shown in Figure I.3. Referring to a radical pair which represents an ensemble average over all radical pairs, the time evolution of the system is described as follows. Two radicals are prepared in a well-defined electron spin state at $t = 0$ and with an interradsical separation r_0 . The spin state evolves in time so that when the radicals collide at $t > t_0$, there is a distribution of population among the singlet state S and the three triplet states T_{+1} , T_0 , T_{-1} (or T_x , T_y , T_z). The singlet radical pairs react to form product, while the triplet pairs separate. The system, now depleted in singlet radical pairs, evolves in time, repopulates the singlet state through intersystem crossing, and either undergoes another collision and forms product or the radicals diffuse apart. Thus, the determination of the geminate recombination yield requires calculation of the time-dependent diffusive motion and time-dependent spin state evolution of the radical pair.

Let the probability per unit time of a collision at time t be represented by $f(t)$, and the probability of product formation upon collision at time t be given by $\lambda(t)$. Including a finite lifetime τ_{RP} for the radical pair, the recombination yield R is given by:

$$R = \int_0^{\infty} \lambda(t) f(t) \exp(-t/\tau_{RP}) dt \quad . \quad (2.1)$$

From the form of Eq. (2.1) it would appear that the problem of calculating R is separable into three parts: determination of $\lambda(t)$, $f(t)$, and τ_{RP} . If only one collision were considered, this would be strictly the case. However, when multiple collisions are considered, $\lambda(t)$ and $f(t)$ cannot be treated separately, and the complexity of the problem increases rapidly. This is explained as follows.

Since with each collision the radical pair is depleted in singlet spin states, the spin state evolution, which governs $\lambda(t)$, cannot be considered apart from the collisions which the radical pair undergoes. The collision probability per unit time $f(t)$ includes contributions from radical pairs which have undergone 1,2,3, ... collisions. Since the outcome of each of these collisions (i.e., reaction or no reaction) depends on the spin state at the time of collision, $f(t)$ depends on $\lambda(t)$. In contrast to $\lambda(t)$ and $f(t)$, τ_{RP} depends on factors which are independent of spin state evolution and radical pair diffusion.

It is evident that if only the first collision is considered, there are no previous collisions or reactions to consider, and $\lambda(t)$ and $f(t)$ are separable. As such, one means of simplifying the solution of R is to formulate the problem using terms which depend only on the probability of first collision. This approach is termed the "First Collision Model" and is described in this chapter. It is important to note that the First Collision Model does not neglect multiple collisions.

It is a multicollision model. However, to simplify the calculation the formalism is developed to calculate each collision as if it were the first collision which the radical pair is undergoing. Within this framework $f(t)$ is calculated in section 2.2, $\lambda(t)$ is calculated in sections 2.3 and 2.5, and the radical pair lifetime τ_{RP} is discussed in section 2.6.

2.2 First-Collision Probability Function

Ignoring the finite lifetime τ_{RP} of the radical pair, the re-encounter probability per unit time $f(t)$ includes terms for all numbers of collisions [12a]:

$$f(t) = \sum_{i=1}^{\infty} p_i(r_0, t) \quad (2.2)$$

where $p_i(r_0, t)$ is the probability per unit time that the radical pair is undergoing its i^{th} collision at time t having started from an initial separation r_0 . Although the initial interradsical separation is written as the vector \underline{r}_0 , $p_i(r_0, t)$ depends only on the magnitude $r_0 = |\underline{r}_0|$, because (1) diffusion is isotropic in solution, and (2) the collision boundary $|\underline{r}| = r_c$ is isotropic. As stated above, the probability of an i^{th} collision depends on the probability of the radical pair having survived an $(i-1)^{\text{th}}$ collision which in turn depends on $\lambda(t)$. To allow for the fact that $\lambda(t)$ changes with each collision, the following quantities are defined:

$$\lambda_1(t_1) \quad \equiv \text{reactivity at first collision at time } t_1 \quad (2.3a)$$

$$\lambda_2(t_1, t_2) \quad \equiv \text{reactivity at second collision at time } t_2 \text{ having undergone one collision at time } t_1 \quad (2.3b)$$

$$\lambda_i(t_1, t_2, \dots, t_i) \quad \equiv \text{reactivity at } i^{\text{th}} \text{ collision at time } t_i \text{ having undergone } i-1 \text{ collisions at times } t_1, t_2, \dots, t_{i-1} \quad (2.3c)$$

Since the probability of surviving a collision at time t is $1 - \lambda(t)$, and since the $(i + 1)^{\text{th}}$ collision is the first re-encounter after the i^{th} collision, then [12a]

$$p_{i+1}(r_0, t) = \int_0^t dt_1 \int_{t_1}^t dt_2 \dots \int_{t_{i-1}}^t dt_i [1 - \lambda_i(t_1, t_2, \dots, t_i)] \\ \times p_i(r_0, t_i) p_1(r_c + d, t - t_i) \quad (2.4)$$

where r_c = separation of centers at radical-radical collision

d = mean diffusive step in solution.

The quantity $r_c + d$ is the interrational separation immediately after an unreactive encounter [12a]. By working back iteratively, it is seen that apart from the $\lambda(t)$'s, it is only necessary to calculate $p_1(r, t)$, the probability per unit time of first collision. This quantity has been worked out by Mozumder [12a] and is given by:

$$p_1(r_0, t) = [(r_c/r_0)(r_0 - r_c)/(\sqrt{4\pi D_R} t^{3/2})] \exp[-(r_0 - r_c)^2/(4D_R t)] \quad (2.5)$$

where D_R is the relative diffusion coefficient for the two radicals.

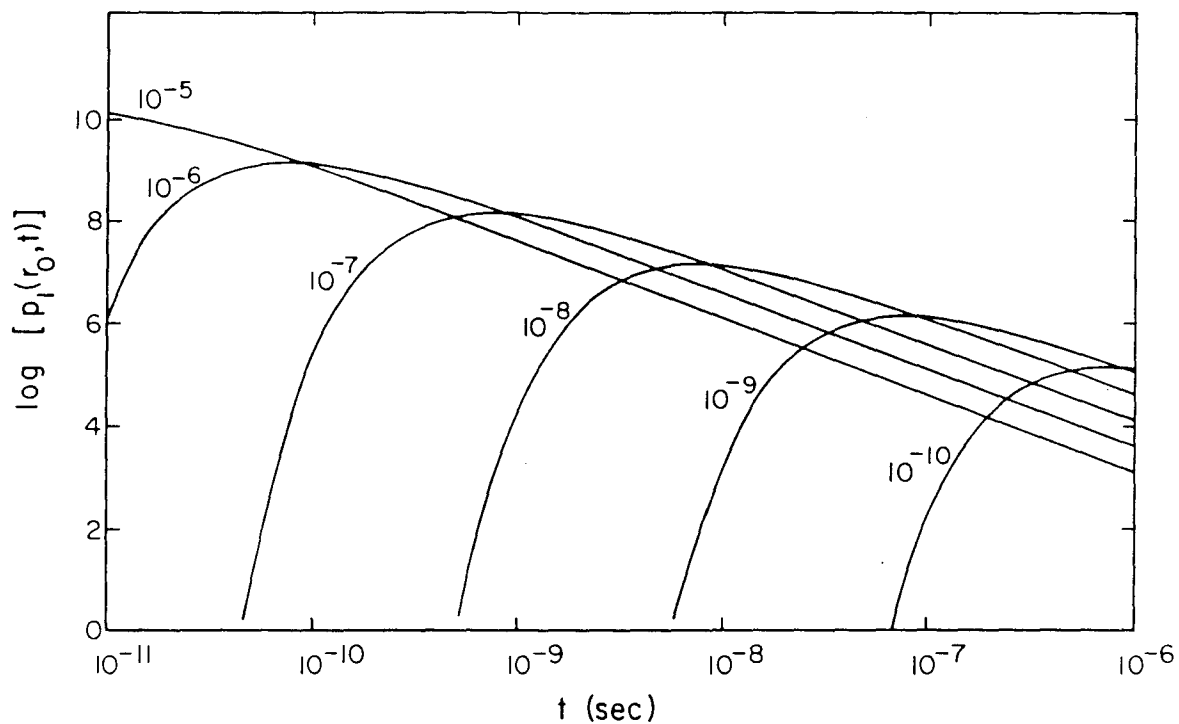
With equations (2.3)-(2.4) the recombination yield can be written using $p_1(r, t)$ instead of $f(t)$:

$$\begin{aligned}
R = & \int_0^{\infty} dt_1 \lambda_1(t_1) p_1(r_0, t_1) \\
& + \int_0^{\infty} dt_1 [1-\lambda_1(t_1)] p_1(r_0, t_1) \int_{t_1}^{\infty} dt_2 \lambda_2(t_1, t_2) p_1(r_c+d, t_2-t_1) \\
& + \int_0^{\infty} dt_1 [1-\lambda_1(t_1)] p_1(r_0, t_1) \int_{t_1}^{\infty} dt_2 [1-\lambda_2(t_1, t_2)] p_1(r_c+d, t_2-t_1) \\
& \times \int_{t_2}^{\infty} dt_3 \lambda_3(t_1, t_2, t_3) p_1(r_c+d, t_3-t_2) \\
& + \dots
\end{aligned} \tag{2.6}$$

where each succeeding term represents the yield from the first, second, third, ... collision. Although the collision radius r_c can be related to the dimensions of the radicals and considered a fixed quantity, there are distributions of values for both the initial interradical separation r_0 and the diffusive length d . Calculations could be performed for several values of r_0 and d , but in this work average values are always used. $p_1(r_0, t)$ is plotted in Figure I.5 for several values of the average diffusion coefficient D_{avg} of the two members of the radical pair. The relative diffusion coefficient D_R is the sum of the two individual diffusion coefficients [8a] or in this case:

$$D_R = 2 D_{\text{avg}} \quad . \tag{2.7}$$

As far as isotope selectivity is concerned, the important point of Figure I.5 is that as D_{avg} becomes smaller, the maximum in $p_1(r_0, t)$ is shifted to longer and longer time.



YBL 8017-12617

Figure I.5. The probability $p_1(r_0, t)$ per unit time that two radicals initially separated by r_0 will have a first collision at time t . The curves are labeled by the average diffusion coefficient D_{avg} for the two radicals; the initial inter-radical separation r_0 is 9 \AA , and the collision radius r_c is 6 \AA .

2.3 Chemical Reactivity

The form assumed for the time-dependent chemical reactivity $\lambda(t)$ is:

$$\lambda(t) = \lambda_S S(t) + \lambda_T T(t) \quad (2.8)$$

where $S(t)$ and $T(t)$ are the time-dependent probabilities that the radical pair is in a singlet or triplet state, respectively, and λ_S and λ_T are the probabilities that bonding will result from either state when the two radicals collide [1]. In this work only the lowest triplet state is considered which is purely repulsive, and, consequently, $\lambda_T = 0$. The singlet surface has a potential minimum at the collision radius r_c , and λ_S may be as large as 1.0. Since the triplets are unreactive, subscripts will be omitted henceforth, and λ will refer only to singlets.

There are various reasons why λ may be less than 1.0; three of these are mentioned below.

1) There may be an activation energy for bond formation. Although no bonds are being broken, some of the radicals considered are delocalized, and the radical center may need to rehybridize from a π -type (much electron delocalization) to a σ -type (electron localized for bond formation). This process may have a small barrier.

2) The radicals may collide with the wrong orientation for bond formation. For some of the large radicals (those with two phenyl groups) this probably reduces λ by a factor of 2 to

3. The smaller radicals are probably close enough to spherical that they can easily rotate into a bonding orientation during collision.

3) The solvent may not be able to dissipate the energy release of bonding quickly enough, causing the product molecule to fall apart. All of the reactions studied in this work involve the formation of carbon-carbon bonds which are typically ~ 80 kcal/mole. Nevertheless, since the product molecules are large (i.e., thirty or more atoms) and the reaction is taking place in a condensed phase, it is assumed that the bonding energy is easily dissipated.

Because of the complexity of the above factors, λ is treated as a phenomenological parameter. For the recombination reactions considered in this work having small, if any, activation energies and taking place in condensed phases, λ is assumed to be fixed for a given reaction independent of solvent, temperature, and viscosity. An estimate gives a value between 0.3 and 1.0.

Having discussed λ , it now remains to determine the time-dependent singlet probability $S(t)$. For this it is necessary to construct the Hamiltonian containing all of the relevant interactions affecting the electron spin states both between and during collisions (section 2.4), and then use an appropriate set of basis functions to calculate the time evolution of the system (section 2.5).

2.4 Spin Hamiltonian

The Hamiltonian \mathcal{H} may be divided into four major terms:

$$\mathcal{H}(t) = \mathcal{H}_{\text{RP}}[\underline{r}(t)] + \mathcal{H}_{\text{R1}}(t) + \mathcal{H}_{\text{R2}}(t) + \mathcal{H}_{\text{SO}} \quad . \quad (2.9)$$

$\mathcal{H}_{\text{RP}}[\underline{r}(t)]$ is the radical pair part of the Hamiltonian, and it contains all of the electron-electron interactions. Because these interactions depend on the interradsical separation $r(t)$, $\mathcal{H}_{\text{RP}}[\underline{r}(t)]$ is coupled to the diffusive motion of the radicals and is therefore time-dependent. $\mathcal{H}_{\text{R1}}(t)$ and $\mathcal{H}_{\text{R2}}(t)$ pertain to isolated radicals and contain only one-electron interactions. These one-electron terms may also be time-dependent due to interactions with the solvent bath surrounding the radicals. \mathcal{H}_{SO} is the spin-orbit coupling Hamiltonian and is composed of one-electron interactions. However, since it must be treated in a special fashion, \mathcal{H}_{SO} is considered separately from $\mathcal{H}_{\text{R1}}(t)$ and $\mathcal{H}_{\text{R2}}(t)$.

The spatial and time dependences of the Hamiltonian introduce a great deal of complexity into the calculation of the time evolution of the radical pair spin states, and it is advantageous to obtain a Hamiltonian which depends only on spin coordinates. As such, the spatial dependence will be integrated out in the course of evaluating each of the Hamiltonian terms. By means of the approximations which follow, the time dependence will either be separated from $\mathcal{H}(t)$ or neglected.

The first approximation is to make $\mathcal{H}_{\text{RP}}[\underline{r}(t)]$ operative only during collisions and to assume that radical rotation makes it

isotropic. This corresponds to giving it the following δ -function dependence on \underline{r} :

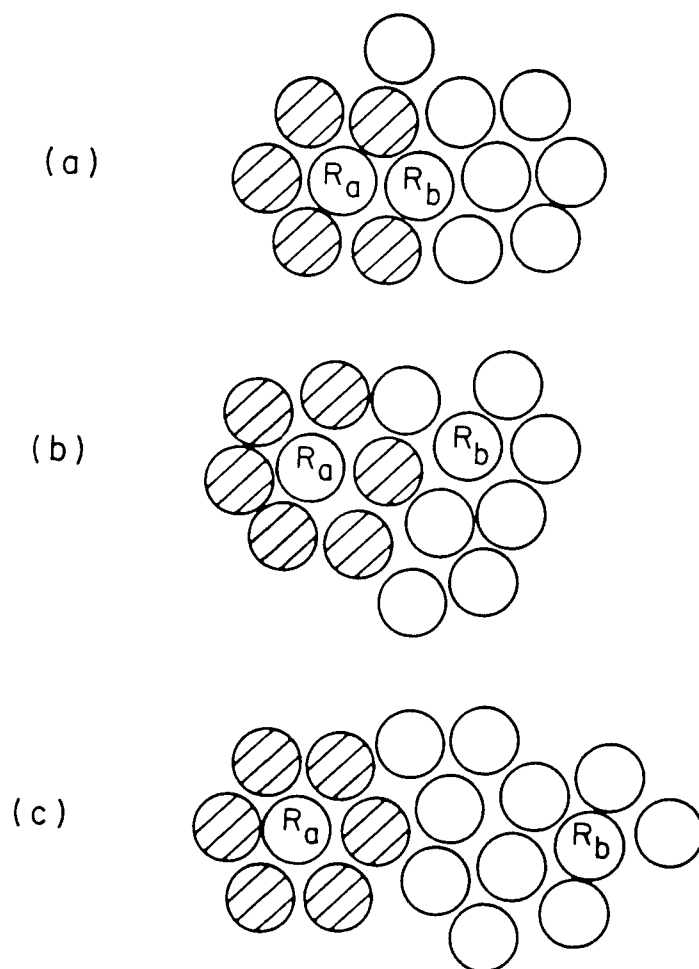
$$\mathcal{H}_{RP}[\underline{r}(t)] = \mathcal{H}_{RP}(r_c) \delta[|\underline{r}(t)| - r_c] \quad . \quad (2.10)$$

The second approximation is that the duration of a collision is short enough that \mathcal{H}_{R1} and \mathcal{H}_{R2} , which are much smaller than $\mathcal{H}_{RP}(r_c)$, can be neglected during collision.

Another way of stating these first two approximations is to say that the radicals travel in and out of two distinct regions as they diffuse. For $|\underline{r}| > r_c$ the time evolution is governed by \mathcal{H}_{R1} and \mathcal{H}_{R2} , and this is termed the "mixing region". For $|\underline{r}| = r_c$ the time evolution is governed by \mathcal{H}_{RP} , and this is termed the "collision region". Since the time-dependent collision probability is determined by $p_1(r_0, t)$, the time dependence of \mathcal{H}_{RP} is determined by this as well. It is assumed that there is no region intermediate to mixing and collision. In other words, the system passes suddenly, or non-adiabatically, between the two regions (see Figure I.6).

Concerning \mathcal{H}_{R1} and \mathcal{H}_{R2} , the unpaired electrons couple to the bath either through interaction with nuclear spins on adjacent solvent molecules (dipole-dipole coupling) or through anisotropic intra-radical couplings which are modulated as the radicals translate and rotate randomly in solution. Two assumptions are made which allow these couplings to be neglected, and \mathcal{H}_{R1} and \mathcal{H}_{R2} to be treated as time-independent.

- 1) The translation and rotation of the radicals in solution



XBL 8010-12620

Figure I.6. Effect of finite particle size on motion of two radicals R_a and R_b in solution. Because the solution is close-packed, two initially touching radicals (a) must separate by an amount comparable to the diameter of the solvent particles (b). At large separations (c) there are many intervening solvent molecules which may be rearranged in various ways to allow the interradsical separation to vary continuously. Because there is a minimum separation which two non-touching radicals may have [see (b)], the transition from the collision region (striped circles) to the mixing region (clear circles) is well defined.

is fast enough compared to the strength of the anisotropic interactions that the Hamiltonian may be treated as isotropic. Rotational diffusion constants measured at room temperature in solvents (i.e., benzene and chloroform) similar to those used in this work are $\sim 10^{11}$ Hz with activation energies of 1 to 2 kcal/mole [14]. Combining this with translational diffusion, the anisotropic interactions are easily averaged out (see below), and, thus, the time dependence is removed.

2) Spin-lattice relaxation is slow compared to geminate recombination and radical lifetimes. Although the fluctuating anisotropic parts may be dropped from the time-averaged Hamiltonian, they are ultimately responsible for bringing the spin system into equilibrium with the bath (lattice). The time scales for geminate recombination and radical removal are typically < 1 μ sec and frequently two to three orders of magnitude shorter. Relaxation times for electron spin polarization have been reported to lie in the range 1 to 80 μ sec for low viscosity liquids at room temperature [15], and, as such, relaxation may be neglected. At very high viscosity the geminate recombination may be so slow that relaxation becomes important. However, under these conditions the rate limiting step for radical pair recombination is diffusion so that the spin interactions, and hence the magnetic isotope effect, should not play a big role anyway (see section 1.5).

2.4.1 Two-Electron Hamiltonian Terms [1]

\mathcal{H}_{RP} is composed of two terms:

$$\mathcal{H}_{\text{RP}} = \mathcal{H}_{\text{e}} + \mathcal{H}_{\text{D}} \quad (2.11)$$

where

\mathcal{H}_e = electron-electron coulombic repulsion

\mathcal{H}_D = electron-electron dipole interaction .

The Hamiltonian term \mathcal{H}_e is diagonalized by the familiar singlet and triplet electronic wave functions. Writing the spatial wave function as $|\chi\rangle$, the proper forms are for singlet:

$$|\chi_S\rangle = (|u_1v_2\rangle + |v_1u_2\rangle)/\sqrt{2} \quad (2.12a)$$

and for triplet:

$$|\chi_T\rangle = (|u_1v_2\rangle - |v_1u_2\rangle)/\sqrt{2} \quad (2.12b)$$

where u and v are molecular orbitals located on different radicals. The subscripts indicate occupation of the orbital by either electron 1 or 2. The associated energies are:

$$E_S = C + J \quad (2.13a)$$

$$E_T = C - J \quad (2.13b)$$

where C is the coulomb integral:

$$C = \langle u_1v_2 | \mathcal{H}_e | u_1v_2 \rangle \quad (2.14a)$$

and J is the exchange integral:

$$J = \langle u_1v_2 | \mathcal{H}_e | v_1u_2 \rangle \quad (2.14b)$$

Theoretical work has shown that C and J depend strongly upon the overlap of the orbitals of the two unpaired electrons [13b]. Thus, C and J fall off rapidly as the radicals separate and are approximated in this work by:

$$C(\underline{r}) = C(r_c) \delta(|\underline{r}| - r_c) \quad (2.15a)$$

$$J(\underline{r}) = J(r_c) \delta(|\underline{r}| - r_c) \quad (2.15b)$$

where rapid rotation is assumed to make the two integrals isotropic on the time scale of a collision (i.e., the radical rotation rate is much greater than the translation rate). Since $C(\underline{r})$ shifts both singlet and triplet levels by the same amount, it may be eliminated by redefining the zero of energy. Having removed $C(\underline{r})$, the time-independent form of \mathcal{H}_e at collision is:

$$\mathcal{H}_e(r_c) = J(r_c) (1/2 + 2 \underline{s}_1 \cdot \underline{s}_2) \quad (2.16)$$

where $J(r_c)$ is a constant and \underline{s}_1 and \underline{s}_2 are the electron spin operators. For organic carbon-centered radicals in the ground state $J(r_c)$ is ~ 80 kcal/mole, or 10^{15} Hz/molecule. The term $(1/2 + 2 \underline{s}_1 \cdot \underline{s}_2)$ gives the appropriate sign of the exchange energy for the singlet and triplet states [Eqs. (2.13a) and (2.13b)].

The classical form of the electron dipole-dipole interaction is:

$$\mathcal{H}_D = (g_1 g_2 \beta_e^2 / r^3) [\underline{s}_1 \cdot \underline{s}_2 - 3(\underline{s}_1 \cdot \underline{r})(\underline{s}_2 \cdot \underline{r}) / r^2] \quad (2.17)$$

where g_1 and g_2 are the isotropic g -factors of the two electrons

and β_e is the Bohr magneton. The factor $g_1 g_2 \beta_e^2 / r^3$ will be used to obtain a rough estimate of the range of \mathcal{H}_D .

6 \AA is a typical particle diameter for the radicals and solvents considered in this work; thus, two radicals separated by an intervening solvent molecule will have an average inter-electron separation of 12 \AA . With $g_1 \approx g_2 \approx 2$ and r equal to 12 \AA , $g_1 g_2 \beta_e^2 / r^3$ equals 30 MHz, which is comparable to \mathcal{H}_{R1} and \mathcal{H}_{R2} . However, since the radicals are generally separated by more than a single solvent molecule between collisions, and since radical diffusion further reduces \mathcal{H}_D , which is completely anisotropic, the approximation is made of neglecting \mathcal{H}_D in the mixing region.

To determine the effect of \mathcal{H}_D on the spin states during collision, it is helpful to cast \mathcal{H}_D in a different form [16]:

$$\mathcal{H}_D = (\underline{s}_1 + \underline{s}_2) \cdot \underline{D} \cdot (\underline{s}_1 + \underline{s}_2) \quad (2.18)$$

where \underline{D} is the second-rank dipolar coupling tensor. Since $(\underline{s}_1 + \underline{s}_2) = 0$ for singlet states, it is evident that \mathcal{H}_D cannot cause intersystem crossing nor mix singlet states in any way. On the other hand, $(\underline{s}_1 + \underline{s}_2)$ is non-zero for the triplet state, and \mathcal{H}_D affects the triplet sublevels. The spherical tensor basis T_x, T_y, T_z diagonalizes \mathcal{H}_D . In this work the Zeeman basis T_{+1}, T_0, T_{-1} is used, and consequently \mathcal{H}_D mixes the triplet sublevels during each collision.

2.4.2 One-Electron Hamiltonian Terms [1]

The Hamiltonian \mathcal{H}_R for a single radical is a sum of four types of interactions (1):

$$\mathcal{H}_R = \mathcal{H}_{HS} + \mathcal{H}_{IS} + \mathcal{H}_{HI} + \mathcal{H}_{II} \quad (2.19)$$

where

\mathcal{H}_{HS} = magnetic field-electron spin interaction

\mathcal{H}_{IS} = electron-nuclear hyperfine interaction

\mathcal{H}_{HI} = magnetic field-nuclear spin interaction

\mathcal{H}_{II} = nuclear spin-spin interaction.

All of these interactions will be written as spin Hamiltonian terms. That is, all spatial integrations have been performed so that g-factors and hyperfine couplings a_i , which depend on orbital populations, may be treated as constants.

The magnetic field-electron spin interaction is written

$$\mathcal{H}_{HS} = g\beta_e \vec{H} \cdot \vec{s} \quad (2.20)$$

where \vec{H} is an externally applied magnetic field, and as in Eq. (2.17) the isotropic g-factor is used. Defining the field axis to be \hat{z} ,

$$\mathcal{H}_{HS} = g\beta_e H s_z \quad (2.21)$$

The electron-nuclear hyperfine interaction consists of an anisotropic through-space dipole-dipole term and a scalar contact

term. Since the strength of the hyperfine coupling in organic radicals is of the order of 10^7 - 10^8 Hz and since this is much smaller than typical rotational diffusion constants (i.e., room temperature values are $\sim 10^{11}$ Hz [14]), the anisotropic term is neglected. The scalar term is:

$$\mathcal{K}_{IS} = \sum_i a_i \mathbf{I}_i \cdot \mathbf{s} \quad (2.22)$$

where the summation is over a single radical, and a_i is the isotropic hyperfine constant and \mathbf{I}_i is the spin of the i^{th} nucleus.

The magnetic field-nuclear spin interaction is:

$$\mathcal{K}_{HI} = -\sum_i \gamma_i \hbar \mathbf{I}_i \cdot \mathbf{H} = -\hbar H \sum_i \gamma_i I_{zi} \quad (2.23)$$

where γ_i is the gyromagnetic ratio, corrected by the isotropic chemical shift, of the i^{th} nuclear spin. \mathcal{K}_{HI} contains no electron spin interactions so it cannot cause intersystem crossing. In low magnetic field this term may be neglected (i.e., $\gamma/2\pi \approx 4 \times 10^3$ Hz/Gauss for protons). In high magnetic field the triplet sublevels T_{+1} and T_{-1} are so widely spaced in energy that intersystem crossing occurs only between singlet S and triplet T_0 and this without change of nuclear spin state (see section 2.5). Since \mathcal{K}_{HI} only serves to shift the energy of a given nuclear spin state, it has no effect on the rate of S to T_0 interconversion and may therefore be neglected at high field. As such, \mathcal{K}_{HI} is dropped from further consideration.

The nuclear spin-spin terms comprising \mathcal{K}_{II} are the anisotropic dipole-dipole coupling and the isotropic through-bond coupling.

Neglecting the anisotropic interactions, the isotropic through-bond couplings are of the order of 10^0 - 10^2 Hz. These clearly cannot affect geminate recombination which takes place on a time scale < 1 μ sec. Thus, \mathcal{H}_{II} is dropped.

In summary, two terms of \mathcal{H}_R are retained: the magnetic field-electron spin coupling Eq. (2.21) and the electron-nuclear isotropic hyperfine interaction Eq. (2.22). Furthermore, there are two one-electron Hamiltonians \mathcal{H}_{R1} and \mathcal{H}_{R2} , one for each electron on a different radical.

2.4.3 Spin-Orbit Coupling

Since spin-orbit coupling is the dominant intersystem crossing mechanism in molecules, it will be discussed in some detail as regards the role it plays in radical pair intersystem crossing. In the literature to date [1,17] arguments have been given for why spin-orbit coupling may be altogether neglected in the treatment of the radical pair. Consequently, it has not been included in any treatment that this author knows of. In this section, however, it is shown that spin-orbit coupling, although zero in first-order, may not be ruled out in second-order. An example demonstrating the strength of the second order coupling is given in section 2.5.6. Nevertheless, due to the complexity of the First Collision Model, the standard assumption of neglecting it will be made. In Chapter 3 the Continuous Diffusion Model is introduced which can easily accommodate spin-orbit coupling. With this latter model the effects of different sizes of spin-

orbit coupling will be shown in Chapter 6.

The standard form of the spin-orbit interaction is that of the "atoms in molecules" approach proposed by McClure [18] where the molecular spin-orbit interaction \mathcal{H}_{SO} is taken to be a sum of single atom contributions. In this work the same approach is used, but, unlike the operator used in molecular problems, here the operator is divided into separate sums for the two radicals:

$$\mathcal{H}_{SO} = \sum_i^a \xi_i(r_{1i}) \tilde{l}_1 \cdot \tilde{s}_1 + \sum_j^b \xi_j(r_{2j}) \tilde{l}_2 \cdot \tilde{s}_2 \quad (2.24)$$

where the superscripts a, b identify the two radicals, the sums are over the nuclei present in each radical, \tilde{l}_k is the orbital angular momentum operator for electron k, and the core electrons have been neglected. The strength of the spin-orbit interaction generated by nucleus i and felt by electron k is $\xi_i(r_{ki})$ where r_{ki} is the distance of the electron from the nucleus. Each nucleus is taken to generate a central field potential (shielded by core electrons) so that $\xi(r_{ki})$ has spherical symmetry (i.e., r_{ki} is used not \tilde{r}_{ki}).

In writing two sums (i.e., treating the two unpaired electrons independently) for \mathcal{H}_{SO} , it is assumed that spin-orbit coupling during collisions may be neglected. This situation is exactly analogous to that of the hyperfine interaction [Eq. (2.22)], and the justification for it lies in the fact that during collision the singlet and triplet states may be separated by ~ 100 kcal/mole, thereby making any mixing between these two states vanishingly small. Phosphorescent lifetimes between such widely separated

levels are typically > 1 msec and often of the order of seconds [18b]. Clearly, it is not necessary to consider this on the time scale of a collision, and Eq. (2.24) may be used for \mathcal{H}_{SO} .

It will now be shown that the radical pair states are not coupled by \mathcal{H}_{SO} in first order. Since spin-orbit coupling is a small perturbation for organic molecules, the two-electron radical pair wave function may be written as a product of space and spin parts:

$$|\Psi_{RP}\rangle = |\chi(\underline{r})\rangle |\phi(\alpha, \beta)\rangle \quad (2.25)$$

where the spatial wave function $|\chi(\underline{r})\rangle$ was introduced in section 2.4.1. With Eq. (2.25) the first-order mixing coefficient between singlet and triplet may be written and the spatial and spin integrals separated as follows:

$$\begin{aligned} & \langle \Psi_{RP,S} | \mathcal{H}_{SO} | \Psi_{RP,T} \rangle / (E_T - E_S) \\ &= \langle \chi_S | \sum_i^a \xi_i(\underline{r}_{1i}) \ell_{i1} | \chi_T \rangle \cdot \langle \phi_S | s_1 | \phi_T \rangle / (E_T - E_S) \\ &+ \langle \chi_S | \sum_j^b \xi_j(\underline{r}_{2j}) \ell_{j2} | \chi_T \rangle \cdot \langle \phi_S | s_2 | \phi_T \rangle / (E_T - E_S) \quad . \quad (2.26) \end{aligned}$$

The spatial integrals in Eq. (2.26) both vanish provided that χ_S and χ_T are real, as will now be demonstrated. In typical organic molecules and radicals all of the molecular orbitals are purely real. That is, the molecular orbitals are real combinations of the purely real atomic orbitals $1s$, $2s$, $2p_x$, $2p_y$, $2p_z$, etc. It is sufficient to show that one of the spatial integrals vanishes:

$$\langle \chi_S | \sum_i^a \xi_i(r_{1i}) \ell_{i1} | \chi_T \rangle = \frac{1}{2} \langle u_1 v_2 + v_1 u_2 | \sum_i^a \xi_i(r_{2i}) \ell_{i1} | u_1 v_2 - v_1 u_2 \rangle \quad (2.27)$$

Integrating over the coordinates of electrons 1 and 2 separately, it follows from the orthogonality of $|u\rangle$ and $|v\rangle$ in the separated radicals that there are two possible non-zero integrals:

$$I_1 = \langle u_1 | \sum_i^a \xi_i(r_{1i}) \ell_{i1} | u_1 \rangle \quad (2.28a)$$

and

$$I_2 = \langle v_1 | \sum_i^a \xi_i(r_{1i}) \ell_{i1} | v_1 \rangle \quad (2.28b)$$

At this point it is necessary to be more specific about the nature of the molecular orbitals u and v . Each orbital is located on a single radical: u is taken to be situated on radical a , and v on radical b . Since the summation in Eqs. (2.28a), (2.28b) is over nuclei on radical a and since $\xi(r) \rightarrow 0$ rapidly with increasing r , matrix elements of the form of Eq. (2.28b) are necessarily zero. In other words, when electron 1 is located on radical b (i.e., molecular orbital v), the spin-orbit coupling it feels from nuclei on radical a is zero.

To evaluate the remaining integral in Eq. (2.28a), it is helpful to consider the angular momentum operator ℓ in spherical coordinates [19]:

$$\ell_x = -i \left[-\sin\phi \frac{\partial}{\partial\theta} - \cos\phi \cot\theta \frac{\partial}{\partial\phi} \right] \quad (2.29a)$$

$$\ell_y = -i[\cos\phi \frac{\partial}{\partial\theta} - \sin\phi \cos\theta \frac{\partial}{\partial\phi}] \quad (2.29b)$$

$$\ell_z = -i \frac{\partial}{\partial\phi} \quad (2.29c)$$

Since $\tilde{\ell}$ has no radial dependence, the spherically symmetric $\xi_i(r_{1i})$ commutes with it, and Eq. (2.28a) may be written:

$$\begin{aligned} \langle u_1 | \sum_i^a \xi_i(r_{1i}) \tilde{\ell}_1 | u_1 \rangle &= \langle \sqrt{\sum_i^a \xi_i(r_{1i})} u_1 | \tilde{\ell}_1 | \sqrt{\sum_k^a \xi_k(r_{1k})} u_1 \rangle \\ &= \langle u_1' | \tilde{\ell}_1 | u_1' \rangle \quad (2.30) \end{aligned}$$

Since the angular momentum operator $\tilde{\ell}$ is Hermitian, its expectation value must be real. However, u and $\xi_i(r_{1i})$ are both purely real functions, and as seen from Eqs. (2.29a)-(2.29c), $\tilde{\ell}$ is purely imaginary. Therefore, the integral in Eq. (2.30) must be identically zero in order to be real [18a,20]. In summary, given that $\xi_i(r_{1i})$ is spherically symmetric and that the molecular orbitals are real, \mathcal{H}_{S0} does not cause first-order mixing between $|\Psi_{RP,S}\rangle$ and $|\Psi_{RP,T}\rangle$.

The second-order mixing coefficient is [21]:

$$\sum_{k \neq RP} \frac{\langle \Psi_{RP,S} | \mathcal{H} | \Psi_k \rangle \langle \Psi_k | \mathcal{H} | \Psi_{RP,T} \rangle}{(E_{RP,S} - E_{RP,T})(E_k - E_{RP,T})}$$

where $|\Psi_k\rangle$ is an excited state which may be either a singlet or triplet. Now it is necessary to determine which terms of the Hamiltonian \mathcal{H} may couple the radical pair states to possible excited states. In the molecular case intersystem crossing is accomplished through the concerted action of vibronic coupling,

or Born-Oppenheimer breakdown, which mixes states of like spin and \mathcal{H}_{SO} which mixes states of different spin. The vibronic coupling results from changes in the electronic wave functions with nuclear motion. This coupling is large only in the collision region [1] where the electronic potential energy surfaces change rapidly with interradsical separation (see Figure I.4), but, as already noted, the mixing is much too weak to be effective on the collisional time scale. Thus, the dominant interaction appearing in both matrix elements of the second order mixing coefficient is \mathcal{H}_{SO} . The fact that \mathcal{H}_{SO} connects $|\Psi_{RP}\rangle$ to excited states is demonstrated by the deviation ($\sim 0.1\%$) of the free radical g-factor of common organic radicals from the free electron value. In fact, the expression for the free radical Δg is very similar to the one which is being treated in this section [22]. Given that the matrix element $\langle \Psi_k | \mathcal{H}_{SO} | \Psi_{RP} \rangle$ is not negligible, and since $(E_{RP,S} - E_{RP,T}) \rightarrow 0$ as the radicals separate, it is no longer valid to use perturbation theory. As such, it is necessary to use the methods to be outlined in the next section, after which the subject of spin-orbit coupling will be picked up again (section 2.5.6) and a simple example provided.

2.5 Time Evolution of the Spin States

The present problem, as defined in section 2.3, is to calculate the probability $S(t)$ that the radical pair is in a singlet electronic state at time t . In order to calculate this quantity there are three things which first need to be specified:

1. An appropriate set of basis functions with which to represent the spin states.
2. Definition of the initial conditions in accordance with the chemical system being described.
3. Formalism for determining the time-evolution of the spin states.

These three requirements will now be described.

2.5.1 Basis functions

Since there are two regions (collision and mixing) in which the time evolution of the electron spins must be determined, it is useful to use two different sets of basis functions. In both regions the basis functions are products of electronic and nuclear spin functions:

$$|\text{Basis Functions}\rangle = |\text{Electronic}\rangle |\text{Nuclear}\rangle \quad . \quad (2.31)$$

Since the Hamiltonian derived in sections 2.4.1 and 2.4.2 is a spin Hamiltonian (spin-orbit coupling will be treated separately in section 2.5.6), the basis functions of Eq. (2.31) involve spin coordinates only. The nuclear spins are weakly coupled

to one another and may be written as a simple product of Zeeman spin functions. These spin functions are grouped together for each radical:

$$|\text{Nuclear}\rangle_a = |m_1 m_2 m_3 \dots\rangle_a \quad (2.32a)$$

$$|\text{Nuclear}\rangle_b = |m'_1 m'_2 m'_3 \dots\rangle_b \quad (2.32b)$$

where the m 's are the magnetic quantum numbers of the nuclei, and the subscripts a, b refer to the two radicals.

In the collision region the two electrons are strongly coupled, and it is therefore necessary to treat them as a pair. The singlet and triplet Zeeman functions are used to describe them in this region. For singlet with spin = 0

$$|S\rangle = (|\alpha_1\rangle |\beta_2\rangle - |\beta_1\rangle |\alpha_2\rangle)/\sqrt{2} \quad M_S = 0 \quad (2.33a)$$

and for triplet with spin = 1:

$$|T_{+1}\rangle = |\alpha_1\rangle |\alpha_2\rangle \quad M_S = +1 \quad (2.33b)$$

$$|T_0\rangle = (|\alpha_1\rangle |\beta_2\rangle + |\beta_1\rangle |\alpha_2\rangle)/\sqrt{2} \quad M_S = 0 \quad (2.33c)$$

$$|T_{-1}\rangle = |\beta_1\rangle |\beta_2\rangle \quad M_S = -1 \quad (2.33d)$$

where M_S is the z projection of the total electronic spin.

Defining the set of two-electron basis functions as $\{\phi_j\}$, a sample function is:

$$|\phi_j\rangle = |S\rangle |m_1 m_2 \dots\rangle_a |m'_1 m'_2 \dots\rangle_b \quad (2.34)$$

In the mixing region the electrons have minimal interaction with one another and may therefore be treated independently. As such, doublet spin functions are used for the electrons. Defining two sets of one-electron basis functions $\{\phi_k\}_a$, $\{\phi_\ell\}_b$, one for each radical, sample functions appear as:

$$|\phi_k\rangle = |m_S\rangle_1 |m_1 m_2 \dots\rangle_a \quad (2.35a)$$

$$|\phi_\ell\rangle = |m'_S\rangle_2 |m'_1 m'_2 \dots\rangle_b \quad (2.35b)$$

where m_S is the z projection of a single electron spin, and in this example electron 1 is localized on radical a and electron 2 on radical b. The two-electron basis functions could be used throughout. The reason for introducing the one-electron functions is a matter of computational convenience. That is, it is a simpler problem to solve for the time-evolution of the radicals individually rather than together. This approach is followed in so far as it is valid (i.e., in the mixing region).

The transition between the two regions is a natural one. For instance, the singlet spin function of Eq. (2.33a) can be re-written in terms of one-electron functions appropriate for the mixing region merely by re-grouping terms:

$$|\phi_j\rangle = \frac{1}{\sqrt{2}} (|\alpha_1\rangle |\beta_2\rangle - |\beta_1\rangle |\alpha_2\rangle) |m_1 m_2 \dots\rangle_a |m'_1 m'_2 \dots\rangle_b \quad (2.36a)$$

$$|\phi_j\rangle = \frac{1}{\sqrt{2}} [|\alpha_1\rangle |m_1 m_2 \dots\rangle_a (|\beta_2\rangle |m'_1 m'_2 \dots\rangle_b) - (|\beta_1\rangle |m_1 m_2 \dots\rangle_a) (|\alpha_2\rangle |m'_1 m'_2 \dots\rangle_b)] \quad (2.36b)$$

$$|\phi_j\rangle = [|\phi_\ell\rangle |\phi'_m\rangle - |\phi_n\rangle |\phi'_o\rangle] / \sqrt{2} \quad (2.36c)$$

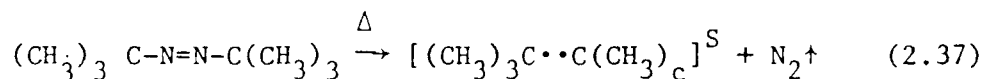
In fact, the two-electron functions may be defined in terms of the one-electron functions from the start.

2.5.2 Initial Conditions

There are three situations which occur commonly in free radical chemical reactions.

a) Singlet Precursor

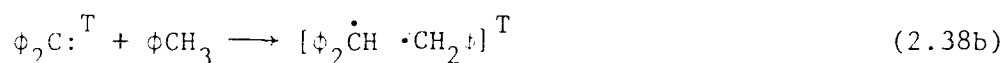
This occurs frequently when the free radical initiation step is through thermolysis:



where the brackets [] indicate that the two radicals are in the vicinity of one another, and the superscript S indicates that the two electrons have singlet spin correlation.

b) Triplet Precursor

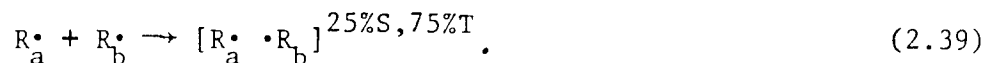
This occurs frequently in reactions involving carbenes or photolysis of ketones:



where ϕ indicates a phenyl group, and the superscript T indicates triplet.

c) Random

This occurs when two radicals formed in different chemical events encounter one another:



In this work the only initial condition considered, besides r_0 , is the fraction f_s of singlet present when the radical pair is formed, which in the three cases cited is 1.0, 0.0, and 0.25, respectively. It is only necessary to be able to solve for the cases of 100% singlet and 100% triplet, however, since a chemical situation of arbitrary f_s can always be written as a linear combination of the two. It is assumed that initially all nuclear spin levels are equally populated (Boltzmann differences are trivial), and any difference in population of the triplet levels T_{+1} , T_0 , T_{-1} is ignored. Although some photolyses occur with preferential population of a given triplet sublevel, it is here assumed that the radical pair is formed with the two radicals in such proximity that the dipole-dipole coupling causes fast relaxation in the triplet manifold (see section 2.4.1).

2.5.3 Time Evolution up to the First Collision

The problem at hand involves an ensemble of radical pairs which were formed at different points in time. Since each pair evolves independently of the others (section 1.2), one can

arbitrarily have all of the radical pairs being formed at $t = 0$ without changing the physical observables at $t = \infty$. With this adjustment it is possible to define a single ensemble averaged radical pair which is generated at $t = 0$ and evolves in time as follows (see also section 2.1).

a) The two radicals start at an initial separation r_0 , which can be taken to be a single diffusive step greater than the collision radius r_c . The initial spin populations are defined by the initial singlet character f_s which is determined by the type of chemical reaction from which the radicals have been formed.

b) Up to the first collision the radical pair evolves solely under the influence of the one-electron Hamiltonian terms \mathcal{H}_{R1} and \mathcal{H}_{R2} . This time evolution proceeds until the pair undergoes collision at time τ . During collision the radical pair evolves under the influence of the two-electron Hamiltonian \mathcal{H}_{RP} , and chemical reaction may occur. Those pairs which do not react separate, and once again the time evolution is governed by \mathcal{H}_{R1} and \mathcal{H}_{R2} . The only difference between the time evolution in this period and that preceding the first collision is that the radical pair, in general, starts evolving under different initial conditions. The problem of calculating the time evolution after collision is identical (except for the initial conditions) to that before collision. Thus, all that is needed is to be able to calculate for arbitrary initial conditions the time evolution of the radical pair up through the first collision, at which point the calculation may be re-started for a subsequent

collision, etc. (see Figure I.3). For this reason the name "First Collision Model" is used.

With these factors in mind, the mathematical details for the time evolution up to the first collision will now be discussed.

A sample singlet wave function was given in Eq. (2.36c):

$$|\Phi_j\rangle = (|\phi_\ell\rangle|\phi'_m\rangle - |\phi_n\rangle|\phi'_o\rangle)/\sqrt{2} \quad .$$

Since the time evolution is governed by the one-electron Hamiltonians \mathcal{H}_{R1} and \mathcal{H}_{R2} , the one-electron wave functions may be treated separately. Thus,

$$|\Phi_j(t)\rangle = (|\phi_\ell(t)\rangle|\phi'_m(t)\rangle - |\phi_n(t)\rangle|\phi'_o(t)\rangle)/\sqrt{2} \quad . \quad (2.40)$$

The time evolution of each wave function is given by the time-dependent Schrödinger equation:

$$i\hbar \frac{\partial}{\partial t} |\phi_k(t)\rangle = \mathcal{H}_R |\phi_k(t)\rangle \quad . \quad (2.41)$$

In order to make Eq. (2.41) amenable to computer treatment, it is necessary to write the operator \mathcal{H} in a matrix representation \mathcal{H}_{\approx} . This is done by calculating the following matrix elements in the basis of the one-electron functions:

$$(\mathcal{H}_{\approx})_{jk} = \langle \phi_j | \mathcal{H} | \phi_k \rangle \quad . \quad (2.42)$$

At this point a simple example will provide the justification for the use of the one-electron basis functions. Suppose each radical contains four spin 1/2 nuclei. Now including the two electrons,

the number of two-electron basis functions is:

$$2^2 \times 2^4 \times 2^4 = 1024$$

since each spin has a multiplicity of two. Consequently, the two-electron Hamiltonian matrix would be 1024×1024 . Now if one-electron basis functions are used, the number of basis states for each radical is:

$$2 \times 2^4 = 32 \quad ,$$

and the size of each one-electron Hamiltonian matrix \mathcal{H}_R is 32×32 . Clearly, the use of one-electron basis functions provides a major reduction in effort.

Another simplification may be realized by considering the operation of the various terms in \mathcal{H}_R on the basis functions.

From Eqs. (2.21) and (2.22):

$$\mathcal{H}_R = g \beta_e H s_z + \sum_i a_i \mathbf{I}_i \cdot \mathbf{s}_i \quad . \quad (2.43a)$$

This may be re-written in terms of raising and lowering operators [23] to give:

$$\mathcal{H}_R = g \beta_e H s_z + \sum_i a_i [(I_i^+ s_i^- + I_i^- s_i^+)/2 + I_{z_i} s_{z_i}] \quad . \quad (2.43b)$$

Since the one-electron basis functions are Zeeman product functions, they are eigenstates of the I_z , s_z operators. Thus, the first and last terms on the right hand side of Eq. (2.43b) do not mix any states. If the total z component of angular momentum is defined:

$$M = m_s + \sum_i m_i \quad , \quad (2.44)$$

it is evident that the raising and lowering terms $I_i^{+} s^{-}$ and $I_i^{-} s^{+}$, while changing m_i and m_s , leave M unchanged. Thus, no term in \mathcal{H}_R mixes states of different M , and the Hamiltonian may be blocked by M values. This simplifying feature along with the use of the one-electron basis functions is employed in the computer program "sing5" (see Appendix A) which performs the calculations described in this section.

Having constructed $\mathcal{H}_{\approx R}$, it may be diagonalized:

$$\underset{\approx}{C}^{-1} \underset{\approx}{\mathcal{H}} \underset{\approx}{C} = \underset{\approx}{\Lambda} \quad . \quad (2.45)$$

It follows from Eq. (2.45) and the time-independent Schrödinger equation (2.52) that the transformation $\underset{\approx}{C}$ contains the eigenvectors as columns, and the diagonal matrix $\underset{\approx}{\Lambda}$ contains the eigenvalues. Since $\underset{\approx}{C}$ is unitary,

$$\underset{\approx}{C}^{\dagger} = \underset{\approx}{C}^{-1} \quad (2.46)$$

where $\underset{\approx}{C}^{\dagger}$ is the Hermitian adjoint of $\underset{\approx}{C}$, and since

$$(\underset{\approx}{C}^{\dagger} \underset{\approx}{C})_{ij} = \sum_k c_{ki}^* c_{kj} = (\underset{\approx}{C}^{-1} \underset{\approx}{C})_{ij} = \delta_{ij} \quad , \quad (2.47)$$

all of the eigenvectors are orthonormal to one another.

Defining (considering only one radical)

$$\{|\theta_j\rangle\} = \text{one-electron eigenfunctions} \quad , \quad (2.48)$$

$$\{\hbar\omega_j\} = \text{one-electron eigenvalues} \quad , \quad (2.49)$$

the eigenfunctions may be written:

$$|\theta_j\rangle = \sum_{\ell} c_{\ell j} |\phi_{\ell}\rangle \quad . \quad (2.50)$$

where the $c_{\ell j}$ are the elements of \underline{C} . From Eq. (2.47) it follows that the basis functions may be written:

$$|\phi_{\ell}\rangle = \sum_j c_{\ell j}^* |\theta_j\rangle \quad . \quad (2.51)$$

For an eigenfunction

$$i\hbar \frac{\partial}{\partial t} |\theta_k\rangle = \mathcal{H}_R |\theta_k\rangle = \hbar\omega_k |\theta_k\rangle \quad (2.52)$$

which has the solution

$$|\theta_k(t)\rangle = \exp[-i\omega_k t] |\theta_k\rangle \quad . \quad (2.53)$$

Substituting this into Eq. (2.51) for the basis functions,

$$|\phi_{\ell}(t)\rangle = \sum_j c_{\ell j}^* \exp[-i\omega_j t] |\theta_j\rangle \quad . \quad (2.54)$$

The time-dependent one-electron basis functions $|\phi_{\ell}(t)\rangle$ may be constructed for radicals a and b, and then substituted into Eq. (2.40) to obtain the time-dependent two-electron basis function $|\phi_j(t)\rangle$.

2.5.4 Time-Dependent Singlet Character

If the system, that is, the ensemble averaged radical pair, starts in the state $|\phi_\ell\rangle$ at $t = 0$, then, assuming no collisions, the probability that the system has evolved into the state $|\phi_m\rangle$ at $t = \tau$ is given by:

$$P_{\ell \rightarrow m}(\tau) = |\langle \phi_m | \phi_\ell(\tau) \rangle|^2 \quad (2.55)$$

where $\langle \phi_m |$ serves as a projection operator for the amplitude of $|\phi_m\rangle$ in $|\phi_\ell(t)\rangle$. The quantity which determines the chemical reactivity during a collision at time τ is the total singlet character $S(\tau)$ of the radical pair. In order to determine this quantity it is necessary to project out all of the two-electron basis functions which have singlet electron spin correlation:

$$S(\tau) = \sum_{j=S} |\langle \phi_j | \phi_\ell(\tau) \rangle|^2 \quad (2.56)$$

where the summation over $j=S$ implies that all singlets are considered. In general, the system will not start in a single state. If the initiation step produces a singlet precursor, then the initial state of the system is:

$$|\text{System}, t=0\rangle = \sum_{\ell=S} |\phi_\ell\rangle \quad (2.57)$$

If there are N singlet states (N is given by the multiplicity of the nuclear spin functions), then the normalized time-dependent singlet character for a singlet precursor is:

$$S_S(\tau) = \sum_{j=S}^N \sum_{\ell=S}^N |\langle \phi_j | \phi_\ell(\tau) \rangle|^2 / N \quad (2.58a)$$

The analogous expression may be written for a triplet precursor (multiplicity of states = 3N):

$$S_T(\tau) = \sum_{j=S}^N \sum_{\ell=T}^{3N} |\langle \phi_j | \phi_\ell(\tau) \rangle|^2 / 3N \quad (2.58b)$$

where the summation over $\ell=T$ is over all 3N triplet electronic states. In Eq. (2.58b) it is necessary to sum over three times as many states as in Eq. (2.58a), thereby requiring three times the computational effort. However, it is possible to write Eq. (2.58b) in terms of summations over singlet states only as is shown in the following proof.

For the sake of this proof, it is assumed that the full two-electron Hamiltonian has been constructed and diagonalized to obtain:

$$\{|\theta_k\rangle\} = \text{set of two-electron eigenfunctions} \quad (2.59)$$

$$\{\hbar\Omega_k\} = \text{set of two-electron eigenvalues} \quad (2.60)$$

With these it will be shown that the following expression holds:

$$N = \sum_{j=S}^N \sum_{\ell=S,T}^{4N} |\langle \phi_j | \phi_\ell(\tau) \rangle|^2 \quad (2.61)$$

where N is the number of singlets, and the second summation is over all states $\ell = S, T$ - singlets and triplets. Expanding Eq. (2.61) in terms of the eigenvectors and eigenvalues:

$$N = \sum_{j=S}^N \sum_{\ell=S,T}^{4N} \left| \sum_m^{4N} c_{jm}^* \sum_n^{4N} c_{\ell n} \exp[-i\Omega_\ell t] \langle \Theta_n | \Theta_j \rangle \right|^2 \quad (2.62)$$

and rearranging

$$N = \sum_{j=S}^N \sum_{\ell=S,T}^{4N} \left| \sum_m^{4N} \sum_n^{4N} c_{jm} c_{\ell n}^* \exp[-i\Omega_\ell t] \langle \Theta_m | \Theta_n \rangle \right|^2 \quad (2.63)$$

Since the eigenvectors are orthogonal, $m=n$, and

$$N = \sum_{j=S}^N \sum_{\ell=S,T}^{4N} \left| \sum_m^{4N} c_{jm} c_{\ell m}^* \exp[-i\Omega_\ell t] \right|^2 \quad (2.64)$$

which may be multiplied out to give

$$N = \sum_{j=S}^N \sum_{\ell=S,T}^{4N} \sum_m^{4N} \sum_{m'}^{4N} c_{jm}^* c_{\ell m} c_{jm'} c_{\ell m'}^* \exp[-i(\Omega_m - \Omega_{m'})t] \quad (2.65)$$

Performing the summation over ℓ first [see Eq. (2.47)],

$$\sum_{\ell=S,T}^{4N} c_{\ell m} c_{\ell m'}^* = \delta_{mm'} \quad (2.66)$$

and with $m = m'$:

$$N = \sum_{j=S}^N \sum_m^{4N} c_{jm}^* c_{jm} = \sum_{j=S}^N 1 = N \quad (2.67)$$

Q.E.D.

Recognizing that Eq. (2.61) can be written

$$N = \sum_{j=S}^N \sum_{m=S}^N |\langle \Phi_j | \Phi_m(t) \rangle|^2 + \sum_{j'=S}^N \sum_{n=T}^{3N} |\langle \Phi_{j'} | \Phi_n(t) \rangle|^2 \quad (2.68)$$

and defining

$$P_S(t) = \sum_{j=S}^N \sum_{m=S}^N |\langle \Phi_j | \Phi_m(t) \rangle|^2, \quad (2.69)$$

then Eqs. (2.58a) and (2.58b) can be rewritten as:

Singlet Precursor

$$S_S(t) = P_S(t)/N \quad (2.70a)$$

Triplet Precursor

$$S_T(t) = \{1 - [P_S(t)/N]\}/3 \quad (2.70b)$$

so that $S_S(t)$ and $S_T(t)$ now both involve the same summations.

Recalling that f_S is the initial fraction of singlet, there follows:

General Precursor

$$S_G(t) = f_S S_S(t) + (1-f_S) S_T(t) \quad (2.71a)$$

or

$$S_G(t) = [(1-f_S) - (1-4f_S)P_S(t)/N]/3 \quad (2.71b)$$

It is noted that for a randomly generated pair $f_S = 0.25$, and $S_G(t) = 0.25$, a constant.

The function $P_S(t)/N$ is calculated in the program "sing5" (Appendix A) for arbitrary magnetic field and up to four spin 1/2 nuclei (of arbitrary hyperfine couplings) on each radical. This program can be run on a mini-computer, and versions of it have

been used on a Data General NOVA 820 computer and a Digital Electronics Corporation PDP 11/70 computer. A calculation is shown in Figure I.7 of the singlet character as a function of time for a radical pair with eight nuclear spins and pure triplet initially. The important feature of Figure I.7 is that the singlet character rises rapidly to near 25% (the equilibrium value) and then oscillates.

It now remains to describe the time evolution of the radical pair during collision.

2.5.5 First Collision and Thereafter

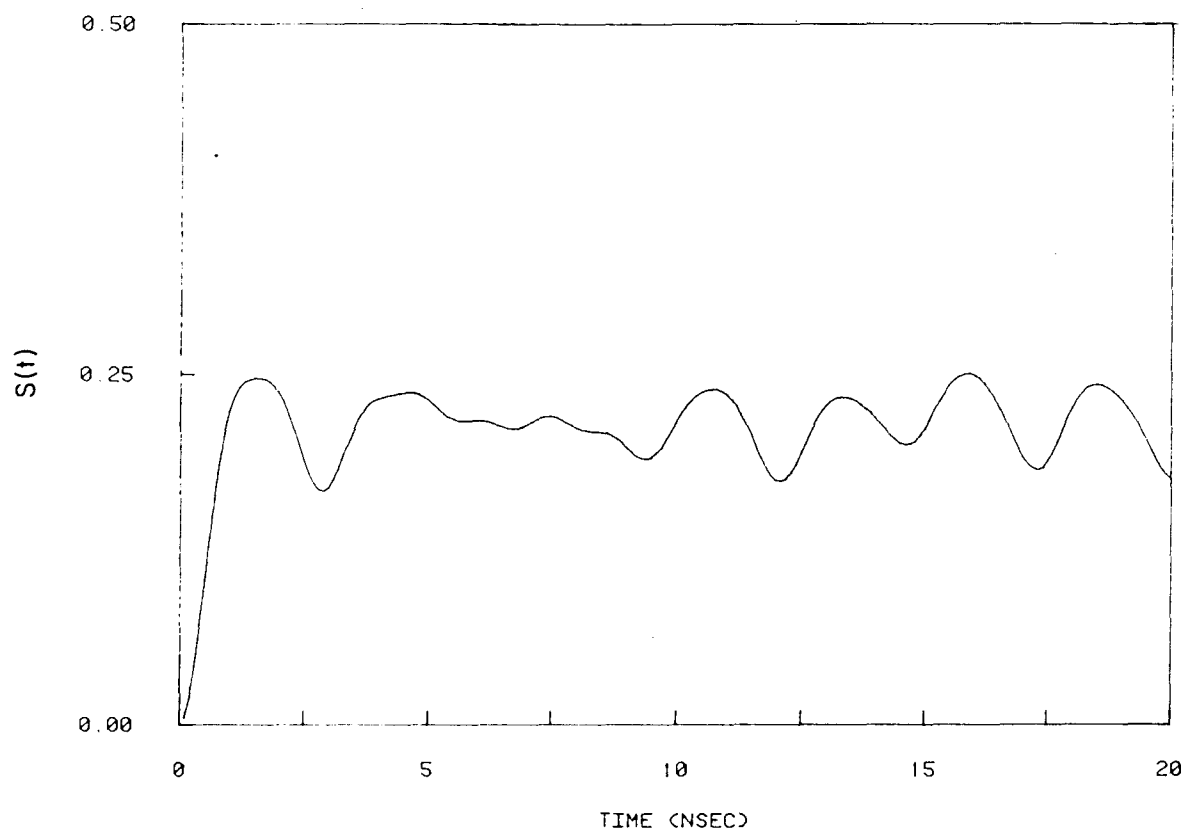
During the time evolution which precedes collision two things happen: (1) The populations of the various spin states change and (2) as the populations change, coherences are generated between spin states that are coupled either directly or indirectly through other states. The effect of a collision on these populations and coherences will now be discussed.

The dominant interaction upon collision is the exchange interaction \mathcal{H}_J . Because of the magnitude of \mathcal{H}_J , the singlet/triplet basis functions are very nearly the true eigenstates. Treating them as approximately so, the following expressions are true for singlet:

$$|\Psi_S(t)\rangle = \exp[-iJt/\hbar] |\Psi_S\rangle \quad (2.72a)$$

and for triplet:

SINGLET CHARACTER



XBL 812- 8114

Figure I.7 Singlet character as a function of time for a radical pair starting in a triplet electronic state. The external magnetic field is zero. The hyperfines on radical R_a are: 12, 34, 56, and 78 gauss; the hyperfines on radical R_b are: 23, 45, 67, and 89 gauss.

$$|\Psi_T(t)\rangle = \exp[+iJt/\hbar] |\Psi_T\rangle \quad . \quad (2.72b)$$

Since a collision time is at least of the order of a molecular vibration $\sim 10^{-14}$ sec (and presumably somewhat longer) and with $J/\hbar \sim 10^{16}$ rad/sec at collision, the argument in the exponential phase factors is $\sim 10^2$ radians. Clearly, any phase coherence between singlet and triplet states is destroyed. Also, since the singlet and triplet energy difference is so large, any inter-system crossing to change these populations may be ignored on the collisional time scale (see section 2.4.3).

Operating among the triplet states is the electron dipole-dipole interaction \mathcal{H}_D . As described in section 2.4.1, \mathcal{H}_D mixes the T_{+1} , T_0 , T_{-1} states, thereby equalizing their populations and destroying coherences between the different triplet levels.

Among the singlet states there is the possibility of their losing enough energy during collision to form a stable chemical bond. As such, a fraction equal to $\lambda S(t)$ of the total number of radical pairs which collide form stable molecules. At this point a simplifying assumption is made about those singlets which survive collision. Although the singlets are unaffected by \mathcal{H}_D , it is assumed that all coherences between them are destroyed and that the surviving $(1-\lambda)$ fraction of singlets represents population which is equally distributed among the singlets. The destruction of all singlet coherences is to be expected since the radical pair is an ensemble average of many different radical pairs. Since the different pairs will undergo collisions of varying duration, they will evolve for different lengths of time under the influence

of \mathcal{K}_J (Eq. (2.72a)), thereby randomizing their phases. This assumption of equalizing the singlet populations is without physical justification and is introduced merely as a computational convenience--it allows the surviving radical pairs to be described by a single independent parameter f_S , the fraction of singlets. Immediately after collision f_S is given by the ratio of surviving singlets to surviving radical pairs:

$$f_S = \frac{(1-\lambda)S(\tau)}{1-\lambda S(\tau)} \quad (2.73)$$

where the collision takes place at time τ . In practice, the assumption about the equalization of the singlet populations during collision has little effect since $\lambda \approx 1$, and most of the singlets do not survive collision.

After collision the time evolution of a new radical pair described by a new f_S value (Eq. (2.73)) is begun, and recombination from a second collision may be calculated. This new pair, of course, is scaled down by the fraction of pairs which have reacted. This is the same picture of radical pair reactivity which was presented in section 2.2 and mathematically stated in Eq. (2.6). The λ_i functions introduced in Eq. (2.3) are accounted for by calculating f_S after each collision and letting the system evolve up to the next collision. The computer program "diffus" (Appendix B) uses the output of the program "sing5" (see section 2.5.4 and Appendix A) to calculate the recombination of radical pairs for up to three collisions. Computationally it is very lengthy to use reasonably sized time increments and account for more than

three collisions

Initiation - τ_1 - Collision - τ_2 - Collision - τ_3 - Collision

when all possible values of τ_1, τ_2, τ_3 are considered up to the disappearance of the radicals (see Figure I.3). In section 2.7 a special case is described where an asymptotic expression is derived including all collisions.

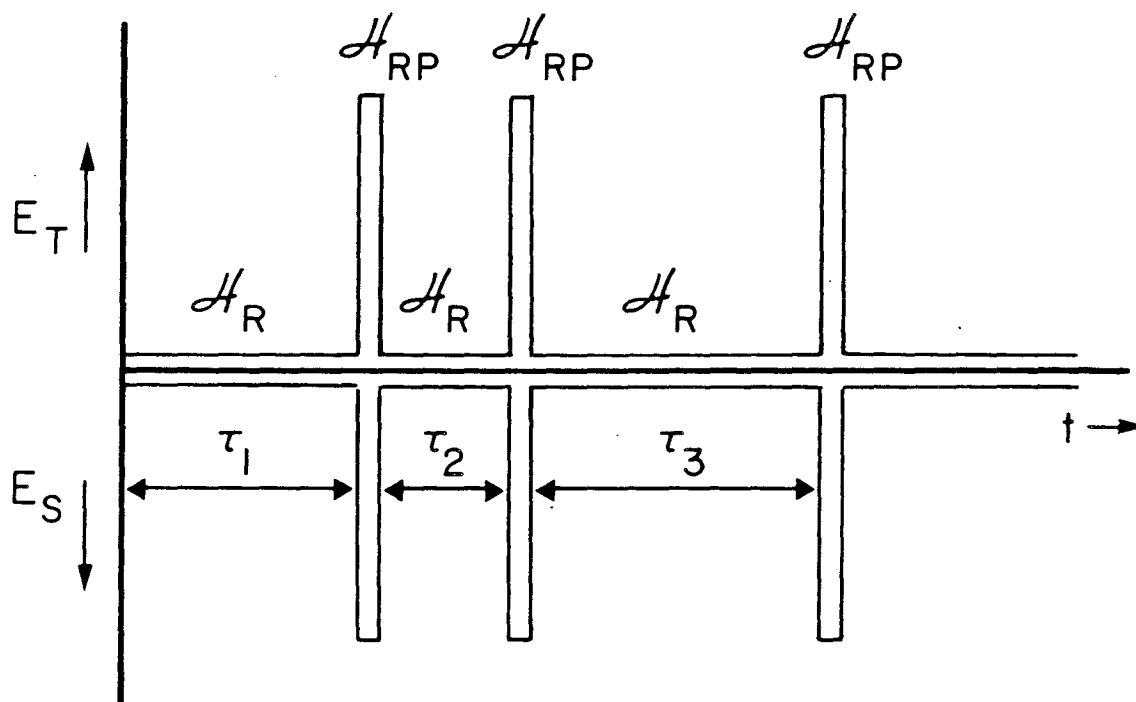
Before proceeding to the next section, the sequence of events in the time evolution is recapitulated and the operation of the various Hamiltonian terms shown schematically in Figures I.8, I.9 and I.10.

2.5.6 Spin-Orbit Coupling

In this section the indirect coupling of the radical pair singlet $|\Psi_{RP,S}\rangle$ and triplet $|\Psi_{RP,T}\rangle$ states through an intermediate excited state $|\Psi_k\rangle$ is considered. Since \mathcal{H}_{SO} is a sum of one-electron operators, the excited state cannot differ from the radical pair states by more than one molecular orbital. The spatial parts of $|\Psi_{RP,S}\rangle$ and $|\Psi_{RP,T}\rangle$ are as defined in Eqs. (2.12a) and (2.12b). $|\Psi_k\rangle$ is taken to be an excited triplet with spatial function:

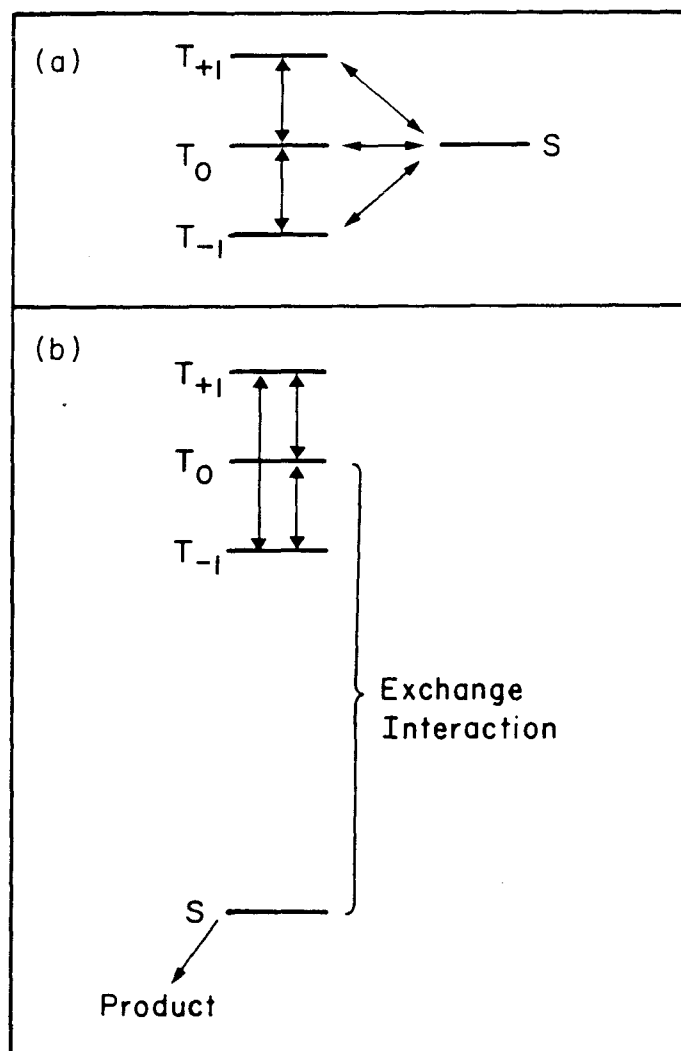
$$|\chi_{k,T}\rangle = (|u_1 w_2\rangle - |w_1 u_2\rangle) / \sqrt{2} \quad . \quad (2.74)$$

For the purpose of this example $|\Psi_{RP,T}\rangle$ is a T_0 spin state and $|\Psi_{k,T}\rangle$ a T_{+1} spin state. The coupling scheme is depicted in Figure I.11.



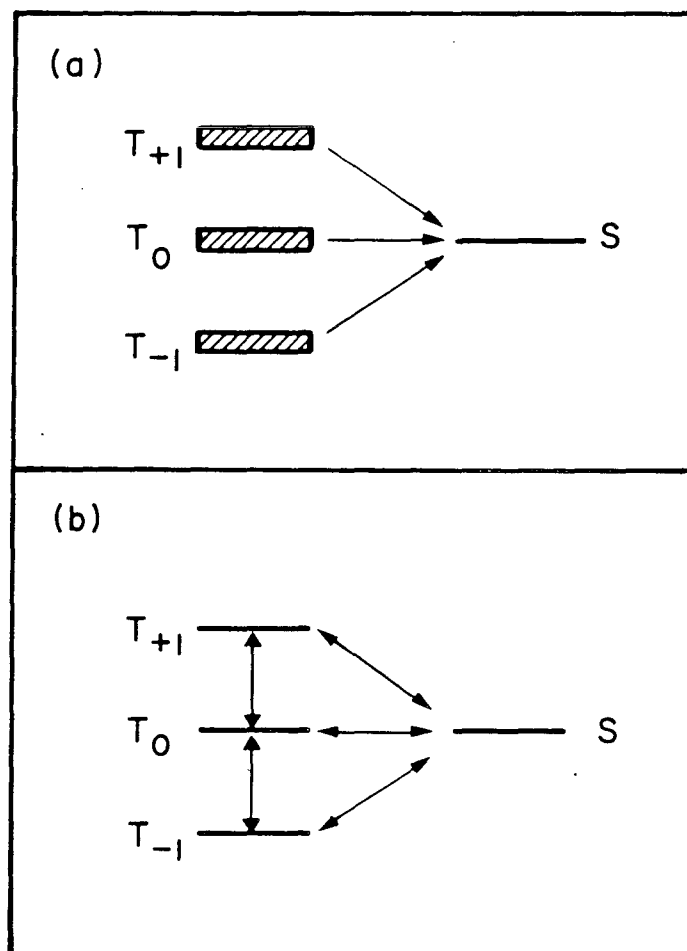
XBL 8010-12462

Figure I.8 Time dependence of the radical pair Hamiltonian. E_T and E_S are the triplet and singlet energies, respectively; τ_1 , τ_2 , and τ_3 are the time intervals between collisions. Between collisions the spins evolve under the influence of the one-electron Hamiltonians \mathcal{H}_R for each radical; during collision the large radical pair Hamiltonian \mathcal{H}_{RP} dominates the time evolution.



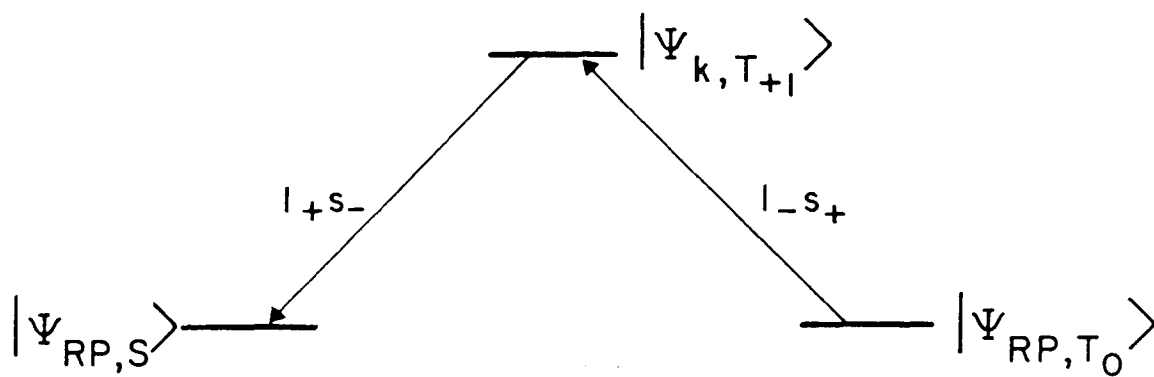
XBL 8010-12459

Figure I.9 Couplings between the electronic spin states in the mixing and collision regions. (a) In the mixing region the one-electron Hamiltonians couple those states differing by $0, \pm 1$ in the z component of the electron angular momentum. (b) In the collision region the two-electron Hamiltonian dominates the time evolution; the dipole-dipole coupling mixes the triplet sublevels and the exchange interaction causes the triplet surface to be repulsive and the singlet surface to be bonding.



XBL 8010-12460

Figure I.10 Time evolution of the electronic spin states after a collision. (a) Immediately after collision the radical pair is depleted in singlet so that there is a net flow of population from the triplet levels to the singlet state. (b) As the radicals diffuse in the mixing region, the spin state populations are equilibrated to give 25% singlet and 75% triplet at zero field.



XBL 8010-12463

Figure I.11 Spin-orbit coupling in second-order. Although spin-orbit coupling cannot connect the radical pair states in first-order, it may couple through an excited triplet state and still be faster than the hyperfine interaction.

The molecular orbital $|w\rangle$ is situated on radical b, and it is therefore necessary to retain only the summation in \mathcal{H}_{SO}^c over the nuclei on radical b. Writing \mathcal{H}_{SO}^c in terms of raising and lowering operators:

$$\mathcal{H}_{SO}^b = \sum_j^b \xi_j(r_{2j}) [(\ell_{2s_2}^+ + \ell_{2s_2}^-)/2 + \ell_{z_2} s_{z_2}] \quad , \quad (2.75)$$

and the following matrix elements are obtained after performing the spin integrations:

$$\langle \Psi_{RP,S} | \mathcal{H}_{SO}^b | \Psi_{RP,T_0} \rangle = 0 \quad (2.76a)$$

$$\langle \Psi_{RP,S} | \mathcal{H}_{SO}^b | \Psi_{k,T_{+1}} \rangle = \langle v_2 | \sum_j \xi_j(r_{2j}) \ell_2^+ | w_2 \rangle / \sqrt{8} \equiv \zeta \quad (2.76b)$$

$$\langle \Psi_{RP,T_0} | \mathcal{H}_{SO}^b | \Psi_{k,T_{+1}} \rangle = \langle v_2 | \sum_j \xi_j(r_{2j}) \ell_2^+ | w_2 \rangle / \sqrt{8} = \zeta \quad . \quad (2.76c)$$

The diagonal elements of \mathcal{H}_{SO}^c are zero since the wave functions are real (see section 2.4.3). The basis functions are numbered as:

$$|\psi_1\rangle = |\Psi_{RP,S}\rangle \quad (2.77a)$$

$$|\psi_2\rangle = |\Psi_{k,T_{+1}}\rangle \quad (2.77b)$$

$$|\psi_3\rangle = |\Psi_{RP,T_0}\rangle \quad . \quad (2.77c)$$

The radical pair states are taken to be degenerate in the mixing region, and the following energies are assigned:

$$E_1 = E_3 = 0 \quad (2.78a)$$

$$E_2 = E \quad . \quad (2.78b)$$

With Eqs. (2.76a)-(2.78b) the Hamiltonian matrix may be constructed (neglecting all other interactions):

$$\mathcal{H} \approx \begin{pmatrix} 0 & \zeta & 0 \\ \zeta^* & E & \zeta^* \\ 0 & \zeta & 0 \end{pmatrix} \quad . \quad (2.79)$$

Diagonalizing \mathcal{H} , the following matrix of eigenvectors \underline{C} are obtained along with the eigenvalues Ω_i for the case of $E \gg |\zeta|$:

$$\underline{C} \approx \begin{pmatrix} 0.707 & \zeta/E & 0.707 \\ 0 & 1 & -\sqrt{2}\zeta^*/E \\ -0.707 & \zeta/E & 0.707 \end{pmatrix} \quad (2.80)$$

$$\Omega_1 = 0 \quad (2.81a)$$

$$\Omega_2 = E + 2\zeta\zeta^*/E \quad (2.81b)$$

$$\Omega_3 = -2\zeta\zeta^*/E \quad . \quad (2.81c)$$

Assuming a triplet precursor, the singlet character as a function of time is given by:

$$S(t) = |\langle \Psi_{RP,S} | \Psi_{RP,T_0}(t) \rangle|^2 \quad . \quad (2.82)$$

From Eqs. (2.54) and (2.80)-(2.82), $S(t)$ is calculated to be

(with $E \gg |\zeta|$):

$$S(t) = \frac{1}{2} - \frac{1}{2} \cos\left(\frac{2\zeta\zeta^*}{E} \frac{t}{\hbar}\right) \quad (2.83)$$

If $|\zeta|$ is of the order of the spin-orbit coupling constant for an electron in a carbon 2p atomic orbital [22]:

$$|\zeta| = 28 \text{ cm}^{-1} = 0.08 \text{ kcal/mole} \quad (2.84)$$

and E is a typical excitation energy in organic molecules:

$$E = 70 \text{ kcal/mole} \quad , \quad (2.85)$$

then the frequency in $S(t)$ is

$$2\zeta\zeta^*/E = 0.18 \text{ cal/mole} = 1.9 \times 10^9 \text{ Hz/molecule} \quad . \quad (2.86)$$

The electron-nuclear hyperfine couplings appearing in \mathcal{H}_{R1} and \mathcal{H}_{R2} (section 2.4.2) are generally in the range 10^7 - 10^8 Hz. Thus, even if the estimate in Eq. (2.86) were reduced by a factor of 10, it would still be comparable to the hyperfines. Furthermore, there is one factor in favor of the estimate of Eq. (2.86). The expression for the free radical electron g-factor contains a second-order perturbation term involving \mathcal{H}_{SO} . The deviation Δg of the free radical g-factor from that of the free electron value is attributed to the spin-orbit interaction which mixes excited electronic states into the ground electronic state of the radical. When the values of $|\zeta|$ and E used above are substituted into the expression for Δg (in an approximate fashion), a value of 10^{-3} is obtained which is characteristic

of all of the radicals studied in this work. For a discussion of the Δg factor along with simple examples the reader is referred to Reference 22.

With these considerations, the neglect of spin-orbit coupling in the standard treatments of radical pair inter-system crossing [1,2,3] seems rather questionable. As mentioned earlier, the complex nature of the First Collision Model precludes the inclusion of spin-orbit coupling, but it is included in the Continuous Diffusion Model which is presented in the following chapter. In Chapter 6 calculations based on the Continuous Diffusion Model are presented which show the sensitivity of both geminate yield and the magnetic isotope effect to spin-orbit coupling. However, it is also shown (section 6.1.2) that CIDNP effects, with which the standard treatments of radical pair recombination are concerned, are far less sensitive to spin-orbit coupling and may be easily observable even when isotope effects are not. Thus, the success of those treatments which neglect the spin-orbit interaction proves little about the importance it may have in radical pair recombination.

magnetic field the precession rate of an electron coupled to a single nucleus is $m\alpha$ where m is the magnetic quantum number and α is the hyperfine interaction of the nucleus. Ignoring differences in electron g -factors [this is easily included by adding a term $(g_1 - g_2)H$], the difference in precession rate $\Delta\nu$ for the two electrons at high fields is [1]:

$$\Delta\nu_{\text{HF}} = \left| \sum_i^a m_i \alpha_i - \sum_j^b m'_j \alpha_j \right| \quad (3.3a)$$

where the sums are over the two radicals for a given nuclear spin state. Since the electrons precess only about the field axis at high field, only the secular part of the hyperfine coupling contributes to $\Delta\nu_{\text{HF}}$. Assuming only spin 1/2 nuclei are present, then at zero field the electron-nuclear coupling becomes α (secular plus non-secular) rather than $m\alpha$. By analogy the zero field expression is defined:

$$\Delta\nu_0 \equiv \left| \sum_i^a n_i \alpha_i - \sum_j^b n'_j \alpha_j \right| \quad (3.3b)$$

where $n = \pm 1$ for each nucleus. By averaging over all possible nuclear spin states, the average difference $\overline{\Delta\nu}$ is calculated for the radical pair. Since a 180° dephasing interconverts singlet and triplet, $k_+ + k_-$ is set equal to $2\overline{\Delta\nu}$. Any additional relaxation terms may be added on to this quantity. This accounts for all time evolution of the spin states between collisions. The only time evolution that takes place during collision is that the singlets react and the triplets are reflected (see section 3.4).

3.3 Chemical Loss

The disappearance of radical pairs through chemical reaction is termed chemical loss and represented by the rate constant k_{loss} . This rate constant is simply the inverse of the radical pair lifetime defined in section 2.6. For the dibenzylketone photolysis with decarbonylation, k_{loss} equals k_{co} , and for the benzophenone/toluene photolysis with scavenging, k_{loss} equals $k_{\text{S}}[\phi\text{SH}]$.

3.4 Time Evolution Equations and Boundary Conditions

The factors discussed in sections 3.1-3.3 can be combined to construct the differential equations describing the time evolution of the radical pair. The solution requires that the equations be integrated with the appropriate boundary and initial conditions imposed on the system. The time evolution equations are

$$\frac{\partial \rho_S}{\partial t}(\underline{r}, t) = [D_R \nabla^2 - k_+ - k_{\text{loss}}] \rho_S(\underline{r}, t) + k_- \rho_T(\underline{r}, t) \quad (3.4a)$$

$$\frac{\partial \rho_T}{\partial t}(\underline{r}, t) = [D_R \nabla^2 - k_- - k_{\text{loss}}] \rho_T(\underline{r}, t) + k_+ \rho_S(\underline{r}, t) \quad (3.4b)$$

The following boundary conditions are introduced:

$$\rho_S(\underline{r}, t) \rightarrow 0 \quad \text{as } |\underline{r}| \rightarrow \infty \quad (3.5a)$$

$$\rho_T(\underline{r}, t) \rightarrow 0 \quad \text{as } |\underline{r}| \rightarrow \infty \quad (3.5b)$$

$$\rho_S(\underline{r}, t) = 0 \quad |\underline{r}| = r_c \quad (3.5c)$$

$$\hat{r} \cdot \nabla \rho_T(\underline{r}, t) = 0 \quad |\underline{r}| = r_c \quad (3.5d)$$

Conditions (3.5a) and (3.5b) hold since there are a finite number of radical pairs. Condition (3.5c) states that all singlets are absorbed when the interradsical separation $|\underline{r}|$ equals r_c the collision radius; that is, $\lambda = 1$ in this model (compare section 2.3). Condition (3.5d) states that all triplets are reflected

when the radicals reach the collision radius.

The initial conditions placed on the system are:

$$\rho_S(\underline{r}, 0) = f_S \delta(\underline{r} - \underline{r}_0) \quad (3.6a)$$

$$\rho_T(\underline{r}, 0) = (1 - f_S) \delta(\underline{r} - \underline{r}_0) \quad (3.6b)$$

where f_S is the fraction of singlets at $t = 0$ and \underline{r}_0 is the initial interracial separation.

Equations (3.4a) and (3.4b) may be separated by the introduction of the following variables:

$$X(\underline{r}, t) = \rho_S(\underline{r}, t) + \rho_T(\underline{r}, t) \quad (3.7a)$$

$$Z(\underline{r}, t) = k_+ \rho_S(\underline{r}, t) - k_- \rho_T(\underline{r}, t) \quad (3.7b)$$

which give:

$$\frac{\partial X}{\partial t}(\underline{r}, t) = [D_R \nabla^2 - k_{\text{loss}}] X(\underline{r}, t) \quad (3.8a)$$

$$\frac{\partial Z}{\partial t}(\underline{r}, t) = [D_R \nabla^2 - (k_+ + k_- + k_{\text{loss}})] Z(\underline{r}, t) \quad (3.8b)$$

3.5 Recombination Yield

The recombination yield R of radical pairs is equal to the flux of singlets into the reaction zone $|\underline{r}| = r_c$ integrated over all time [12b]. This time-dependent flux $F(t)$ of singlets is given by:

$$F(t) = \int_{|\underline{r}|=r_c} d\tilde{A} D_R \hat{r} \cdot \nabla_{\tilde{S}} \rho_{\tilde{S}}(\underline{r}, t) = \int_{|\underline{r}|=r_c} d\tilde{A} D_R \hat{r} \cdot \nabla_{\tilde{X}} X(\underline{r}, t) \quad (3.9)$$

where the two integrals are equal for $|\underline{r}|=r_c$ by Eqs. (3.5d) and (3.7a). Since the diffusion is isotropic, $X(\underline{r}, t)$ and $Z(\underline{r}, t)$ may be written as functions with only time-dependent radial parts:

$$X(\underline{r}, t) = \sum_{l,m} x_{l,m}(r, t) Y_{l,m}(\theta, \phi) \quad (3.10a)$$

$$Z(\underline{r}, t) = \sum_{l,m} z_{l,m}(r, t) Y_{l,m}(\theta, \phi) \quad (3.10b)$$

where the $Y_{l,m}(\theta, \phi)$'s are spherical harmonics. The only angular dependence in the integral of Eq. (3.9) is from $X(\underline{r}, t)$ so that when the angular integration is performed, only the spherically symmetric $Y_{0,0}$ term survives:

$$F(t) = \int_{|\underline{r}|=r_c} d\tilde{A} D_R \frac{\partial X}{\partial r}(\underline{r}, t) = \sqrt{4\pi} r_c^2 D_R \frac{\partial x_{0,0}}{\partial r}(\underline{r}, t) \Big|_{r=r_c} \quad (3.11)$$

The recombination yield is:

$$R = \int_0^{\infty} dt F(t) = \sqrt{4\pi} r_c^2 D_R \left[\frac{\partial}{\partial r} \int_0^{\infty} dt x_{0,0}(r,t) \right]_{r=r_c} \quad (3.12)$$

The integral over time is equivalent to a Laplace transform:

$$L\{F(t)\} = \int_0^{\infty} dt \exp(-qt) F(t) = \tilde{F}(q) \quad (3.13)$$

where the Laplace transform variable q is zero. Thus,

$$R = \tilde{F}(0) = \sqrt{4\pi} r_c^2 D_R \left. \frac{\partial \tilde{x}_{0,0}}{\partial r}(r,0) \right|_{r=r_c} \quad (3.14)$$

Since the Laplace-transformed $\tilde{x}(r,0)$ is the desired quantity, the time evolution equations (3.8a) and (3.8b) may be Laplace transformed:

$$[D_R \nabla^2 - k_{\text{loss}}] \tilde{X}(r,0) = -X(r,0) \quad (3.15a)$$

$$[D_R \nabla^2 - (k_+ + k_- + k_{\text{loss}})] \tilde{Z}(r,0) = -Z(r,0) \quad (3.15b)$$

where use has been made of the fact that $X(r,t)$ and $Z(r,t)$ equal zero at $t = \infty$ because of chemical loss and recombination.

From the initial conditions Eqs. (3.6a) and (3.6b) and the definitions of $X(r,t)$ and $Z(r,t)$ [Eqs. (3.7a) and (3.7b), respectively], there follows:

$$X(r,0) = \delta(r-r_0) \quad (3.16a)$$

$$Z(r,0) = [f_S(k_+ + k_-) - k_-] \delta(r-r_0) \equiv \gamma k_- \delta(r-r_0) \quad (3.16b)$$

The δ -function may be written in terms of spherical harmonics:

$$\delta(\underline{r}-\underline{r}_o) = \frac{1}{r^2} \delta(r-r_o) \sum_{\ell,m} Y_{\ell,m}^*(\theta_o, \phi_o) Y_{\ell,m}(\theta, \phi) \quad (3.17)$$

Since the spherical harmonics are linearly independent, Eqs. (3.15a) and (3.15b) must be true for each individual pair of l, m values. From Eq. (3.11) only the $l=m=0$ term is of interest. Thus,

$$[D_R \nabla_r^2 - k_{\text{loss}}] \tilde{x}_{o,o}(r,0) = -\delta(r-r_o) / (\sqrt{4\pi} r^2) \quad (3.18a)$$

$$[D_R \nabla_r^2 - (k_+ + k_- + k_{\text{loss}})] \tilde{z}_{o,o}(r,0) = -\gamma k_- \delta(r-r_o) / (\sqrt{4\pi} r^2) \quad (3.18b)$$

where now it is only necessary to keep the radial part ∇_r^2 of the Laplacian.

The homogeneous equation may be written:

$$\frac{\partial^2}{\partial r^2} f(r) + \frac{2}{r} \frac{\partial}{\partial r} f(r) - \ell^2 f(r) = 0 \quad (3.19)$$

where $f(r)$ may be \tilde{x} or \tilde{z} . The solutions of Eq. (3.19) are zeroth-order modified spherical Bessel functions [27]:

$$f(r) = c_1 \exp[-\ell r]/r + c_2 \exp[+\ell r]/r \quad (3.20)$$

Eqs. (3.18a) and (3.18b) can thus be solved for $\tilde{x}_{o,o}(r,0)$ and $\tilde{z}_{o,o}(r,0)$ and solutions obtained for the two regions $r_c \leq r \leq r_o$ and $r_o \leq r \leq \infty$. Matching the solutions at r_o by assuming their continuity and using the boundary conditions Eqs. (3.5a)-(3.5d) (Laplace transforming them, etc.), the functions $\tilde{x}_{o,o}(r,0)$

and $\tilde{z}_{o,o}(r,0)$ are completely determined. Taking the derivative of $\tilde{x}_{o,o}(r,0)$ at $r = r_c$ [Eq. (3.14)], the recombination yield R is determined in analytical form. The result is:

$$R = \frac{r_c}{r_o} \frac{(1+\beta r_c) \exp[-\alpha(r_o-r_c)] + \gamma(1+\alpha r_c) \exp[-\beta(r_o-r_c)]}{(1+\beta r_c) + (1+\alpha r_c)k_+/k_-} \quad (3.21)$$

where

$$\alpha = [k_{\text{loss}}/D_R]^{1/2} \quad (3.22a)$$

$$\beta = [(k_+ + k_- + k_{\text{loss}})/D_R]^{1/2} \quad (3.22b)$$

$$\gamma = f_S [1 + (k_+/k_-)] - 1 \quad (3.22c)$$

Using Eqs. (3.21)-(3.22c) it is possible to calculate ^{13}R and ^{12}R from which a suitable enrichment parameter may be defined (Chapter 6) for comparison with experiment.

Before proceeding to the next chapter, the Continuous Diffusion Model will be modified by the addition of an extra boundary condition in order to treat a case of special experimental interest--that of diffusion in a restricted volume.

3.6 Restricted Volume and Micelles

Surfactants are molecules consisting of one or more hydrocarbon chains attached to a polar head group. In solution these molecules form aggregates, or micelles, of various sizes and shapes in which the nonpolar parts (i.e., the hydrocarbon chains) of the molecules associate together and the polar parts (i.e., the head groups) associate together [28]. The type of micelle treated in this section is that in which the surfactant molecules are more or less radially arranged into a sphere with the hydrocarbon chains forming the interior and the polar head groups forming the surface. An organic molecule may be solubilized into the interior of the micelle which is roughly equivalent to a liquid hydrocarbon droplet [28]. A nonpolar organic molecule will be repelled from the polar head groups at the surface of the sphere. In aqueous solution the concentration of nonpolar organic molecules will be much higher in the micelle interiors than in the bulk H₂O solution. Thus, when such a solution is photolyzed, the photochemistry of the organic molecule of interest takes place within the micelle [6].

The Continuous Diffusion Model is adapted to such a situation by replacing the boundary conditions (3.5a) and (3.5b), which are relevant for infinite solution, with the new conditions:

$$\hat{r} \cdot \nabla_{\underline{r}} \rho_S(\underline{r}, t) = 0 \quad |\underline{r}| = r_b \quad (3.23a)$$

$$\hat{r} \cdot \nabla_{\underline{r}} \rho_T(\underline{r}, t) = 0 \quad |\underline{r}| = r_b \quad (3.23b)$$

where r_b is the micelle radius. Since it is the interradical separation \tilde{r} and not the individual position vectors of the radicals which enters the calculation, one radical is always positioned at the origin. Thus, Eqs.(3.23a) and (3.23b) state that the singlet and triplet radical pairs are reflected when they separate to the micelle boundary radius r_b . For the infinite volume case (sections 3.4, 3.5) the constraint of fixing one radical and considering the relative diffusion of the other was simply a matter of reference frame and was inconsequential. In the micelle case the artificial constraint of having one radical remain at the center is a source of error. Nevertheless, the model still accounts for the general features of diffusion in a restricted volume.

Replacing Eqs. (3.5a) and (3.5b) with Eqs. (3.23a) and (3.23b), and following the same analysis as in sections 3.4 and 3.5, the expression obtained for recombination in a micelle is

$$R = \{(\Delta_3\phi_1 + \Delta_1\phi_2)(1 + \alpha r_c) \exp[\alpha(r_o - r_c)] - (\Delta_4\phi_1 + \Delta_2\phi_2)(1 - \alpha r_c) \exp[-\alpha(r_o - r_c)]\} / (\Delta_1\Delta_4 - \Delta_2\Delta_3) \quad (3.24)$$

where

$$\Delta_1 = 1 - \alpha r_b \quad (3.25a)$$

$$\Delta_2 = (1 + \alpha r_b) \exp[-2\alpha(r_b - r_o)] \quad (3.25b)$$

$$\begin{aligned} \Delta_3 = & \{(1-\beta r_b)[k_+(1-\alpha r_c) + k_-(1+\beta r_c)] \exp[\beta(r_o-r_c)] \\ & - q[k_+(1-\alpha r_c) + k_-(1-\beta r_c)] \exp[-\beta(r_o-r_c)]\} \exp[-\alpha(r_o-r_c)] \end{aligned} \quad (3.25c)$$

$$\begin{aligned} \Delta_4 = & \{(1-\beta r_b)[k_+(1+\alpha r_c) + k_-(1+\beta r_c)] \exp[\beta(r_o-r_c)] \\ & - q[k_+(1+\alpha r_c) + k_-(1-\beta r_c)] \exp[-\beta(r_o-r_c)]\} \exp[\alpha(r_o-r_c)] \end{aligned} \quad (3.25d)$$

$$\phi_1 = (\Delta_1 - \Delta_2) / (2\alpha r_o) \quad (3.25e)$$

$$\phi_2 = (r_c/r_o) \gamma k_-(1-\beta r_b - q) \quad (3.25f)$$

$$q = (1+\beta r_b) \exp[-2\beta(r_b-r_o)] \quad (3.25g)$$

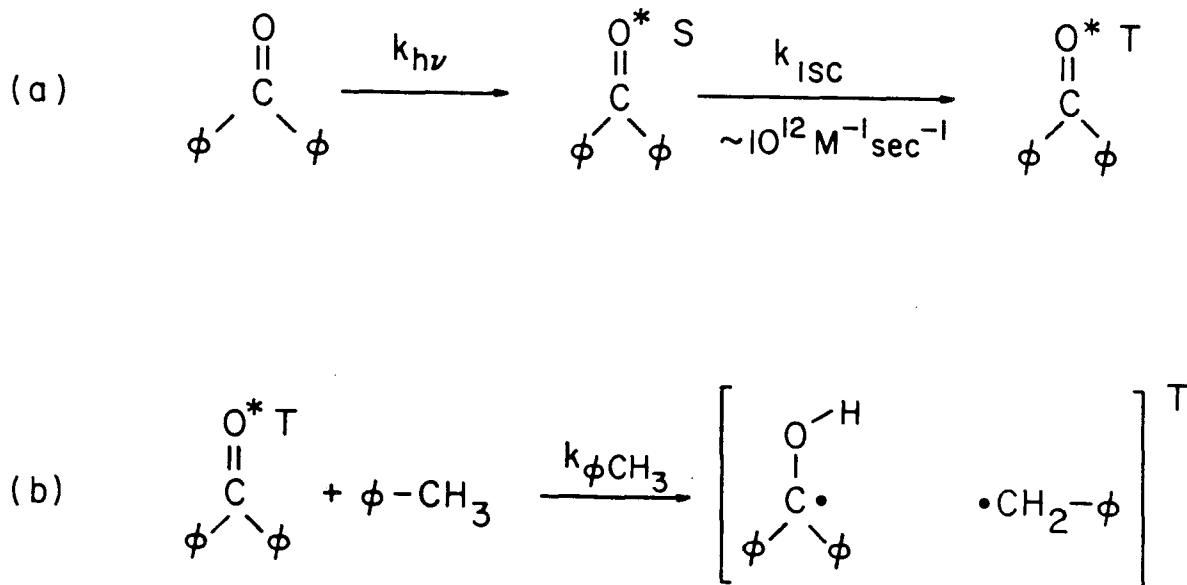
Although the micelle was introduced as a special case of the derivation of the preceding section, in fact, the opposite is true. Eq. (3.21) for recombination in an infinite volume is a special case of Eq. (3.24) and is obtained directly from Eq. (3.24) in the limit of $r_b \rightarrow \infty$ (see Chapter 6, Figure I.42).

4. PHOTOCHEMISTRY

4.1 Benzophenone and Toluene

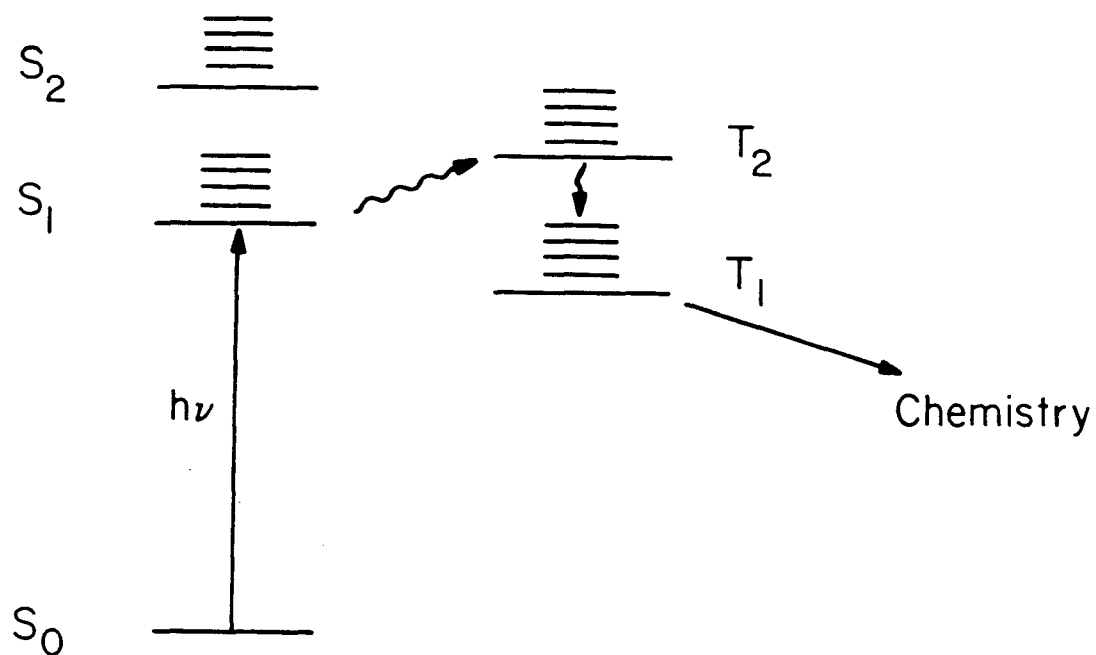
The benzophenone photochemistry involves two steps as shown in Figure I.12: (a) production of photoexcited benzophenone and (b) reaction of the excited benzophenone with toluene. For the photoexcitation step irradiation was performed with a high pressure mercury UV lamp with all light of wavelength shorter than $3450 \overset{\circ}{\text{A}}$ filtered out so that only the lowest excited singlet S_1 of benzophenone could be populated.

S_1 occurs 74 kcal/mole above the ground state [29] and has an absorption maximum $\sim 3500 \overset{\circ}{\text{A}}$ in cyclohexane [30]. S_1 intersystem crosses to the first excited triplet T_1 , in $\sim 3 \times 10^{-11}$ sec with near unit probability [31]. From theoretical considerations [32] and chemical reactivity, S_1 and T_1 are identified as n, π^* states. That is, they are formed by the excitation of a non-bonding electron on oxygen to the π^* orbital of the carbonyl group. Since the two states have the same orbital make-up, the spin-orbit interaction cannot couple them directly, and the fast intersystem crossing must involve an intermediate T_2 state (see Figure I.13). Furthermore, since S_1 and T_1 are separated by 5.7 kcal/mole [29], the high rate of intersystem crossing indicates that there is significant Franck-Condon overlap between S_1 and an excited vibrational state of T_1 giving a near degenerate condition as shown in Figure I.13. T_2 is presumably a π, π^* state (i.e., $\pi \rightarrow \pi^*$ excitation).



XBL 8010-7377

Figure I.12 (a) Benzophenone is photoexcited to a singlet state which decays to a metastable triplet. (b) The alkoxy-like triplet state abstracts a hydrogen from toluene and, conserving spin correlation, produces a triplet radical pair.

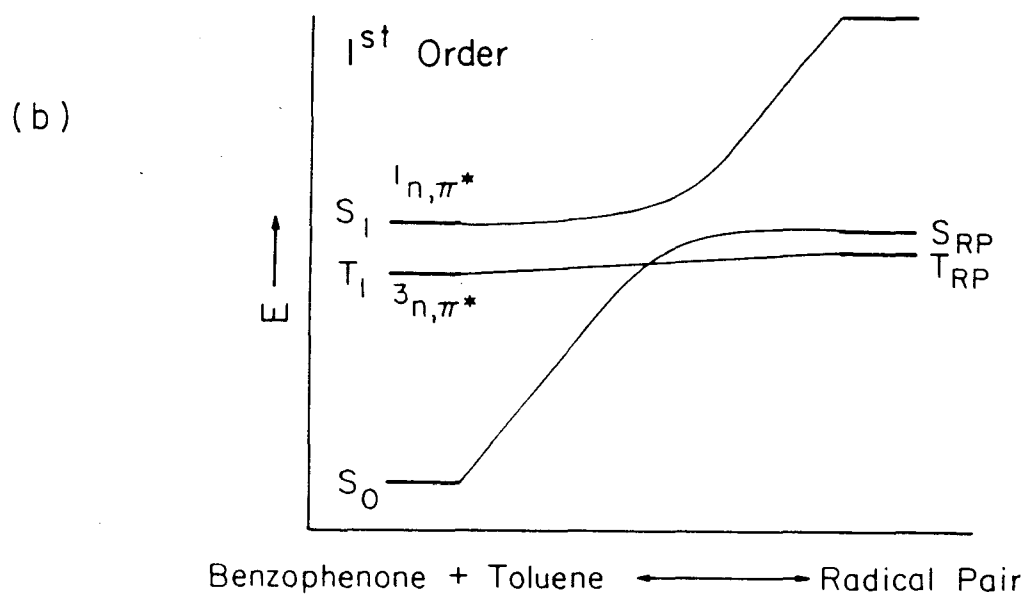
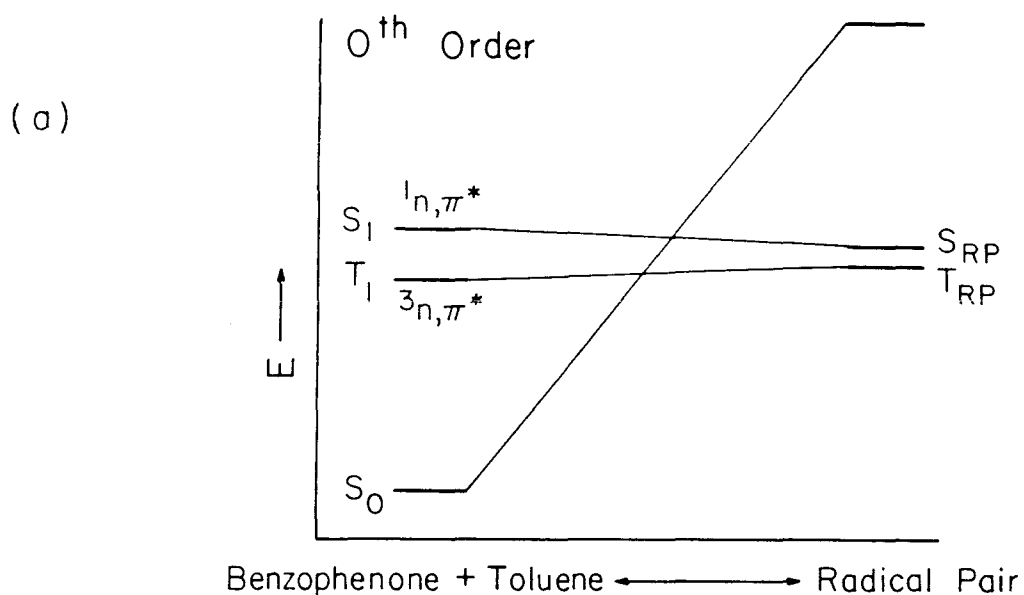


XBL 8010-12621

Figure I.13 Photochemical route to produce triplet state chemistry. The carbonyl moiety is photoexcited to the first excited singlet state. The excited singlet S_1 decays to the lowest triplet via the spin-orbit interaction which operates through an intermediate excited triplet T_2 (see sections 2.4.3 and 2.5.6). The metastable triplet T_1 can react to form a triplet radical pair.

The excited triplet T_1 has a room temperature lifetime in "inert" organic solvents of $\sim 4 \times 10^{-3}$ sec [33]. Because a non-bonding electron has been excited from the carbonyl oxygen, the excited state appears radical-like, that is, like an alkoxy radical [34]. The radical-like oxygen abstracts a hydrogen from toluene with rate constant $k_{\phi\text{CH}_3}$ equal to $6 \times 10^{-5} \text{ M}^{-1} \text{ sec}^{-1}$ [33,35]. The toluene concentrations used were 1 to 10 M, and thus the abstraction reaction took $\leq 10^{-6}$ sec, well within the excited state lifetime. The hydrogen abstraction takes place without change of electron spin [36], and since S_1 decays to T_1 much faster than the rate of hydrogen abstraction, the radical pairs are formed with 100% triplet electron spin correlation.

An important consideration in regard to radical pair intersystem crossing arises when the state correlation diagram for carbonyl hydrogen abstraction is examined. A schematic correlation diagram is shown in Figure I.14. In zero order the S_1 and S_0 potential energy surfaces cross. Thus, in zero order if the radical pair state T_{RP} crosses over to S_{RP} , the radical pair still remains on an unbound surface. In first order, mixing between S_1 and S_0 is allowed, but T_1 - S_0 mixing is forbidden because of the different electronic spin. The S_1 - S_0 mixing causes an avoided crossing as shown in the second part of Figure I.14, and now S_{RP} correlates with the bound state S_0 . The strength of the avoided crossing and the rate at which the radicals move on the surfaces (i.e., adiabatic versus non-adiabatic motion) are major factors in determining (1) the



XBL 8010-12624

Figure I.14 Correlation diagrams for benzophenone and toluene radical pair. These figures are based on the work of Salem [36] for formaldehyde plus methane. (a) In zeroth-order there is no interaction to mix the ground and excited singlet states; thus, the singlet radical pair state may not lead to product. (b) In first-order the excited and ground singlet energy surfaces cannot cross; therefore, the singlet radical pair lies on a bound potential energy surface.

reactivity λ of singlets during collision (see section 2.3) and (2) the preparation of a pure triplet radical pair. The fact that triphenylethanol is a product of the benzophenone/toluene photolysis indicates that the surface crossing is indeed avoided. The geminate recombination process for the triplet radical pair from benzophenone and toluene (or from dibenzylketone; see below) is shown schematically in Figure I.15.

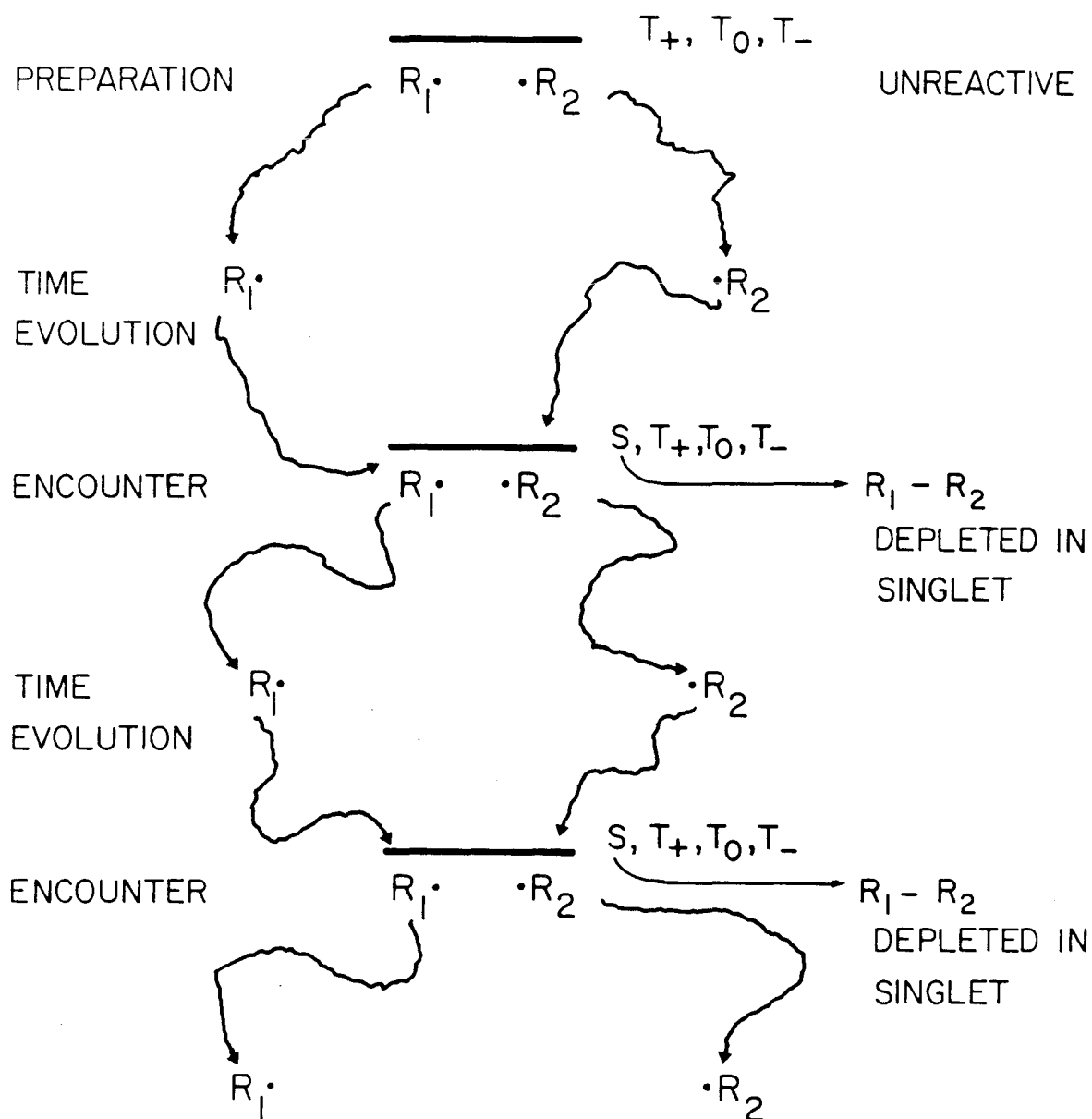
The hyperfine couplings for the radical pair are shown in Figure I.16. Although the ketyl radical is drawn with the electron localized at the central carbon, the ^{13}C at this position does not have a very large hyperfine coupling, because the unpaired electron resides in a π^* orbital and is really delocalized over both aromatic rings. In addition, the π^* molecular orbital is made up of p atomic orbitals which have nodes at the nuclei.

The isotropic g-factors are [37]:

$$g_{\text{Ketyl}} = 2.003$$

$$g_{\text{Benzyl}} = 2.0026 \quad .$$

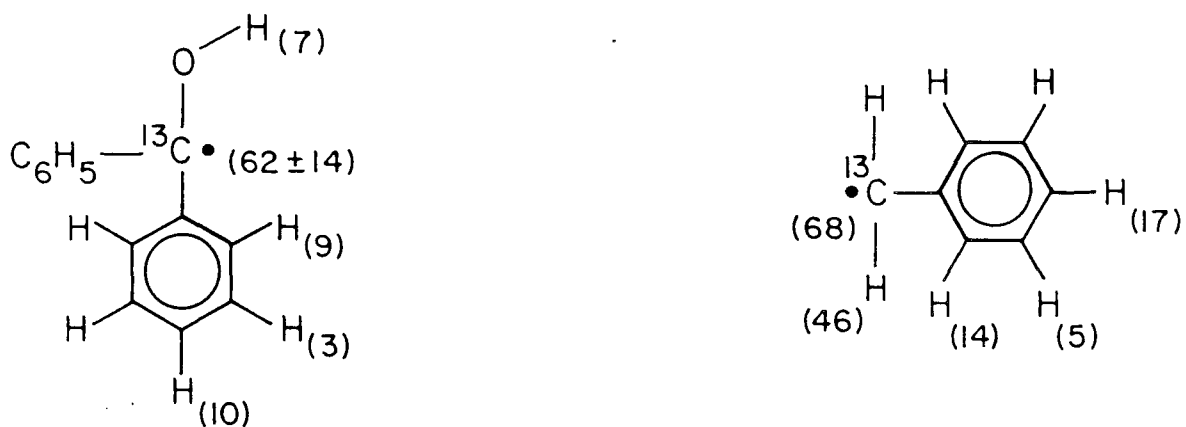
The deviation from the free electron g-factor of 2.0023 indicates that spin-orbit coupling is non-zero (see sections 2.4.3 and 2.5.6).



XBL 802-8352

Figure I.15 Diffusive behavior of a triplet radical pair. The overbar indicates collision. The initially prepared triplet cannot bond so it separates. During separation the hyperfine couplings interconvert triplet and singlet, and upon re-encounter bonding is possible. Those radicals with the largest hyperfines interconvert the fastest and are most likely to form product.

HYPERFINE CONSTANTS IN MHz

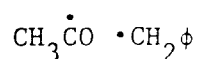


XBL 8010-12622

Figure I.16 Hyperfine coupling constants for the radical pair produced by photolysis of benzophenone and toluene. All values are taken from Reference 37.

4.2 Dibenzylketone

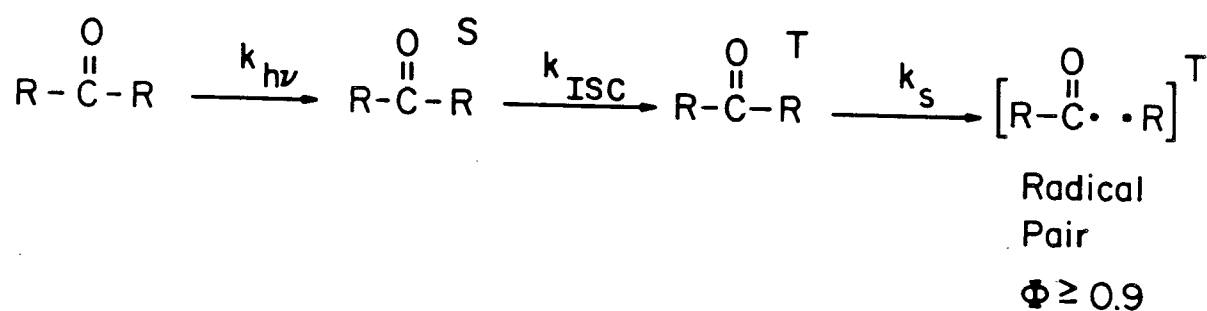
The photolysis of dibenzylketone to produce a radical pair is shown in Figure I.17. Photolysis was performed with irradiation $> 3000 \text{ \AA}$ which should populate only the n, π^* singlet. Engel [38] has determined the energy of $^1n, \pi^*$ to be 88 kcal/mole (3250 \AA) and of $^3n, \pi^*$ to be 79 kcal/mole. The triplet energy is more than sufficient to accomplish bond scission since the bond strength of a similar carbon-carbon bond:



is listed as 63 kcal/mole [39]. From singlet and triplet sensitization and quenching experiments Engel [38] has determined that the $^3n, \pi^*$ level is populated with near unit quantum yield (see Figure I.13, section 4.1) and that bond scission occurs in $\sim 10^{-10}$ sec. Since decay of T_1 to S_0 cannot compete with the rate of bond scission, triplet radical pairs are formed with near unit quantum yield as shown in Figure I.17.

A schematic zero-order correlation diagram for the ketone cleavage is shown in Figure I.18a. When first-order mixing of the triplet states is allowed, the correlation diagram of Figure I.18b results. From the latter diagram it is reasonable to expect the formation of a triplet radical pair since the cleavage of S_1 is endothermic and the cleavage of T_1 is estimated from the above stated energies to be exothermic by 16 kcal/mole. As

Preparation



XBL 803-8420

Figure I.17 Preparation of the dibenzylketone triplet radical pair. $\text{R} = \text{C}_6\text{H}_5\text{CH}_2$. Photolysis proceeds through an excited singlet state which decays to an excited triplet (see Figure I.13). The triplet decays via bond scission to a triplet radical pair. The quantum yield for loss of CO is ~ 0.9 [6b]; this value is a lower limit for production of the radical pairs since some of the pairs recombine.

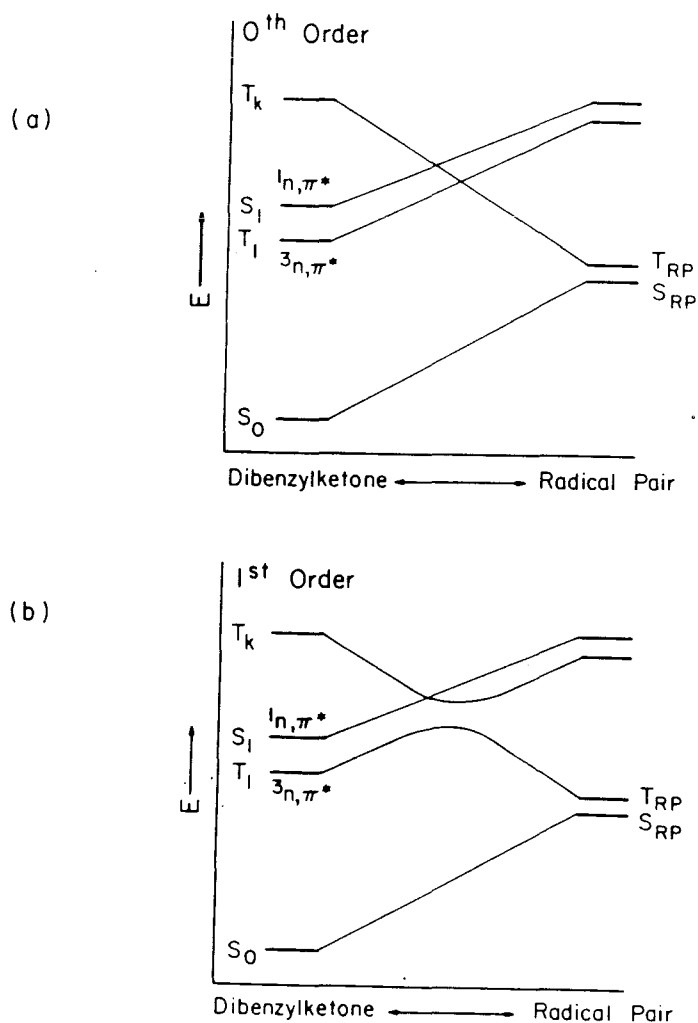


Figure I.18 Correlation diagrams for the dissociation of dibenzylketone into a radical pair. These figures are based on the work of Salem [36] for acetone. (a) In zeroth-order the n, π^* states cannot dissociate into radical pair states. (b) In first-order only the excited triplet state can dissociate into a radical pair; thus, the photoexcited dibenzylketone produces a pure triplet radical pair.

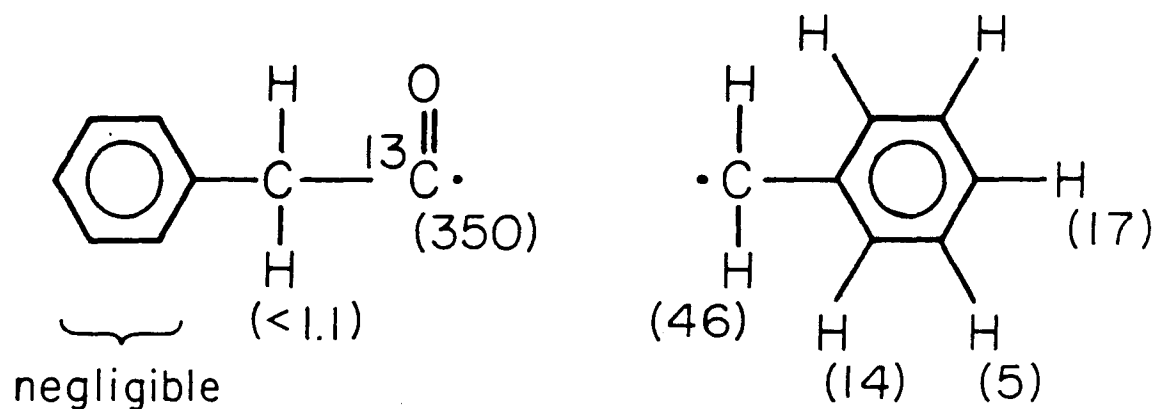
in the case of benzophenone, radical pair intersystem crossing is a viable route to geminate recombination since S_{RP} is a bound state. Thus, the triplet radical pair evolves as shown in Figure I.15 (section 4.1).

The radical pair is shown in Figure I.19 with the relevant hyperfine couplings. In contrast to the benzophenone generated radical pair, the ketyl radical from dibenzylketone is a σ radical. That is, the unpaired electron on the ketyl radical is localized in a sp^2 σ orbital on the carbonyl group. Due to the localization and s character of the orbital, the carbonyl ^{13}C has a large hyperfine constant. The g-factor for the ketyl radical is [37]:

$$g = 2.0007$$

with g for the benzyl radical given in section 4.1.

HYPERFINE CONSTANTS IN MHz



XBL 785-8667

Figure I.19 Hyperfine coupling constants for the radical pair produced by photolysis of dibenzylketone. All values are taken from Reference 37.

5. EXPERIMENTAL DETAILS

All photolyses were performed with a high pressure mercury capillary lamp (Illumination Industries AH-6). The reaction conditions, irradiation set-up, and product work-up are described below under the three reactions studied.

5.1 Benzophenone and Toluene

Photoexcited benzophenone abstracts a hydrogen atom from toluene and forms a triplet radical pair (Chapter 4), and for geminate recombination to occur, there must be intersystem crossing. Because a ^{13}C at the radical center of either benzophenone or toluene will speed up the intersystem crossing, the geminate product 1,1,2-triphenylethanol is expected to be enriched in ^{13}C . On the other hand, the radicals which diffuse apart are slightly de-enriched in ^{13}C , and, consequently, the 1,1,2-triphenylethanol formed homogeneously has less ^{13}C than the reactants. Thus, the magnetic isotope effect in the benzophenone/toluene reaction was measured as follows:

1) Benzophenone and toluene were photolyzed to form 1,1,2-triphenylethanol both geminately and homogeneously. The ^{13}C content of the isolated product should be essentially the same as that of the reactants.

2) Benzophenone and toluene were photolyzed in the presence of excess scavenger (thiophenol) which scavenges the benzyl radicals and prevents homogeneous formation of the

triphenylethanol. Thus, the isolated 1,1,2-triphenylethanol is pure geminate product and should be ^{13}C enriched. The condition of complete scavenging was determined by varying the thiophenol concentration and determining the region where the 1,2-diphenylethane disappears, and the yield of the 1,1,2-triphenylethanol approaches a constant value (asymptotic geminate yield).

3) By comparing the ^{13}C content of the triphenylethanol formed under the two conditions of no scavenger and excess scavenger, the magnetic isotope effect was determined.

Using the above procedure the reactions summarized in Table I.1 were studied. Reaction volumes were typically 5 ml, and the reactions were performed in 25 ml pyrex erlenmeyer flasks. The flasks were stoppered with rubber septa, and O_2 was flushed out by bubbling dry N_2 through the solutions for ~ 1 hour. The ^{13}C -enriched and deuterated benzophenone compounds were purchased from Merck, Sharp, and Dohme of Canada. The ^{13}C -toluene was synthesized according to the procedure outlined in Appendix F. Spectralgrade solvents were used without further purification.

Photolysis times were typically 45 minutes which gave 75% reaction of the benzophenone. The flasks were suspended in a pyrex dish/water bath with the UV lamp below the dish. The water bath contained a copper coil with running water and the bath was stirred to maintain the temperature $\sim 22^\circ\text{C}$. The lamp to reaction flask distance was ~ 10 cm. Within the water bath in the path between lamp and flask was a 1 cm thick piece of

Table I.1 Reaction Conditions for Benzophenone plus Toluene
Photolyses

Reaction	Solvent	$[\phi_2\text{CO}] \times 10^3 \text{ M}$	$[\phi\text{SH}] \times 10^3 \text{ M}$	$[\phi\text{CH}_3]\text{M}$
1-1	Benzene	3.0	0.0	3.1 ^a
1-2	"	2.9	4.4	3.0 ^a
1-3	"	2.7	14	2.8 ^a
2-1	Acetonitrile	3.0	0.0	3.1 ^a
2-2	"	2.9	4.4	3.1 ^a
2-3	"	2.7	14	2.8 ^a
3-1	Acetonitrile	2.7	0.0	0.30 ^a
3-2	"	2.7	7.3	0.30 ^a
3-3	"	2.7	15	0.30 ^a
4-1	Acetonitrile	0.27 ^b	0.0	0.94
4-2	"	0.27 ^b	1.7	0.94
5-1	Acetonitrile	1.3 ^b	0.0	4.7
5-2	"	1.3 ^b	7.8	4.7
6-1	Acetonitrile	3.0 ^c	0.0	4.7
6-2	"	2.9 ^c	17	4.5

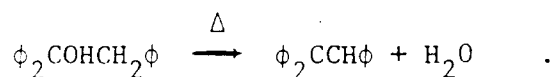
^aToluene initially enriched to 40% in the α position.

^bBenzophenone initially enriched to 40% in the carbonyl position.

^cBenzophenone initially enriched to 40% in the carbonyl position,
and rings deuterated to 99% ²D.

plexiglass which served to filter out all light of wavelength $< 3450 \text{ \AA}$. The use of this filter minimized the occurrence of unwanted side reactions by allowing only the $^1_{n,\pi^*}$ of benzophenone at 3500 \AA to be produced. Furthermore, because of the water bath there was 2-3 cm of H_2O in the light path which served as an IR filter and helped prevent solution heating.

The reactions were characterized by gas chromatography using standards of benzophenone, 1,2-diphenylethane, 1,1,2-triphenylethanol, and tetraphenyl-1,2-ethanediol. The last product was not observed in the GC, presumably because it either decomposed or had such a long retention time that its peak was not detected. The 1,1,2-triphenylethanol gave two peaks which were attributed to the alcohol and its dehydration product triphenylethylene:



This assignment was further substantiated by the fact that only the dehydration product could be detected in the mass spectrum. A Varian 3740 Flame Ionization Detector gas chromatograph was used. The columns were 6' by 1/8" 3% SE-30 (80/100 mesh Supelcoport) and 3% OV-17 (100/120 mesh Supelcoport) and were run in the temperature range 160-210°C.

For product analysis the reaction solvents were evaporated and the mass spectroscopy of the residue performed without further separation. The dehydration product of the triphenylethanol, triphenylethylene, appeared in the mass spectra without complication from other reaction products. The mass spectrometer

was an MS-12, and multiple spectra (20-40 scans) were recorded of each reaction. Although the dehydration reaction could not be avoided, further fragmentation was prevented by running the mass spectrometer at low ionization voltage ~ 12 eV. Peak intensities were determined by an online computer which introduced much unnecessary fluctuation into the data. After rejection of anomalous values, the data were averaged and theoretical spectra calculated to determine the isotopic content.

5.2 Dibenzylketone

The dibenzylketone (DBK) photolysis is a cyclic reaction where the geminate recombination regenerates the starting material. Since the initial radical pair is a triplet (Chapter 4), the nuclear magnetic isotope effect favors recombination of ^{13}C containing radical pairs so that as the photolysis proceeds the DBK becomes progressively enriched in ^{13}C . Those pairs which diffuse apart cannot reform the ketone, because decarbonylation of the acyl radical is much faster than homogeneous recombination. In the benzophenone/toluene reaction the relevant quantity to measure was ^{13}C in the homogeneous product versus ^{13}C in the geminate product. In the DBK reaction the relevant observable is the ^{13}C content of partially reacted ketone versus the ^{13}C content of unreacted ketone. The experimental procedure was to photolyze the ketone, monitor the reaction progress by comparing the relative amounts of the ketone and the homogeneous product 1,2-diphenylethane, and monitor the ^{13}C content of the ketone.

Because the reaction is cyclic, the enrichment is sensitive not only to the differential in geminate recombination of ^{12}C and ^{13}C , but also to the total amount of geminate return since this determines the number of cycles a molecule may go through. As such, the enrichment is very sensitive to the decarbonylation rate (i.e., temperature dependence) and the diffusion rate (i.e., viscosity dependence) which determine the ratio of homogeneous to geminate product. The experimental approach taken was to optimize the dibenzylketone enrichment through manipulation of

temperature and viscosity, and Table I.5 (section 6.2.2) summarizes the reaction conditions used.

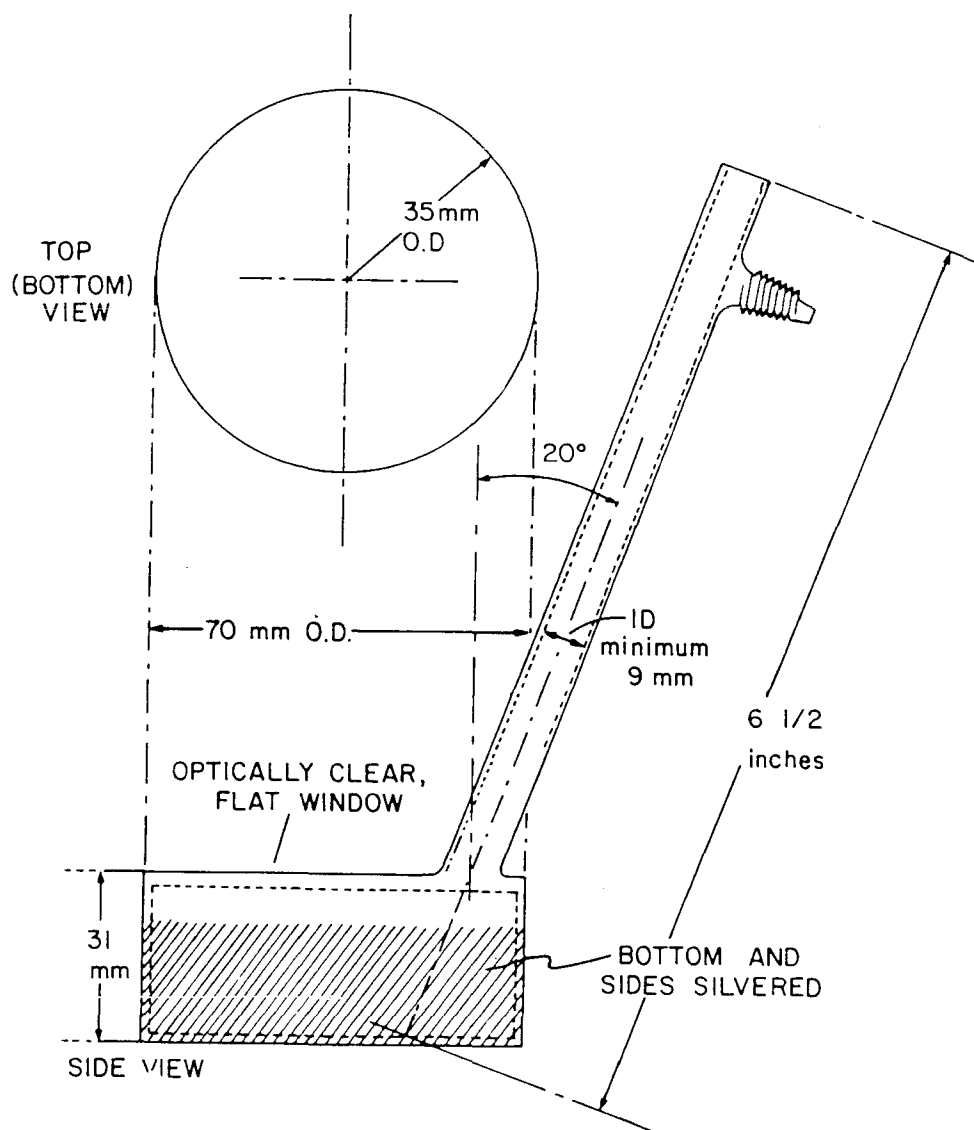
Reaction volumes were typically 25 ml, and the DBK concentration was ~ 0.1 M. Because frequent aliquots were taken, no attempt was made at degassing the samples. However, to keep the reactions dry, the reaction cells were kept under a positive pressure of dry N_2 . The ^{13}C -enriched DBK reagent was synthesized according to the procedure outlined in Appendix F. Reagent grade solvents were used without further purification. Because DBK absorbs at a shorter wavelength than benzophenone, quartz glassware was used for the photolyses. For room temperature experiments a similar photolysis set-up was used as for benzophenone. For the low temperature experiments a specially designed all quartz 100 ml cell was used which could be immersed in a constant temperature bath and irradiated from above. The cell is pictured in Figure I.20.

Three bath set-ups were used:

- 1) Ice/ H_2O
- 2) Dry ice/ethanol
- 3) Ethanol bath cooled by cold N_2 flowing through an immersed copper coil.

The temperature was measured using a copper/constantan thermocouple inserted in the cell, and temperature stabilization was achieved through a combination of varying the bath temperature and the irradiation intensity (i.e., the lamp to cell distance).

Typically the lamp to cell distance was 15 cm with the cell 1 cm below the surface of the bath.



XBL 812-8105

Figure I.20 Immersible quartz reaction cell. The cell may be immersed in a constant temperature bath for temperature control and has an optically flat window to allow photolysis from above. The bottom and sides are silvered to increase the light intensity in the cell. The side arm is designed to allow removal of aliquots while keeping a positive pressure of dry N_2 in the cell. During photolysis a copper/constantan thermocouple is inserted in the cell.

The reaction progress was easily characterized using gas chromatography (Varian 3740 Gas Chromatograph and the columns previously described) to measure the DBK and 1,2-diphenylethane peaks.

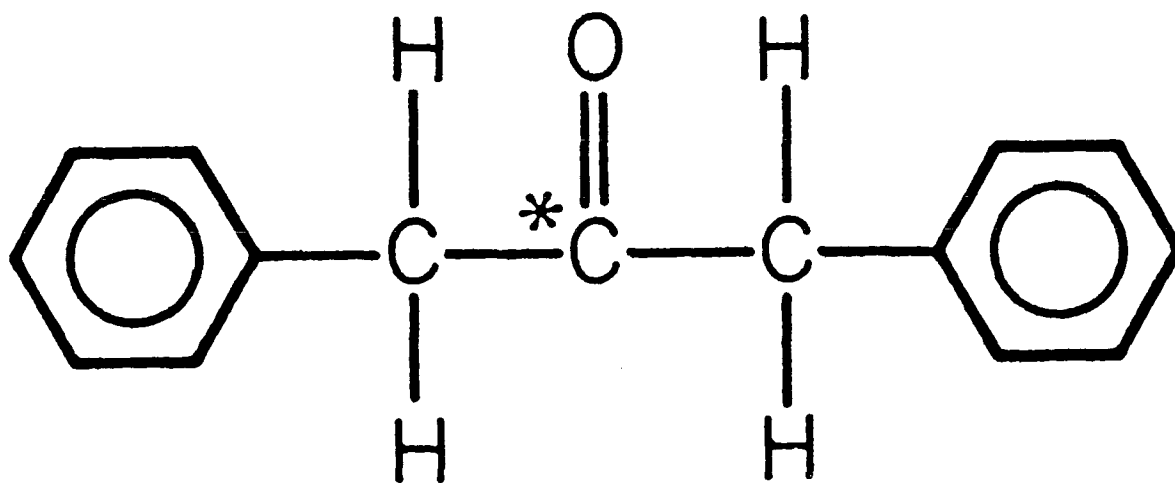
The peak areas were computed by triangulation and compared with peaks from standard solutions of known concentration. Before performing the isotopic analysis, the DBK was purified by two steps of separation. The first step was preparative thin layer chromatography. A 50/50 methylene chloride/hexane solvent was used with Analtech Uniplates of 2000 μ thick Silica Gel GF. The 8" x 8" plates were typically loaded with 100-200 mg of material obtained by taking a reaction aliquot and distilling off the solvent. For loading the plates, the material was dissolved in hexane. After collecting the DBK band, the ketone was further purified by preparative gas chromatography. A 10' by 1/4" 10% SE-30 (80/100 mesh Gas-Chrom Q) column was used with temperature equal to 200°C. Column injections were 50 μ l of a DBK/acetone solution.

With the purified DBK the ^{13}C enrichment of the carbonyl carbon (initially enriched to 30% for ease of analysis) was measured with two different methods: mass spectrometry and NMR spectroscopy. In the former method a mass spectrum was taken for the molecular ion of the DBK. The MS-12 mass spectrometer was used as with the benzophenone/toluene, but it was found that rather than using computer analysis the mass spectra could be determined far more accurately and reproducibly by obtaining a

strip chart recording of the ion flux and measuring the peak heights by hand. 20-40 scans were obtained as before, although the reproducibility was such that there was little need to average. To minimize fragmentation of the molecular ion, the mass spectrometer was run at very low ionization voltage ~ 12 eV. The mass spectra were analyzed by assuming natural abundance isotopes at all positions except for the carbonyl carbon.

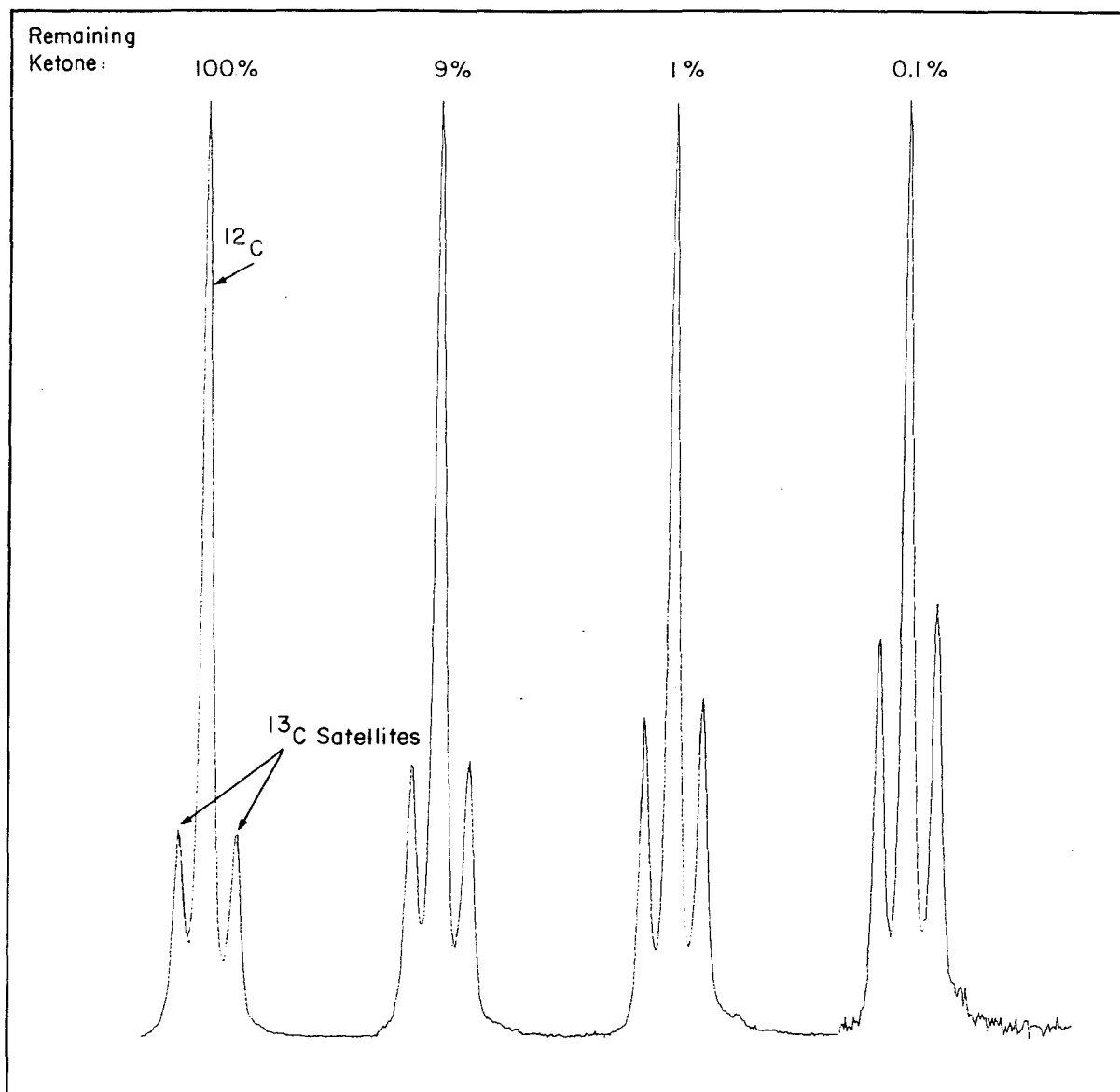
Although mass spectrometry is more accurate, NMR was also used, because it has the advantage of monitoring the isotopic content at the carbonyl position directly. A carbonyl ^{13}C splits the proton resonance at the adjacent methylene position (see Figure I.21) by 6.3 Hz. By observing the proton NMR spectrum and comparing the integrated areas of the ^{13}C satellites to the unsplit methylene resonance, the percent ^{13}C is obtained. One set of results where the NMR spectrum was recorded as a function of the percent of ketone remaining is shown in Figure I.22.

The accuracy of the NMR is limited by the fact that with the small coupling constant of 6.3 Hz the methylene resonances are not fully resolved from one another. In order to find the peak areas it was necessary to use a curve fitting program (Nicolet Curve Analysis Program) with the positions, widths, and heights of three Lorentzians as variables (see Figure I.23). Because of phase errors in the NMR spectra and line broadening which distorts the Lorentzian lineshapes, the fitting did not give very accurate numbers (i.e., $\sim 5\%$ error), but it did serve to confirm that the carbonyl carbon was being enriched (see Fig. I.22).



XBL 785-8668

Figure I.21 Dibenzylketone molecule. In the absence of ^{13}C the methylene protons give a single NMR line. With ^{13}C at the carbonyl position the methylene resonance is split by 6.3 Hz.



XBL 806-9851

Figure I.22 Methylene proton NMR signal as a function of remaining ketone for photolysis of dibenzylketone in cyclohexanol at 0°C.

Isotopic analysis by curve fitting the methylene triplets gives:

100% ketone, 29% ^{13}C ; 9% ketone, 36% ^{13}C ; 1% ketone, 40% ^{13}C ;

0.1% ketone, 47% ^{13}C . Total photolysis time is 409 min.

Peak Analysis of Dibenzylketone Methylene Triplet

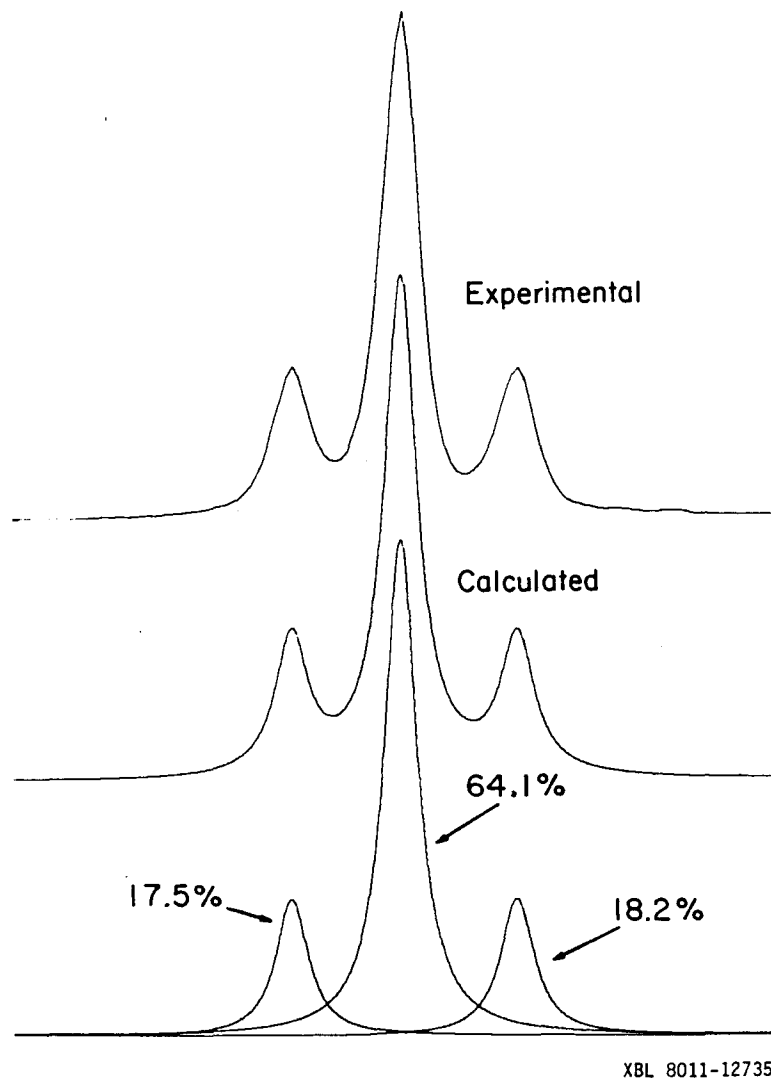


Figure I.23 Curve fitting analysis of the dibenzylketone methylene triplet. The center line is the proton resonance in the absence of ^{13}C . The outer resonances are from molecules containing a ^{13}C at the carbonyl position. The accuracy of the fit is limited by the overlap of the long Lorentzian tails and by phase errors.

The NMR spectra were taken with a pulsed 180 MHz spectrometer, and for some of the very dilute samples (10^{-2} - 10^{-3} M since 99.9% of the ketone was reacted), several thousand shots were required for good signal/noise. 16 K FID's were acquired for maximum peak resolution, and the acquisition time per shot was ~ 6 seconds. To avoid error due to the protons (satellite lines) coupled to ^{13}C having a different relaxation time than the protons (center line) "coupled" to ^{12}C , the relaxation after saturation of the methylene triplet was observed (see Figure I.24) with the results:

$$^1\text{H to } ^{13}\text{C (upfield):} \quad T_1 = 2.5 \pm 0.1 \text{ sec}$$

$$^1\text{H to } ^{13}\text{C (downfield):} \quad T_1 = 2.6 \pm 0.1 \text{ sec}$$

$$^1\text{H to } ^{12}\text{C:} \quad T_1 = 2.6 \pm 0.1 \text{ sec}$$

Thus, no error is expected from having a short recycle time (recycle time is equal to the acquisition time).

For the dilute samples (10^{-2} - 10^{-3} M) it was necessary to exclude H_2O since its resonance could swamp out the ketone resonance. For this purpose dry, clean NMR tubes (0.5 ml) were soaked several hours in D_2O and then washed and dried with d_6 -acetone. 99.95% deuterated chloroform was used as solvent for the NMR samples.

Viscosities for the neat reaction solvents were interpolated from the tables in Reference 40. For the 70/30 and 80/20 cyclohexanol/isopropanol (weight/weight) solvents the viscosities

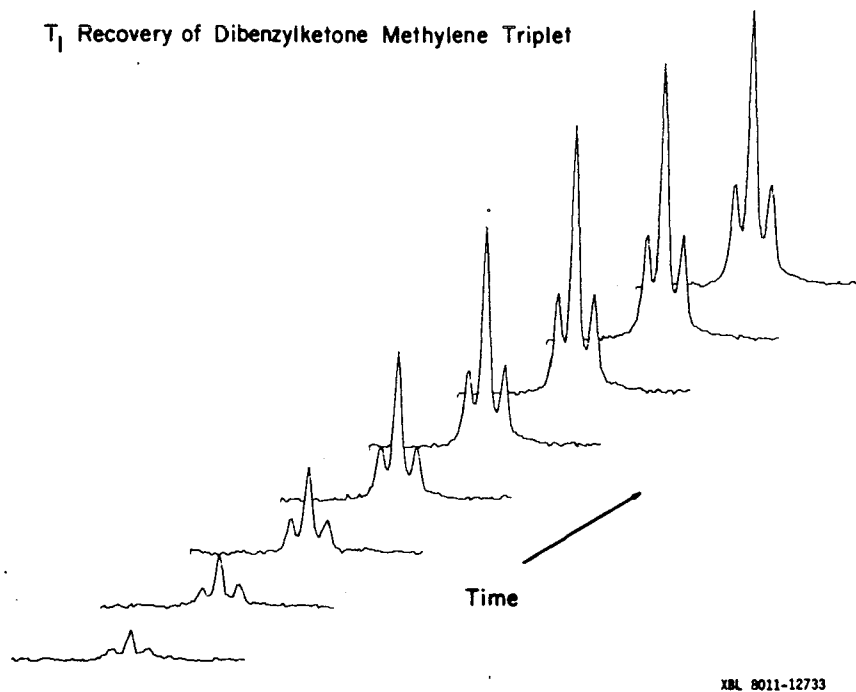


Figure I.24 T_1 recovery of dibenzylketone methylene triplet. To within experimental error, the relaxation time of the protons is independent of whether they are coupled to ^{13}C or not. Thus, there is no distortion in the intensities when a short recycle delay is used in signal averaging. The measured relaxation time is 2.6 ± 0.1 sec.

were measured with a falling ball viscosimeter as follows (see Figure I.25). Stainless steel balls of 1/16", 1/8", 5/32", and 3/16" were dropped through a tube containing the solvent mixture of interest, and from the fall times of the balls the viscosity of the solvent could be calculated using the treatment of Laughlin and Uhlmann [41]. The drop tube had a 40 cm long neck of 0.6 cm inner diameter which slowed the drop rate of the balls and also allowed them to temperature equilibrate with the solvent. Below the neck was the area calibrated for the fall. This region had a 2.66 cm inner diameter and 10 cm length. The drop tube was completely immersed in an ethanol bath in a silvered vacuum jacketed glass dewar with an unsilvered (i.e., clear) strip down the side for observation. The temperature of the bath was regulated by bubbling cold N₂ through the liquid. During measurements the N₂ was turned off to avoid disturbing the drop tube. The temperature within the drop tube was measured by a copper/constantan thermocouple. It was also necessary to measure the solvent densities. This was done by immersing a graduated cylinder with solvent in the temperature bath and measuring the solvent volume as a function of temperature. Assuming a cubical coefficient of expansion of glass of 2.5×10^{-5} per degree centigrade [39], the error in the density measurements due to contraction of glass components is $\leq 0.2\%$ over the temperature range studied. With the falling ball and density data the results of the viscosity as a function of temperature measurements are shown in Figure I.26.

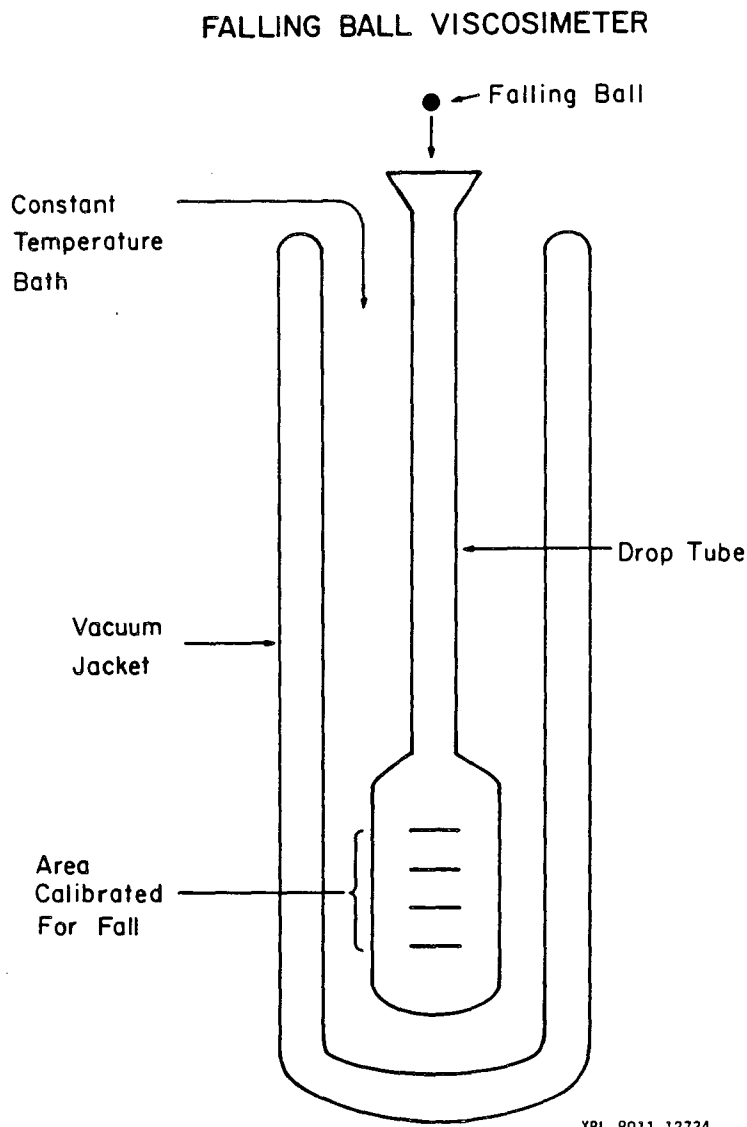
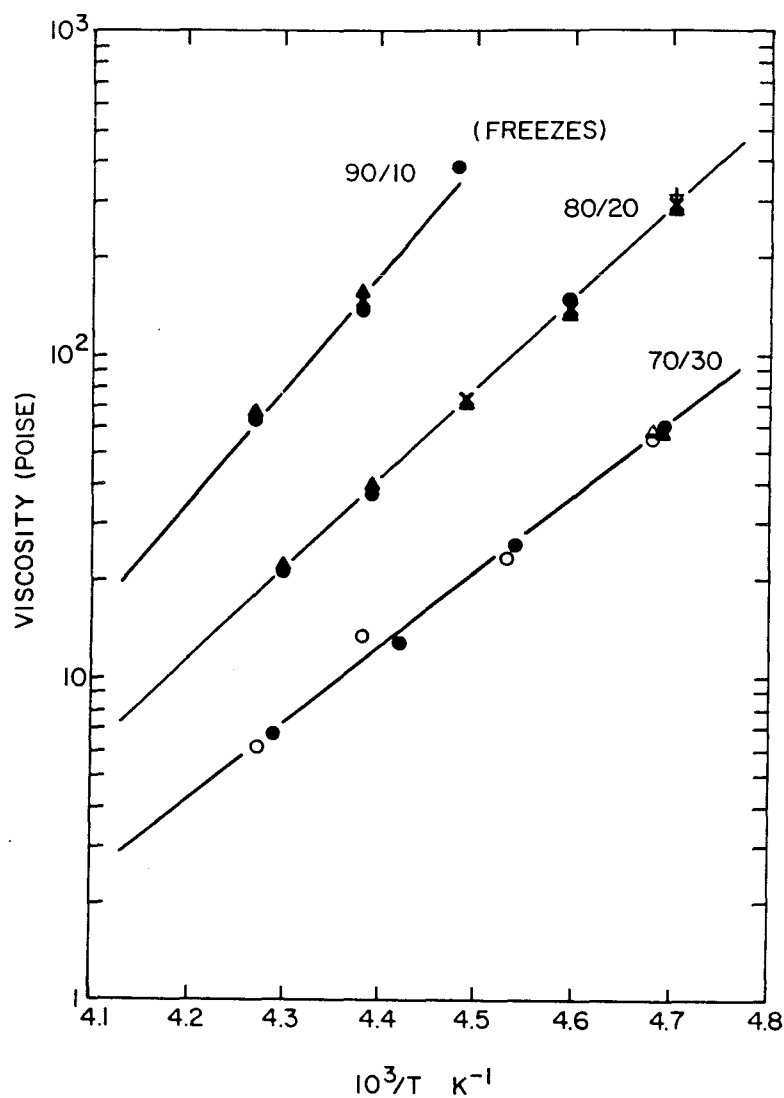


Figure I.25 Falling ball viscosimeter. The long neck of the drop tube (not drawn to scale) allows temperature equilibration of the falling ball with the solvent before reaching the calibrated area. Ethanol was used for the bath, and its temperature was regulated by blowing cold N_2 through the bath. During measurements the N_2 was turned off to avoid disturbing the drop tube.

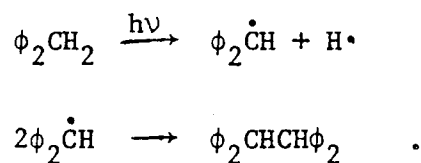


XBL 8011-12731

Figure I.26 Viscosity measurements for cyclohexanol/isopropanol solutions. Each curve is labeled by the weight/weight ratio of cyclohexanol to isopropanol. Using the falling ball viscosimeter of Figure I.25 and the treatment of Reference 41, the measured viscosities were independent of ball size: ● 1/16", ▲ 1/8", × 5/32", + 3/16" diameter stainless steel balls. The results were unchanged by the addition of 0.06 M 1,2-diphenylethane to simulate experimental conditions: ○ 1/16", Δ 1/8" diameter balls with 0.06 M 1,2-diphenylethane. Fitting the lines with an Arrhenius expression the following activation energies are obtained: 70/30, 11 kcal/mole; 80/20, 13 kcal/mole; 90/10 17 kcal/mole.

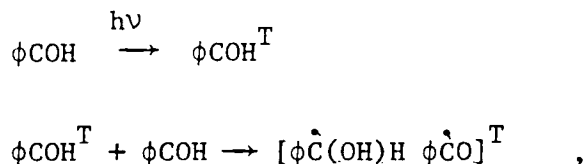
5.3 Benzaldehyde

Photoexcited benzaldehyde (ϕCOH) was studied as a candidate for production of triplet radical pairs through hydrogen abstraction from a substrate. In initial experiments benzaldehyde was photolyzed at high concentration (2 M) in toluene and in cyclohexane. In both cases a polymeric material was formed which was not amenable to further analysis. It was assumed that the benzaldehyde was reacting too efficiently with itself, and, therefore, a substrate with a more labile hydrogen was needed. Diphenylmethane ($\phi_2\text{CH}_2$) was chosen as substrate (and solvent), but it was found to be unstable under photolysis conditions [42]. When pure diphenylmethane was photolyzed, 1,1,2,2-tetraphenylethane was formed, presumably through the following free radical mechanism:

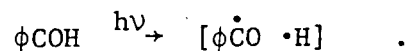


After these failures benzaldehyde was eliminated from further consideration.

In retrospect, benzaldehyde reacting with itself via hydrogen abstraction could provide a very interesting system to study [43]:



since the acyl radical ($\phi\dot{\text{C}}\text{O}$) is a σ radical and therefore has a large ^{13}C hyperfine (359 MHz) at the carbonyl position [37]. It is reported that benzaldehyde undergoes unimolecular reaction [44]:



This also produces the acyl radical but now via a mechanism which allows a cyclic reaction to be studied as in the case of dibenzylketone. Since the phenyl radical ($\phi\cdot$) is less stable than the benzyl radical ($\phi\dot{\text{C}}\text{H}_2$), the acyl radical from benzaldehyde should decarbonylate more slowly than that from dibenzylketone and therefore give a more efficient geminate recombination and enrichment system (see section 6.2).

6. CALCULATIONS AND EXPERIMENTAL RESULTS

Results are presented in this chapter for the benzophenone plus toluene and the dibenzylketone reactions. For the calculations with the First Collision Model eight hyperfines were used: the four largest from each radical. For the Continuous Diffusion Model calculations, Eq. (3.3b) was used to determine $\overline{\Delta v}$ with all of the known hyperfine constants included in the summations. In both models unit reactivity of singlets during collision was assumed; that is, $\lambda = 1$. The same values of r_c and r_o were used for both reactions. r_c was calculated from the molecular density of toluene, and r_o was derived from experimental results for dibenzylketone (section 6.2.2). For the benzophenone plus toluene reaction a value of 1 msec was used for the radical pair lifetime τ_{RP} ; Eq. (2.89) was used to calculate τ_{RP} for dibenzylketone. The parametrization of the isotope enrichment is discussed below with the experimental results.

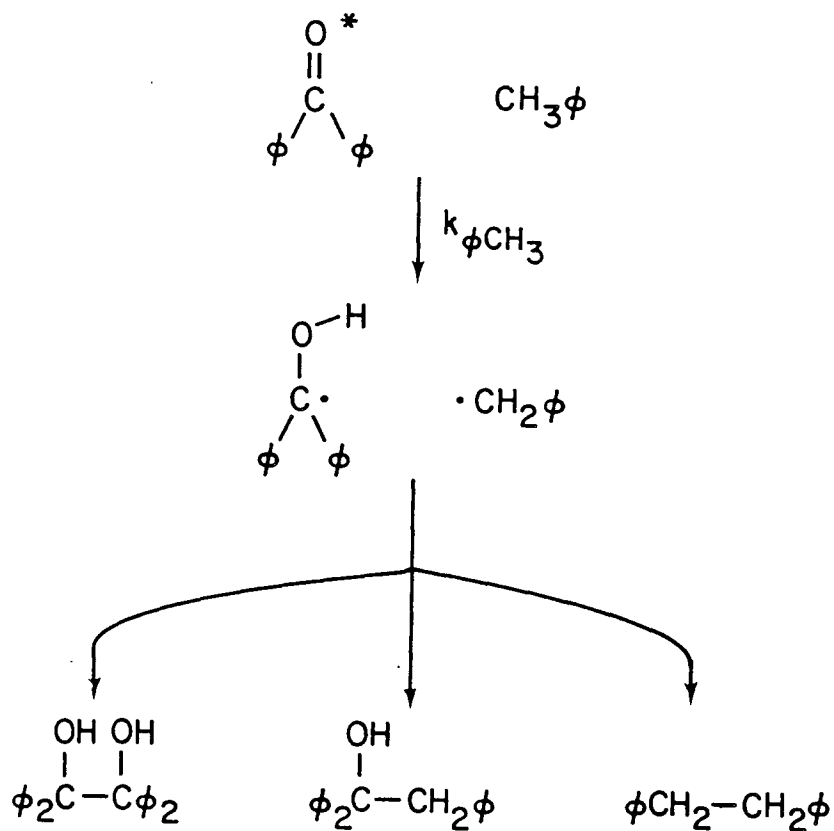
6.1 Benzophenone and Toluene

6.1.1 Geminate Recombination

The photolysis of benzophenone in toluene to produce 1,2-diphenylethane, 1,1,2-triphenylethanol, and tetraphenyl-1,2-ethanediol (see Figure I.27) has been previously established [45]. The first-order dependence on benzophenone is demonstrated in Figure I.28 where it is shown that the yields of triphenylethanol and diphenylethane vary linearly with the initial concentration of benzophenone.

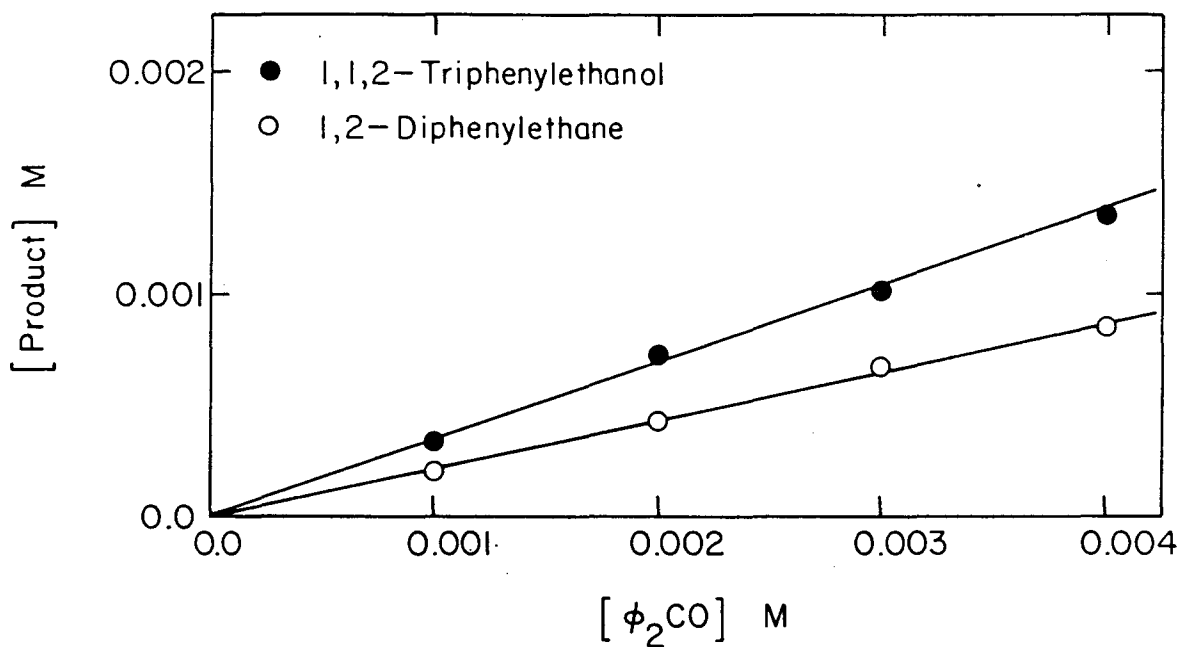
The efficiency of bubbling N_2 through the reaction solutions to remove O_2 is shown in Table I.2 where it is seen that the diphenylethane yield drops markedly when there is no degassing (i.e., no removal of O_2). The drop is attributed to the reaction of O_2 with the benzyl radicals [45]. Assuming that the benzyl radicals remove all of the O_2 from solution, the difference in yields of the diphenylethane gives an estimate of $\sim 10^{-3}$ M for the concentration of O_2 present in undegassed solution.

The experimentally determined ratio of 1,1,2-triphenylethanol to 1,2-diphenylethane formed is 1.6 ± 0.1 (see Figure I.28). From this number it follows that 45% of the benzophenone which abstracts a hydrogen from toluene forms triphenylethanol. To isolate that fraction of the triphenylethanol which is formed geminately, it is necessary to scavenge all radicals escaping fast geminate recombination before they have a chance to undergo homogeneous reaction. The results of an experiment with varying



XBL 8011-12736

Figure I.27 Radical-radical coupling products from the photolysis of benzophenone and toluene. The product 1,1,2-triphenylethanol is formed homogeneously and geminately.



XBL 812-8110

Figure I.28 Linear dependence of the yields of 1,1,2-triphenylethanol and 1,2-diphenylethane on the initial concentration of benzophenone. Toluene was the solvent. Each reaction was photolyzed for 1 hour. The simple linear dependence of the yields indicates that the reaction as illustrated in Figure I.27 is uncomplicated by impurities or side reactions. The ratio of the triphenylethanol yield to diphenylethane is 1.6 ± 0.1 .

Table I.2 Efficiency of Flushing out O_2 with N_2

Reactant ^a [ϕ_2CO]M	N_2 Flushing ^b (minutes)	Product [$\phi CH_2 CH_2 \phi$]M
0.003	0	0.0002
"	30	0.001
"	60	0.001
"	90	0.001

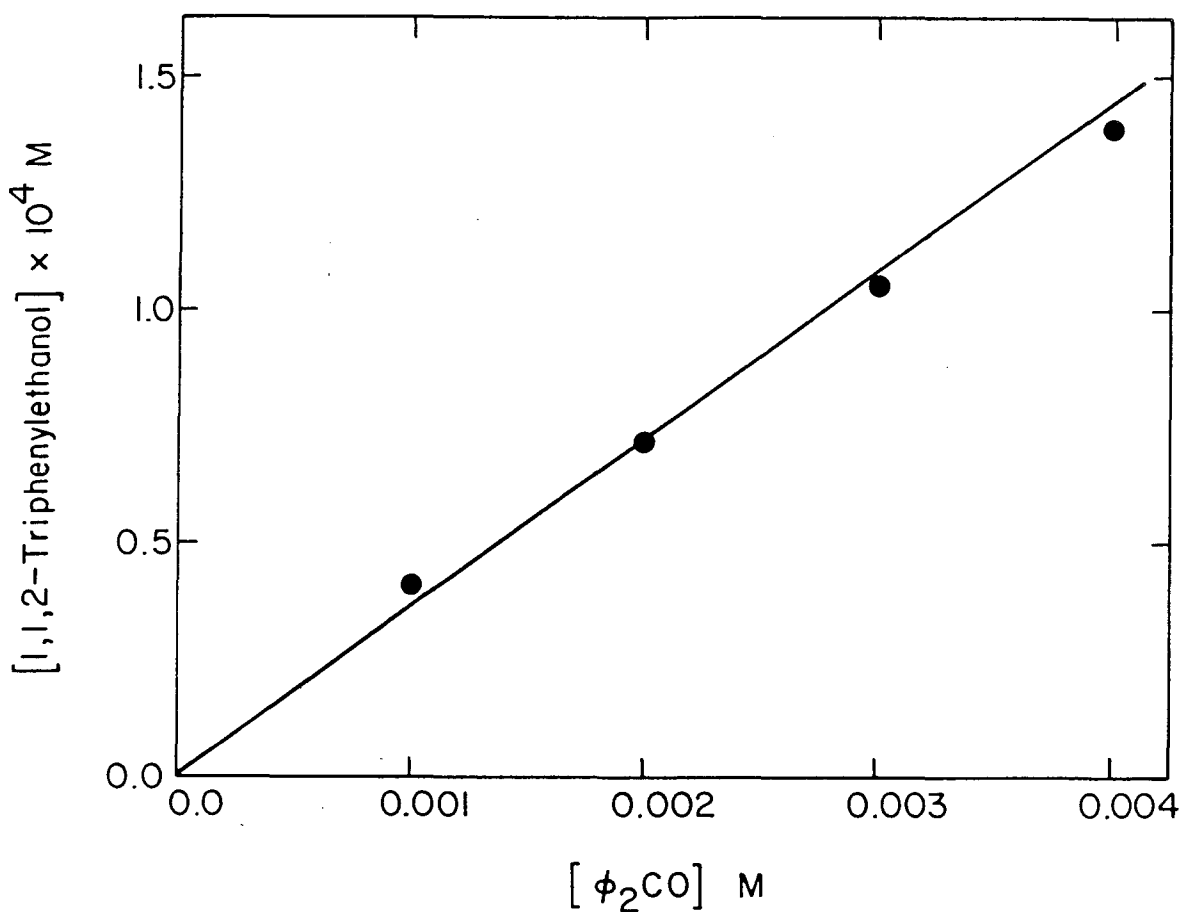
^aToluene is the solvent.

^bBefore photolysis the stoppered reaction flasks were immersed in an ice bath to reduce the toluene vapor pressure, and dry N_2 gas was bubbled through them.

concentration of the radical scavenger thiophenol ϕSH are shown in Figure I.2 (section 1.2). The 1,2-diphenylethane disappears for $[\phi\text{SH}]/[\phi_2\text{CO}] \sim 2$ (i.e., $[\phi\text{SH}] \sim 5 \times 10^{-3}$ M), which indicates very efficient scavenging of the benzyl radicals by the thiol. (See section 2.6 for an estimate of the scavenging rate constant k_s). The 1,1,2-triphenylethanol, however, persists all the way out to $[\phi\text{SH}]/[\phi_2\text{CO}] = 6$ and appears to be leveling off at a non-zero value. This non-zero value represents the geminate fraction. The time scale of geminate recombination is far too fast (10^{-9} - 10^{-8} sec) for the dilute scavenger ($\sim 10^{-2}$ M) to compete with. This may also be shown as follows.

Since the homogeneous concentration of radicals depends on the concentration of benzophenone, in the presence of scavenger the homogeneous radical-radical coupling products are formed more efficiently as the benzophenone concentration increases. The linear dependence of the triphenylethanol yield on benzophenone concentration shown in Figure I.29 indicates, therefore, that at 0.015 M thiophenol ($[\phi\text{SH}]/[\phi_2\text{CO}] = 5$ in Figure I.2) the triphenylethanol is formed only geminately. Together the data of Figures I.2 and I.29 demonstrate that thiophenol serves as an efficient radical scavenger.

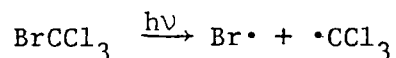
Many other scavengers were tried but had to be rejected because of complicating side reactions. One example is bromotrichloromethane BrCCl_3 which has been used frequently elsewhere [2]. When BrCCl_3 was photolyzed in toluene (no benzophenone present) both α -bromotoluene and 1,2-diphenylethane were formed.



XBL 812-8113

Figure I.29 Linear dependence of the 1,1,2-triphenylethanol yield on the initial benzophenone concentration in the presence of scavenger. The concentration of the scavenger thiophenol is 0.015 M; toluene is the solvent. Each reaction was photolyzed for 1 hour. If triphenylethanol were being formed from radicals produced by different benzophenone molecules, then the efficiency of scavenging would go up as the benzophenone concentration goes down. However, the simple linear dependence of the yield indicates that the reaction is first-order in benzophenone; that is, the triphenylethanol is formed only geminately.

Presumably the BrCCl_3 dissociates under photolysis conditions



due to the relatively weak (55 kcal/mole [39]) bromine-carbon bond. Both of the radicals produced can abstract hydrogen from toluene since the bond energies of hydrogen to bromine (87.4 kcal/mole) and hydrogen to trichloromethyl (96 kcal/mole) are both greater than hydrogen to benzyl (85 kcal/mole). Thus, BrCCl_3 serves as an alternate source of benzyl radicals. Furthermore, the α -bromotoluene formed by scavenging



was found to be unstable under photolysis conditions as photolysis of α -bromotoluene in toluene produced 1,2-diphenylethane.

Returning to thiophenol, the data of Figure I.2 are plotted relative to the unscavenged reaction and only show the change in yield as scavenger is added. To obtain the actual geminate recombination yield R , it is necessary to correct for reaction between the thiophenol scavenger and triplet benzophenone. The rate constants for reaction of triplet benzophenone with toluene and thiophenol are [35]:

$$k_{\phi\text{CH}_3} = 6.3 \times 10^5 \text{ M}^{-1} \text{ sec}^{-1}$$

$$k_{\phi\text{SH}} = 2.6 \times 10^8 \text{ M}^{-1} \text{ sec}^{-1}$$

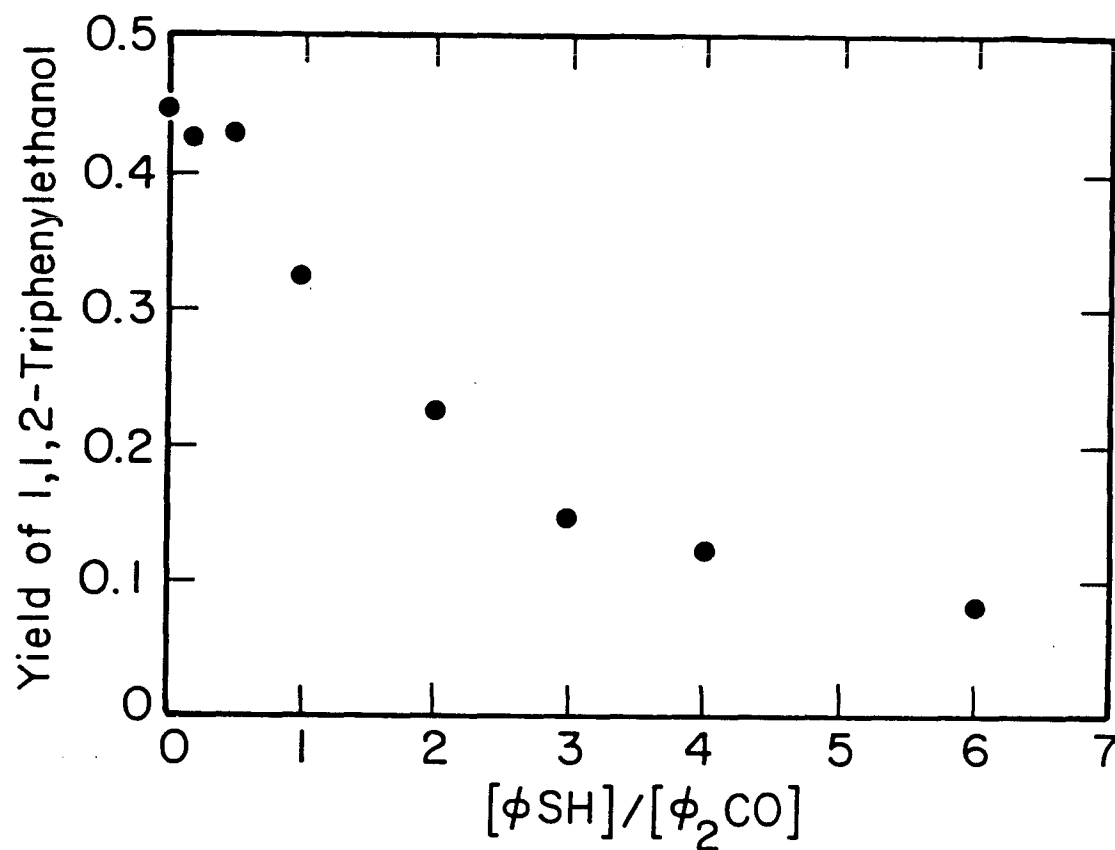
Given the large value of $k_{\phi\text{SH}}$, the thiophenol competes effectively for the photoexcited benzophenone in spite of the large difference in concentrations:

$$[\phi\text{CH}_3] = 9.4 \text{ M}$$

$$[\phi\text{SH}] = 0.016 \text{ M} \quad .$$

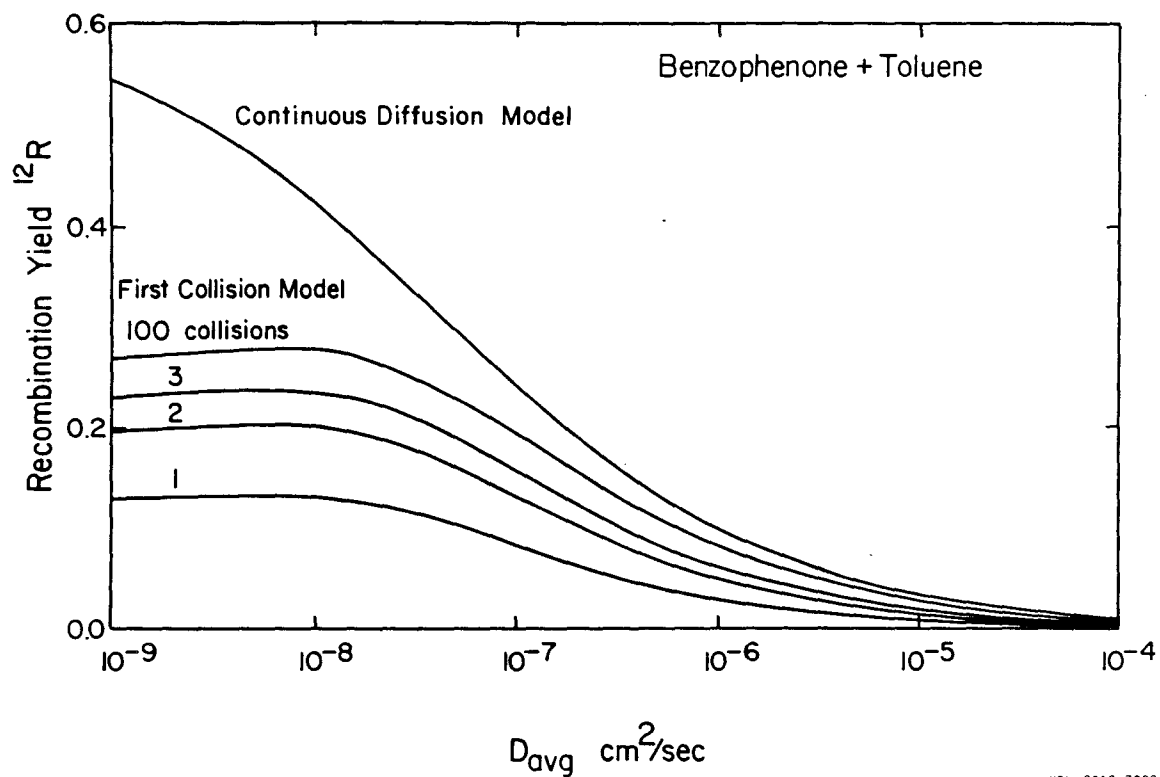
The effect of the scavenger is easily accounted for, since it is known that thiophenol does not photoreduce but only quenches the excited benzophenone [46]. The labile thiyl hydrogen is believed to be reversibly abstracted by the excited benzophenone, resulting in ground state ketone and thiol [46]. Thus, for the data of Figure I.2 after 45 minutes of photolysis, 75% of the benzophenone is consumed when no thiophenol is present, but 54% is consumed when $[\phi\text{SH}]/[\phi_2\text{CO}] = 6$.

The true geminate yield is obtained by dividing the moles of 1,1,2-triphenylethanol produced by the moles of benzophenone consumed, as is shown in Figure I.30. Assuming no homogeneous reaction at $[\phi\text{SH}]/[\phi_2\text{CO}] = 6$, the geminate yield is seen to be 8%. This value for photolysis of benzophenone and toluene with natural abundance ^{12}C is to be compared with Figure I.31 where ^{12}R is calculated as a function of D_{avg} , the average diffusion coefficient for the two members of the radical pair. The diffusion coefficient of the benzyl radical in toluene should be close to the self-diffusion coefficient of toluene which is $2.3 \times 10^{-5} \text{ cm}^2/\text{sec}$ [47]. Since the ketyl radical is about twice the size of the benzyl radical, it should diffuse somewhat more



XBL 8010-7373

Figure I.30 Determination of the geminate yield of 1,1,2-triphenylethanol. The yield is the moles of triphenylethanol formed per mole of benzophenone consumed. The ratio of thiophenol to benzophenone is for the beginning of photolysis. The initial concentration of benzophenone is 0.003 M. As the concentration of radical scavenger increases, only the triphenylethanol which is formed geminately remains. For $[\phi SH]/[\phi_2 CO] < 1$ all of the thiophenol is consumed by radicals, so the yield of homogeneous product does not fall off rapidly.



XBL 8010-7380

30

Figure I.31 Calculated recombination (i.e., geminate) yield ^{12}R for benzophenone and toluene with ^{12}C . D_{avg} is the average diffusion coefficient for the two members of the radical pair.

slowly, and 10^{-5} cm²/sec is chosen as a rough estimate of D_{avg} for the radical pair.

Included in Figure I.31 are the predictions of both the First Collision Model (FCM) and the Continuous Diffusion Model (CDM). It is seen that the First Collision Model is close to convergence after three collisions. The two models agree reasonably well for $D_{\text{avg}} > 10^{-6}$ cm²/sec and begin diverging below 10^{-7} cm²/sec. Since the experimental value is at $D_{\text{avg}} \cong 10^{-5}$ cm²/sec, the two models cannot be distinguished. The predicted values at 10^{-5} cm²/sec are

$${}^{12}R_{\text{FCM}} = 2.8\%$$

$${}^{12}R_{\text{CDM}} = 3.5\%$$

where the converged value is used for the First Collision Model. Both models underestimate the experimental value by more than a factor of two. One explanation for this may be the presence of spin-orbit coupling, which enhances the geminate recombination of triplets. This will be further discussed below.

6.1.2 Isotope Enhancement Factor

The isotopic content of the geminate product is determined by the relative recombination probabilities for the radical pairs containing different isotopes. Thus, considering ¹³C and ¹²C-containing radical pairs:

$$\left(\frac{^{13}\text{C}}{^{12}\text{C}}\right)_{\text{Product}} = \left(\frac{^{13}\text{R}}{^{12}\text{R}}\right) \left(\frac{^{13}\text{C}}{^{12}\text{C}}\right)_{\text{Initial}} \quad (6.1)$$

from which the "enhancement factor" Q is defined to be:

$$Q \equiv \frac{^{13}\text{R}}{^{12}\text{R}} = \frac{\left(\frac{^{13}\text{C}}{^{12}\text{C}}\right)_{\text{Product}}}{\left(\frac{^{13}\text{C}}{^{12}\text{C}}\right)_{\text{Initial}}} \quad (6.2)$$

Or in the case of triphenylethanol from the benzophenone and toluene reaction:

$$Q = \frac{\left(\frac{^{13}\text{C}}{^{12}\text{C}}\right)_{\text{Scavenger}}}{\left(\frac{^{13}\text{C}}{^{12}\text{C}}\right)_{\text{No - Scavenger}}} \quad (6.3)$$

where "scavenger" and "no-scavenger" represent geminate and homogeneous product, respectively. A more illustrative quantity is $Q-1$ since this gives zero when the reactants and products have the same isotopic content.

The theoretically predicted $Q-1$ for benzophenone and toluene is plotted in Figure I.32, where it is seen that the agreement between the First Collision Model and Continuous Diffusion Model is quite reasonable. Over the range of readily realizable viscosities the biggest effect is expected for D_{avg} between 10^{-5} and 10^{-4} cm^2/sec . Experiments were performed using both ^{13}C enriched benzophenone (carbonyl carbon) and ^{13}C enriched toluene (methyl carbon), but since they have comparable hyperfines (62 MHz for benzophenone and 68 MHz for toluene), the calculations were performed only for enriched benzophenone. The experimental results are given in Table I.3 (see Table I.1, section 5.1, for the reaction conditions).

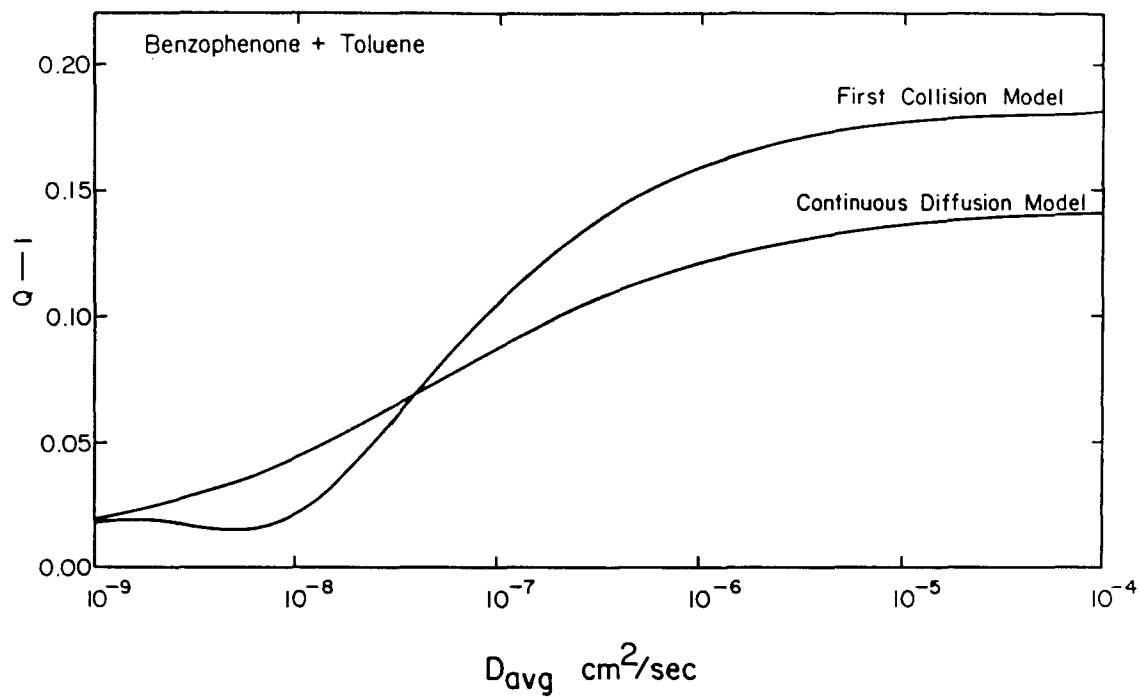


Figure I.32 Isotope enhancement factor for the benzophenone plus toluene photolysis. Q is the ratio of recombination yields $^{13}\text{R}/^{12}\text{R}$ for ^{13}C and ^{12}C containing radical pairs. Q greater than one indicates the ability of ^{13}C to facilitate geminate recombination of the triplet radical pairs.

Table I.3 Enrichment Results for Benzophenone plus Toluene
Photolyses.

Reaction	$[\phi SH]/[\phi_2 CO]$	% $^{13}C^a$	% Fragmentation ^b
1-1	0.0	38.8 ± 0.2	
1-2	1.5	40 ± 2	
1-3	5	38.8 ± 0.4	
2-1	0.0	41 ± 1	
2-2	1.5	39.2 ± 0.7	
2-3	5	40 ± 1	
3-1	0.0	37.8 ± 0.2	
3-2	2.7	36 ± 1	
3-3	5.5	---	
4-1	0.0	41.0 ± 0.2	6.6
4-2	6.3	41.3 ± 0.4	5.9
5-1	0.0	42.1 ± 0.2	6.1
5-2	6.0	41.0 ± 0.3	0.8
6-1	0.0	39.0 ± 0.1 ^c	4.8
6-2	6.0	39.3 ± 0.3 ^c	4.2

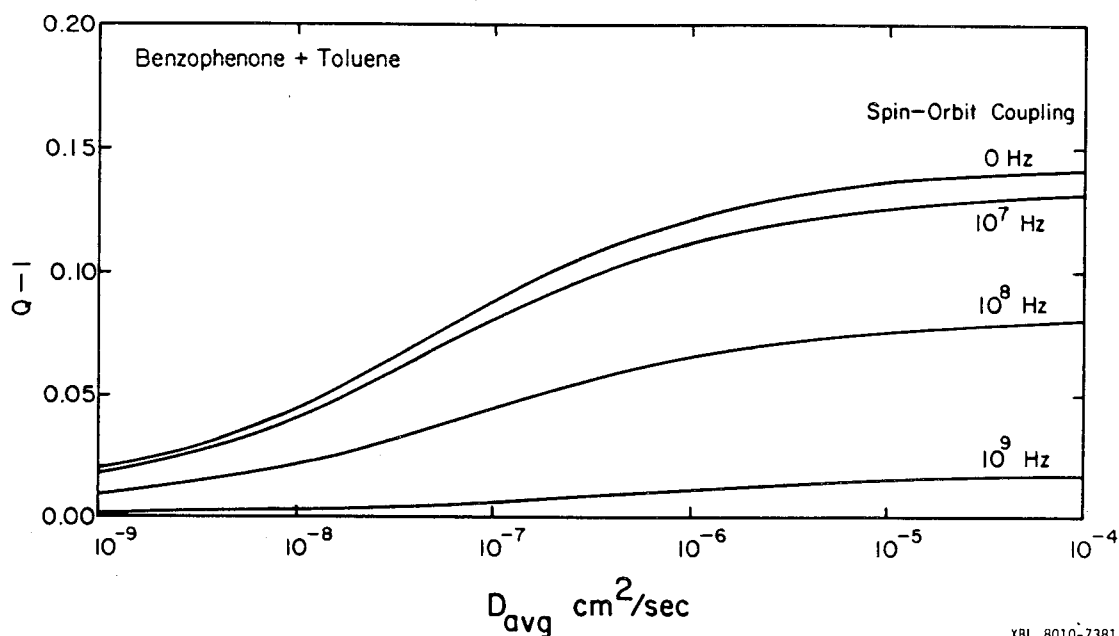
^aMass spectra are fitted for the triphenylethylene ion. Natural abundance isotopes are assumed at all positions (Reaction 6 excepted) except for ^{13}C at one position. 20 to 40 mass spectra were averaged, and the estimated ^{13}C errors are one-sigma values for the means. Systematic errors are ignored, since enrichment is the differential of two measurements.

^bThe ion of interest, triphenylethylene, has a base mass of 256. For mass spectra with a peak at 255, the percent fragmentation is used as an extra fitting parameter for the overlapping triphenylethylene-minus-one-hydrogen spectrum.

^cReaction 6 is fitted with 98.9% 2D per position for the two benzophenone phenyl rings which appear in the product.

Among the six sets of reactions displayed in Table I.3 the only evident result is the absence of any trend toward enrichment as the scavenger concentration is increased. For each reaction set, the enrichments are more or less equal within experimental error (the error estimates are one-sigma values). Given that the mass spectroscopy technique (i.e., computer integration of peak intensities) was not very accurate, nevertheless, with the number of experiments done and the amount of averaging for each experiment, the conclusion seems justifiable that the enrichment in this system is zero.

With $D_{\text{avg}} \cong 10^{-5} \text{ cm}^2/\text{sec}$ the theoretical value of $Q-1$ which is intermediate to the predictions of the two models (see Figure I.32) is 0.16. With an initial ^{13}C of 40% and a Q value of 1.16, the final enrichment of the geminate product should be 43.6% [see Eq. (6.2)]. No change of this size was detected in any of the experiments. One possible explanation for this discrepancy is that spin-orbit coupling dominates intersystem crossing in the radical pair and thereby diminishes any magnetic isotope selectivity. The effect of spin-orbit coupling on the enhancement factor is shown in Figure I.33. Since the radical pair starts as a triplet, any intersystem crossing contribution from spin-orbit coupling will increase the geminate yield. This trend is shown in Table I.4 where geminate yield and ^{13}C enrichment are given as a function of the spin-orbit coupling strength. It is seen that for a spin-orbit coupling of 10^9 Hz, both the predicted geminate yield and ^{13}C enrichment are in reasonable



XBL 8010-7381

Figure I.33 Effect of spin-orbit coupling on the benzophenone plus toluene isotopic enrichment. The curves are labeled by the rate of intersystem crossing due to spin-orbit coupling. Since this coupling does not distinguish between ^{13}C and ^{12}C , it dilutes any isotope effects on geminate recombination. 10^9 Hz is the estimated value of spin-orbit coupling for organic radicals (see sections 2.4.3 and 2.5.6). The curves were calculated with the Continuous Diffusion Model.

Table I.4 Effect of Spin-Orbit Coupling on Geminate Recombination
and Isotope Enrichment

Spin-Orbit Coupling (Hz) ^a	Geminate Recombination ^b	Q ^c	% ¹³ C in Product ^d
0	0.035	1.136	43.1
10 ⁷	0.037	1.126	42.9
10 ⁸	0.047	1.076	41.8
10 ⁹	0.097	1.015	40.4

^aThe values are the rates of intersystem crossing due to spin-orbit coupling.

^bThis is ¹²R; these calculated values should be compared with Figure I.30 where the geminate yield is determined to be 0.08 for natural abundance reactants.

^cQ values are calculated with the Continuous Diffusion Model assuming an average diffusion coefficient of 10⁻⁵ cm²/sec.

^dProduct values are calculated from Eq. (6.2) assuming 40% ¹³C in the reactant benzophenone.

agreement with the experimental values.

One objection that may be raised regarding the presence of spin-orbit coupling is that Chemically Induced Dynamic Nuclear Polarization (CIDNP), which depends upon the same factors as the magnetic isotope effect, is a very general phenomenon which gives large enhancements in NMR signals for a variety of systems. In fact, when the benzophenone plus toluene reaction is observed by NMR during photolysis [48], the methylene NMR signal of the 1,1,2-triphenylethanol product is seen to be enhanced by a factor of 250. Nevertheless, this does not contradict the results of this work. When measuring ^{13}C enrichments, one is looking for differences of the order of a few percent. However, in NMR one is concerned with population differences on the order of parts per million. For example, if a population difference of two parts per million is enhanced by a factor of 250

$$Q(10^6+1)/(10^6-1) = (10^6+250)/(10^6-250) \quad ,$$

a Q value of only 1.0005 is required. Thus, the Q values required for CIDNP effects are easily accommodated within a reaction system where the spin-orbit coupling prevents an observable magnetic isotope effect.

In conclusion, the results presented in this section indicate that spin-orbit coupling is the dominant mechanism for inter-system crossing in the benzophenone plus toluene generated radical pair. The required strength of the spin-orbit coupling is 10^9 Hz, and this value was shown in section 2.5.6 to be

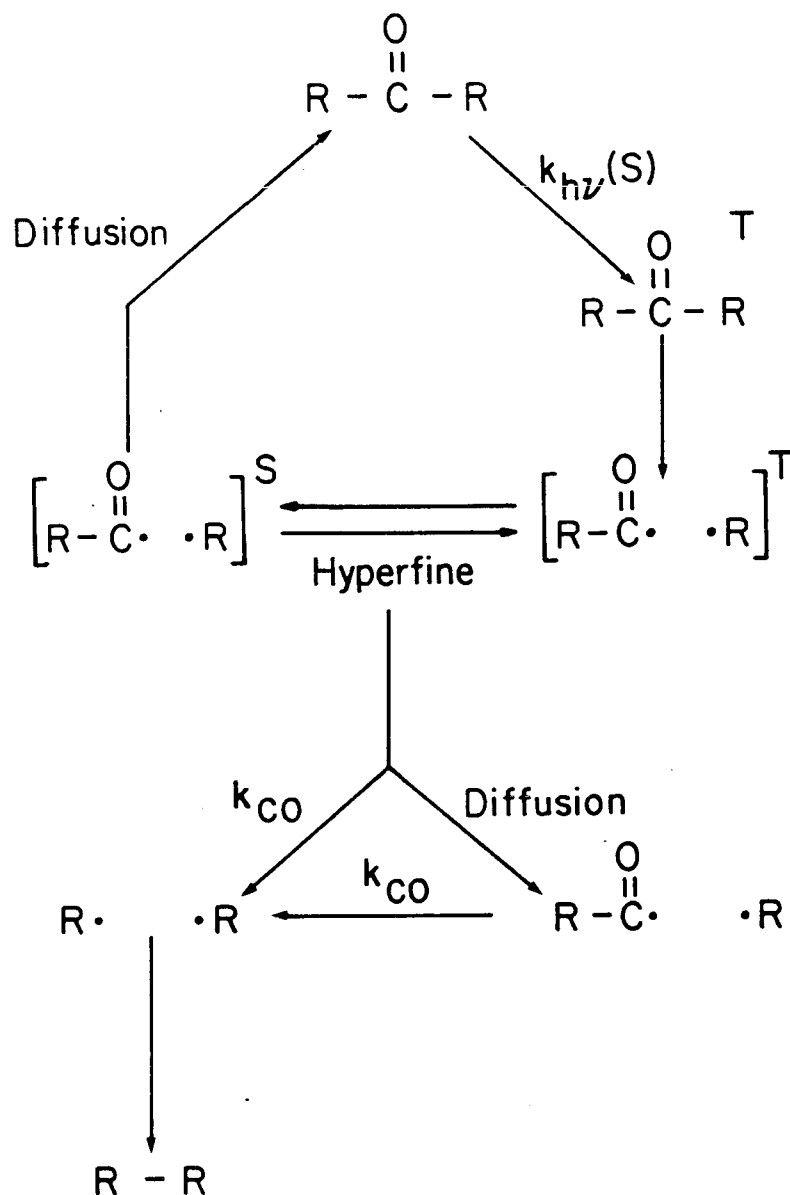
consistent with expectations for a carbon-centered radical with spin-orbit coupling operating through an intermediate state of 70 kcal/mole excitation.

6.2 Dibenzylketone

6.2.1 Geminate Recombination

The photolysis of dibenzylketone is a cyclic process in which the geminate product and the reactant molecule are identical (see Figure I.34). Hence, the geminate yield cannot be determined by product analysis (it can be gotten by quantum yield measurements where it is assumed that every molecule which absorbs a photon forms a radical pair [6,49]). The disadvantage of such a system is that any isotopic enrichment of the geminate product is diluted by mixture with unreacted dibenzylketone. The advantage, which is of greater importance, is that as photolysis proceeds the dibenzylketone may go through many cycles of geminate recombination and become progressively enriched in ^{13}C .

Because of the two factors of dilution of geminate product by reactant and multiple photolysis cycles, it is important to maximize the recombination yield R . R is plotted in Figure I.35 as a function of D_{avg} . The agreement between the two models is fair, and, as before, the First Collision Model is near convergence after three collisions. In contrast to the benzophenone and toluene reaction, the geminate yield of dibenzylketone does not continue to go up as D_{avg} becomes smaller and smaller. The difference is that whereas the action of the scavenger is limited by the rate of diffusion and therefore becomes slower as the solution becomes more viscous, decarbonylation is independent of



XBL 802-8353

Figure I.34 Overall reaction scheme for photolysis of dibenzylketone ($R = C_6H_5CH_2$); S and T stand for singlet and triplet electron correlation, respectively; $k_{hv}(S)$ indicates that photolysis involves an excited singlet state; the brackets [] indicate radical pairs that have a finite probability of diffusive reencounter. Hyperfine couplings equilibrate S and T while diffusive encounter of singlets reforms the ketone; diffusive separation and decarbonylation (k_{CO}) form 1,2-diphenylethane.

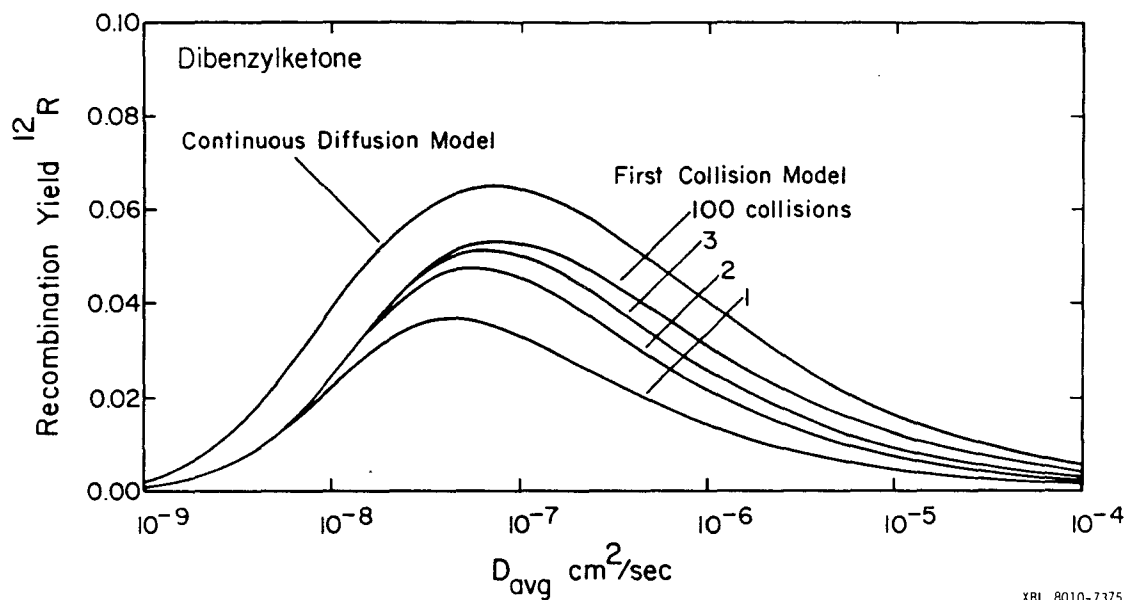


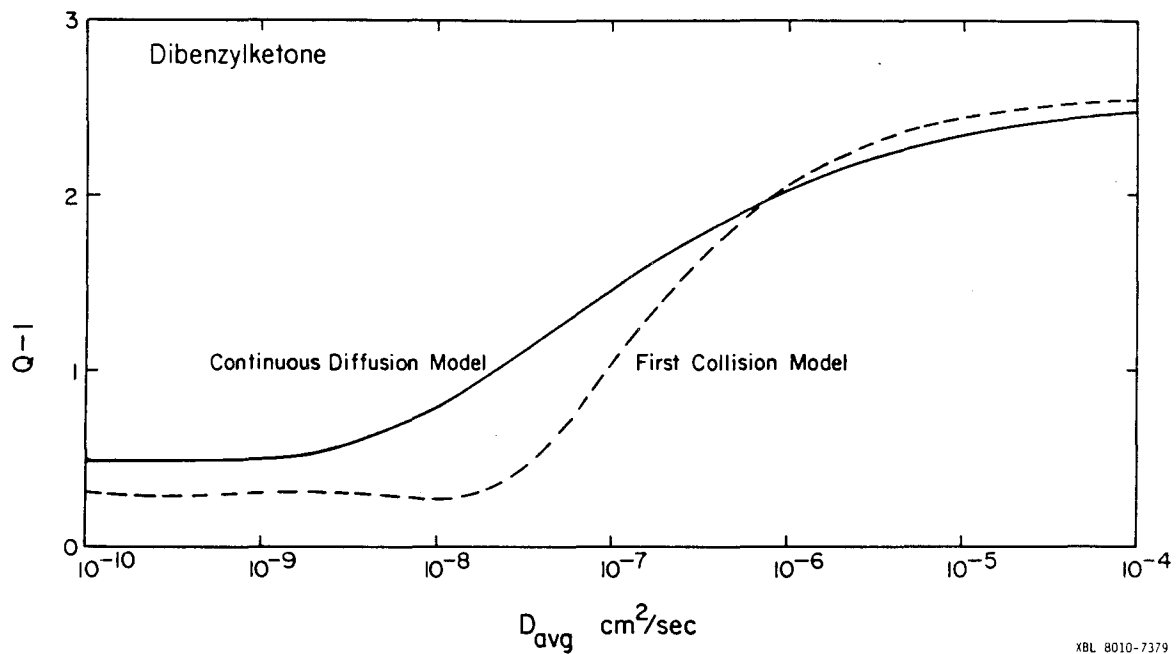
Figure I.35 Calculated recombination yield ^{12}R for dibenzylketone with ^{12}C . Unlike benzophenone and toluene (Figure I.31), the geminate recombination yield falls to zero as the diffusion slows down, because decarbonylation destroys the phenylacetyl radicals $\text{C}_6\text{H}_5\text{CH}_2\dot{\text{C}}\text{O}$.

diffusivity and therefore destroys a greater and greater fraction of radical pairs as recombination slows down. Thus, the recombination yield goes through a maximum at intermediate values ($\approx 10^{-7}$ cm²/sec) of the diffusion coefficient.

6.2.2 Isotope Enrichment Factor

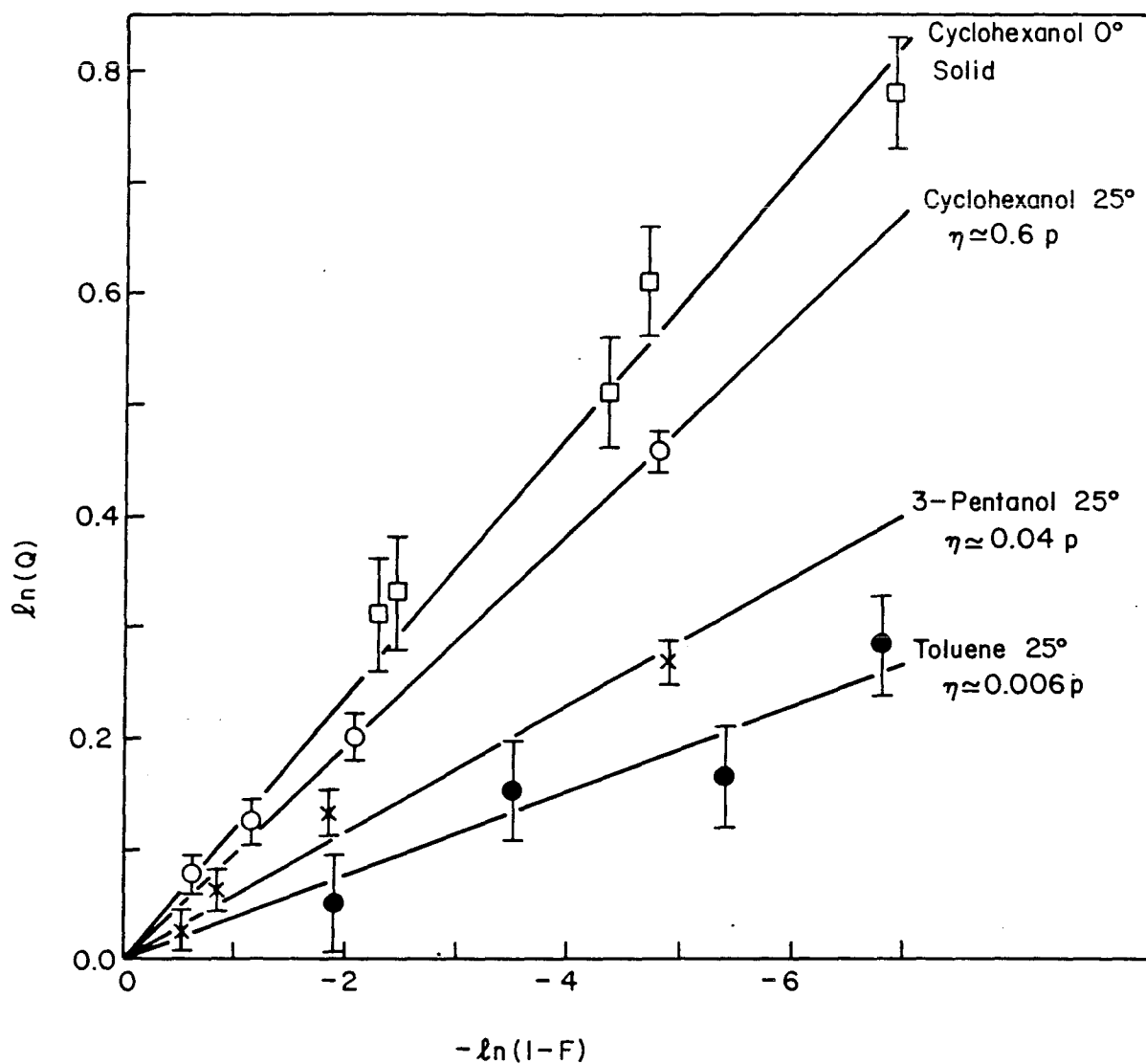
In Figure I.36 are plotted the predicted values of $Q-1$. It is noted that the First Collision Model and Continuous Diffusion Model agree rather well over most of the range of D_{avg} . Because of the large hyperfine coupling (350 MHz) of the carbonyl ¹³C in the acyl radical from dibenzylketone, the $Q-1$ values are an order of magnitude larger than those of benzophenone and toluene. Here, as for the benzophenone and toluene system, Q increases as D_{avg} increases. The observed behavior, however, is quite a bit different from what this might imply.

In Figure I.37 are shown the results of photolyses performed at four different viscosities. It is seen that there is indeed isotope enrichment and that, furthermore, for a given amount of photolysis (i.e., a given fraction of ketone consumed), the enrichment increases as the viscosity increases. This viscosity dependence is a consequence of the cyclic nature of the reaction. Since Q describes neither the viscosity dependence nor the progressive enrichment with photolysis time, it is not a meaningful quantity for describing a cyclic reaction. It is the slopes of the lines, not the Q values, which characterize the data of Figure I.37. Rather than using Q which is the ratio of



XBL 8010-7379

Figure I.36 Isotope enhancement factor for the dibenzylketone photolysis. Because of its large ^{13}C hyperfine coupling, dibenzylketone's $Q-1$ value is an order of magnitude larger than that for benzophenone and toluene, Figure I.32.



XBL 806-9850

Figure I.37 ^{13}C enrichment of dibenzylketone for photolysis in three different solvents. η is the viscosity in units of poise. The form of the plot corresponds to the analysis (valid for small enhancement factors) proposed by Bernstein [50]. Q is the ratio of ^{13}C to ^{12}C in the ketone relative to the ratio at zero photolysis. F is the fraction of ketone which has decarbonylated.

recombination probabilities (i.e., $^{13}R/^{12}R$), what is needed is a quantity related to the ratio of disappearance probabilities, that is, $(1-^{13}R)/(1-^{12}R)$.

Defining $k_{h\nu}$ as the rate constant for photolytic production of triplet radical pairs, there follows for the disappearance of ^{13}C and ^{12}C -containing dibenzylketone:

$$[^{13}C] = [^{13}C]_0 \exp[-(1-^{13}R)k_{h\nu}t] \quad (6.4a)$$

and

$$[^{12}C] = [^{12}C]_0 \exp[-(1-^{12}R)k_{h\nu}t] \quad (6.4b)$$

where $[^{13}C]$ and $[^{12}C]$ are the concentrations of dibenzylketone with ^{13}C and ^{12}C at the carbonyl position, respectively. The factor $(1-R)$ is equivalent to a quantum yield for destruction of the ketone. From the above equations it is easily seen that

$$\ln([^{13}C]/[^{13}C]_0) = -(1-^{13}R)k_{h\nu}t \quad (6.5a)$$

and

$$\ln([^{12}C]/[^{12}C]_0) = -(1-^{12}R)k_{h\nu}t \quad (6.5b)$$

so that

$$\ln([^{13}C]/[^{13}C]_0) = \frac{(1-^{13}R)}{(1-^{12}R)} \ln([^{12}C]/[^{12}C]_0) \quad (6.6)$$

Plotting $\ln([^{13}C]/[^{13}C]_0)$ versus $\ln([^{12}C]/[^{12}C]_0)$ for a photolysis, the slope $(1-^{13}R)/(1-^{12}R)$ may be obtained, and,

relating to this, the enrichment factor ϵ is defined to be:

$$\epsilon = 1 - \left\{ \frac{(1-^{13}\text{R})}{(1-^{12}\text{R})} \right\}. \quad (6.7)$$

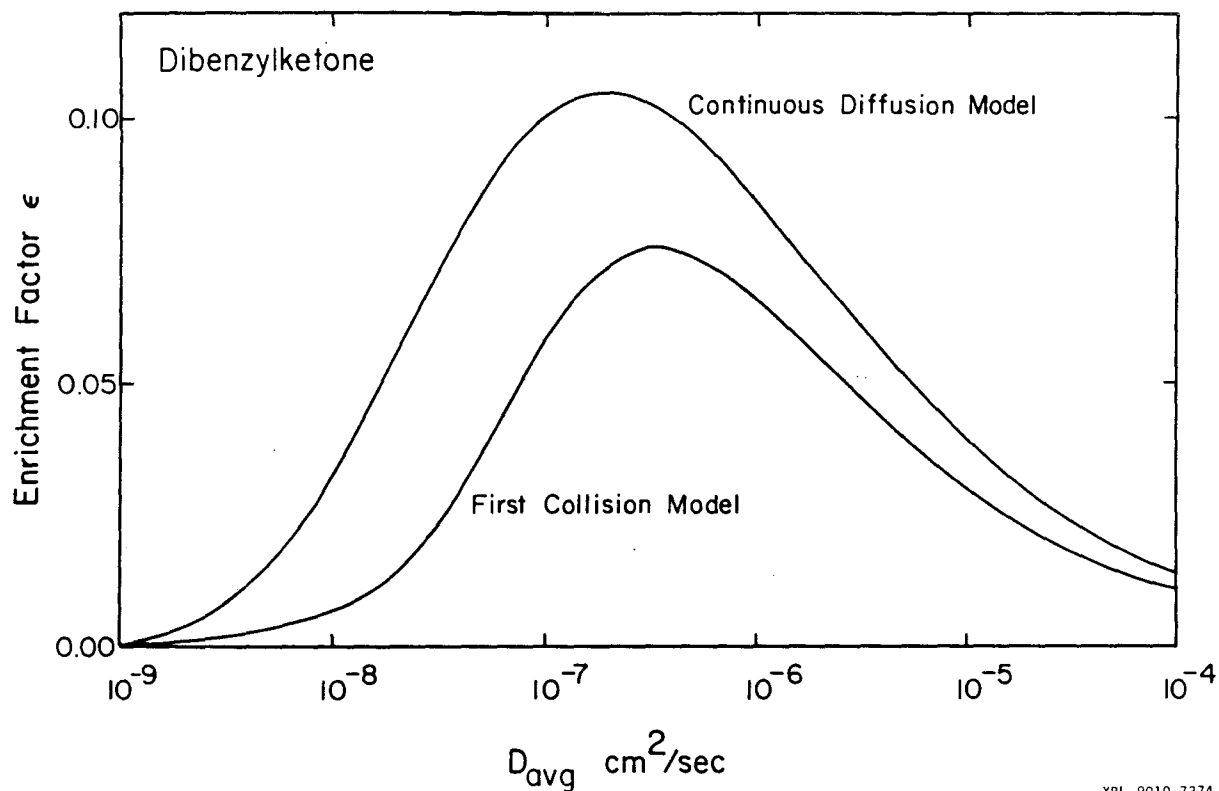
Alternatively, ϵ may be viewed as the differential loss between ^{12}C and ^{13}C relative to the loss of ^{12}C . ϵ is plotted as a function of diffusion coefficient in Figure I.38 where it is seen that the two models predict a maximum for $D_{\text{avg}} \approx 10^{-7} - 10^{-6} \text{ cm}^2/\text{sec}$. ϵ is calculated from the data shown in Figure I.37 and presented in Table I.5 along with the theoretical predictions. For the theoretical calculation of ϵ it was necessary to estimate the diffusion coefficients of the radicals from the known viscosities of the solvents. For this purpose the Stokes-Einstein equation was used with a factor of 1/4 to correspond to "slip" boundary conditions [11]:

$$D = \frac{1}{4} \frac{kT}{\pi\sigma\eta} \quad (6.8)$$

where σ is the radical radius and η is the solvent viscosity in poise. For the dibenzylketone radical pair σ is taken to be the molecular radius of toluene since the toluene molecule is intermediate in size to the two radicals. From the molecular density of toluene

$$\sigma \approx 3 \times 10^{-8} \text{ cm}.$$

Also appearing in the calculation is the radical-radical collision radius r_c which equals the sum of the radii of the ketyl and benzyl radicals:



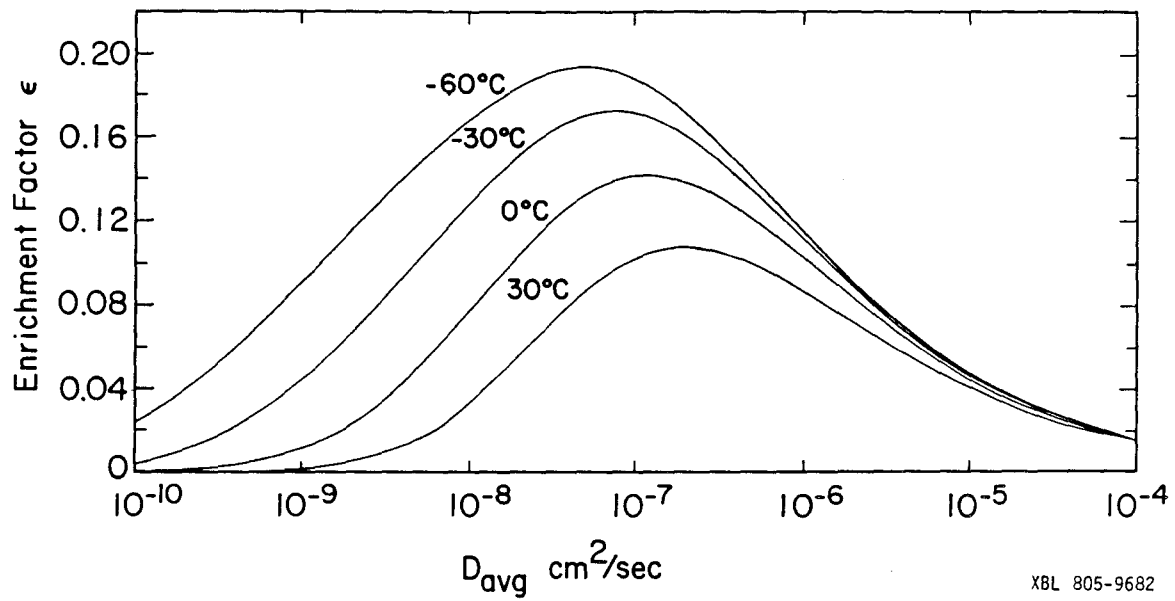
XBL 8010-7374

Figure I,38 Enrichment factor ϵ for the dibenzylketone photolysis. Cyclic reactions are better characterized by the enrichment factor ϵ than by the enhancement factor Q . ϵ is the differential loss between ^{12}C and ^{13}C relative to the loss of ^{12}C for a single stage of photolysis.

$$r_c \approx 2\sigma \quad .$$

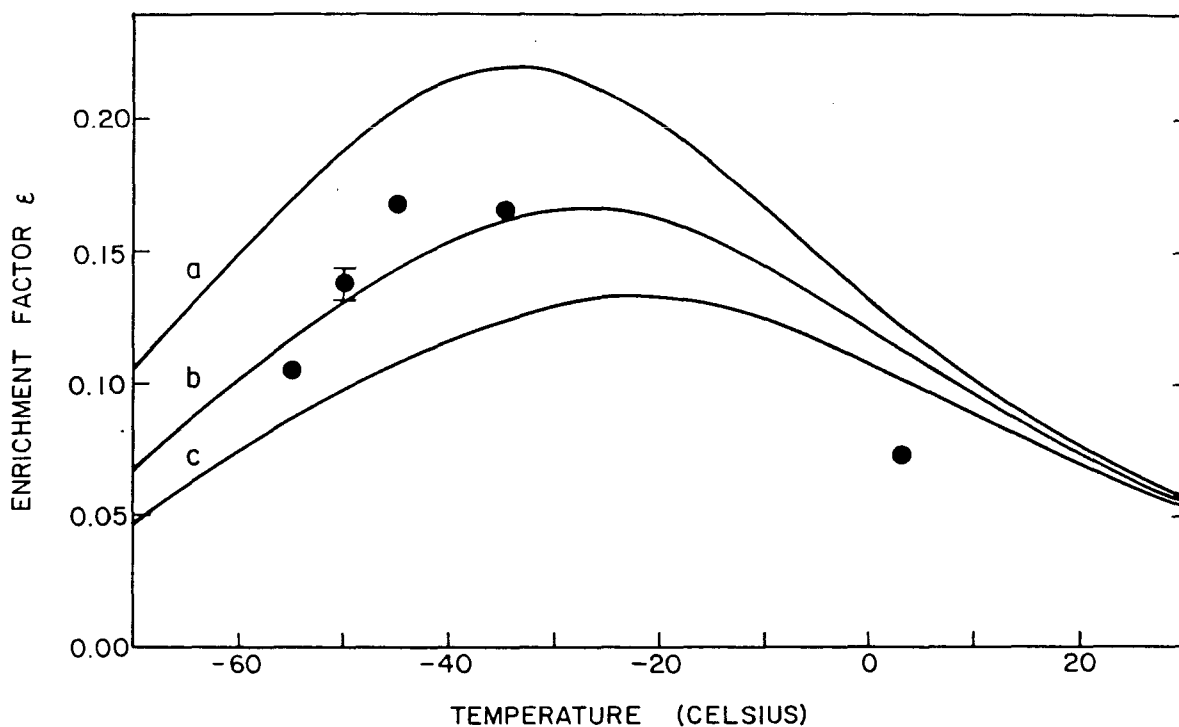
The dependence of ϵ on the decarbonylation rate of the ketyl radical is shown in Figure I.39 where a set of curves are plotted for different temperatures. The important feature is that as the temperature drops (i.e., less decarbonylation), the geminate recombination and, concomitantly, the enrichment factor increase.

In order to study the enrichment over a large viscosity range, 70/30 and 80/20 weight/weight mixtures of cyclohexanol and isopropanol were used as solvents and the temperature varied to control the viscosity. Since the decarbonylation has a smaller activation energy (i.e., $E_a = 7.3$ kcal/mole) than do the viscosities of the two solvents (i.e., 11 kcal/mole for the 70/30 and 13 kcal/mole for the 80/20), it does not change as rapidly as viscosity with temperature. Thus, although both decarbonylation rate and viscosity enter into the enrichment factor and are included in the computation of ϵ , the main features in the temperature dependence for these solvents are due to viscosity changes. The temperature dependence of the enrichment factor for photolysis in 70/30 cyclohexanol/isopropanol solvent is shown in Figure I.40 along with theoretically predicted curves. In contrast to the data shown in Figure I.37 where the enrichment factor increases with viscosity, the data in Figure I.40 show that at very high viscosity the enrichment factor begins to fall off. If the viscosity were not changing more rapidly than decarbonylation, the enrichment would be



XBL 805-9682

Figure I.39 Calculated dibenzylketone enrichment factor as a function of temperature and average diffusion coefficient. The temperature dependence is due to the activated decarbonylation process. The curves were calculated with the Continuous Diffusion Model.



XBL 806-9849

Figure I.40 Enrichment factor as a function of temperature for photolysis of dibenzylketone in a 70/30 cyclohexanol/isopropanol weight/weight solvent. The viscosities of the data points are given in Table I.5. Uncertainties are given by error bars or size of point. The Continuous Diffusion Model was used for the theoretical curves which were calculated for different values of r_0 , the radical-radical separation immediately after scission of the ketone: (a) $r_0 = 8 \text{ \AA}$, (b) $r_0 = 9 \text{ \AA}$, (c) $r_0 = 10 \text{ \AA}$. For the theoretical curves the measured viscosities were fitted to an Arrhenius expression.

expected to increase with decreasing temperature as indicated in Figure I.39.

Also shown in Figure I.40 is the dependence of the model calculation on the initial separation r_0 of the radical pair. The best fit is for $r_0 = 9 \text{ \AA}$ which is a reasonable value since this gives $r_0 - r_c = 3 \text{ \AA}$, a number comparable to the molecular dimensions (i.e., microscopic graining of the cyclohexanol/isopropanol solvent). To avoid the use of variable fit parameters for each reaction, this value of r_0 was used in all of the calculations in this work, although it is expected to vary with solvent, temperature, and reactant.

The deviation of the 3°C point from the theoretically predicted curves may be a real discrepancy between theory and experiment. However, it may also be attributed to extrapolating, using an Arrhenius law, the viscosity over such a large temperature range with data measured from -60 to -40°C . An accurate measurement of the viscosity (or diffusion coefficient) at 3°C is needed before the model calculation can be considered to be in true disagreement with experiment. Nevertheless, the experimental data do show the expected maximum in the enrichment as a function of the rate of diffusion, and in the range of accurate viscosity measurements (-40 to -60°C) an r_0 value of 9 \AA gives the best agreement between theory and experiment. The experimental and theoretical values for the 70/30 cyclohexanol/isopropanol solvent are tabulated in Table I.5 along with two values for the 80/20 solvent at higher viscosity.

Table I.5 Dibenzylketone Enrichment ϵ as a Function of Viscosity and Temperature

Solvent	Viscosity ^a (Poise)	Temperature ^b (Celsius)	ϵ Experimental ^c	ϵ Theoretical ^d
Toluene	0.006	25	0.038 \pm 0.003	0.031
	0.008	0	0.061 \pm 0.003	0.040
3-Pentanol	0.04	25	0.056 \pm 0.002	0.069
Cyclohexanol	0.6	25	0.093 \pm 0.002	0.114
	Solid ^e	0	0.112 \pm 0.003	--
70% Cyclohexanol 30% Isopropanol w/w	0.2 (?)	3	0.073 \pm 0.002	0.112
	3.8	-35	0.166 \pm 0.002	0.163
	11	-45	0.168 \pm 0.003	0.144
	18	-50	0.138 \pm 0.006	0.131
	32	-55	0.105 \pm 0.003	0.117
80% Cyclohexanol 20% Isopropanol w/w	36	-45	0.086 \pm 0.007	0.099
	270	-60	0.088 \pm 0.008	0.050

^aThe viscosities are all approximate. Viscosities for the neat solvents were interpolated from the tables in Reference 40. For the 70/30 and 80/20 cyclohexanol/isopropanol (weight/weight) solvents the viscosities were measured with a falling ball viscosimeter. The 3°C and -35°C viscosities for 70/30 cyclohexanol/isopropanol were extrapolated (using an Arrhenius law) from data measured from -60°C to -40°C.

^bTemperatures are average values over the course of a photolysis and typically varied by \pm 3°C. Photolysis times varied from 1 hour at 25°C (1% ketone remaining) to 50 hours at -60°C (25% ketone remaining).

^cThe enrichment factor ϵ is the differential loss between ^{12}C and ^{13}C relative to the loss of ^{12}C for a single stage of photolysis.

^dThe theoretical values of ϵ are calculated with the Continuous Diffusion Model. All values assume $r_0 = 9 \text{ \AA}$.

^eCyclohexanol forms a plastic crystal from -10°C to 24°C [51].

The overall agreement between theory and experiment, as demonstrated by the values in Table I.5, is reasonably good. The model calculations are not expected to be of high accuracy since some error is introduced by using the Stokes-Einstein equation, Eq. (6.8), rather than directly measuring the diffusion coefficients.

As in the case of the benzophenone and toluene reaction, it is interesting to include spin-orbit coupling in the model calculations and estimate what role it plays in radical pair intersystem crossing. In Figure I.41 are shown the enrichment curves expected for various values of the spin-orbit coupling strength. It is clear that a value of 10^9 Hz, as is required for benzophenone and toluene, would introduce substantial disagreement between the experimental and theoretical enrichment factors for dibenzylketone.

If it is oxygen, and not carbon, that is responsible for spin-orbit coupling, then it is not surprising that spin-orbit coupling is more important in the benzophenone than in the dibenzylketone reaction. The ketyl radical from benzophenone and toluene is a π radical. Thus, the unpaired electron is delocalized and would perhaps spend some time on the oxygen. The acyl radical from dibenzylketone, however, is a σ radical with the unpaired electron highly localized at a carbon center. On the other hand, it is possible that spin-orbit coupling is important in the dibenzylketone case, and the theoretical predictions could be brought in line with experimental results

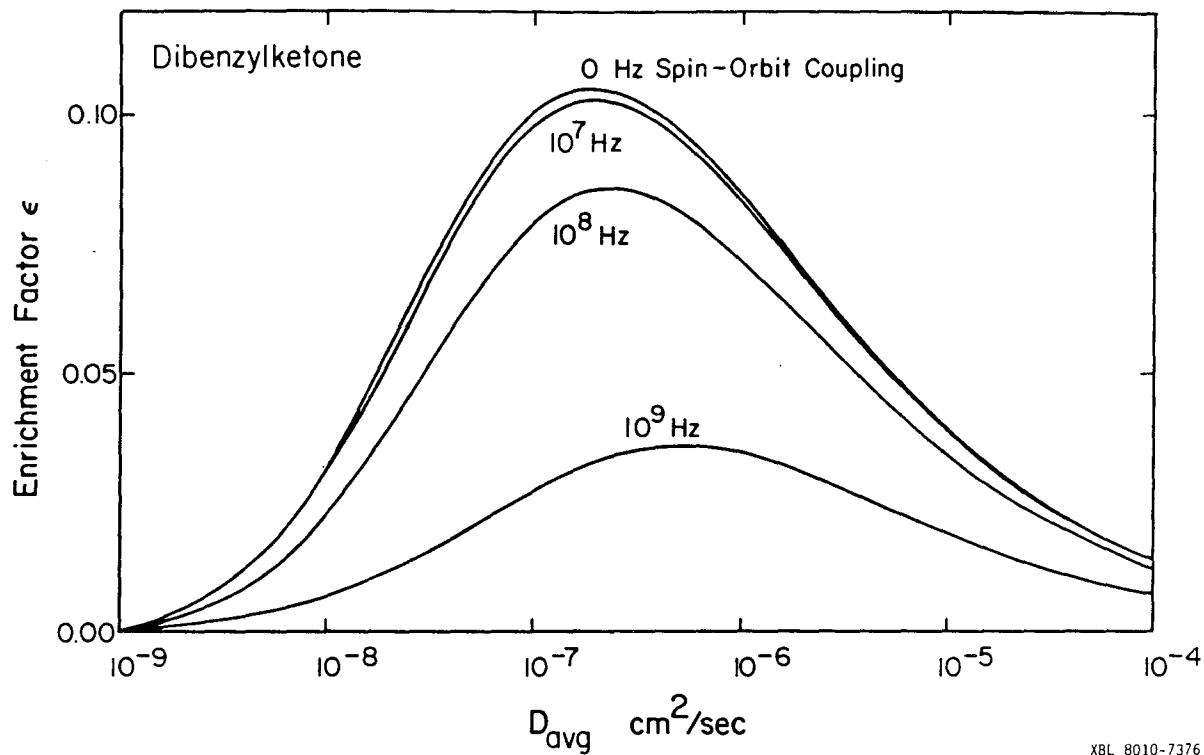
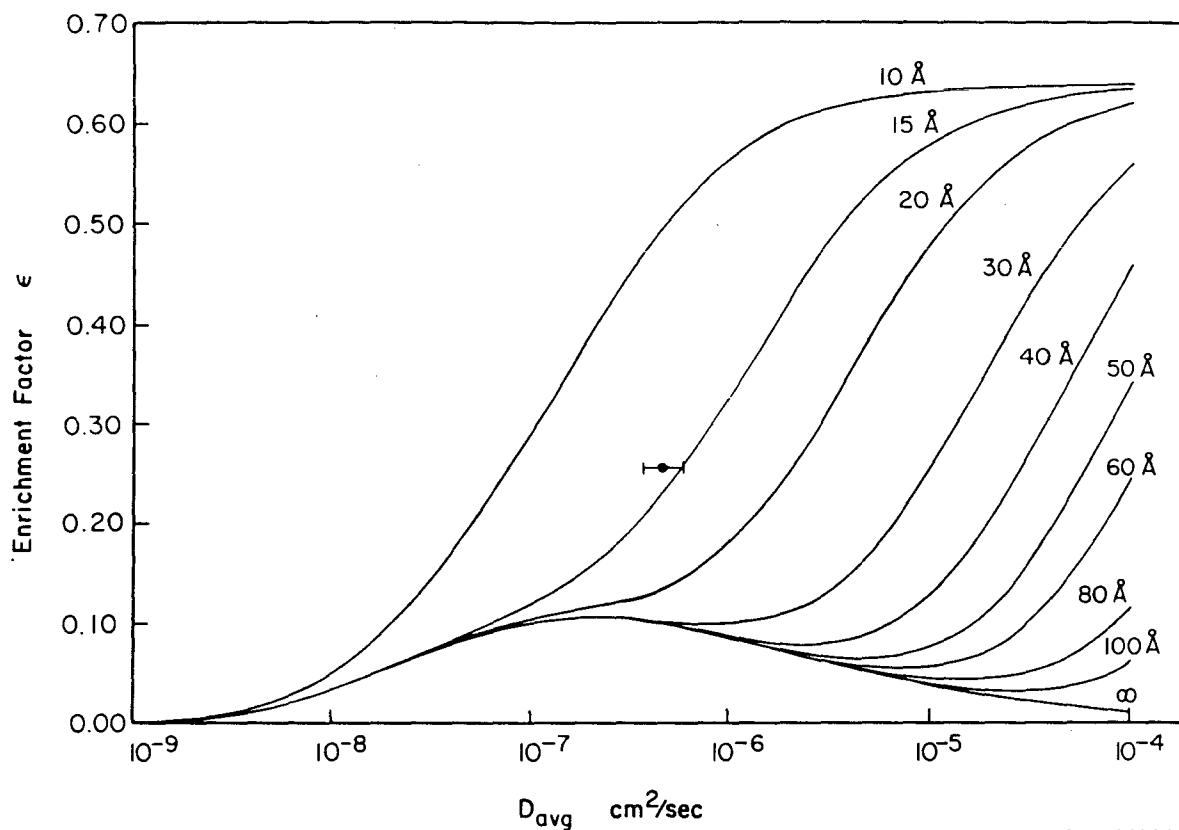


Figure I.41 Effect of spin-orbit coupling on the dibenzylketone enrichment factor. The curves are labeled by the rate of inter-system crossing due to spin-orbit coupling. 10^9 Hz is the estimated value of spin-orbit coupling for organic radicals (see sections 2.4.3 and 2.5.6). The curves were calculated with the Continuous Diffusion Model.

by a better choice of r_0 . As such, until a better understanding of r_0 is attained or else quantum yield measurements are made over a large viscosity range to estimate geminate recombination yields, the exclusion of spin-orbit coupling from consideration is only tentative.

In Figure I.42 are shown the model calculations for photolysis of dibenzylketone in different size micelles. The notable result is that large enhancements in the enrichment factor ϵ are possible by restricting the volume for diffusion. The explanation for this enhancement is simply that as the two members of the radical pair are kept in close proximity to one another, the geminate yield goes up thereby aiding the enrichment process. For the benzophenone and toluene system where only the relative probabilities of recombination are important, it would be disadvantageous to perform the reaction in a micelle.

In conclusion, large enrichments in ^{13}C have been observed in the dibenzylketone photochemical reaction. This enrichment was substantially enhanced at intermediate values of viscosity and at low temperatures in good agreement with theoretical predictions based on the Continuous Diffusion Model.



XBL 805-9681A

Figure I.42 Enrichment factor for photolysis of dibenzylketone within a sphere with a reflecting wall (e.g., a micelle). The curves are labeled by the radius r_b of the sphere in angstroms. The single data point is taken from the results of Turro [6] for photolysis of dibenzylketone in the hexadecyltrimethylammonium chloride (HDTCl) micelle. The radius of the organic portion of the HDTCl micelle is 21.7 \AA as measured by X-ray scattering [52]. With a radical radius of 3 \AA , the actual boundary radius r_b is 18.7 \AA . The diffusion coefficient for the radicals in the micelle was estimated [Eq. (6.8)] from the measured viscosities in a similar micelle hexadecyltrimethylammonium bromide [53].

7. SUMMARY AND DISCUSSION

In the foregoing chapters the theoretical basis for the magnetic isotope effect has been presented along with two models for predicting the effects of nuclear spin on radical pair recombination. In the First Collision Model the radical pair diffusion is treated via a first collision probability function and the evolution of electron-nuclear spin states treated quantum mechanically. Geminate recombination is calculated by numerically integrating as a function of time the first collision probability times the probability the radical pair is in a singlet state times a decaying exponential to account for a finite radical lifetime. Because of the quantum mechanical treatment it is difficult to account for more than about eight nuclear spins, while the numerical integration makes it difficult to include more than three collisions of the two radicals. It was shown, however, that in the case of high singlet reactivity (i.e., $\lambda \approx 1$) a simple closed form solution could be obtained to account for all possible collisions (see section 2.7).

In the Continuous Diffusion Model singlet-triplet intersystem crossing and chemical loss of radicals are treated via first order rate constants. These rate constants are added on to two different equations, one for singlets and one for triplets. The equations are separated and analytically solved for the geminate recombination yield R , thereby accounting for all possible collisions. Although the Continuous Diffusion Model treats the spins as a system approaching equilibrium and neglects all quantum mechanical

oscillations, it is in fair agreement with the First Collision Model in predicting geminate yields and isotopic enrichments for the two radical pairs studied.

As might be expected, the qualitative agreement between the predictions of the two models is much better than their quantitative agreement. This is a reflection of the fact that although the various physical terms are treated very differently in the two models, they still give the same time scales for diffusion, intersystem crossing, and radical lifetimes in both treatments. Given this agreement the Continuous Diffusion Model is certainly the method of choice for calculation and prediction because of its simplicity and general applicability. In addition, the model was generalized to treat geminate recombination within a reflecting sphere, such as a micelle.

It was argued that although spin-orbit coupling has been neglected in other published treatments, it can be a major and even dominant mode of intersystem crossing in the radical pair. Spin-orbit coupling is easily included in the Continuous Diffusion Model, and its importance was shown in the treatment of the benzophenone and toluene data. It was found that for the benzophenone and toluene reaction the measured geminate yield was too large and the enrichment too small (i.e., not observed) to agree with model calculations which consider only the hyperfine couplings. Both of these observations were shown to be consistent with the operation of spin-orbit coupling.

In the dibenzylketone case ^{13}C enrichment was observed, and because of the cyclic nature of the reaction, it was found to be easily manipulated by viscosity and temperature changes. Experiments with dibenzylketone in a variety of solvents and at different temperatures showed that the ^{13}C enrichment factor can be greatly enhanced at intermediate viscosities (~ 10 poise) and at low temperature. Furthermore, the experimental results showed the Continuous Diffusion Model to be of good utility in characterizing the reaction.

There are certainly many possibilities for future extension of the magnetic isotope effect so that this technique may be of practical value in isotope separation. There are other good candidates for study, as benzaldehyde, and use can be made of solvents of restricted volume (e.g., micelles) or restricted dimensionality (e.g., liquid crystals, bilayers) to get large geminate yields and therefore large enrichments in cyclic reactions. Free radical reactions with heavier atoms, as in organometallic chemistry [54], with much bigger hyperfine couplings [7c] may produce large magnetic isotope effects if not complicated by spin-orbit coupling. In any event, the Continuous Diffusion Model allows easy estimation of magnetic isotope effects for other nuclei and prediction of the optimum conditions for performing the reactions.

REFERENCES

1. R. Kaptein, *J. Am. Chem. Soc.* 94, 6251 (1972).
2. *Chemically Induced Magnetic Polarization*, edited by A. R. Lepley and G. L. Closs (Wiley, New York, 1973).
3. *NATO Advanced Study Institute Series, Vol. C34, Chemically Induced Magnetic Polarization*, edited by L. T. Muus, P. W. Atkins, K. A. McLauchlan, and J. B. Pedersen (Reidel, Dordrecht, 1977).
4. A. L. Buchachenko, E. M. Galimov, V. V. Ershov, G. A. Nikiforov, and A. D. Pershin, *Dokl. Phys. Chem.* 228, 451 (1976).
5. (a) L. Sterna and A. Pines, 1977 Annual Report of the Materials and Molecular Research Division, Lawrence Berkeley Laboratory, LBL-7355, p. 265.
(b) L. Sterna, D. Ronis, S. Wolfe, and A. Pines, *J. Chem. Phys.* 73, 5493 (1980).
6. (a) N. J. Turro and B. Kraeutler, *J. Am. Chem. Soc.* 100, 7432 (1978).
(b) N. J. Turro, B. Kraeutler, and D. R. Anderson, *J. Am. Chem. Soc.* 101, 7435 (1979).
7. (a) R. Z. Sagdeev, T. V. Leshina, M. A. Kamkha, O. I. Belchenko, Yu. N. Molin, and A. I. Rezvukhin, *Chem. Phys. Lett.* 48, 89 (1977).
(b) V. A. Belyakov, V. I. Mal'tsev, E. M. Galimov, and A. L. Buchachenko, *Dokl. Chem.* 243, 561 (1979).
(c) A. V. Podoplelov, T. V. Leshina, R. Z. Sagdeev,

- Yu. N. Molin, and V. I. Gol'danskii, JETP Lett. 29, 380 (1979).
- (d) H.-J. Werner, H. Staerk, and A. Weller, J. Chem. Phys. 68, 2419 (1978).
- (e) W. Bube, R. Haberkorn, and M. E. Michel-Beyerle, J. Am. Chem. Soc. 100, 5993 (1978).
8. (a) R. M. Noyes, J. Chem. Phys. 22, 1349 (1954).
(b) R. M. Noyes, J. Am. Chem. Soc. 77, 2042 (1955).
(c) R. M. Noyes, J. Am. Chem. Soc. 78, 5486 (1956).
9. (a) F. J. Adrian, J. Chem. Phys. 53, 3374 (1970).
(b) F. J. Adrian, J. Chem. Phys. 54, 3912 (1971).
10. G. S. Hammond, J. N. Sen, and C. E. Boozer, J. Am. Chem. Soc. 77, 3244 (1955).
11. E. McLaughlin, Trans. Faraday Soc. 55, 28 (1959).
12. (a) K. M. Salikov, F. S. Sarvarov, R. Z. Sagdeev, and Yu. N. Molin, Kinet. Catal. 16, 239 (1975).
(b) Z. Schulten and K. Schulten, J. Chem. Phys. 66, 4616 (1977).
(c) J. H. Freed, Reference 3, p. 309.
(d) A. Mozumder, J. Chem. Phys. 69, 1384 (1978).
13. (a) W. Kolos and L. Wolniewicz, J. Chem. Phys. 43, 2429 (1965).
(b) J. N. Murrell and J. J. C. Teixeira-Dias, Mol. Phys. 19, 521 (1970).
14. W. T. Huntress, J. Phys. Chem. 73, 103 (1969).
15. Reference 2, p. 60.

16. A. Carrington and A. D. McLauchlan, Introduction to Magnetic Resonance (Harper and Row, New York-Evanston-London, 1967), pp. 116-118.
17. P. W. Atkins and K. A. McLauchlan, Reference 2, p. 41.
18. (a) D. C. McClure, J. Chem. Phys. 20, 682 (1952).
(b) S. P. McGlynn, T. Azumi, M. Kinoshita, Molecular Spectroscopy of the Triplet State (Prentice-Hall, Englewood Cliffs, New Jersey, 1969).
19. C. S. Johnson and L. G. Pedersen, Problems and Solutions in Quantum Chemistry and Physics (Addison-Wesley, Reading-Menlo Park-London-Amsterdam-Don Mills-Sydney, 1976), p. 135.
20. C. P. Slichter, Principles of Magnetic Resonance (Springer, Berlin-Heidelberg-New York, 1978), pp. 78-82, 296-299.
21. Reference 19, p. 165.
22. Reference 16, pp. 133-138.
23. Reference 16, pp. 18, 19.
24. G. Brunton, H. C. McBay, and K. U. Ingold, J. Am. Chem. Soc. 99, 4447 (1977).
25. W. K. Robbins and R. H. Eastman, J. Am. Chem. Soc. 92, 6077 (1970).
26. G. L. Closs. 23rd International Congress on Pure and Applied Chemistry, 1971, Vol. 4, p. 19.
27. E. Butkov, Mathematical Physics (Addison-Wesley, Reading-Menlo Park-London-Amsterdam-Don Mills-Sydney, 1968). p. 381 ff.
28. L. R. Fisher and D. G. Oakenfull, Chem. Soc. Reviews 6, 25 (1977).

29. A. Beckett and G. Porter, *Trans. Faraday Soc.* 59, 2038 (1963).
30. N. J. Turro, *Modern Molecular Photochemistry* (Benjamin/Cummings, Menlo Park-Reading-London-Amsterdam-Don Mills-Sydney, 1978) p. 108.
31. R. M. Hochstrasser, H. Lutz, and G. W. Scott, *Chem. Phys. Lett.* 24, 162 (1974).
32. Reference 30, pp. 105-109.
33. L. Giering, M. Berger, and C. Steel, *J. Am. Chem. Soc.* 96, 953 (1974).
34. Reference 30, p. 364 ff.
35. S. J. Formosinho, *J. C. S. Faraday II*, 72, 1313 (1976).
36. L. Salem, *J. Am. Chem. Soc.* 96, 3486 (1974).
37. Landolt-Börnstein, *Numerical Data and Functional Relationships, New Series* (Springer, Berlin-Heidelberg-New York, 1977), Group II, Vol. 9, Part b.
38. P. S. Engel, *J. Am. Chem. Soc.* 92, 6074 (1970).
39. *CRC Handbook of Chemistry and Physics* (CRC Press, Cleveland, 1977), 58th edition.
40. Landolt-Börnstein, *Numerical Data and Functional Relationships* (Springer, Berlin-Heidelberg-New York, 1969), 6th edition, Vol. II, Part 5a.
41. W. T. Laughlin and D. R. Uhlmann, *J. Phys. Chem.* 76, 2317 (1972).
42. G. Porter and M. W. Windsor, *Nature* 180, 187 (1957).
43. G. L. Closs and D. R. Paulson, *J. Am. Chem. Soc.* 92, 7229 (1970).

44. M. Cocivera and A. M. Trozzolo, *J. Am. Chem. Soc.* 92, 1772 (1970).
45. G. S. Hammond, W. P. Baker, and W. M. Moore, *J. Am. Chem. Soc.* 83, 2795 (1961).
46. J. B. Guttenplan and S. G. Cohen, *J. Org. Chem.* 38, 2001 (1973).
47. D. E. O'Reilly and E. M. Peterson, *J. Chem. Phys.* 56, 2262 (1972).
48. G. L. Closs and L. E. Closs, *J. Am. Chem. Soc.* 91, 4550 (1969).
49. W. K. Robbins and R. H. Eastman, *J. Am. Chem. Soc.* 92, 6076 (1970).
50. (a) R. B. Bernstein, *J. Phys. Chem.* 56, 893 (1952).
(b) R. B. Bernstein, *Science* 126, 119 (1957).
51. P. A. Windsor, in *Liquid Crystals and Plastic Crystals*, edited by G. W. Gray and P. A. Windsor (Halsted, New York, 1969), Vol. 1, p. 48.
52. F. Reiss-Husson and V. Luzzati, *J. Phys. Chem.* 68, 3504 (1964).
53. M. Shinitzky, A. C. Dianoux, C. Gitler, and G. Weber, *Biochemistry* 10, 2106 (1971).
54. (a) R. G. Lawler and P. Livant, *J. Am. Chem. Soc.* 98, 3710 (1976).
(b) B. J. Schaart, H. W. H. J. Bodewitz, C. Blomberg, and F. Bickelhaupt, *J. Am. Chem. Soc.* 98, 3712 (1976).
(c) R. Benn, *Chem. Phys.* 15, 369 (1976).

PART II: INTERACTIONS BETWEEN NUCLEAR SPIN AND METHYL GROUP
ROTATIONAL AND TORSIONAL DEGREES OF FREEDOM

8. INTRODUCTION

The focus of this work is to use nuclear spin as a probe of methyl group motion in the solid state. The role of the nuclear spin is not merely a passive one where the NMR spectrum reflects the type of structural and motional environment in which the nuclear spins are located. Rather, the Pauli exclusion principle provides a rigid coupling between the dynamics of nuclear spin-lattice relaxation and torsional transitions of the methyl group. This coupling is evidenced by the bi-exponential relaxation observed for the nuclear spin system. Spin thermodynamics [1,2] provides a useful framework for elucidating the nature of this coupling and in providing the motivation for the experiments which were performed. Consequently, a brief overview is given in Chapter 9 of the main features of the spin thermodynamic picture. In Chapter 10 are presented those properties of methyl groups in solids which guide the application of spin thermodynamics to a suitable description of the experimental situation. Following the discussion of spin diffusion and spin-lattice relaxation in Chapter 11, the experimental arrangement is described in Chapter 12. The experiments and calculations are given in Chapter 13. Results are presented for studies of the coupling between nuclear spin and rotational polarization, the methyl group magnetic moment, methyl-methyl steric interactions, and the relation between hindered rotation and tunneling. A brief summary and discussion is given in Chapter 14.

8.1 Partitioning of States in Space and Spin

In describing a system of N particles it is frequently advantageous to partition the system into various subsystems which may be considered more or less independently and therefore more easily described than the system as a whole. Thus, the methyl iodide molecule (CH_3I) is described in terms of center of mass motion, rotations, vibrations, and electronic states, or degrees of freedom. The choice of these different categories is largely determined by classical expectations, and the validity of the picture is generally based on the fact that each category is associated with its own characteristic range of energies.

In a quantum mechanical picture the system is described by its Hamiltonian. The division into subsystems is accomplished by partitioning the Hamiltonian as:

$$\mathcal{H} = \mathcal{H}_{\text{elect}}^{\circ} + \mathcal{H}_{\text{vib}}^{\circ} + \mathcal{H}_{\text{rot}}^{\circ} + \mathcal{H}'_{\text{elect-vib}} + \mathcal{H}'_{\text{elect-rot}} + \mathcal{H}'_{\text{vib-rot}} \quad (8.1)$$

where translational energies and couplings to the radiation field have been neglected. The first three terms on the right hand side of Eq. (8.1) represent pure electronic, vibrational and rotational subsystems, respectively:

$$[\mathcal{H}_{\text{elect}}^{\circ}, \mathcal{H}_{\text{vib}}^{\circ}] = 0, \quad (8.2)$$

etc. The last three terms represent those interactions which cause mixing between the different "pure" states. Thus,

$$[\mathcal{H}_{\text{elect}}^{\circ}, \mathcal{H}'_{\text{elect-vib}}] \neq 0 \quad (8.3a)$$

$$[\mathcal{H}_{\text{elect}}^{\circ}, \mathcal{H}'_{\text{vib-rot}}] = 0 \quad , \quad (8.3b)$$

etc. The validity of the partitioning into subsystems is dependent upon the magnitude of the mixing terms \mathcal{H}' and the type of measurement performed on the system.

In describing the nuclear spin states of a molecule the same considerations may be applied as were used above. Restricting the discussion to spin 1/2 particles in the solid state, the relevant Hamiltonian is:

$$\mathcal{H} = \mathcal{H}_{\text{Zeeman}} + \mathcal{H}_{\text{Dipolar}} \quad (8.4)$$

$\mathcal{H}_{\text{Zeeman}}$ refers to interactions between single spins and an external magnetic field, and $\mathcal{H}_{\text{Dipolar}}$ refers to spin-spin dipole-dipole interactions. Writing $\mathcal{H}_{\text{Zeeman}}$ as \mathcal{H}_Z and decomposing $\mathcal{H}_{\text{Dipolar}}$ into a part \mathcal{H}_D° which commutes with \mathcal{H}_Z and a part \mathcal{H}'_D which does not, an analogous form to Eq. (8.1) is obtained:

$$\mathcal{H} = \mathcal{H}_Z + \mathcal{H}_D^{\circ} + \mathcal{H}'_D \quad (8.5)$$

This Hamiltonian leads to the natural choice of Zeeman states (eigenstates of \mathcal{H}_Z) and dipolar states (eigenstates of \mathcal{H}_D°) for partitioning the system. In high magnetic fields (i.e., ≥ 1 kilogauss) the Zeeman energies are much larger than dipolar energies, and it is valid to treat Zeeman and dipolar as two independent subsystems. In low magnetic fields Zeeman and

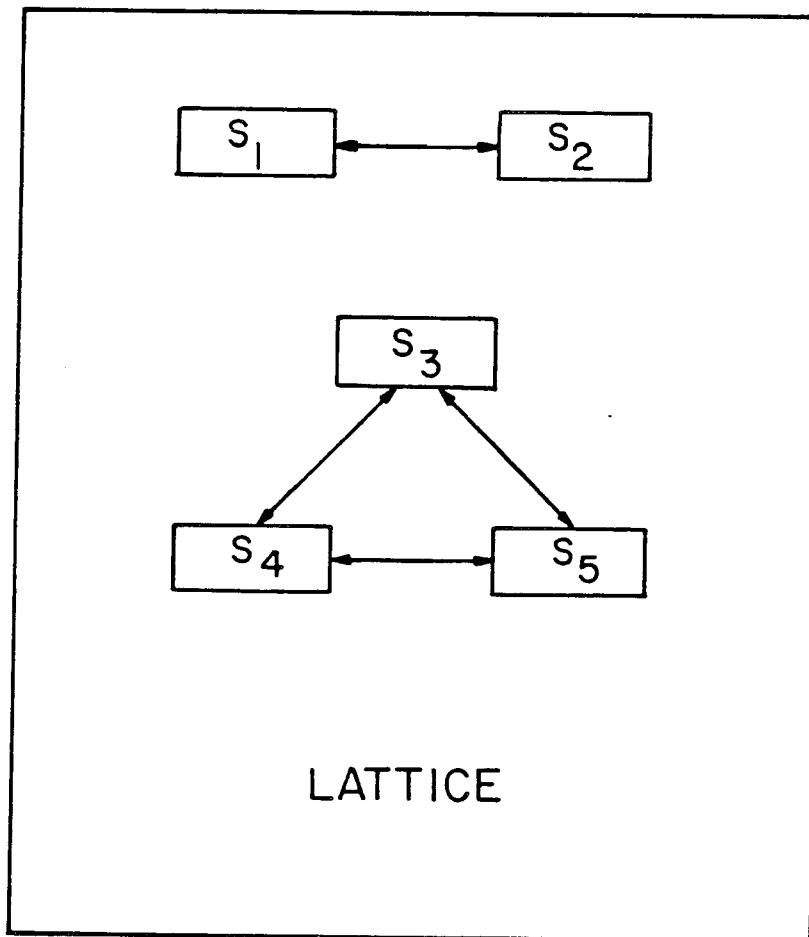
dipolar energies are comparable, the two systems interact strongly, and the partitioning breaks down [1,3]. In this work only very high magnetic fields of 24 and 42 kilogauss are used so that Zeeman and dipolar are always valid subsystems. However, as shown in the next section, they fail to completely describe the state of the methyl group. Alternately stated, the energies alone are insufficient to describe the complete state of the spins. An analogous situation occurs in the case of chiral molecules, where a knowledge of the energy gives no indication as to the number of left and right-handed molecules present.

The selection of the appropriate variables to describe the spin system fully is guided by a consideration of the spatial properties of the methyl group and of the spin-spin interactions within the solid state. Before these factors are discussed, the spin thermodynamic picture is presented to provide the framework within which the variables are used.

9. SPIN THERMODYNAMICS [1,2]

The object of this chapter is to develop a description of the spin system in terms of coupled reservoirs, or subsystems, embedded in a lattice of enormous heat capacity (see Figure II.1). The spin system is taken to be an ensemble of equivalent methyl groups, that is, methyl groups which have the same barrier to rotation and whose C_3 axes all have the same orientation with respect to the magnetic field. Methyl groups at different orientations to the field and non-methyl spins will be considered in Chapter 11.

The ensemble of equivalent methyl groups may be described by the properties of one methyl group which is the average of the ensemble. Consider this methyl group. It has three spin $1/2$ protons, each of which has two possible states of angular momentum $+1/2$ or $-1/2$ as defined within a given axis system. Thus, there are $2^3 = 8$ possible nuclear spin states for the three methyl protons. Requiring the total population of all the states to be a constant, there still remain seven population variables to specify [4]. (The question of specifying the phases of states will be taken up in section 9.3). Treating the methyl group as a thermodynamic system in contact with the lattice, seven subsystems can be constructed corresponding either to individual spin states or, where it is advantageous, to linear combinations of spin states. This approach is described below. To allow for exchange of energy or population between the various reservoirs, the grand canonical ensemble is used.



XBL 812-8111

Figure II.1 Examples of subsystems embedded in a lattice and exhibiting various couplings among themselves. All of the subsystems are coupled to the lattice. Since S_1 and S_2 are coupled to one another, the relaxation of either after being driven from equilibrium would be bi-exponential (see section 13.1). S_3 , S_4 , and S_5 would exhibit tri-exponential relaxation behavior.

9.1. Grand Canonical Ensemble

The methyl group spins constitute a thermodynamic system which is maintained in equilibrium by the lattice (non-nuclear degrees of freedom). This thermodynamic system is described by the grand canonical ensemble:

$$p = \exp\left[\left(\sum_i \mu_i n_i - E\right)/kT\right] / \Xi \quad (9.1)$$

where p is the probability for a given distribution of population (normalized) among the spin levels, the n_i 's are the populations of the levels, the μ_i 's are the chemical potentials of the levels, E is the total energy of the spin system, and Ξ is the partition function. Since the energy of each spin level is fixed, the total energy is specified by the populations:

$$E = \sum_i e_i n_i \quad (9.2)$$

where e_i is the energy of the i^{th} level. Thus, E is not an independent parameter and it may be dropped, leaving the populations $\{n_i\}$ to describe the system:

$$p = \exp\left[\sum_i (\mu_i/kT)n_i\right] / \Xi \quad (9.3)$$

There are two criticisms in regard to expressing p as a function of the level populations. The first is that NMR measurements are never concerned with the populations of individual levels, but rather with population differences (or energy differences)

between levels. As such, the individual populations can only be indirectly related to experiment. The second criticism has to do with the time scales for NMR relaxation and is discussed in the next section under the title of quasi-equilibrium. Following the discussion of this second criticism an alternative set of variables known as the "number operators" is introduced in section 9.3.

This page is for number sequence only.

9.2 Quasi-equilibrium [1,6]

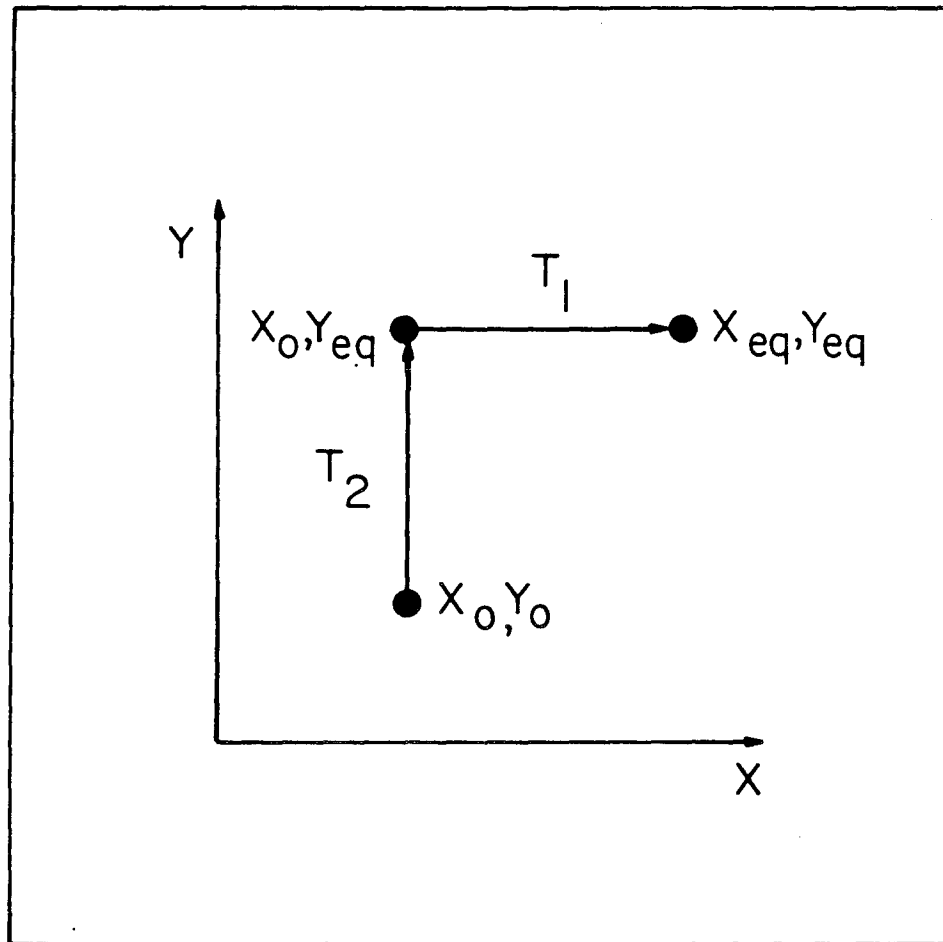
In studying relaxation it is frequently the case that transitions between some levels are much faster than transitions between other levels. Thus, when the spin system starts in some general non-equilibrium configuration, it is found that some population differences, although not the populations themselves, approach equilibrium much faster than other population differences do. As a consequence of this the number of variables required to describe the relaxation is dependent upon the time scale of the measurement. This is illustrated quite simply in Figure II.2. Since the required number of variables will always be less than or equal to the total number for the system, a judicious choice of variables may greatly simplify the description of the relaxation.

In general, if the individual level populations are chosen as the variables, a reduction in effort will not be achieved. If, however, the problem is re-parameterized in terms of population differences, the separation of relaxation equations by time scales is straightforward. This work is concerned with proton spin relaxation in the solid state, and the relevant feature to be taken advantage of is the vast difference in time scales (i.e., five to six orders of magnitude) between T_1 and T_2 relaxation processes. Spin diffusion (section 11.1) takes the proton spin system to a state of quasi-equilibrium in $\sim 20\text{-}50 \mu\text{sec}$ (T_2). Those population differences which have equilibrated need not be considered further in describing the

relaxation. In other words, for each set of levels which have equilibrated a constraint may be introduced which fixes the ratios of the relevant populations; each constraint reduces the number of independent variables.

The system relaxes from a state of quasi-equilibrium to a state of complete equilibrium in 1-100 sec (T_1) as a result of spin-lattice relaxation (section 11.3). The slowly varying parameters which characterize the relaxation of the quasi-equilibrium state are termed the quasi-constants, or quasi-invariants, of the motion [1,6]. The quasi-constants are linear combinations of the level populations, and constructing the appropriate set of linear combinations is analogous to finding the constants of the motion in mechanics.

Of interest in this work is the quasi-equilibrium state, because of the physical significance of the quasi-constants. The choice and significance of the quasi-constants is informed by the considerations presented in Chapters 10 and 11. Before entering upon these considerations, an operator formalism for the quasi-constant variables is presented in the following section.



XBL 812-8116

Figure II.2 Relaxation of a system which is described by two variables and which passes through a quasi-equilibrium state. The system is prepared in the state X_0, Y_0 . The variable Y relaxes to its equilibrium value in a time T_2 which is short compared to the relaxation time of X . The relaxation of the quasi-equilibrium state is characterized by the single variable X and requires a time T_1 to reach complete equilibrium.

9.3 Number Operators

In Eq. (9.3) p was written as a function of the level populations n_i . It is clear that any complete set of variables which are made up of linear combinations of the n_i 's will work equally well. In this section the quantum mechanical density operator $\hat{\rho}$ is introduced with the density operator $\hat{\rho}$ replacing the thermodynamic probability function p and with a generalized set of number operators $\{\hat{O}_k\}$ replacing the set of level populations $\{n_i\}$. The transition from scalar to operator is made via the level population operators \hat{n}_i :

$$\hat{n}_i = |i\rangle\langle i|, \quad (9.4)$$

the eigenvalues of which are the level populations. The number operators at quasi-equilibrium are defined:

$$\hat{O}_k = \sum_i c_{ki} |i\rangle\langle i| \quad . \quad (9.5)$$

The matrix c which defines the number operators is given in section 11.2 following the introduction of all of the quasi-constants.

In analogy with Eq. (9.3) [6],

$$\hat{\rho} = \exp\left(\sum_k \alpha_k \hat{O}_k\right) / \Xi \quad (9.6)$$

where the α_k 's are the intensive parameters (i.e. entropy derivatives) associated with the number operators. The point of contact between the density operator Eq. (9.6) and the thermodynamic probability function Eq. (9.3) is that the

probability p is the expectation value of the operator $\hat{\rho}$ for a given state of the system. In the formalism of section 9.1 a state of the system is defined by a given set of populations $\{n_i\}$. In the formalism of this section the system is specified by the expectation values of the \hat{O}_k operators.

Because the \hat{O}_k 's are defined in Eq. (9.5) as diagonal in the spin level basis, the density operator $\hat{\rho}$ is also diagonal in this basis. Since the off-diagonal matrix elements $\langle i|\hat{\rho}|j\rangle$ represent coherences between the $|i\rangle$ and $|j\rangle$ nuclear spin states, Eq. (9.5) states that there can be no coherences in the spin system. This corresponds to the treatment of section 9.1 where it was assumed that the system was entirely specified by the level populations $\{n_i\}$ with no regard to phase relations between the states. This conforms to the usual treatment of spin thermodynamics [7,8] where the random phase approximation is invoked, and all of the coherences are assumed to be zero. In NMR experiments, however, coherently prepared ensembles are the rule rather than the exception (the exception being π pulses or saturation). This is not a problem though, since this work is concerned primarily with the time evolution of the system after quasi-equilibrium is reached, and the relaxation processes (i.e., T_2) which produce quasi-equilibrium destroy all of the coherences. Thus, the random phase approximation is valid, and the \hat{O}_k 's are diagonal.

At high temperature the α_k 's are small, and Eq. (9.6) may be expanded to first order:

$$\hat{\rho} = \hat{1} + \sum_k \alpha_k \hat{O}_k \quad (9.7)$$

where $\hat{1}$ is the unit operator and Ξ which is only a normalization constant has been dropped. The number operators are defined so that their expectation values are deviations from equal distribution of population.

Thus,

$$\text{Tr } \hat{O}_k = \text{Tr } \hat{O}_k \hat{1} = 0 \quad ; \quad (9.8)$$

that is, the number operators are all traceless [6]. The number operators are defined to be orthogonal and normalized [6]:

$$\text{Tr } \hat{O}_k \hat{O}_\ell = \delta_{k\ell} \quad (9.9)$$

With Eqs. (9.7) - (9.9) the expectation values of the number operators are [6]:

$$\text{Tr } \hat{O}_k \hat{\rho} = \alpha_k \quad (9.10)$$

at high temperature.

With the above factors and the discussion of the previous sections in view the properties of the number operators may be summarized:

- 1) They form a complete set of variables for the system.
- 2) They are linearly independent and normalized.
- 3) They are traceless.

- 4) They correspond to Hamiltonian terms where possible.
- 5) They are chosen with regard to describing the quasi-equilibrium state.
- 6) They are not unique.

On the basis of these properties the number operators are defined in the next two chapters where the methyl group properties and spin relaxation are discussed.

10. METHYL GROUP DESCRIPTION

10.1 Spatial Hamiltonian

The methyl group is a C_3 rotor which in this work is treated as moving in a three-fold cosine potential. Including rotational kinetic energy the Hamiltonian for a rigid methyl rotor is [9]:

$$\mathcal{H} = \frac{-\hbar^2}{2I} \frac{\partial^2}{\partial \phi^2} + \frac{V_3}{2} (1 - \cos 3\phi) \quad (10.1)$$

where ϕ is the angle of rotation and the moment of inertia I about the C_3 axis is $\approx 5.5 \times 10^{-40} \text{ g cm}^2$ [10]. The barrier V_3 results from both intramolecular steric interactions and intermolecular hindrances within the crystalline sample. To construct the Hamiltonian matrix of Eq. (10.1) and diagonalize it, the basis set of free rotor wave functions is chosen:

$$|m\rangle = \exp(-im\phi) / \sqrt{2\pi} \quad (10.2)$$

which are the exact solutions for $V_3 = 0$.

The full symmetry group of the methyl rotor is C_{3v} , but since only rotational dynamics are being considered here, it is sufficient to use only the rotational subgroup C_3 . There are three irreducible representations of the group C_3 , and they transform under the symmetry operations as shown in Table II.1. Using Table II.1 to project the symmetrized wave functions out of the basis set it is found that for

$$A \text{ symmetry: } m = 3n \quad (10.3a)$$

$$E^a \text{ symmetry: } m = 3n - 1 \quad (10.3b)$$

$$E^b \text{ symmetry: } m = 3n + 1 \quad (10.3c)$$

where $n = 0, \pm 1, \pm 2, \dots$. The energy levels and angular momenta of a free rotor are shown in Figure II.3.

The program "methyl" (Appendix C) is used for the hindered rotor calculations, and in Figure II.4 are shown the results of a calculation for $V_3 = 1$ kcal/mole which is a medium size solid state barrier. In contrast to the free rotor wave functions, the hindered rotor, or torsional, wave functions are not eigenfunctions of angular momentum. Nevertheless, the expectation values of the angular momentum operator $-i\hbar\partial/\partial\phi$ can still be calculated. Since each torsional wave function $|\psi_\ell\rangle$ is a linear combination of free rotor basis functions,

$$|\psi_\ell\rangle = \sum_k a_{k\ell} \exp(-im_k\phi)/\sqrt{2\pi} \quad , \quad (10.4)$$

and the expectation value of angular momentum is given by:

$$\langle m \rangle_\ell = \sum_k a_{k\ell}^* a_{k\ell} m_k \quad . \quad (10.5)$$

Comparing Figures II.3 and II.4, it is seen that below the top of the barrier the angular momentum of the torsional levels is greatly reduced, whereas above the barrier the E states rapidly approach free rotor behavior. Since the free rotor A states occur in degenerate pairs (i.e., $m = \pm 3n$), the two members of

Table II.1 Character Table for C_3 Symmetry

	E	C_3	C_3^2
A	1	1	1
E^a	1	ϵ	ϵ^*
E^b	1	ϵ^*	ϵ

$$\epsilon = \exp(i2\pi/3)$$

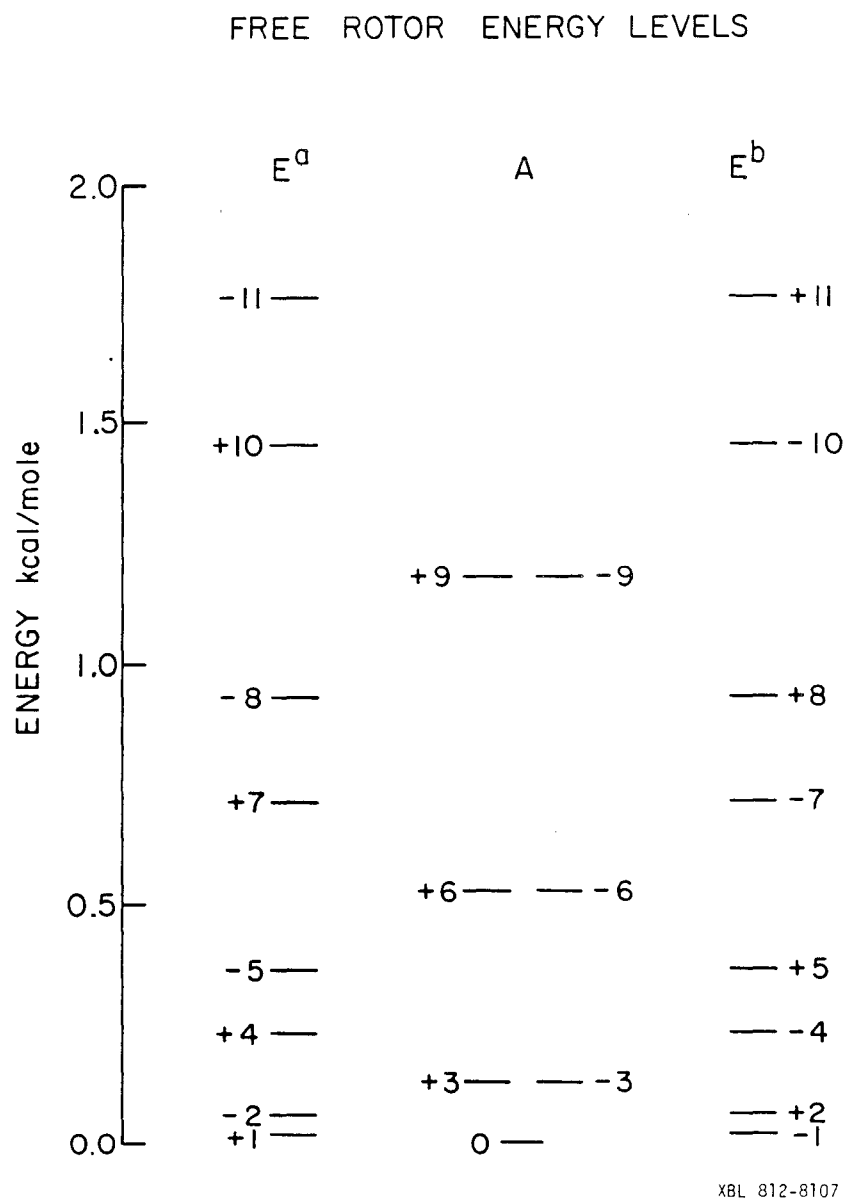


Figure II.3 Energy levels for an unhindered C_3 rotor. There are three symmetry manifolds: E^a , A, and E^b . Each level is labeled by its angular momentum eigenvalue.

each pair mix very effectively, even well above the barrier, to form symmetric and antisymmetric combinations which have $m = 0$.

The convention used in this work is to label each set of A, E^a, E^b states as torsional level i (starting with zero) and to define the energy difference between the E _{i} and A _{i} states as the tunneling splitting Δ_i :

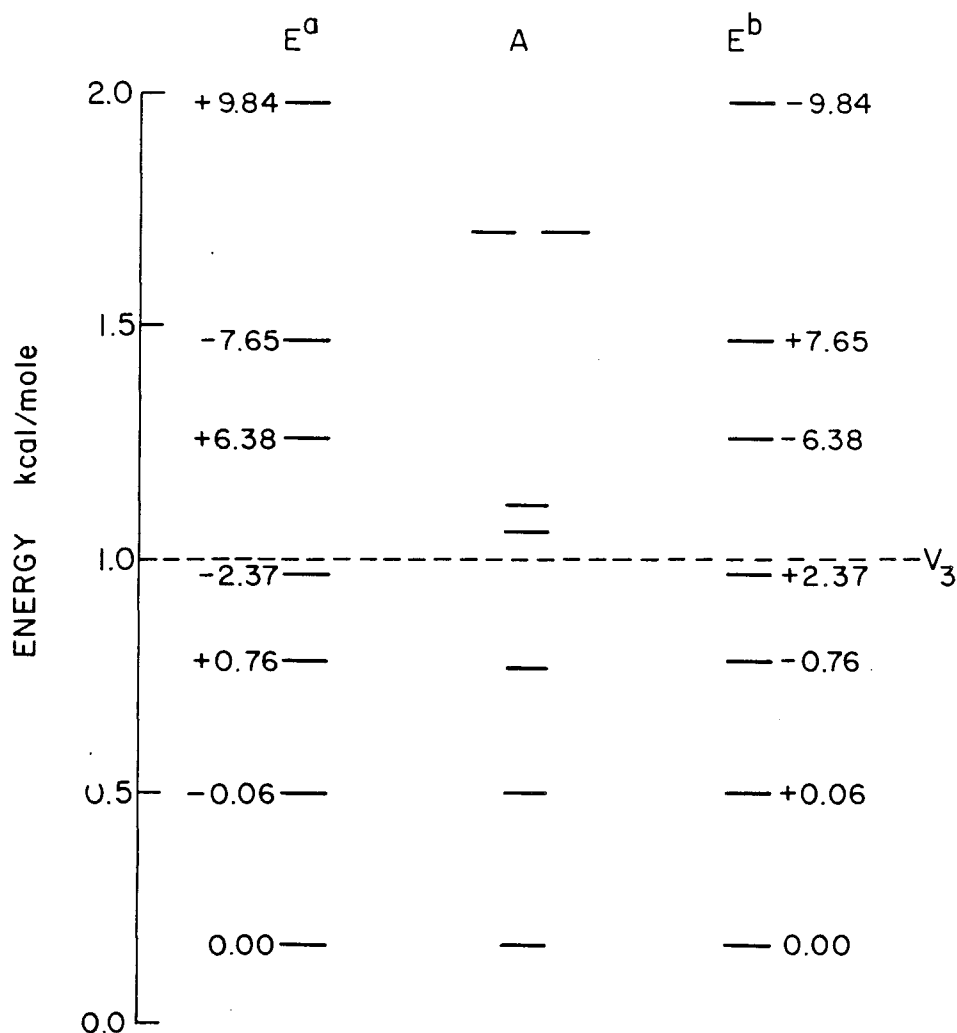
$$\Delta_i = e_i^E - e_i^A \quad (10.6)$$

where e_i^E and e_i^A are the energies of the E and A states, respectively, of the i^{th} torsional level. As seen in Figures II.3 and II.4, Δ_i alternates in sign from one torsional level to the next.

There are a variety of experimental observables which depend on the average energy difference between A and E states. For high barriers where the energy differences between torsional levels are much greater than the tunneling splittings, the average A-E energy difference may be equated to the average tunneling splitting ω_t . Assuming equilibrium with the lattice, the temperature dependent average tunneling splitting may be straightforwardly calculated from the Boltzmann distribution of populations [11]:

$$\omega_t(T) = \frac{\sum_i \Delta_i [\exp(-e_i^E/kT) + \exp(-e_i^A/kT)]}{\sum_j [\exp(-e_j^E/kT) + \exp(-e_j^A/kT)]} \quad (10.7)$$

The E and A states are weighted equally in Eq. (10.7) since they

ROTOR LEVELS FOR $V_3 = 1$ kcal/mole


XBL 812-8108

Figure II.4 Energy levels for a C_3 rotor with a 1 kcal/mole three-fold cosine barrier. Each level is labeled by its angular momentum expectation value. The A states are linear combinations of $+3n$ and $-3n$ levels and have zero average angular momentum. The three levels at ~ 0.2 kcal/mole comprise the zeroth torsional level; the three levels at 0.5 kcal/mole comprise the first torsional level, etc.

have the same degeneracy as is shown in section 10.3 where the spin-rotor coupling is discussed. Although equations of the form of Eq. (10.7) have been used extensively in the literature [11,12,13,14,15,16], there are important restrictions on its use as shown in Chapter 13, section 6.

An important feature of the methyl group dynamics is that transitions within a symmetry manifold (i.e., A_i to A_{i+1} , E_j^a to E_{j-1}^a , etc.) are much faster than transitions between different symmetries. The symmetry conserving transitions are caused by the rotor-phonon interaction which has A symmetry [17,18]. The transitions between symmetries are caused by the dipolar Hamiltonian which is much weaker [17]. The time scale for the symmetry conserving transitions is given by the correlation time τ_c for methyl group motion which at room temperature equals $\sim 10^{-12}$ - 10^{-11} sec. The time scale for the transitions between rotor symmetries is given by the spin-lattice relaxation time T_1 which at room temperature is ~ 1 -100 sec.

10.2 Spin Hamiltonian

10.2.1 Zeeman Hamiltonian

Using a three-spin Zeeman product basis $|\alpha\alpha\alpha\rangle$, $|\alpha\alpha\beta\rangle$, $|\beta\beta\alpha\rangle$, etc., the C_3 -symmetrized wave functions are:

$$|A_{+3/2}\rangle = |\alpha\alpha\alpha\rangle \quad (10.8a)$$

$$|A_{+1/2}\rangle = (|\alpha\alpha\beta\rangle + |\alpha\beta\alpha\rangle + |\beta\alpha\alpha\rangle)/\sqrt{3} \quad (10.8b)$$

$$|A_{-1/2}\rangle = (|\beta\beta\alpha\rangle + |\beta\alpha\beta\rangle + |\alpha\beta\beta\rangle)/\sqrt{3} \quad (10.8c)$$

$$|A_{-3/2}\rangle = |\beta\beta\beta\rangle \quad (10.8d)$$

$$|E_{+1/2}^a\rangle = (|\alpha\alpha\beta\rangle + \epsilon|\alpha\beta\alpha\rangle + \epsilon^*|\beta\alpha\alpha\rangle)/\sqrt{3} \quad (10.8e)$$

$$|E_{-1/2}^a\rangle = (|\beta\beta\alpha\rangle + \epsilon|\beta\alpha\beta\rangle + \epsilon^*|\alpha\beta\beta\rangle)/\sqrt{3} \quad (10.8f)$$

$$|E_{+1/2}^b\rangle = (|\alpha\alpha\beta\rangle + \epsilon^*|\alpha\beta\alpha\rangle + \epsilon|\beta\alpha\alpha\rangle)/\sqrt{3} \quad (10.8g)$$

$$|E_{-1/2}^b\rangle = (|\beta\beta\alpha\rangle + \epsilon^*|\beta\alpha\beta\rangle + \epsilon|\alpha\beta\beta\rangle)/\sqrt{3} \quad (10.8h)$$

Having defined the spin states, it is now possible to define the appropriate number operator corresponding to each term of the spin Hamiltonian.

The Zeeman Hamiltonian is:

$$\mathcal{H}_z = -\gamma\hbar H_0 I_z \quad (10.9)$$

where the magnetic field H_0 is taken to be along the z axis. The basis functions of Eqs. (10.8a)-(10.8h) are eigenfunctions of \mathcal{H}_z with

$$I = I_1 + I_2 + I_3 \quad , \quad (10.10a)$$

$$I_z = I_{z1} + I_{z2} + I_{z3} \quad , \quad (10.10b)$$

etc., for the methyl spins. The eigenvalues of \mathcal{H}_z are:

$$e_z = -\gamma\hbar H_0 m_z \quad (10.11)$$

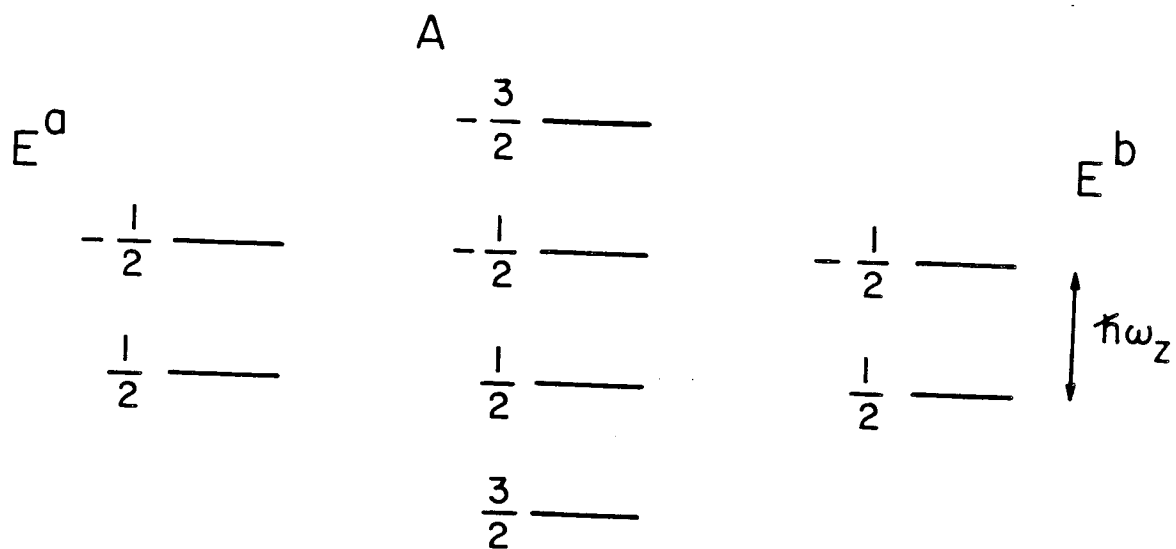
where m_z for the spins is distinguished from the m value defined for the rotor in the preceding section. The spin states in the presence of an external magnetic field appear as shown in Figure II.5.

Recalling that the number operators represent excess populations and are normalized, \hat{O}_1 is defined:

$$\hat{O}_1 = \sum_i m_{zi} \hat{n}_i / \sqrt{6} \quad (10.12)$$

where the \hat{n}_i are the population operators for the spin levels defined in Eq. (10.8). With $\omega_z = \gamma H_0$, it follows that

$$\mathcal{H}_z = -\hbar\omega_z \hat{O}_1 \quad . \quad (10.13)$$



XBL 812-8117

Figure II.5 The energy levels of the three protons of a methyl group considering only the Zeeman interaction. The levels are labeled by the component of spin angular momentum along the magnetic field axis. The C_3 -symmetrized wave functions are given in Eq. (10.8).

10.2.2 Dipolar Hamiltonian

The intramethyl dipolar Hamiltonian was written in Eq. (8.5) as the sum of two terms \mathcal{H}_D° and \mathcal{H}_D^{\prime} . Since \mathcal{H}_D° commutes with the Zeeman Hamiltonian \mathcal{H}_z , the wave functions of Eq. (10.8) are also eigenfunctions of \mathcal{H}_D° . \mathcal{H}_D^{\prime} which does not commute with \mathcal{H}_z or \mathcal{H}_D° is responsible for spin-lattice relaxation of the spin states.

The standard form of \mathcal{H}_D° is:

$$\mathcal{H}_D^{\circ} = \sum_i \sum_j D_{ij} [2I_{zi} I_{zj} - (I_i^+ I_j^- + I_i^- I_j^+)/2] \quad (10.14)$$

where the two summations are over the three protons of the methyl group. The factor D_{ij} is given by:

$$D_{ij} = \gamma^2 \hbar^2 P_2(\cos\beta_{ij})/r^3 \quad (10.15)$$

where r is the distance between each pair of spins of the methyl triangle, β_{ij} is the angle between the internuclear vector of spins i and j and the magnetic field, and $P_2(\cos\beta_{ij})$ is the second Legendre polynomial. Since the rotation rate of the methyl group is typically much greater than D_{ij} , an average dipolar coupling D may be factored out of Eq. (10.14) and the summations performed separately over the spin operators. Thus,

$$\mathcal{H}_D^{\circ} = D[2I_z^2 - (I^+ I^- + I^- I^+)/2] \quad (10.16)$$

where I_z is defined in Eq. (10.10b) and

$$I^+ = \sum_i I_i^+ \quad (10.17a)$$

$$I^- = \sum_i I_i^- \quad (10.17b)$$

From the definitions of the raising and lowering operators it follows straightforwardly that:

$$\mathcal{H}_D^{\circ} = D[3I_z^2 - I(I+1)] \quad (10.18)$$

where I is the magnitude of \tilde{I} . When the C_3 axis is parallel to the magnetic field, all of the internuclear vectors are perpendicular to the field, and D equals $\gamma^2 \hbar^2 / r^3$. For arbitrary angle θ between the C_3 axis and the field it is recognized that Eq. (10.18) transforms as the second-rank tensor T_0 so that

$$D = \gamma^2 \hbar^2 P_2(\cos\theta) / r^3 \quad (10.19)$$

Since the E^a and E^b spin states are equivalent to spin 1/2 particles, it is obvious from Eq. (10.18) that they can have no dipolar energy. On the other hand, the A spin states which are identical to a spin 3/2 particle are all shifted by \mathcal{H}_D° . By convention the number operator for the dipolar states is \hat{O}_5 and is defined:

$$\hat{O}_5 = [\hat{n}(A_{3/2}) + \hat{n}(A_{-3/2}) - \hat{n}(A_{1/2}) - \hat{n}(A_{-1/2})] / 2 \quad (10.20)$$

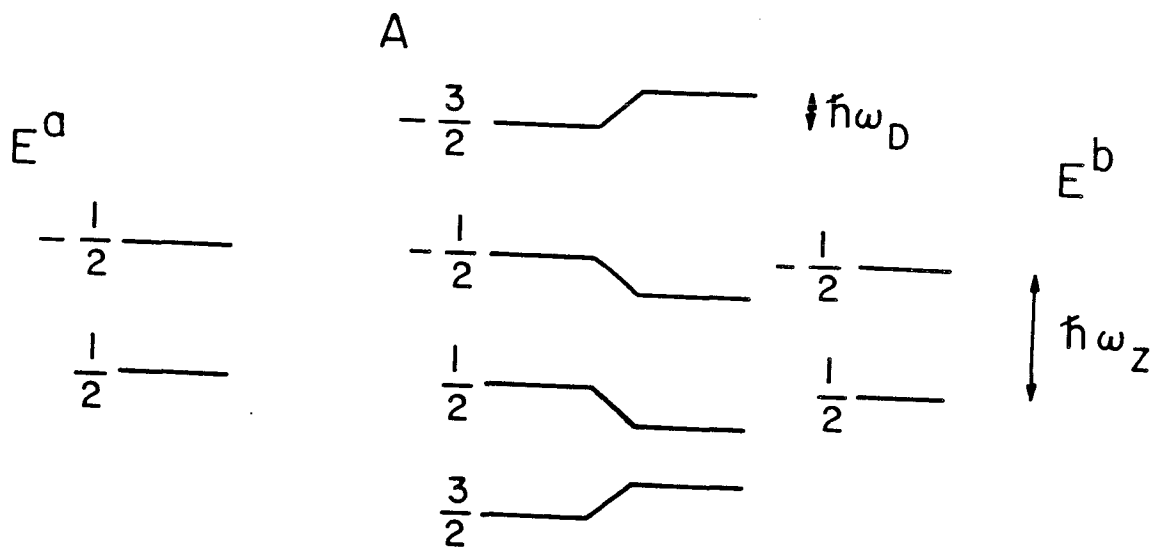
The secular dipolar Hamiltonian may now be written:

$$\mathcal{H}_D^{\circ} = \hbar \omega_D \hat{O}_5 \quad (10.21)$$

where

$$\hbar\omega_D = 3D \quad (10.22)$$

as defined by Eq. (10.18) and Figure II.6.



XBL 812-8118

Figure II.6 The energy levels of the three protons of a methyl group considering the Zeeman and intramethyl dipolar interactions. The intermethyl and non-methyl dipolar interactions may be viewed as broadening all of the levels.

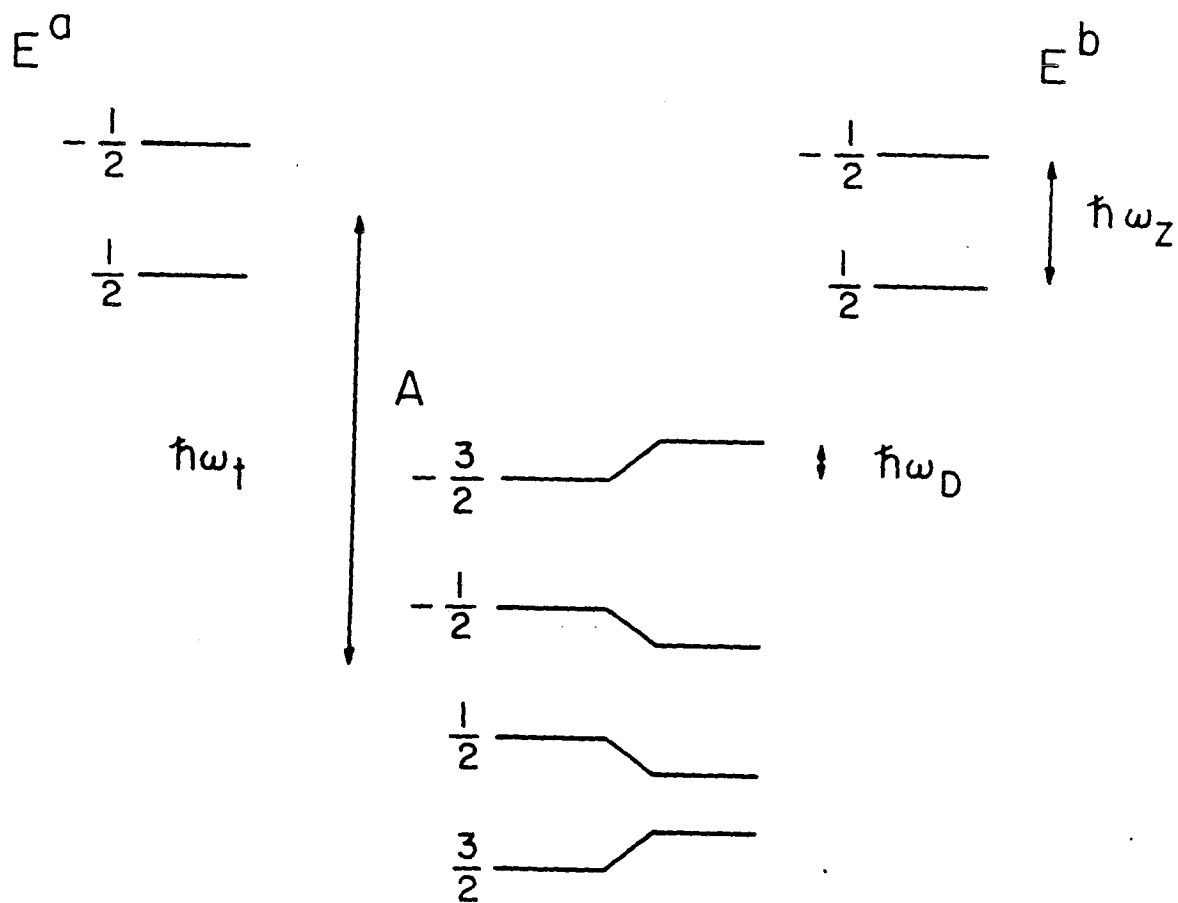
10.3 The Pauli Principle and the Tunneling System

Before closing this description of the methyl group it is necessary to consider the Pauli exclusion principle which introduces an important coupling between the spatial and spin wave functions. The Pauli principle requires that the total wave function change sign with every exchange of two protons since they are fermions. Since a C_3 rotation of the methyl group is exactly equivalent to two pair exchanges of the protons, the overall change in the wave functions is $(-1)(-1) = +1$. To insure, therefore, that the phase of the wave function remains unchanged under a C_3 rotation, it is necessary that the symmetries of the spatial and spin wave functions correlate to give A symmetry. Thus, the symmetries, in analogy with ortho and para hydrogen, couple as shown in Table II.2.

One important feature of Table II.2 is that E spin states correlate only with E rotor states and A spin states correlate only with A rotor states. This accounts for the equal weighting given to the E and A states in Eq. (10.7); there are two E spin doublets and one A spin quartet for each torsional level. It also follows from this coupling that the tunneling splitting ω_t may be associated directly with the spin states (similar to the exchange interaction and singlet and triplet electronic states discussed in Part I, section 2.4.1). That is, the wave functions associated with the E and A spin states are necessarily separated in energy by the tunneling splitting. This feature is shown in Figure II.7 and suggests the addition of the tunneling system \hat{O}_6 ,

Table II.2 Correlation of Spin and Rotor Symmetries

Spin	Rotor
A	A
E ^a	E ^b
E ^b	E ^a



XBL 812-8119

Figure II.7 The energy levels of the three protons of a methyl group considering the Zeeman, intramethyl dipolar, and tunneling interactions. The appearance of a tunneling energy in the spin Hamiltonian is a consequence of the Pauli exclusion principle which couples spin and rotor symmetries.

by convention, as another number operator:

$$\hat{O}_6 = [\sum_i \hat{n}_i(A) - \sum_j \hat{n}_j(E^a) - \sum_k \hat{n}_k(E^b)] / (2\sqrt{2}) \quad (10.23)$$

where the sums are over all the population operators of the specified symmetry. The tunneling energy is

$$\mathcal{H}_T = \hbar\omega_t \hat{O}_6 \quad (10.24)$$

The remaining number operators will be introduced in Chapter 11.

11. SPIN DIFFUSION AND SPIN-LATTICE RELAXATION

11.1 Symmetry Restricted Spin Diffusion [6,11,19,20]

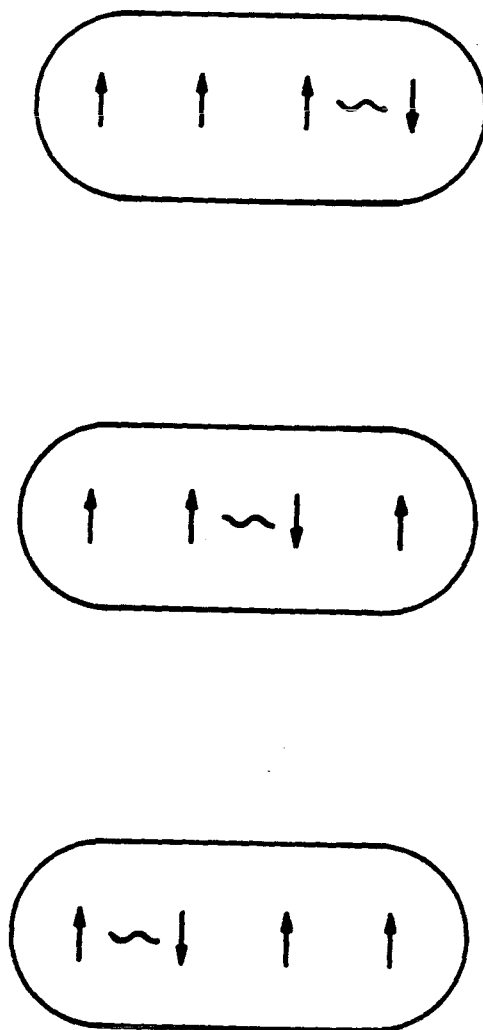
The intramethyl dipolar Hamiltonian was discussed in section 10.2.2. In this section the intermethyl (and non-methyl) dipolar Hamiltonian $\mathcal{H}_{D,inter}^c$ is introduced. As before, the dipolar Hamiltonian is separated into a secular and a non-secular part:

$$\mathcal{H}_{D,inter}^c = \mathcal{H}_{D,inter}^{\circ} + \mathcal{H}_{D,inter}^{\prime} \quad (11.1)$$

$\mathcal{H}_{D,inter}^{\circ}$ contains a term $I_{zi} I_{zj}$ which shifts energy levels and a flip-flop term $I_i^+ I_j^- + I_i^- I_j^+$ [see Eq. (10.14)] which is responsible for spin diffusion among the individual methyl groups and any other surrounding like spins. Spin diffusion propagates the magnetization throughout a crystal as shown in Figure II.8 and thereby establishes a uniform magnetization, or spin temperature [21]. When the spin system is prepared in a non-equilibrium state, spins in different motional or structural environments will, in general, relax at different rates. For protons in solids spin diffusion is typically four or five orders or magnitude faster than spin-lattice relaxation so that the assumption of a single Zeeman spin temperature within a crystal is valid during relaxation. This situation may be termed unrestricted spin diffusion, and it must be qualified when treating rapidly rotating methyl groups.

Unless the methyl group is very hindered, methyl group rotation is orders of magnitude faster than the dipolar interaction.

SPIN DIFFUSION



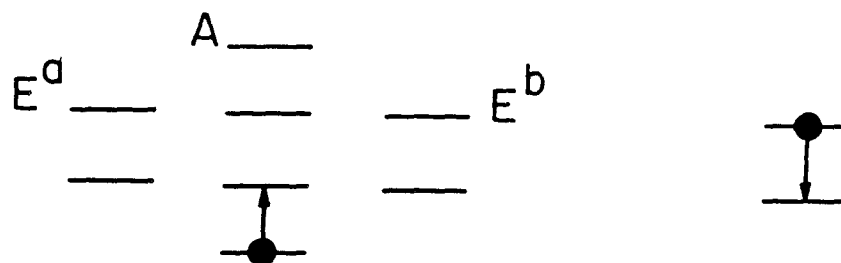
XBL 802-8350

Figure II.8 Propagation of spin magnetization by spin diffusion. For abundant protons the flip-flop terms of the dipolar Hamiltonian allow the magnetization to diffuse throughout a crystal and thereby establish a uniform Zeeman temperature. In the figure the pairwise flip-flop term propagates a $-1/2$ spin magnetization among a group of $+1/2$ spins.

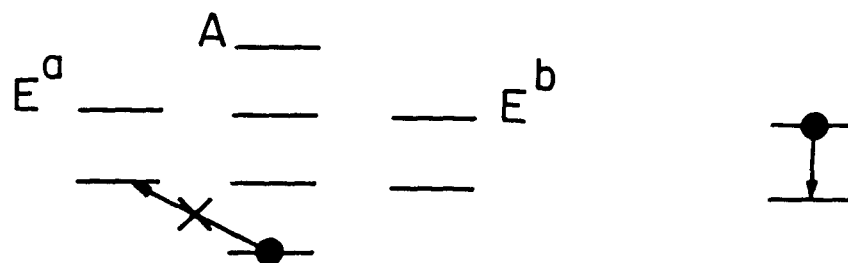
Hence, $\mathcal{H}_{D,inter}^{\circ}$ affects all three protons of a given methyl group in identical fashion. Alternately stated, spin diffusion operates as a totally symmetric interaction on the methyl group [6]. The importance of this fact is that spin diffusion, although affecting the magnetization of a particular methyl group, cannot change the symmetry state of the methyl group. This is indicated pictorially in Figure II.9. This situation is termed symmetry restricted spin diffusion (SRSD) [6,11,19,20], and as a consequence of it additional quasi-constants are present.

Symmetry restricted spin diffusion is discussed further in the next section. The non-secular interaction $\mathcal{H}_{D,inter}'$ which contributes to spin-lattice relaxation is treated in section 11.3.2.

(a) ALLOWED FLIP-FLOP



(b) FORBIDDEN FLIP-FLOP



XBL 812-8106

Figure II.9 Symmetry Restricted Spin Diffusion (SRSD). The average dipolar interaction between a rapidly rotating methyl group and an adjacent spin is totally symmetric [6]. Thus, it cannot change the methyl group symmetry. The symmetry-conserving flip-flop (a) is therefore allowed, and the symmetry-nonconserving flip-flop (b) is forbidden.

11.2 Rotational Polarization

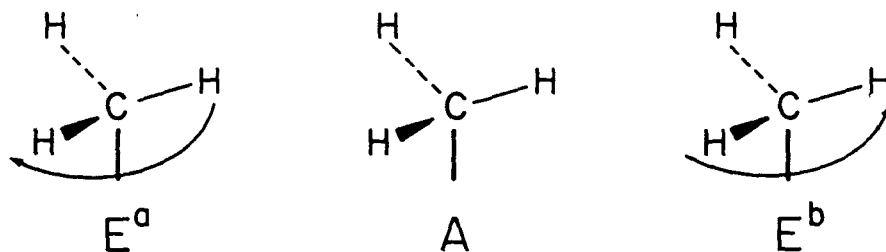
The rapid spin diffusion is the phenomenon responsible for bringing the initially prepared non-equilibrium spin system into a state of quasi-equilibrium. Spin diffusion maintains the Zeeman and dipolar polarizations as quasi-constants [22]. Since SRSD conserves the symmetry of each methyl group, there is now an additional one quasi-constant per methyl group. If each of these quasi-constants were distinct and coupled to the Zeeman subsystem, then the Zeeman relaxation would be extraordinarily complex. In fact, it is only necessary to add one more quasi-constant to the three previously defined. This is proven as a general result in section 11.3. For now this may be illustrated in simple fashion by considering an ensemble of equivalent methyl groups.

Since SRSD conserves the symmetries of the methyl groups, the population within each spin symmetry manifold (A , E^a , and E^b) is constant. Since the total number of methyl groups is a constant, there are two independent symmetry population variables which specify the ensemble [6]. One has already been defined in Eq. (10.23) as the tunneling system. Presently the remaining quasi-constant is defined as the difference between E^a and E^b spin populations and is termed the rotational polarization system \hat{O}_4 [6,11,19,20,23]:

$$\hat{O}_4 = [\sum_i \hat{n}_i(E^a) - \sum_j \hat{n}_j(E^b)] / 2 \quad (11.2)$$

where the sums are over all of the states within the specified symmetry. \hat{O}_4 is called rotational polarization, since for a hindered rotor the E^a and E^b spin states correlate with rotor states of opposite angular momentum within a given torsional level (see Figure II.10).

The complete set of number operators and their spin state eigenvalues are given in Table II.3.



NUCLEAR SPIN STATE	ROTATION
E^a	E^b
A	A (No Rotation)
E^b	E^a

XBL 802-8351

Figure II.10 Correlation of nuclear spin states with methyl group rotation. The spin and rotor symmetries are coupled as a consequence of the Pauli exclusion principle. Since within a given torsional level the E^a and E^b rotor states have opposite angular momenta and the A rotor state has no average angular momentum, then the E^a and E^b spin states may be associated with opposite senses of methyl group rotation.

Table II.3 Eigenvalues^a of the Number Operators^{b,c}

	$A_{3/2}$	$A_{1/2}$	$A_{-1/2}$	$A_{-3/2}$	$E_{1/2}^a$	$E_{-1/2}^a$	$E_{1/2}^b$	$E_{-1/2}^b$
$\sqrt{6} \hat{O}_1$	3/2	1/2	-1/2	-3/2	1/2	-1/2	1/2	-1/2
$\sqrt{2} \hat{O}_2$	1/2	-1/2	1/2	-1/2	-1/2	1/2	-1/2	1/2
$\sqrt{3} \hat{O}_3$	0	1	-1	0	-1/2	1/2	-1/2	1/2
\hat{O}_4	0	0	0	0	1/2	1/2	-1/2	-1/2
\hat{O}_5	1/2	-1/2	-1/2	1/2	0	0	0	0
$\sqrt{2} \hat{O}_6$	1/2	1/2	1/2	1/2	-1/2	-1/2	-1/2	-1/2
\hat{O}_7	0	0	0	0	1/2	-1/2	-1/2	1/2

^aThe eigenvalues are for the spin eigenstates of the Zeeman and secular dipolar Hamiltonians. At quasi-equilibrium all of the number operators are diagonal.

^bThe identity operator which may be taken as the eighth number operator is not needed since the total population of the spin states is a constant.

^cThis table is taken from reference 6.

11.3 Spin Lattice Relaxation

11.3.1 Independent Methyl Groups

Reiterating, the four quasi-constants of the methyl group spin system are:

$$\begin{aligned}\hat{O}_1 &= \text{Zeeman Magnetization} \\ \hat{O}_4 &= \text{Rotational Polarization} \\ \hat{O}_5 &= \text{Dipolar Order} \\ \hat{O}_6 &= \text{Tunneling Polarization.}\end{aligned}$$

The relevant quantity associated with each is its expectation value which at high temperature is given by Eq. (9.10):

$$\text{Tr } \hat{O}_k \hat{\rho} = \alpha_k \quad .$$

The object of the present section is to obtain the time-dependent solutions of [6]:

$$\dot{\tilde{\alpha}} = -\tilde{S} \cdot (\tilde{\alpha} - \tilde{\alpha}_{eq}) \quad (11.3)$$

where $\tilde{\alpha}$ is the vector of α_k 's with equilibrium value $\tilde{\alpha}_{eq}$ and \tilde{S} is the relaxation matrix.

It is assumed that the intramethyl non-secular dipolar interaction \mathcal{H}'_D dominates the spin-lattice relaxation to such an extent that $\mathcal{H}'_{D,inter}$ may be neglected. The basis for this is that the methyl groups are the only molecular groups undergoing rapid phonon-modulated motion in the samples studied. Furthermore, it is assumed that the intramethyl proton distance

is somewhat shorter than the distance between methyl and non-methyl protons [the relaxation efficiency falls off as $1/r^6$; see Eqs. (11.4a)-(11.5)]. In any event, it is extremely difficult to treat $\mathcal{J}'_{D,inter}$ analytically [24], and if necessary it can always be added on as a phenomenological contribution [25] to the relaxation equations developed in this and the following section.

The intramethyl relaxation rate constants for the α_k 's at high temperature are [6]:

$$S_{11}(\theta) = 2K (1+3 \cos^2\theta) \quad (11.4a)$$

$$S_{14}(\theta) = S_{41}(\theta) = 2\sqrt{6} K \cos\theta \quad (11.4b)$$

$$S_{44} = 3K \quad (11.4c)$$

$$S_{55} = 3K \quad (11.4d)$$

$$S_{56}(\theta) = S_{65}(\theta) = 3\sqrt{2} K P_2(\cos\theta) \quad (11.4e)$$

$$S_{66} = 6K \quad (11.4f)$$

where θ is the angle between the methyl group C_3 axis and the magnetic field and

$$K = (9/16) \hbar^2 \gamma^4 \tau_c / r^6 \quad (11.5)$$

where γ is the gyromagnetic ratio of the proton, τ_c is the correlation time for methyl group motion, and r is the intra-methyl proton-proton separation. No couplings exist at high temperature between α_1 , α_4 and α_5 , α_6 . Since only Zeeman relaxation (i.e., T_1) is studied in this work, α_5 and α_6 are dropped from further consideration. For convenience the following definitions are made:

$$M = \alpha_1 \quad (11.6a)$$

$$R = \alpha_4 \quad (11.6b)$$

where M represents the magnetization of the Zeeman states and R represents the rotational polarization.

The remaining problem is to obtain the quasi-constants for a system of inequivalent methyl groups. The correct quasi-constant for the Zeeman system follows straightforwardly from a consideration of spin diffusion. Restricting the discussion to two methyl groups and neglecting the coupling to the rotational polarization system, the Zeeman relaxation equations are:

$$\dot{\tilde{M}}_1 = -S_{11}(\theta_1)\tilde{M}_1 - V(\tilde{M}_1 - \tilde{M}_2) \quad (11.7a)$$

$$\dot{\tilde{M}}_2 = -S_{11}(\theta_2)\tilde{M}_2 - V(\tilde{M}_2 - \tilde{M}_1) \quad (11.7b)$$

where

$$\tilde{M} = M - M_{eq} \quad (11.8)$$

and V is the spin diffusion interaction which serves to equalize the two magnetizations (see Figure II.13a). Writing Eqs. (11.7a) and (11.7b) in matrix form:

$$\begin{pmatrix} \dot{\tilde{M}}_1 \\ \dot{\tilde{M}}_2 \end{pmatrix} = - \begin{pmatrix} S_{11}(\theta_1) + V & -V \\ -V & S_{11}(\theta_2) + V \end{pmatrix} \begin{pmatrix} \tilde{M}_1 \\ \tilde{M}_2 \end{pmatrix} \quad (11.9)$$

and rotating the relaxation matrix by 45° , the following equation is obtained:

$$\begin{pmatrix} \dot{\tilde{M}}_1 + \dot{\tilde{M}}_2 \\ \dot{\tilde{M}}_1 - \dot{\tilde{M}}_2 \end{pmatrix} = - \begin{pmatrix} S_{11} & [S_{11}(\theta_1) - S_{11}(\theta_2)]/2 \\ [S_{11}(\theta_1) - S_{11}(\theta_2)]/2 & S_{11} + 2V \end{pmatrix} \begin{pmatrix} \tilde{M}_1 + \tilde{M}_2 \\ \tilde{M}_1 - \tilde{M}_2 \end{pmatrix} \quad (11.10)$$

where S_{11} is the average of the two rate constants $S_{11}(\theta_1)$ and $S_{11}(\theta_2)$. Since $V \gg S_{11}$, spin diffusion drives the Zeeman difference $(\tilde{M}_1 - \tilde{M}_2)$ to zero long before the sum $(\tilde{M}_1 + \tilde{M}_2)$ relaxes. Hence, $(\tilde{M}_1 - \tilde{M}_2)$ may be dropped, and the quasi-equilibrium state is described by the quasi-constant $(\tilde{M}_1 + \tilde{M}_2)$. It follows that for N methyl groups the appropriate Zeeman quasi-constant is:

$$\tilde{M} = \sum_i^N \tilde{M}_i \quad (11.11)$$

with the auto-relaxation rate constant

$$S_{11} = \sum_i^N S_{11}(\theta_i)/N \quad (11.12)$$

Any non-methyl protons may be simply added onto the above sums with N being redefined to include all of the protons.

Because there is no mechanism comparable to spin diffusion to transfer rotation polarization among all of the methyl groups, rotational polarization is more difficult to treat than the Zeeman system. Nevertheless, there is only one rotational polarization quasi-constant which couples to the Zeeman system. The relaxation equations and results are stated in this section with the derivation being given in Appendix D.

Having defined the Zeeman quasi-constant \tilde{M} in Eq. (11.11), the relaxation matrix S is now asymmetric. The reason is that the rotational polarization R_i of an individual methyl group couples to \tilde{M} as before, but only $1/N$ of \tilde{M} couples to R_i .

Thus,

$$\begin{pmatrix} \dot{\tilde{M}}/M_{eq} \\ \dot{R}_1/M_{eq} \\ \dot{R}_2/M_{eq} \\ \vdots \\ \vdots \\ \vdots \end{pmatrix} = - \begin{pmatrix} S_{11} & S_{14}(\theta_1) & S_{14}(\theta_2) & \cdots \\ S_{14}(\theta_1)/N & S_{44} & 0 & \cdots \\ S_{14}(\theta_2)/N & 0 & S_{44} & \cdots \\ \vdots & \vdots & \vdots & \vdots \\ \vdots & \vdots & \vdots & \cdots \\ \vdots & \vdots & \vdots & \vdots \end{pmatrix} \begin{pmatrix} \tilde{M}/M_{eq} \\ R_1/M_{eq} \\ R_2/M_{eq} \\ \vdots \\ \vdots \\ \vdots \end{pmatrix} \quad (11.13)$$

where M_{eq} , the equilibrium value of \tilde{M} , has been introduced as a normalization factor. Eq. (11.13) could be diagonalized by standard techniques, but for N methyl groups the relaxation matrix is $(N+1) \times (N+1)$, and the general solution is intractable. However, by considering the determinant

$\det(S-\lambda I)$ for the eigenvalue problem, it is easily seen that as long as S_{44} is independent of angle (i.e., at high temperature), there will be $N-1$ eigenvectors with relaxation rate S_{44} which are not coupled to the Zeeman system. The remaining two eigenvectors result in a Zeeman relaxation characterized by two quasi-constants so that the relaxation is bi-exponential [6,23,25]. The relaxation rates λ_1 , λ_2 and eigenvectors are derived in Appendix D and given in References 23 and 25:

$$\lambda_{1,2} = (S_{11}+S_{44})/2 \pm \frac{1}{2} [(S_{11}-S_{44})^2 + 4 S_{14}^2]^{1/2} \quad (11.14)$$

where

$$S_{14}^2 = \sum_i^N S_{14}^2(\theta_i)/N \quad (11.15)$$

The required rotational polarization quasi-constant is [6,25]:

$$P_r(t) = \sum_i^N \cos(\theta_i) R_i(t) \quad (11.16)$$

resulting in the following relaxation equations:

$$\tilde{M}(t)/M_{eq} = C_1 \exp(-\lambda_1 t) + C_2 \exp(-\lambda_2 t) \quad (11.17a)$$

and

$$2\sqrt{6} K P_r(t)/M_{eq} = (\lambda_1 - S_{11}) C_1 \exp(-\lambda_1 t) + (\lambda_2 - S_{11}) C_2 \exp(-\lambda_2 t) \quad (11.17b)$$

where

$$C_1 = [(S_{11} - \lambda_2) \tilde{M}(0) - 2\sqrt{6} K P_r(0)] / [(\lambda_1 - \lambda_2) M_{eq}] \quad (11.18a)$$

and

$$C_2 = [\tilde{M}(0) - C_1] / M_{eq} \quad (11.18b)$$

The importance of the above equations is that the Zeeman relaxation is dynamically coupled to the rotational polarization of the spin states, and, therefore, through the Pauli principle it is dynamically coupled to the rotor states. There are some interesting consequences of this coupling which relate to the angular momentum which the E^a , E^b rotor states possess. One such consequence is the possibility of measuring the methyl group magnetic moment in the solid state (see section 13.2). Another is the ability to detect gearing between methyl groups which is discussed in the following section and also in section 13.3.

11.3.2 Coupled Methyl Groups

A question of long standing interest is whether or not two adjacent methyl groups rotate together as two clogged gears [26,27,28,29]. If they do, that behavior should have a marked effect on rotational polarization as will now be shown.

Consider two methyl groups geared together in a perfectly classical fashion. Since they are constrained to rotate at the same speed, they must be in the same torsional level. And since they must have opposite angular momenta, they necessarily

form an $E^a E^b$ rotor pair as shown in Figure II.11. Complete gearing, therefore, prevents the formation of a non-zero rotational polarization. However, since it is the projection of rotational polarization along the magnetic field axis [see Eq. (11.16)] that is important, the rotational polarization system may still couple to the Zeeman system as shown in Figure II.12.

The gearing interaction is accounted for in a manner analogous to the treatment of spin diffusion. That is, defining W as the gearing interaction and ignoring for the moment the coupling to the Zeeman system, the relaxation equations for the rotational polarizations of two adjacent methyl groups are [compare Eqs. (11.7a) and (11.7b)]:

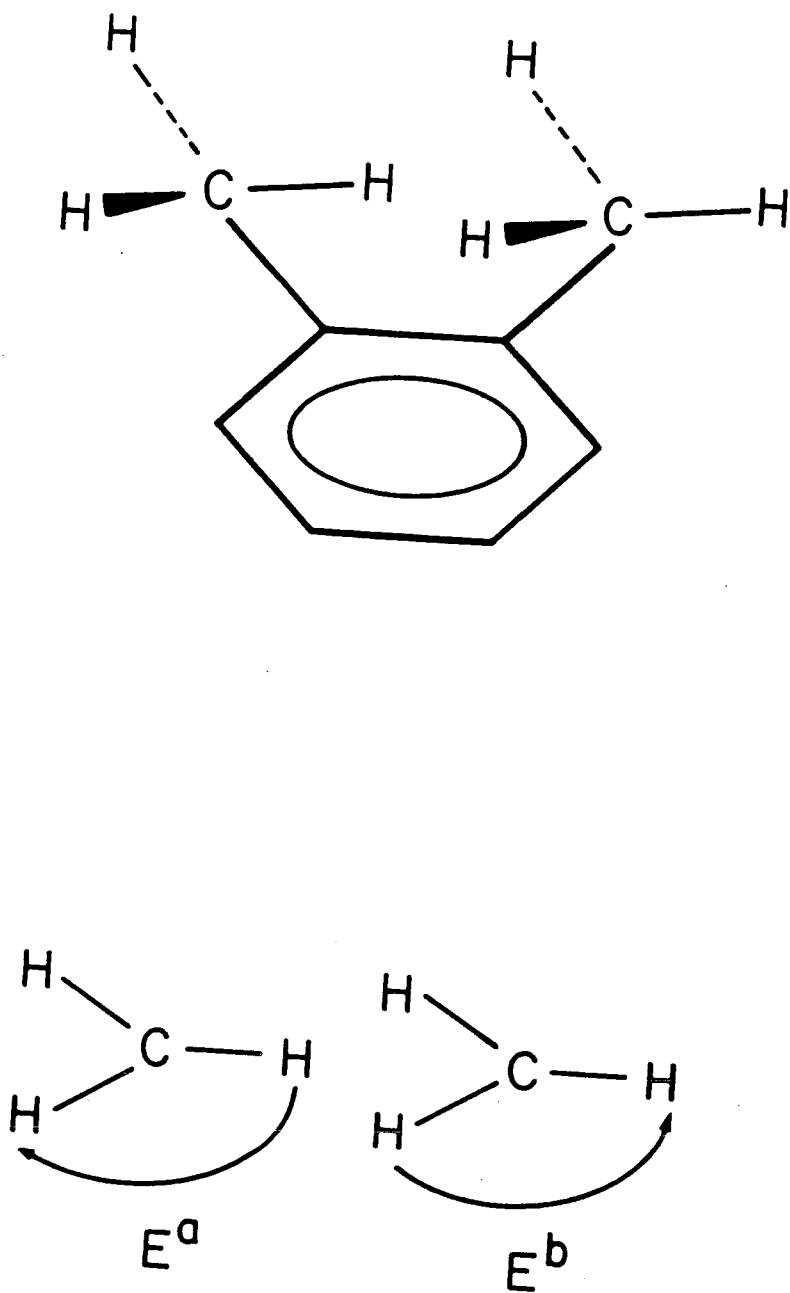
$$\dot{R}_1 = -S_{44}R_1 - W(R_1 + R_2) \quad (11.19a)$$

$$\dot{R}_2 = -S_{44}R_2 - W(R_1 + R_2) \quad (11.19b)$$

where, in contrast to spin diffusion, W causes the sum of the polarizations rather than the differences to go to zero. This is illustrated in Figure II.13.

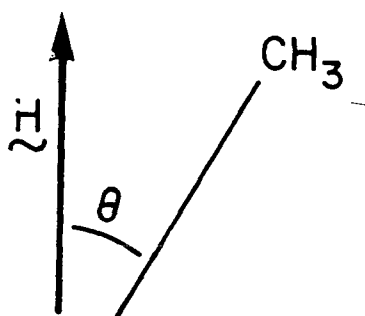
With Eqs. (11.19a) and (11.19b) and the Zeeman system the complete relaxation equation for two adjacent methyl groups is:

$$\begin{pmatrix} \dot{\tilde{M}} \\ \dot{R}_1 \\ \dot{R}_2 \end{pmatrix} = - \begin{pmatrix} S_{11} & S_{14}(\theta_1) & S_{14}(\theta_2) \\ S_{14}(\theta_1)/2 & S_{44}+W & W \\ S_{14}(\theta_2)/2 & W & S_{44}+W \end{pmatrix} \begin{pmatrix} \tilde{M} \\ R_1 \\ R_2 \end{pmatrix} \quad (11.20)$$

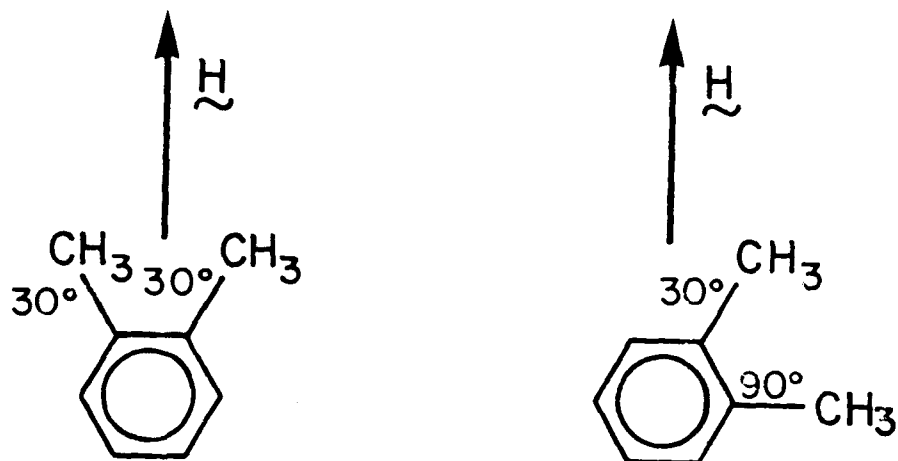


XBL 802-8346

Figure II.11 Cancellation of rotational polarization for geared methyl groups.



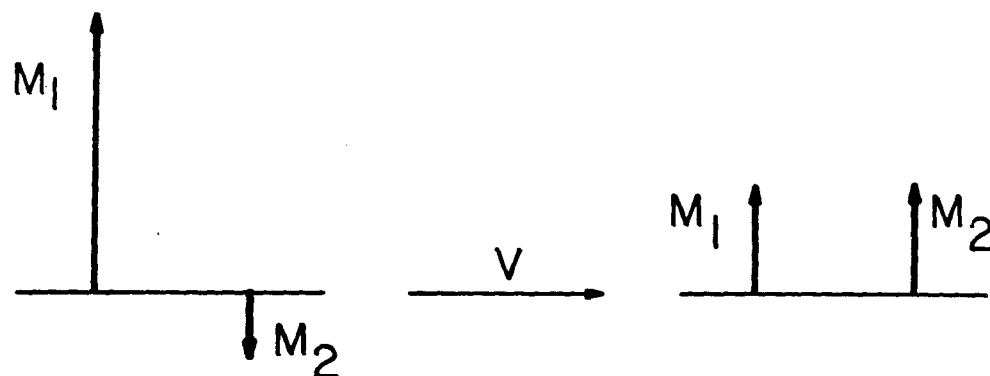
ZEEMAN TO ROTATIONAL POLARIZATION $\sim \cos\theta$



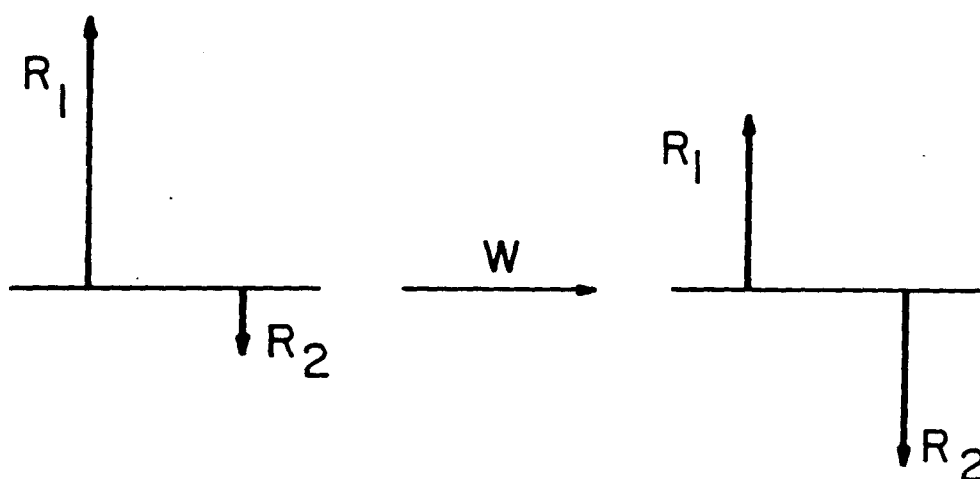
XBL 802-8349

Figure II.12 Angular dependence of the net rotational polarization of two geared methyl groups. Because of the $\cos\theta$ dependence of the Zeeman to rotational polarization coupling, it is the magnetic field projection of the rotational polarization which is a quasi-constant. Thus, if the methyl groups are geared, the xylene molecule on the left will exhibit no rotational polarization, but the molecule on the right will.

(a) SPIN DIFFUSION (FLIP-FLOP)



(b) STERIC INTERACTION



XBL 813-8357

Figure II.13 Comparison of the effects of spin diffusion and steric interaction on two adjacent methyl groups. (a) The spin diffusion causes the difference in the two Zeeman magnetizations to go to zero. (b) The steric interaction causes two adjacent methyl groups to rotate in opposite directions, and the sum of rotational polarizations goes to zero.

The rotational polarizations are rotated by 45° to obtain:

$$\begin{pmatrix} \dot{\tilde{M}} \\ \dot{R}_1 - \dot{R}_2 \\ \dot{R}_1 + \dot{R}_2 \end{pmatrix} = - \begin{pmatrix} S_{11} & [S_{14}(\theta_1) - S_{14}(\theta_2)]/2 & [S_{14}(\theta_1) + S_{14}(\theta_2)]/2 \\ [S_{14}(\theta_1) - S_{14}(\theta_2)]/2 & S_{44} & 0 \\ [S_{14}(\theta_1) + S_{14}(\theta_2)]/2 & 0 & S_{44} + 2W \end{pmatrix} \times \begin{pmatrix} \tilde{M} \\ R_1 - R_2 \\ R_1 + R_2 \end{pmatrix} . \quad (11.21)$$

The case of $W = 0$ was treated in section 11.2 where it was shown that the Zeeman relaxation is described by two exponentials. For arbitrary W the solution of Eq. (11.21) has two quasi-constants coupled to the Zeeman system so that the relaxation is tri-exponential (see the computer program "couple.c" in Appendix E). If the two methyl groups are strongly geared, then $W \gg S_{11}, S_{44}$ and the sum $(R_1 + R_2)$ goes rapidly to zero leaving a quasi-equilibrium state described (ignoring the dipolar and tunneling systems) by \tilde{M} and the difference $(R_1 - R_2)$.

Thus, in the limit of large W , (R_1+R_2) may be dropped and the following relaxation matrix obtained for N methyl groups:

$$\begin{pmatrix} \dot{M}/M_{eq} \\ (\dot{R}_1 - \dot{R}_2)/M_{eq} \\ (\dot{R}_3 - \dot{R}_4)/M_{eq} \\ \vdots \\ \vdots \end{pmatrix} = - \begin{pmatrix} S_{11} & [S_{14}(\theta_1) - S_{14}(\theta_2)]/2 & [S_{14}(\theta_3) - S_{14}(\theta_4)]/2 \dots \\ [S_{14}(\theta_1) - S_{14}(\theta_2)]/N & S_{44} & 0 & \dots \\ [S_{14}(\theta_3) - S_{14}(\theta_4)]/N & 0 & S_{44} & \dots \\ \vdots & & & \\ \vdots & & & \end{pmatrix} \times \begin{pmatrix} \tilde{M}/M_{eq} \\ (R_1 - R_2)/M_{eq} \\ (R_3 - R_4)/M_{eq} \\ \vdots \\ \vdots \end{pmatrix}$$

(11.22)

where the normalization M_{eq} has been included, and the methyl groups interact sterically in isolated pairs: (R_1-R_2) , (R_3-R_4) , (R_5-R_6) , etc. Eq. (11.22) is of exactly the same form as Eq. (11.13) and may be solved by the techniques outlined in Appendix D. Following this procedure a bi-exponential solution is obtained with relaxation rate constants:

$$\lambda'_{1,2} = (S_{11} + S_{44})/2 \pm \frac{1}{2} [(S_{11} - S_{44})^2 + 4 S_{14}^2]^{1/2} \quad (11.23)$$

where

$$S_{14}^2 = \sum_{i=1,3,5,\dots}^{N-1} [S_{14}(\theta_i) - S_{14}(\theta_{i+1})]^2 / (2N) \quad (11.24)$$

The new rotational polarization quasi-constant is defined to be:

$$Q_r(t) = \sum_{i=1,3,5,\dots}^{N-1} [\cos(\theta_i) - \cos(\theta_{i+1})] [R_i(t) - R_{i+1}(t)] / 2, \quad (11.25)$$

resulting in the following relaxation equations:

$$\tilde{M}(t)/M_{eq} = C'_1 \exp(-\lambda'_1 t) + C'_2 \exp(-\lambda'_2 t) \quad (11.26a)$$

and

$$2\sqrt{6} K Q_r(t)/M_{eq} = (\lambda'_1 - S_{11}) C'_1 \exp(-\lambda'_1 t) + (\lambda'_2 - S_{11}) C'_2 \exp(-\lambda'_2 t) \quad (11.26b)$$

where

$$C'_1 = [(S_{11} - \lambda'_2) \tilde{M}(0) - 2\sqrt{6} K Q_r(0)] / [(\lambda'_1 - \lambda'_2) M_{eq}] \quad (11.27a)$$

and

$$C_2' = [\tilde{M}(0) - C_1'] / M_{eq} \quad . \quad (11.27b)$$

Eqs. (11.22)-(11.27b) should be compared with the analogous Eqs. (11.13)-(11.18b) for independent methyl groups. The critical factors which distinguish the two sets of equations are the cross-relaxation terms S_{14}^2 and $S_{14}'^2$ and the associated quasi-constants $P_r(t)$ and $Q_r(t)$, respectively.

One problem that arises in considering strongly interacting methyl groups is that the adjacent methyl groups may contribute significantly to one another's relaxation. This can be accounted for as follows. If the methyl groups do not exert a strong gearing interaction W on one another, it is unlikely that at high temperature the individual protons (i.e., the gear teeth) can remain in registry with one another for periods of time comparable to $1/\mathcal{H}_{D,inter}^c$ [29]. Consequently, $\mathcal{H}_{D,inter}^c$ is averaged over the methyl protons and contributes predominantly to symmetry conserving transitions. Defining this contribution to be Δ_{11} :

$$S_{11}' = S_{11} + \Delta_{11} \quad . \quad (11.28)$$

On the other hand, if the gearing is very strong, $\mathcal{H}_{D,inter}^c$ will not be averaged over the methyl protons, and it will cause $E^a \rightarrow E^b$ transitions. [Actually, such transitions are implicitly assumed in W , Eqs. (11.19a) and (11.19b)]. Defining this contribution to be Δ_{44} :

$$S'_{44} = S_{44} + \Delta_{44} \quad . \quad (11.29)$$

There is no reason for $\mathcal{K}_{D,inter}$ to affect S_{14} [25]. Estimates of Δ_{11} and Δ_{44} may be obtained by semi-empirical considerations (see section 13.5.1). Since $\mathcal{K}_{D,inter}$ may contribute to relaxation whether there is steric interaction or not, S'_{11} and S'_{44} may be used in the treatment of either independent or coupled methyl groups [25].

Although bi-exponential relaxation is predicted for either extreme of no gearing or large gearing, all three measurable quantities λ_1 , λ_2 , and C_1 (or λ'_1 , λ'_2 , and C'_1) differ in the two cases. Results of experiments on molecules containing methyl groups of varying degrees of steric interaction are presented in section 13.5.

12. EXPERIMENTAL DETAILS

12.1 Samples

All experiments were performed on powder samples except for some studies which were done on single crystals of durene (1,2,4,5-tetramethylbenzene) and 2,3-dimethylmaleicanhydride. Methyl iodide (CH_3I) was studied at -105°C and -150°C . Since it froze suddenly at -80°C (published M.P. = -66.5°C [30]), it presumably did not form a glass. The methyl iodide was typically cooled over a period of 1 to 2 hours.

Several experiments were performed using single crystals of 2,3-dimethylmaleicanhydride. All of the single crystals contained 10% of perdeuterated molecules. The level of deuteration was 98% so that any CH_2D , which might have significantly different relaxation properties [31] than CH_3 , was very dilute. The deuterium quadrupole splitting of the rapidly rotating CD_3 depends only on the angle between the C_3 axis and the magnetic field. Hence, it was hoped that the deuterium NMR spectrum could be used to orient the single crystal and thereby obtain the angular dependence of rotational polarization. This had to be abandoned, however, due to the complexity of the deuterium spectrum. The spectrum appeared to contain eight pairs of lines (i.e., eight methyl orientations, thus, four molecules per unit cell) although the signal to noise precluded saying this with great certainty.

The advantage of using a single crystal is that spin diffusion is effective over the entire sample. For a powder

the separation of the crystallites prevents effective spin diffusion, and the crystallites relax independently. Thus, there may be multiple spin temperatures and a markedly non-exponential relaxation curve for the powder. However, if there are multiple methyl group orientations per unit cell, the relaxation is relatively isotropic with little difference between powder and crystal. This probably explains the success of Emid in applying SRSD theory to powders [11,23,25]. As shown in section 13.3, however, the powder and single crystal of 2,3-dimethylmaleicanhydride have different temperature dependences.

The powder samples were pressed into pellets 6 mm in diameter and 6 mm in length. The single crystals were approximately the same size. The solids were inserted into 8 mm glass tubes and held in place with teflon plugs. The CH_3I was degassed and sealed in an 8 mm tube.

Syntheses for those samples which are not commercially available are described in Appendix F. Also contained in Appendix F are the details of the single crystal preparation.

12.2 Signal to Noise

All of the measurements reported in this work are basically intensity measurements. Consequently, the critical experimental parameters were signal to noise and spectrometer linearity (linearity is discussed separately under each spectrometer). Linewidth was a minimal concern except for the unsuccessful crystal alignment by deuterium NMR where the field was shimmed to give a 1 ppm linewidth for H_2O .

Very little could be done to improve signal to noise other than signal averaging. The proton signals were large, but fluctuations in electronics and ambient noise picked up by the probe were not negligible. Signal averaging was made difficult by the very feature which is of interest in this work: rotational polarization. Ordinarily, the recycle delay between measurements is one T_1 . Furthermore, the relaxation is generally independent of recycle delay if the spin system is saturated at the start of each cycle. Since rotational polarization is a separate quasi-constant, it is not removed by saturating the Zeeman spin system. In fact, it is unaffected if the saturation time is much less than S_{14} . Consequently, the rotational polarization must be allowed to relax to a negligible level between measurements. The rotational polarization lifetime, or $1/e$ decay time, was generally two to four times as long as T_1 . Allowing four lifetimes, two to three minutes was typically required for each measurement. With fifteen different time values for a given relaxation experiment, it was prohibitive to average more than about 10 times. This

was generally sufficient to obtain S/N of 50 or better.

Since the proton spectrum was a single Gaussian of 30 to 50 KHz linewidth, it was unnecessary to Fourier transform the FID's. Typically, each FID was averaged and then integrated (after linearity correction if necessary), allowing 15 μ sec deadtime after the detection pulse.

12.3 106 MHz Spectrometer

12.3.1 Magnet

The spectrometer is based around a Westinghouse 24.4 kGauss superconducting magnet with 2.5 inch bore. Although the magnet is low resolution, in all cases the homogeneous linewidths were much greater than any inhomogeneous broadening.

12.3.2 Pulse Generation

The proton RF is generated by mixing the 30 MHz LO from a General Radio 1164-A frequency synthesizer with 136 MHz (generated by doubling 68 MHz output by the same synthesizer) and keeping the lower sideband. The RF is gated by a 16-step home-built pulse programmer. After various stages of intermediate amplification the pulse is finally amplified to 200 watts with a class C tuned transmitter built from a Millen ham radio kit. 90° pulse lengths are 1 to 1.25 μ sec, thus, providing sufficient spectral width to cover the proton spectrum.

12.3.3 Probe

The probe uses a simple coil-and-capacitor tank circuit (see Figure II.14a) with a Q of \sim 150 at 106.2 MHz. The coil is 8 turns of 18 gauge bare copper wire and has a diameter of 8 mm and length of 1.5 cm. The coil is mounted on a teflon block (\sim 2.25" diameter) and covered with a glass dewar for thermal insulation.

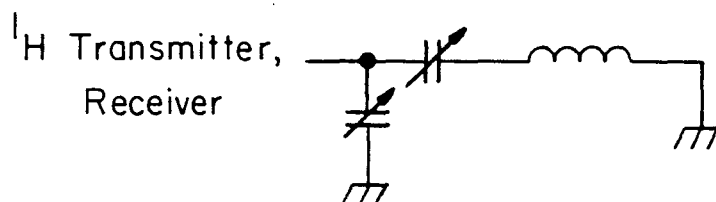
Temperature control is achieved by regulating the flow and temperature of cold N_2 or warm air over the sample. Before reaching the sample the input gas flows over a small coil of Advance wire which is heated by a voltage proportional current source. A copper/constantan thermocouple is read by a nanovoltmeter which outputs a differential voltage to drive the current source. By calibrating the nanovoltmeter with a digital thermometer, the temperature may be regulated to within $\pm 0.1^\circ\text{C}$ over the range -170°C to 80°C .

The sample mount is similar to that shown in Figure II.15. The sample is mounted in the larger of a pair of two-to-one 90° bevel gears. The shaft of the smaller gear is attached to a flexible cable external to the probe which allows manual rotation of the sample: 180° in ~ 1 sec.

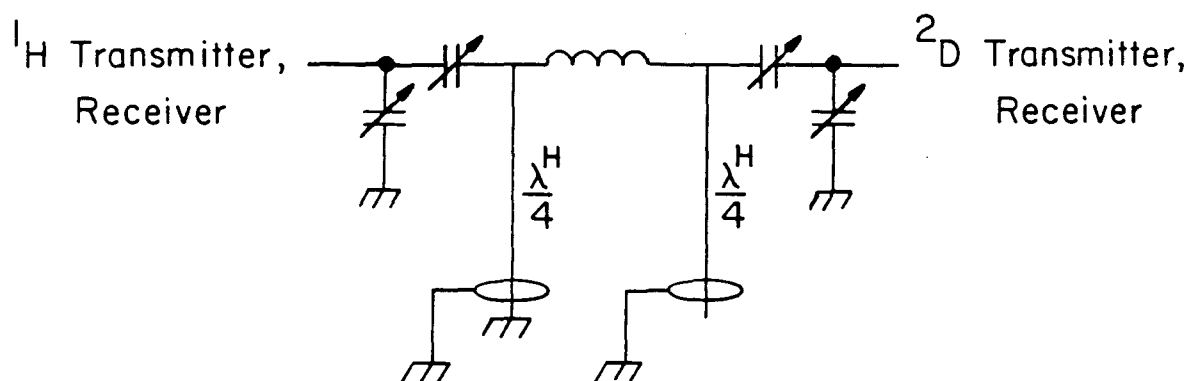
12.3.4 Receiver

The proton receiver has two stages of amplification: a wideband low noise preamplifier (Avantek UTO-511, UA-102, UA-103 cascade) with 34 dB gain and a 30 MHz low noise IF amplifier with 43 dB gain. The IF amp is home-built and is based on a cascaded pair of Siliconix E420 dual J-FET's [32]. Between the wideband and IF amplifiers the NMR signal is mixed down to 30 MHz and then attenuated to avoid saturating the IF amp. The output of the IF amp is split by a 0° - 90° tee to allow quadrature detection. The two phases are each mixed with 30 MHz and one is selected to be digitized.

(a) SINGLE-TUNED PROBE



(b) DOUBLE-TUNED PROBE

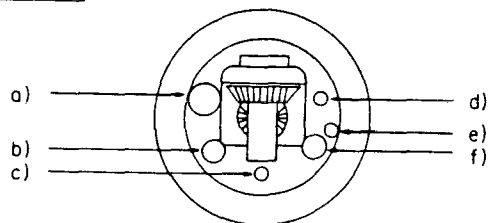


XBL 812-8109

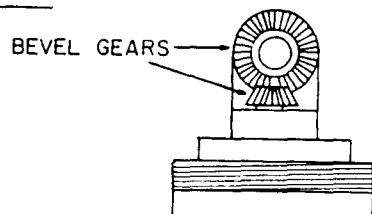
Figure II.14 Single and double-tuned probe circuits. λ^H is the wavelength corresponding to the proton Larmor frequency; λ^H is corrected for the reduced velocity ($0.7c$) of an electromagnetic wave in a solid coaxial cable.

PROBE HEAD AND SAMPLE MOUNT

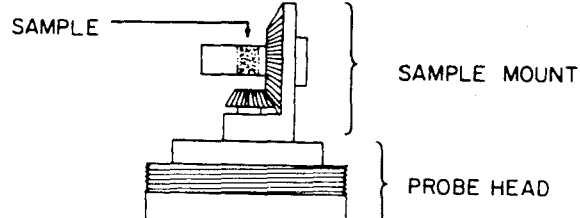
TOP VIEW



FRONT



SIDE



SCALE \longleftarrow 2" \longrightarrow

XBL 812-8128

Figure II.15 Probe head and sample mount. The probe head is made of glass-impregnated teflon, and the sample mount is aluminum with a teflon sleeve. The probe head is threaded for attaching a bell jar dewar. The labeled openings are for a) gas transfer line, b) grounded $\lambda^H/4$ stub, c) proton capacitor, d) deuterium capacitor, e) copper/constantan thermocouple, and f) open $\lambda^H/4$ stub. The straight bevel gears are brass and have a 32 pitch; the larger gear is 1" in diameter with 32 teeth, and the smaller is 1/2" in diameter with 16 teeth.

The maximum gain of the receiver is greater than 60 dB. With 25 dB attenuation before the IF amp, the spectrometer is linear to within 2% over a range of input signals from 0.6 μ Vrms to 0.6 mVrms. The linearity of the IF amp over this range could not be matched by two commercial IF amps (RHG EVT-3010's) that were tried. Error from non-linearity was less than or equal to the statistical errors generally present.

12.3.5 Digitizer

The audio signal is digitized by an 8 bit Biomation Transient Recorder Model 802. The maximum digitization rate is 1000 points in 500 μ sec which is more than sufficient for solid state proton spectra.

Typical audio signals ranged from 1 to 100 mVpp.

12.4 185 MHz Spectrometer

12.4.1 Magnet

The magnet is a Bruker 42.5 kGauss superconducting magnet with 3.5 inch bore. The magnet has both superconducting and room temperature shims and was shimmed to a 1 ppm H₂O linewidth for the experiments.

12.4.2 Pulse Generation

The RF and LO generation is very similar to that previously described (section 12.3.2). The 30 MHz LO is generated by tripling the 10 MHz output of a General Radio 1061 frequency synthesizer. 155 MHz from the same synthesizer is mixed with the 30 MHz, and the upper sideband kept. After various stages of intermediate amplification the 185 MHz is gained up to 200 watts with a class C cavity-tuned transmitter built from a Millen ham radio kit.

The pulse is gated with a 16-step home-built pulse programmer which can be loaded and run under computer control (a NOVA 820 computer is used). 90° pulses were typically around 5 μsec long which provided adequate spectral width.

12.4.3 Probe

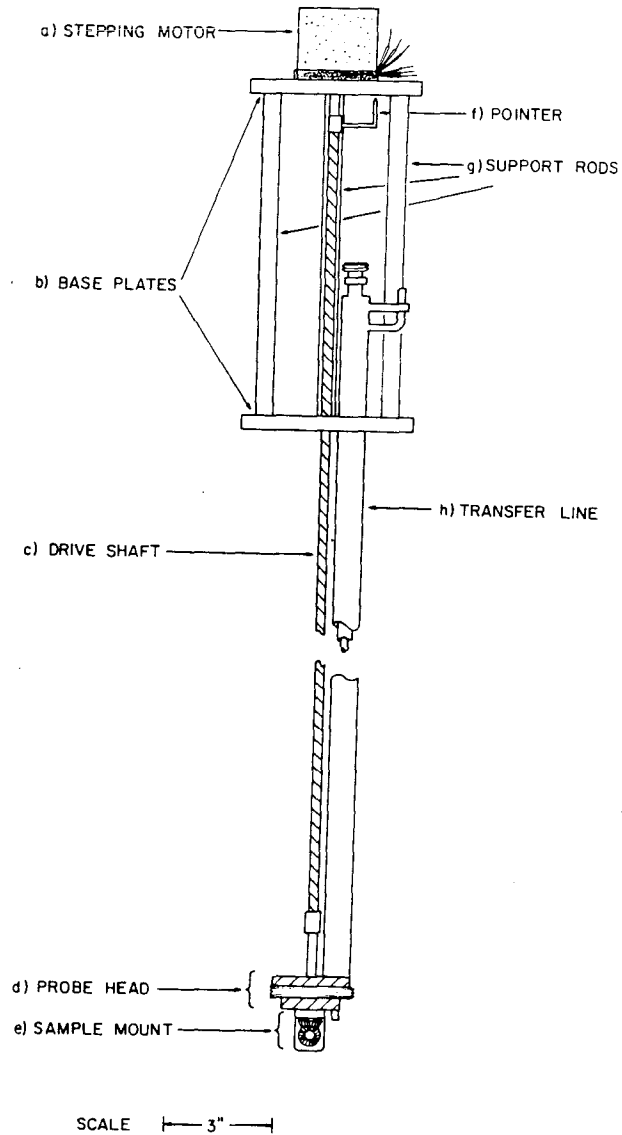
The probe uses a single coil double-tuned tank circuit as shown in Figure II.14b (similar to Reference 33). The circuit

is simultaneously tuned for ^1H at 185 MHz and ^2D at 28.4 MHz. The coil uses 8 turns of 18 gauge bare copper wire and is 8 mm in diameter and 1.5 cm in length.

The temperature control is similar to that described in section 12.3.3 except that a digital thermometer with internal reference controls the heater current supply. Thus, the nanovoltmeter arrangement described previously is bypassed, and the desired temperature may be dialed in directly.

The probe is designed for automated sample flipping. The sample mount of the probe is as shown in Figure II.15. The sample sits in the larger of a pair of two-to-one 90° brass bevel gears. The shaft of the smaller gear runs along the length of the probe (~ 4 feet) and is attached to the shaft of a SLO-SYN MO61-FC08 stepping motor mounted at the end of the probe (see Figure II.16). The motor mount is extended 9" beyond what is normally the end of the probe. This is to allow clearance for the tuning capacitors and temperature-control connections and also to provide greater separation between the motor (which contains permanent magnets) and the superconducting magnet. The step increment of the motor is 1.8° so that the 2 to 1 gearing provides a 0.9° step increment for the sample. The motor is driven by an STM101 translator module which requires a 24 VDC, 6 amp power supply. The stepping motor and translator module are manufactured by Superior Electric Company.

The translator module is driven by negative going logic pulses (10 μsec minimum width) from the spectrometer pulse



XBL 812-8126

Figure II.16 Sample flipping probe. The tuning capacitors, $\lambda^H/4$ stubs, and thermocouple, which run parallel to the transfer line, are not shown. The base plates and support rods are aluminum; the drive shaft and gas transfer line, which supports the probe head, are stainless steel. The rotation angle is marked by a pointer and azimuthal chart on the upper base plate. The total probe length is ~ 4 feet.

programmer and has two inputs to allow the motor to be stepped clockwise or counterclockwise. The translator module also has an internal oscillator for continuous rotation of the motor. The translator module is rated at 1000 pulses per second and the motor at 500 pulses per second maximum. In practice, however, it was found that the motor could be run at 1000 pulses per second (i.e., 180° sample flip in 0.2 sec) without error.

12.4.4 Receiver

The receiver is very similar to the one described in section 12.3.4, the major exception being that a commercial 30 MHz IF amp (RHG EVT 3010) is used. There are two stages of amplification (preamp and IF), and the output of the IF amp is divided into 0° and 90° components and mixed with 30 MHz to obtain the audio signal in quadrature.

The receiver was found to have poor linearity characteristics with the gain of a 1 μ Vrms input signal being 2 to 3 dB less than the gain of a 0.1 mVrms input. Since non-linearity can severely distort a relaxation curve, it was necessary to record a calibration curve for each experiment and correct the data accordingly.

12.4.5 Digitizers

The two audio components are sampled and digitized by a pair of Datel Model SHM2 S/H's in series with a pair of 10 bit

Datel Model ADCE10B A/D's. The digitization rate is limited by the rate of data transfer to the NOVA 820 computer. The fastest acquisition rate without error is 5 μ sec per point which is marginal with T_2 's around 20 μ sec.

S

I

S

I

I

I

II

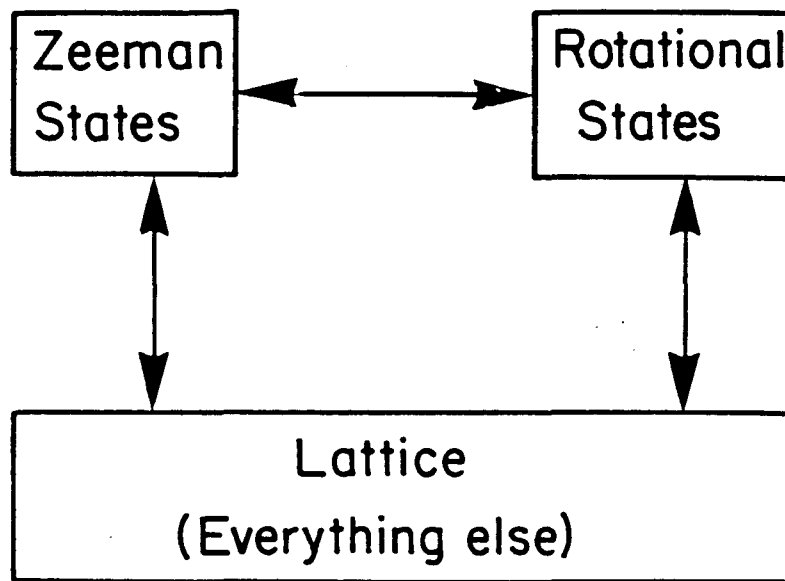
13. EXPERIMENTAL RESULTS AND CALCULATIONS

13.1 Bi-exponential Relaxation

The equilibrium spin system is shown in Figure II.17. At equilibrium there is no net flow of energy or particles between any of the subsystems or between subsystem and lattice. The effect of the RF pulse is depicted in Figure II.18. The NMR probe circuit is coupled only to the Zeeman spin states; the rotational polarization subsystem and lattice can be detected only indirectly through their influence on the Zeeman states. After the Zeeman system is driven from equilibrium it relaxes as shown in Figure II.19. If the Zeeman system were the only quasi-constant or if it was uncoupled from the other subsystems, then it would relax as a single exponential. The coupling to the rotational polarization brings about the bi-exponential relaxation described in section 11.3.1.

The measured bi-exponential relaxation of 2,6-dimethylphenol is shown in Figure II.20. A saturation recovery pulse sequence was used with a recycle delay of 150 sec. For saturation of the spin system three 90° pulses were used; the pulses were separated by 1.5 msec which is much greater than T_2 and much less than T_1 . 2,6-dimethylphenol has been studied extensively by Emid [20,23,25] using CW NMR techniques.

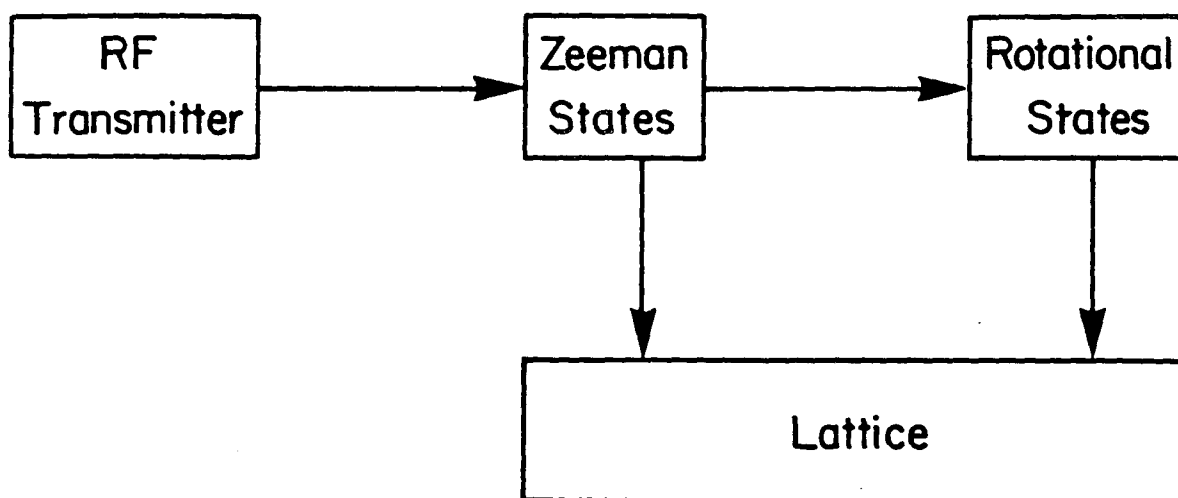
Thermodynamic Picture of System at Equilibrium



XBL 803-8421

Figure II.17 Thermodynamic picture of system at equilibrium. There is no net flow of energy or particles between the three reservoirs.

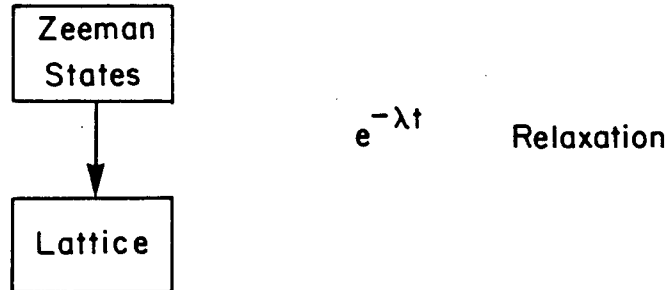
Drive from Equilibrium



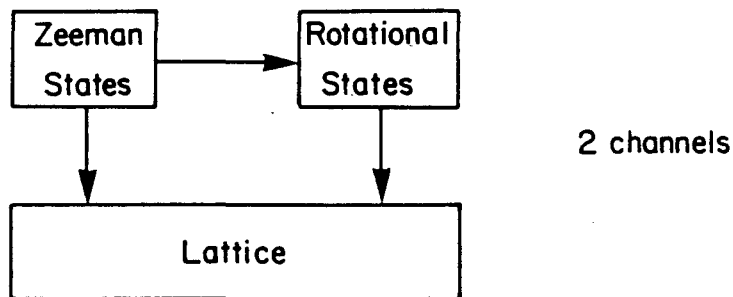
XBL 803-8422

Figure II.18 Use of RF irradiation to drive the system from equilibrium. The RF circuit (i.e., the probe coil) is coupled directly to the Zeeman subsystem and indirectly to the rotational polarization subsystem and the lattice.

Without Rotational Coupling



With Rotational Coupling



$C_1 e^{-\lambda_1 t} + C_2 e^{-\lambda_2 t}$ Relaxation

XBL 803-8419

Figure II.19 Return to equilibrium. After RF irradiation the Zeeman subsystem returns to equilibrium by losing energy to the lattice. If there is only one coupling to the lattice, the relaxation is exponential. If the Zeeman subsystem couples to rotational polarization, the relaxation is bi-exponential.

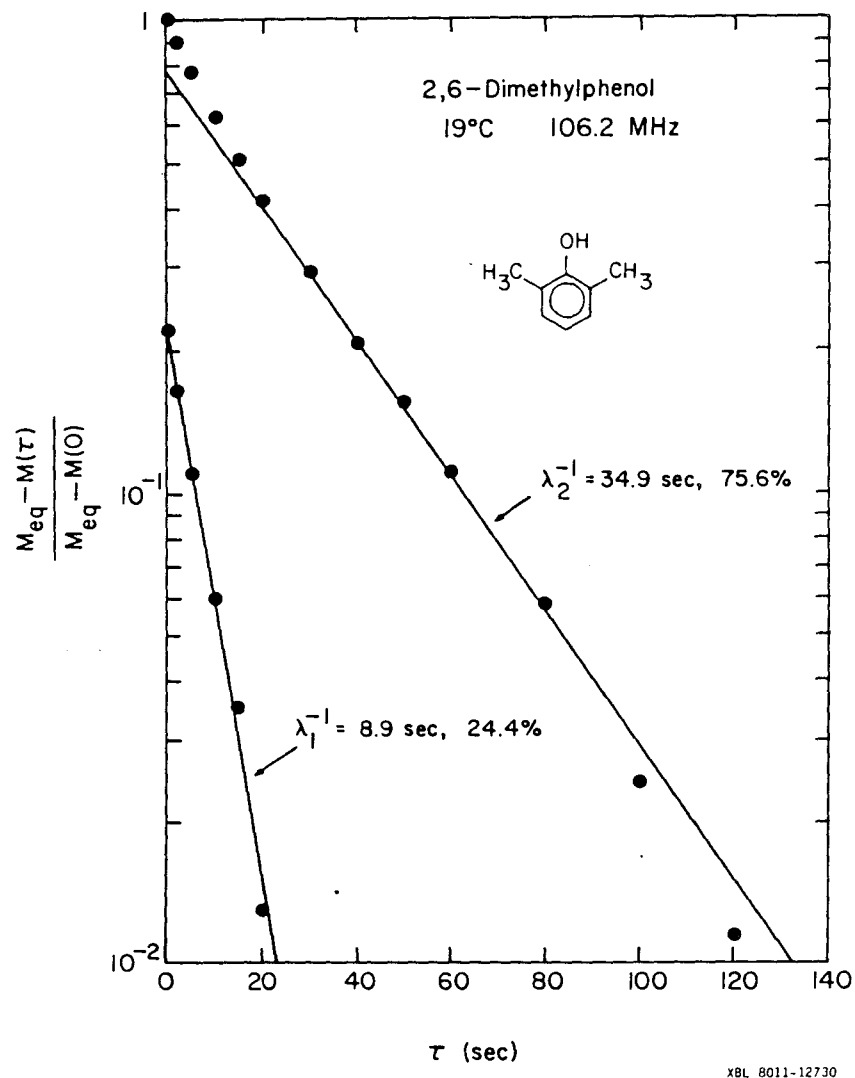


Figure II.20 Bi-exponential T_1 relaxation observed for a polycrystalline sample of 2,6-dimethylphenol. The line for the fast component was obtained by subtracting the slow component from the measured curve.

13.2 Time Dependence of Rotational Polarization

Once the Zeeman system is driven from equilibrium (i.e., heated by the RF pulses), it in turn drives the rotational polarization system away from equilibrium [19,23]. The size of the rotational polarization which is generated may be monitored through the Zeeman signal as follows.

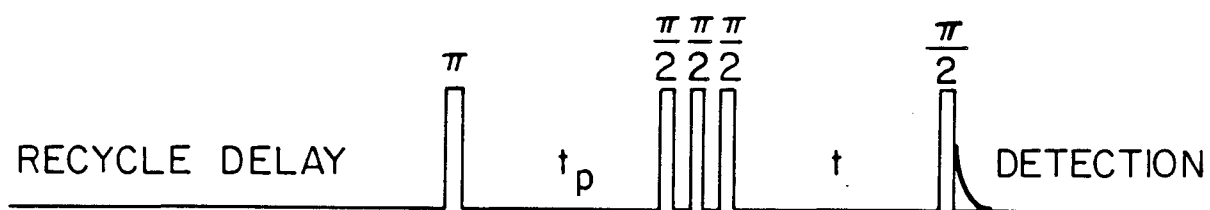
The Zeeman system is given a π pulse and then allowed to relax for a time t_p . During this time the rotational polarization subsystem is being pumped. Immediately after t_p the Zeeman system is saturated by a series of 90° pulses and then sampled at a time t later as shown in Figure II.21. If there were no rotational polarization, the size of the sampled Zeeman signal would depend only on the time interval t . However, since rotational polarization is not affected when the Zeeman system is saturated, $P_r(t_p)$ is present after saturation, and this in turn influences the Zeeman recovery. The Zeeman signal is dependent upon both evolution periods and is written explicitly as $\tilde{M}(t_p, t)$. $P_r(t_p)$ may be measured through the changes in $\tilde{M}(t_p, t)$ as a function of t_p .

From Eqs. (11.17a)-(11.18b)

$$\frac{[\tilde{M}(t_p, t) - \tilde{M}(0, t)]}{M_{eq}} = -2\sqrt{6} K P_r(t_p) \frac{[\exp(-\lambda_1 t) - \exp(-\lambda_2 t)]}{[(\lambda_1 - \lambda_2) M_{eq}]} \quad (13.1)$$

and

$$2\sqrt{6} K P_r(t_p) / M_{eq} = 2(\lambda_1 - S_{11})(\lambda_2 - S_{11}) \frac{[\exp(-\lambda_1 t_p) - \exp(-\lambda_2 t_p)]}{(\lambda_1 - \lambda_2)} \quad (13.2)$$



XBL 812-8122

Figure II.21 Pulse sequence for determining the time dependence of rotational polarization. The rotational polarization is pumped by the Zeeman relaxation during the time t_p , and its magnitude is determined by its effect on the Zeeman relaxation during the time t .

where

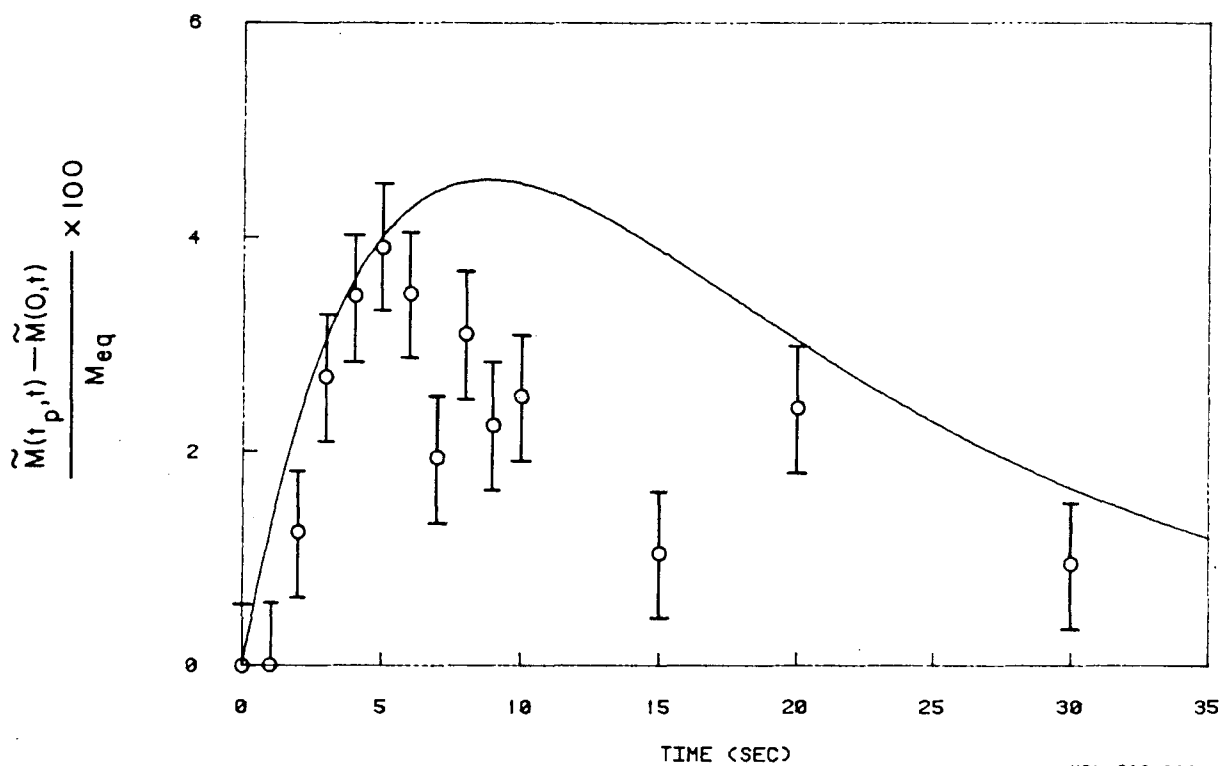
$$\tilde{M}(0,0)/M_{eq} = -2 \quad (13.3a)$$

$$P_r(0)/M_{eq} = 0 \quad (13.3b)$$

The quantity $[\tilde{M}(t_p, t) - \tilde{M}(0, t)]/M_{eq}$, which is directly proportional to $P_r(t_p)/M_{eq}$, was measured for 1,4,5,8-tetramethylantracene as a function of t_p with t equal to 6 sec. The data are plotted in Figure II.22, and apart from the poor signal to noise the data do show the rise and fall of $P_r(t_p)$ as predicted by Eq. (13.2).

The T_1 relaxation curve of 1,4,5,8-tetramethylantracene was measured (see section 13.5.1) to obtain the quantities λ_1 , λ_2 , and C_1 . Using these measured quantities and Eqs. (11.17a)-(11.18b), (13.1)-(13.3b), the predicted time dependence of $P_r(t_p)$ is shown in Figure II.22. Presumably a part of the discrepancy between the predicted curve and the experimental data may be attributed to the fact that the non-exponentiality of the T_1 curve contains contributions from rotational polarization plus powder anisotropy (i.e., incomplete spin diffusion), whereas the data of Figure II.22 are strictly a measurement of rotational polarization.

TIME DEPENDENCE OF ROTATIONAL POLARIZATION



XBL 813-8360

Figure II.22 Time dependence of rotational polarization. The sample was polycrystalline 1,4,5,8-tetramethylantracene. The proton resonance frequency was 185 MHz, and the temperature was 25°C. The abscissa is the time t_p , and the time t was fixed at 6 sec (see Figure II.21). The theoretical curve was calculated using Eqs. (11.17a)-(11.18b), (13.1)-(13.3b), and the T_1 relaxation data of Figure II.32.

13.3 Angular Dependence of Rotational Polarization

The rotational polarization quasi-constant was shown to be [Eq. (11.16)]:

$$P_r(t) = \sum_i \cos(\theta_i) R_i(t)$$

where $R_i(t)$ is the E^a-E^b population difference of the i^{th} methyl group and θ_i is the angle between the methyl C_3 axis and the magnetic field. Considering $R_i(t)$ as a vector of length $R_i(t)$ parallel to the i^{th} C_3 axis, $P_r(t)$ is the total projection of rotational polarization along the magnetic field. $R_i(t)$ may be written:

$$R_i(t) = [\sin\theta_i \cos\eta_i \hat{x} + \sin\theta_i \sin\eta_i \hat{y} + \cos\theta_i \hat{z}] R_i(t) \quad (13.4)$$

where η_i is the azimuthal angle and \hat{x} , \hat{y} , \hat{z} are the unit axis vectors. If the sample is rotated about the x axis by the angle ϕ , then the new rotational polarization quasi-constant immediately after rotation is:

$$P_r(t, \phi) = \sum_i [\cos\theta_i \cos\phi - \sin\theta_i \sin\eta_i \sin\phi] R_i(t) \quad (13.5)$$

Assuming that a powder average is valid, then the average value of $\sin\eta$ is zero, and from Eqs. (11.16) and (13.5):

$$P_r(t, \phi) = \cos(\phi) P_r(t, 0) \quad (13.6)$$

where the notation has been changed to account for the sample

rotation. Eq. (13.6) may be tested experimentally to confirm the vector nature of rotational polarization and the validity of the z projection P_r as the correct quasi-constant.

$P_r(t_p, 0)$ was pumped as demonstrated in the previous section, the sample rotated (see Figure II.23), and resultant rotational polarization measured by its effect on the Zeeman T_1 recovery. The necessary pulse sequence is shown in Figure II.24 with the first sample rotation (≤ 0.2 sec) being controlled by the pulse programmer (automated probe described in section 12.4.3). Incorporating the time intervals t_p and t and the rotation angle Φ into the notation, there follows from Eqs. (11.17a)-(11.18b):

$$\begin{aligned} [\tilde{M}(t_p, \Phi, t) - \tilde{M}(t_p, 0, t)] / M_{eq} &= -2\sqrt{6}K [P_r(t_p, \Phi) - P_r(t_p, 0)] \\ &\times [\exp(-\lambda_1 t) - \exp(-\lambda_2 t)] / [(\lambda_1 - \lambda_2) M_{eq}] \end{aligned} \quad (13.7)$$

According to Eq. (13.6)

$$P_r(t_p, \Phi) - P_r(t_p, 0) = (\cos\Phi - 1) P_r(t_p, 0) \quad (13.8)$$

Thus,

$$[\tilde{M}(t_p, \Phi, t) - \tilde{M}(t_p, 0, t)] / [\tilde{M}(t_p, \pi, t) - \tilde{M}(t_p, 0, t)] = (1 - \cos\Phi) / 2 \quad (13.9)$$

where Eq. (13.7) is taken relative to its value for a π rotation of the sample.

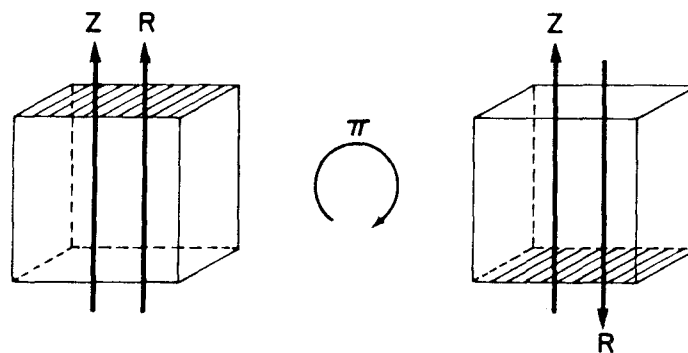
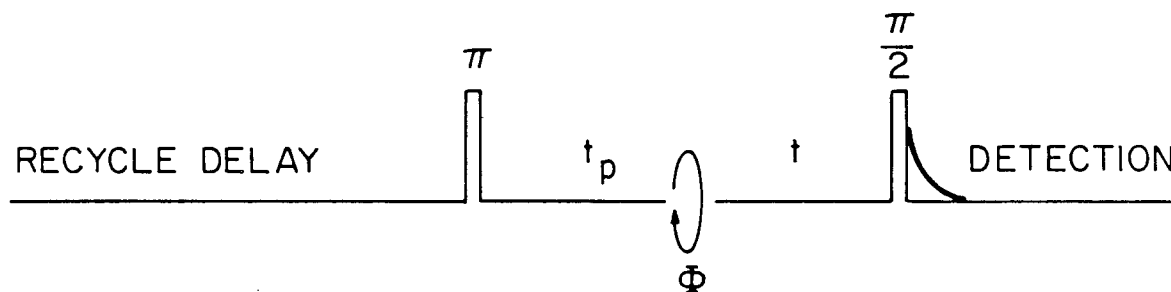


Figure II.23 Effect of a 180° sample flip on the Zeeman (Z) and rotational polarization (R) subsystems. The Zeeman subsystem depends only on spin coordinates and is unaffected, therefore, by a sample flip. Rotational polarization is associated with the spin symmetries which are coupled to the spatial symmetries through the Pauli exclusion principle. Thus, rotational polarization follows the motion of the methyl C_3 axes and is inverted by a sample flip.

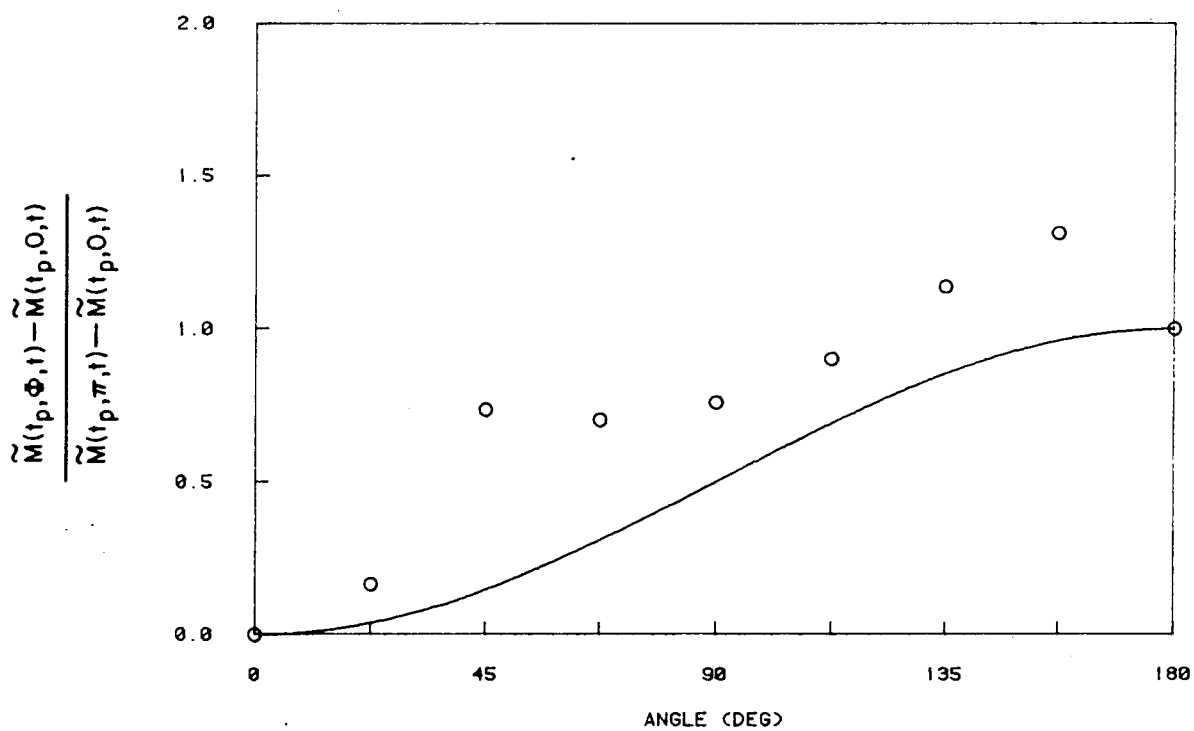


XBL 812-8121

Figure II.24 Pulse sequence for determining the angular dependence of rotational polarization. The rotational polarization is pumped by the Zeeman relaxation during the time t_p . The sample is then quickly rotated by an angle Φ , and the resulting rotational polarization measured by its effect on the Zeeman relaxation during the time t .

The quantity expressed in Eq. (13.9) has been measured for a 1,4,5,8-tetramethylantracene powder with $t_p = t = 9$ sec, and the results are plotted in Figure II.25 as a function of Φ . The agreement between the experimental results and Eq. (13.9) is fair considering that there should be some contribution to the results from T_1 anisotropy in the powder.

ANGULAR DEPENDENCE OF ROTATIONAL POLARIZATION



XBL 813-8359

Figure II.25 Angular dependence of rotational polarization. The sample was polycrystalline 1,4,5,8-tetramethylantracene. The proton resonance frequency was 185 MHz, and the temperature was 25°C. The abscissa is the angle Φ ; the times t_p and t were fixed at 9 sec (see Figure II.24). The theoretical curve was calculated from Eq. (13.9).

13.4 Equilibrium Rotational Polarization

Implicit in the use of C_3 symmetry for the methyl group is the degeneracy of the E^a and E^b rotor states within a torsional level (it is assumed throughout this discussion that degeneracy refers either to an individual torsional level or to an average over torsional levels). This may be rigorously affirmed on the basis of time reversal since the E^a and E^b states are mirror images of one another. However, in the presence of an external magnetic field the two symmetries need not be degenerate, since time reversing the methyl group does not change the direction of the field. The degree to which the field breaks the degeneracy and the C_3 symmetry depends upon the degree of interaction between the methyl group rotation and the magnetic field. This interaction will now be elucidated.

In the gas phase the rapidly rotating ($\geq 10^{13}$ Hz) methyl group of methyl iodide CH_3I generates a magnetic moment which can be detected through shifts in the rotational spectrum of CH_3I in a magnetic field [34]. The magnetic moment may be written:

$$\underline{\mu} = \beta \underline{g} \cdot \underline{J} \quad (13.10)$$

where β is the nuclear magneton, \underline{g} the molecular g-tensor, and \underline{J} the angular momentum of the molecule. Considering only the component due to rotation of the methyl group about its C_3 axis:

$$\mu_{CH_3} = \beta g_k \hbar m \quad (13.11)$$

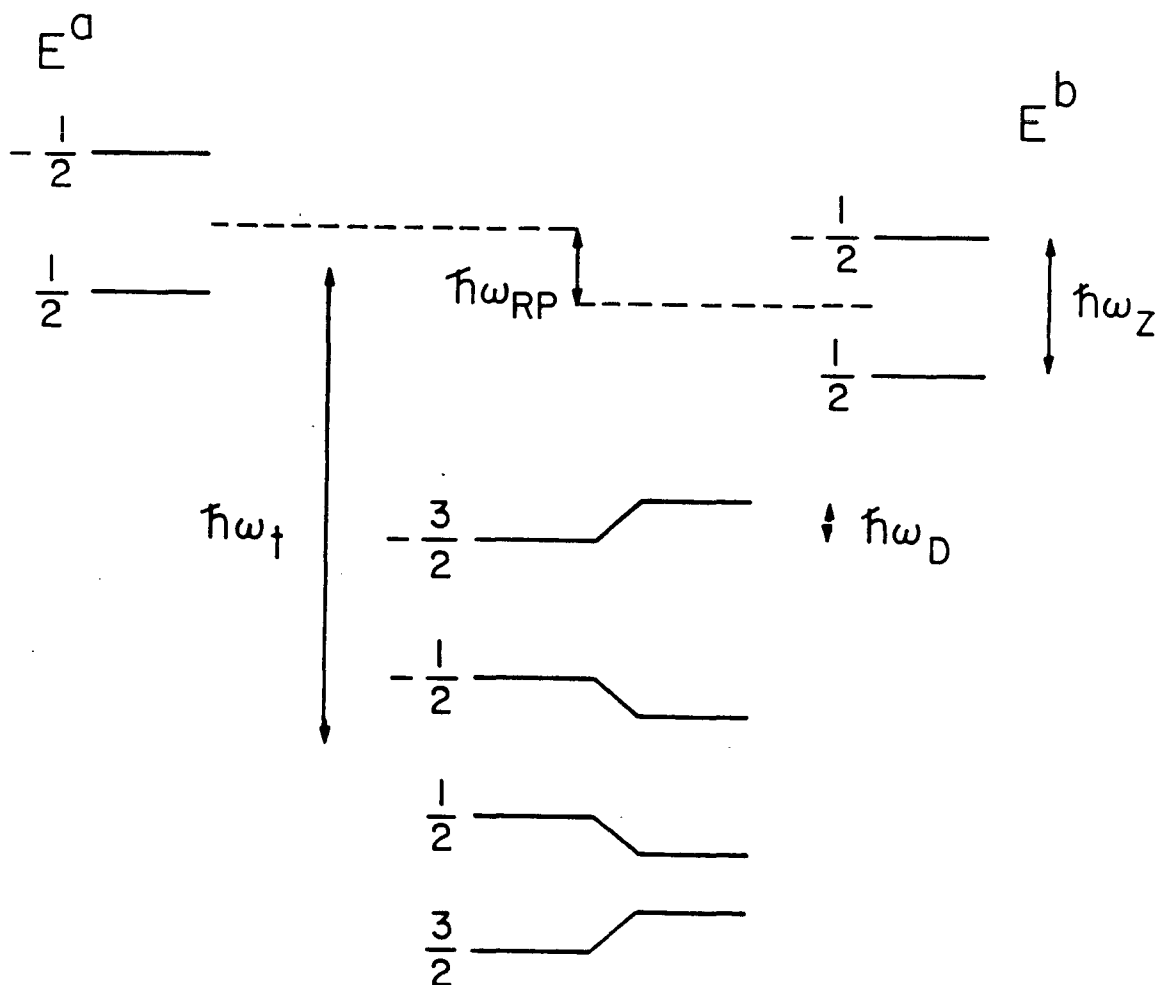
where g_k is the methyl group g-factor and m is the angular

momentum quantum number along the C_3 axis (see section 10.1)

g_k has been measured for a few molecules: CH_3F , CH_3Br , CH_3I , CH_3CCH [35,36]. All of the measured values are ~ 0.3 with the value for CH_3I equal to 0.310 ± 0.016 [35].

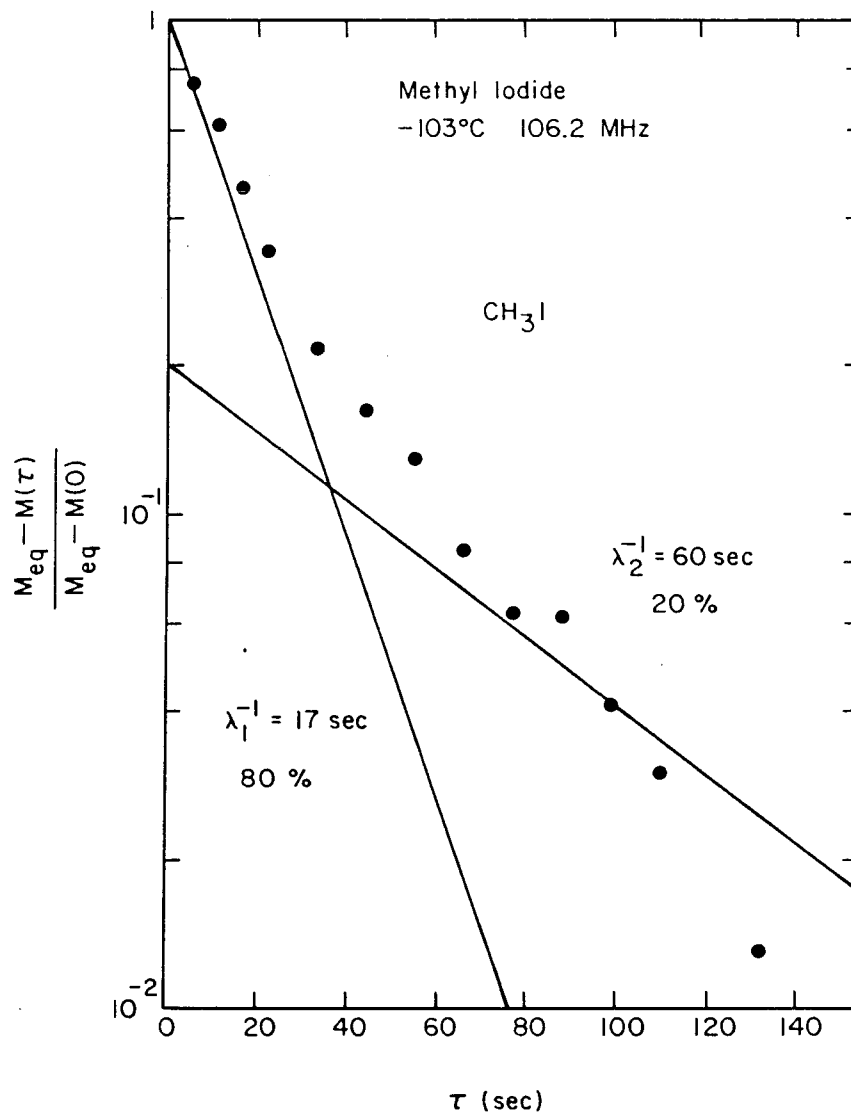
In section 10.1, Eq. (10.5) it was shown that although angular momentum is no longer a good quantum number for hindered rotors, hindered methyl groups do rotate and an expectation value of angular momentum $\langle m \rangle$ can be associated with each E^a and E^b state (see Figure II.4). Furthermore, by calculating a Boltzmann average over the torsional states, it is possible to associate a temperature-dependent expectation value of angular momentum with each symmetry manifold E^a and E^b . Thus, in the presence of an external magnetic field the E^a and E^b spin states which are associated with the E^b and E^a rotor states, respectively, through the Pauli principle are no longer degenerate [18]. This is illustrated in Figure II.26 where the energy $\hbar\omega_{RP}$ is associated with rotational polarization. The net effect of this is that at equilibrium the populations of the E^a and E^b spin states are no longer equal so that $P_{r,eq}$ is non-zero.

Experiments were performed to measure the equilibrium value of rotational polarization $P_{r,eq}$ for solid CH_3I at $-103^\circ C$. The non-exponential relaxation of solid CH_3I is shown in Figure II.27. From the temperature dependence of T_1 (measured at -103 and $-150^\circ C$) the barrier to CH_3 rotation was found to be 420 ± 60 cal/mole. $P_{r,eq}$ was measured by the combination of pulse sequences shown in Figure II.28. In the first sequence a 90° pulse is given to the spins, after a time t_p the sample is flipped by 180° , and then



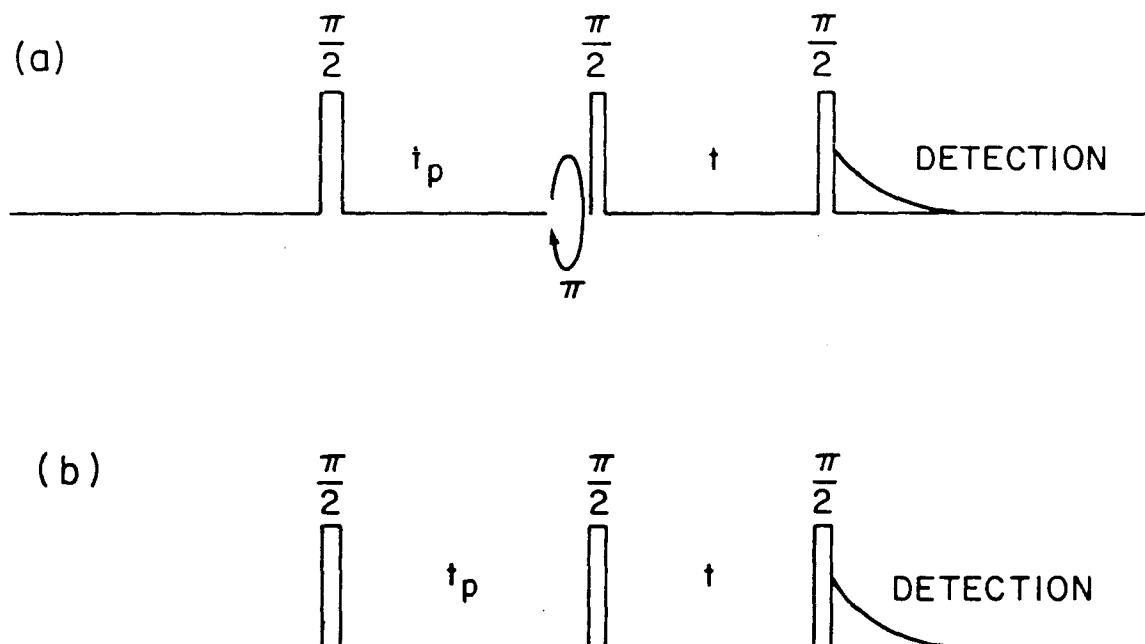
XBL 812-8120

Figure II.26 The energy levels of the three protons of a methyl group considering the Zeeman, intramethyl dipolar, and tunneling interactions and the coupling between the methyl group rotation and the external magnetic field. Because the magnetic field lifts the degeneracy of the E^a and E^b states, the methyl group symmetry is only approximately C_3 .



XBL 812-8124

Figure II.27 Bi-exponential T_1 relaxation observed for a sample of frozen methyl iodide. The parameters for the fast relaxation component are accurate to within 20%, and the parameters for the slow component are within a factor of 2. Additional values which were included in the fit but not plotted are: 2.47 at 176 sec, 0.48 at 219 sec, and 0.35 at 263 sec.



XBL 812-8112

Figure II.28 Pulse sequences used for determination of equilibrium rotational polarization. The rotational polarization is pumped by the Zeeman relaxation during the time t_p , and it is observed by its effect on the Zeeman relaxation during the time t . Pulse sequence (a) contains a 180° sample flip. The difference in Zeeman signals from sequences (a) and (b), for given values of t_p and t , is directly proportional to the rotational polarization present at time t_p . By fixing t and increasing t_p , the data may be extrapolated to obtain the equilibrium rotational polarization. Note: since the difference of (a) and (b) was recorded, the second $\pi/2$ pulse of each sequence was unnecessary.

after a time t the Zeeman signal is sampled. The second sequence is the same except the sample flip is omitted. The difference between the two Zeeman signals (i.e., flip and no flip) is proportional to $P_r(t_p)$ [see Eqs. (13.7), (13.8)]. By increasing t_p while holding t fixed, the asymptotic equilibrium value $P_{r,eq}$ may be measured. The results of such an experiment are shown in Figure II.29.

$P_r(t_p)$ appears to be converging to a non-zero equilibrium value although the data are far from conclusive. A non-linear least squares routine was used to fit the data to the equation:

$$f(t) = A + B \exp(-\lambda t) \quad (13.12)$$

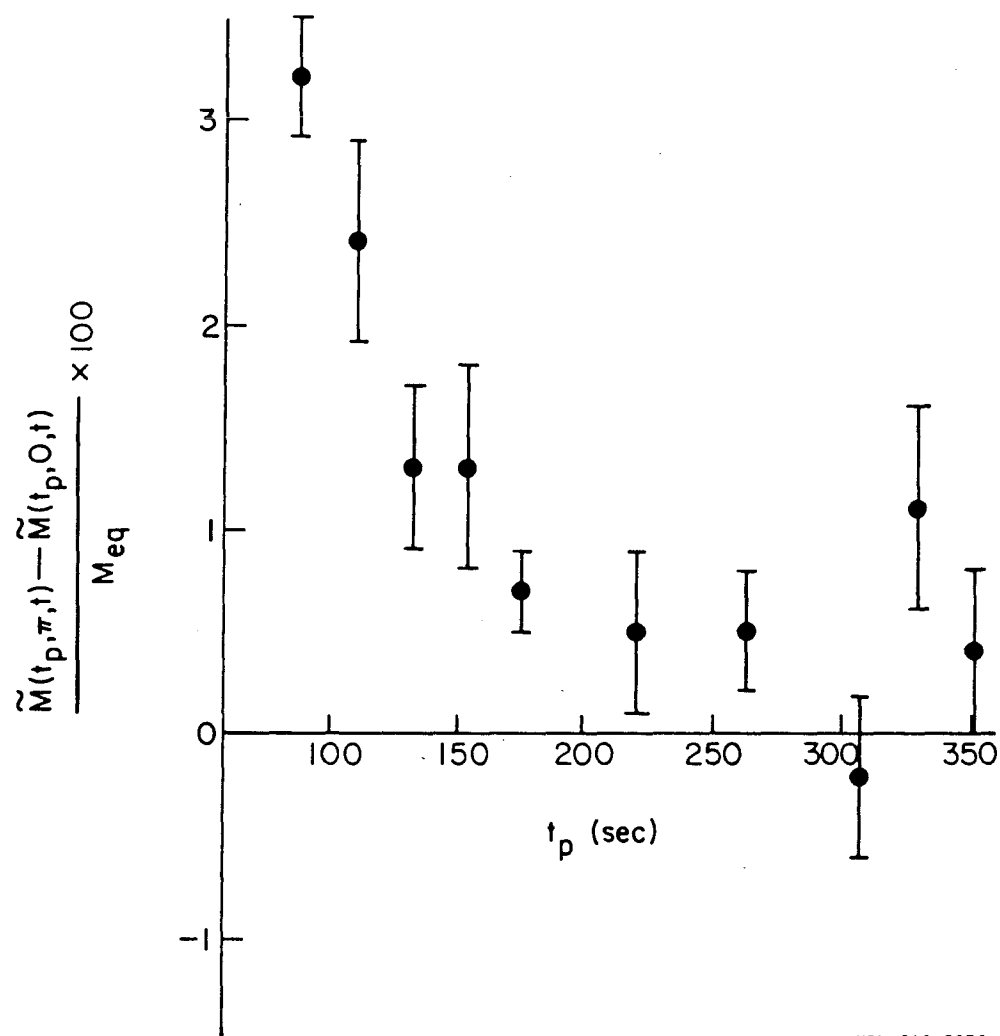
where A and λ are related to $P_{r,eq}$ and λ_2 , respectively. The fit was performed using the FORTRAN subroutine "VARPRO" [37,38,39] obtained from the Lawrence Berkeley Laboratory Computer Center. It is not advisable to take the logarithm of Eq. (13.12) and use a linear least-squares method since this is ill-behaved for $f(t)$ near zero and meaningless for a negative $f(t)$. The results of the VARPRO fit are:

$$A = 0.004 \pm 0.002 \quad (13.13a)$$

$$B = 0.2 \pm 0.1 \quad (13.13b)$$

$$\lambda = 0.022 \pm 0.006 \text{ sec}^{-1} \quad (13.13c)$$

From Eqs. (13.7) and (13.8) and the experimental parameters obtained from the data of Figures II.27 and II.29 there is obtained:

$P_{r,eq}$ MEASUREMENT

XBL 813-8356

Figure II.29 Measurement of the equilibrium rotational polarization $P_{r,eq}$ of solid methyl iodide. The proton frequency was 106.2 MHz, and the temperature was -103°C . The time t was fixed at 15 sec (see Figure II.28). A non-linear least squares fit of the data gave a decay time of 50 ± 25 sec, in fair agreement with λ_2 of Figure II.27, and an equilibrium value $P_{r,eq}/M_{eq}$ of 0.003 ± 0.002 (note: the data in the figure are scaled up by a factor of 100).

$$P_{r,eq}/M_{eq} = 0.003 \pm 0.002 \quad (13.14)$$

where K was calculated from Eqs. (11.4a) and (11.18a) assuming a powder average for S_{11} .

The program "methyl" (Appendix C) was used to calculate the theoretical value of $P_{r,eq}/M_{eq}$ as follows. With the high temperature approximation

$$P_{r,eq} = \hbar \omega_{RP}/kT = \beta g_k \hbar [\langle m(E^a) \rangle - \langle m(E^b) \rangle] H \quad (13.15a)$$

$$M_{eq} = \hbar \omega_z/kT = \beta g_H \hbar H \quad (13.15b)$$

where g_H is the proton g -factor. With

$$\langle m(E^b) \rangle = -\langle m(E^a) \rangle \quad (13.16)$$

by time reversal symmetry, it follows that

$$P_{r,eq}/M_{eq} = 2 \langle m(E^a) \rangle g_k/g_H = 0.111 \langle m(E^a) \rangle \quad (13.17)$$

where the experimental values of g_k (0.31) and g_H (5.585) have been used. Using "methyl" to calculate the temperature-dependent $P_{r,eq}/M_{eq}$ (i.e., the angular momentum of the rotor is temperature-dependent) for a 420 cal/mole barrier, the results of Figure II.30 are obtained. Given the negligible value predicted at -103°C , the experimental results of Figure II.29 and Eq. (13.14) must be considered very tentative. Furthermore, in the calculation all methyl groups were assumed parallel to the field \underline{H} , whereas a powder average would be more appropriate. With the magnetic interaction given by $\underline{\mu} \cdot \underline{H}$, the energy varies as $\cos\theta$. Performing

a powder average, the calculations of Figure II.30 are reduced by a factor of two (note: methyl groups pointing in opposite directions do not cancel since the coupling to the Zeeman system is proportional to $\cos\theta$).

An interesting calculation would be to see if a larger value of $P_{r,eq}$ is predicted for a sixfold rather than a threefold barrier.

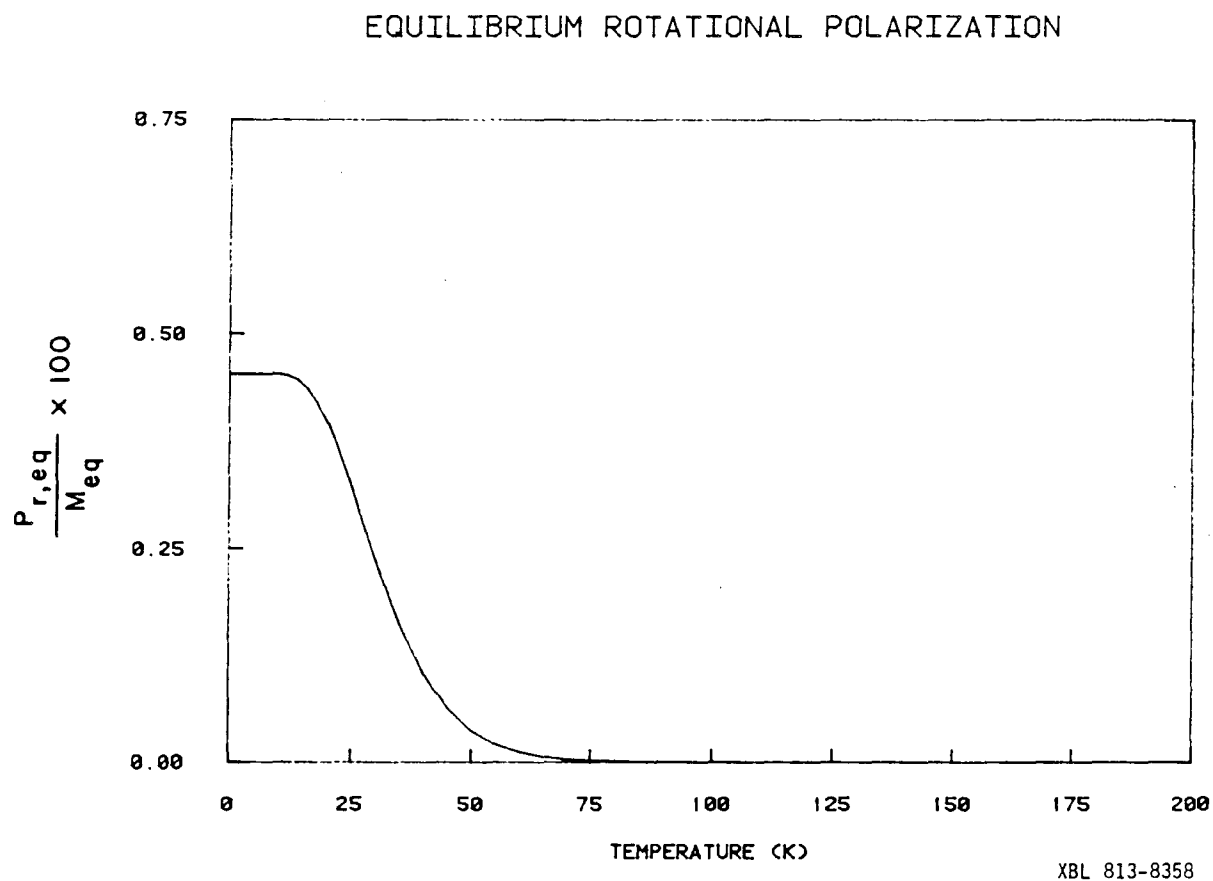


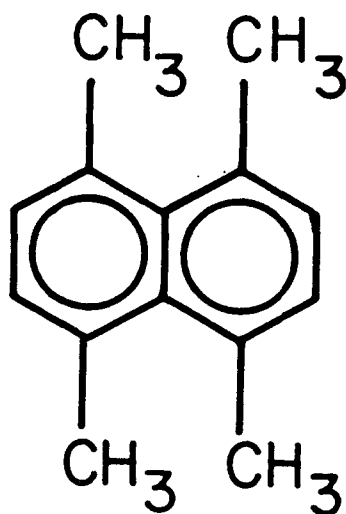
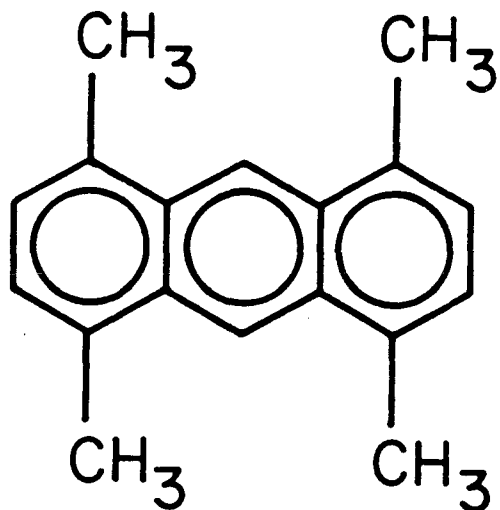
Figure II.30 Theoretical equilibrium rotational polarization $P_{r,eq}$ as a function of temperature. The activation energy 420 ± 60 cal/mole, which was obtained from the CH_3I relaxation data, was used as the barrier to methyl group rotation. All methyl groups were assumed to have their C_3 axes along the magnetic field. For an isotropic distribution of methyl groups the above calculation should be reduced by a factor of 2.

13.5 Methyl-methyl Steric Interaction

13.5.1 Strong and Weak Coupling

The molecules 1,4,5,8-tetramethylantracene and 1,4,5,8-tetramethylnaphthalene (see Figure II.31) provide an interesting comparison for observing the effect of steric interaction on rotational polarization. In 1,4,5,8-tetramethylantracene the methyl groups are well separated, and the bi-exponential relaxation of independent methyl groups is expected. The T_1 relaxation curve of 1,4,5,8-tetramethylantracene is shown in Figure II.32. The data are fitted well with a bi-exponential decay curve (the nonlinear least-squares fitting routine "VARPRO" [37,38,39] was used to fit all of the relaxation data discussed in sections 13.5.1 and 13.5.2).

On the other hand, 1,4,5,8-tetramethylnaphthalene, which has very strong steric interaction between adjacent methyl groups, exhibits the strictly exponential decay behavior shown in Figure II.33. This is in exact accordance with the predictions of section 11.3.2 for strongly coupled methyl groups. According to Eq. (11.24) the coupling between Zeeman and rotational polarization depends on the difference $[S_{14}(\theta_i) - S_{14}(\theta_{i+1})]$ for two coupled methyl groups. This difference is zero for 1,4,5,8-tetramethylnaphthalene since both members of each coupled pair are parallel (or nearly so), and, therefore, the Zeeman system relaxes independently (and exponentially) of rotational polarization. The strong coupling is found to persist from 20°



XBL 802-8347A

Figure II.31 Examples of weak and strong steric coupling. The well-separated methyl groups of 1,4,5,8-tetramethylantracene (top) are expected to relax as independent methyl groups, whereas the closely-spaced methyl groups of 1,4,5,8-tetramethylnaphthalene (bottom) are expected to relax as strongly geared methyl groups.

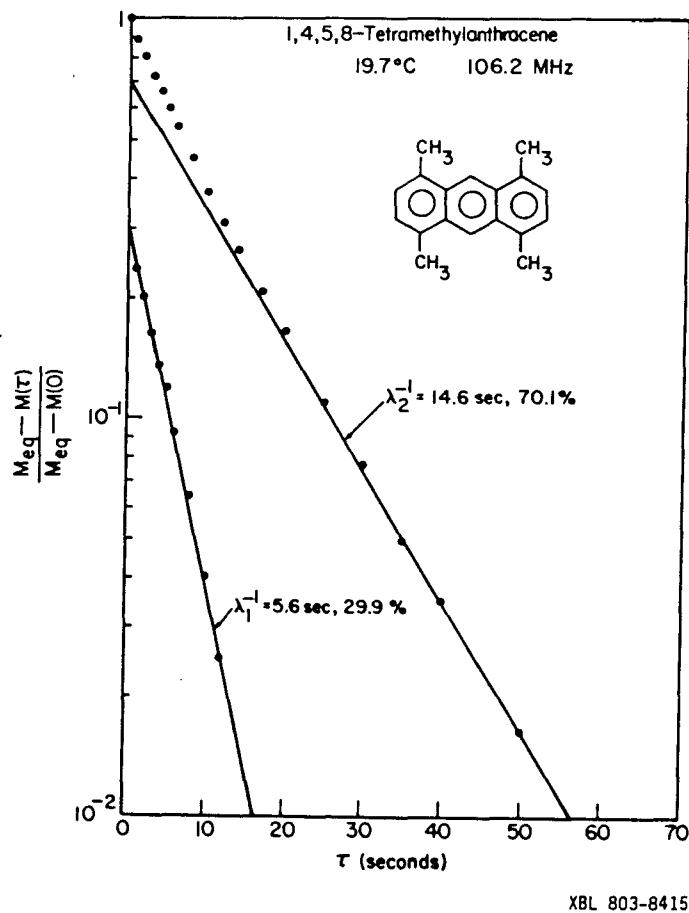


Figure II.32 Bi-exponential T_1 relaxation observed for a polycrystalline sample of 1,4,5,8-tetramethylanthracene. The line for the fast component was obtained by subtracting the slow component from the measured curve. The bi-exponential relaxation is indicative of independent methyl groups.

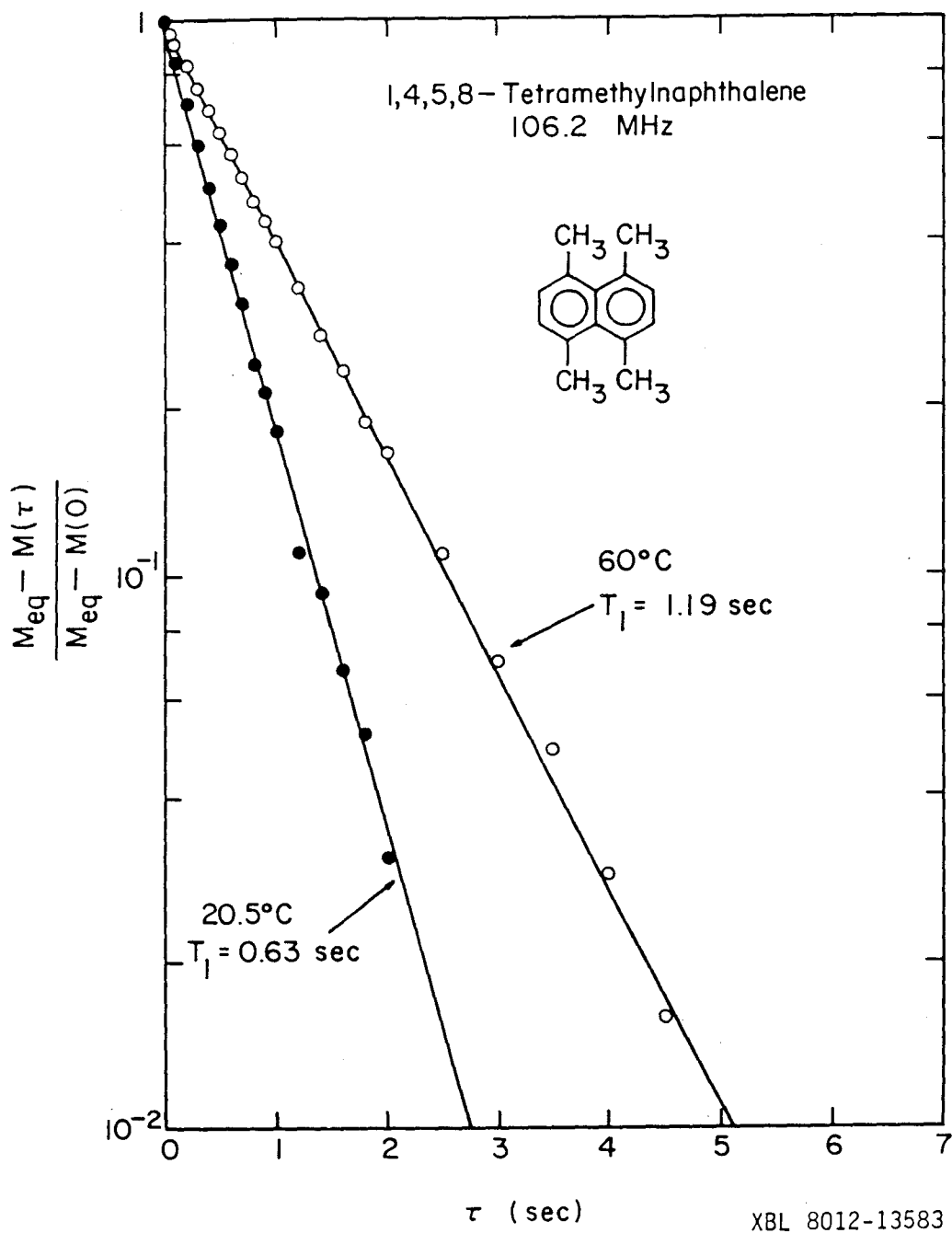


Figure II.33 Exponential T_1 relaxation observed for a polycrystalline sample of 1,4,5,8-tetramethylnaphthalene. The relaxation times are accurate to within 1%. The exponential relaxation can be attributed to the combined effects of strong methyl gearing and intermethyl relaxation.

to 60° as shown in Figure II.33. Assuming an Arrhenius law for the correlation time, the calculated barrier to methyl group reorientation is 3.1 ± 0.1 kcal/mole. This value is essentially the same as that for 1,8-dimethylnaphthalene which has been reported as 3.2 ± 0.1 kcal/mole [40] and 3 kcal/mole [41]; the barriers for other dimethylnaphthalenes range from 0.4 to 2.5 kcal/mole [40].

The objection could be made that the intermethyl contribution to the relaxation seriously alters the treatment of section 11.3.2. This may be easily checked. It was previously stated that $\mathcal{H}_{D,inter}$ increases S_{11} and S_{44} but not S_{14} [25]. Assuming that either S_{11} and S_{44} become large due to $\mathcal{H}_{D,inter}$ or S_{14} becomes small due to the steric interaction, then $\lambda_{1,2}$ may be expanded in the quantity $4 S_{14}^2 / (S_{11} - S_{44})^2$ to obtain from Eq. (11.14) or (11.23)

$$\lambda_1 \cong S_{11} + x \quad (13.18a)$$

$$\lambda_2 \cong S_{44} - x \quad (13.18b)$$

where

$$x = S_{14}^2 / (S_{11} - S_{44}) \quad (13.19)$$

And with $P_r(0)$ equal to zero,

$$C_1 \cong [(S_{11} - S_{44} + x) / (S_{11} - S_{44} + 2x)] \tilde{M}(0) / M_{eq} \quad (13.20a)$$

$$C_2 \cong [x / (S_{11} - S_{44} + 2x)] \tilde{M}(0) / M_{eq} \quad (13.20b)$$

As x goes to zero, C_2 goes to zero, and the relaxation is exponential. Thus, this technique cannot distinguish S_{14} going to zero from S_{11} , S_{44} becoming very large.

From Figures II.32 and II.33 it is seen that S_{11} of 1,4,5,8-tetramethylnaphthalene is about ten times larger than that of 1,4,5,8-tetramethylantracene. If this difference is due to $\mathcal{H}_{D,inter}^c$, then the effects due to steric coupling may be diluted considerably. However, if the difference is due to the tetramethylnaphthalene having a much larger methyl group rotational barrier than the tetramethylantracene, then the steric coupling model is correct since S_{11} , S_{44} , and S_{14} are all proportional to the correlation time and scale by the same factor. Thus, it is necessary to distinguish between changes due to barrier height and changes due to intermethyl relaxation. Two methods are suggested below for determining this.

S_{44} for 1,4,5,8-tetramethylnaphthalene may be obtained by measuring the dipolar relaxation rate S_{55} [42] since S_{44} and S_{55} are equal [see Eqs. (11.4c) and (11.4d)]. S_{11} is obtained simply from Figure II.33. If S_{11} and S_{44} have changed by a common factor relative to the same quantities for 1,4,5,8-tetramethylantracene, then it may be assumed that the rates have simply scaled with the increase in barrier. Alternatively, if one methyl group of each coupled pair were deuterated, then the relaxation could be measured at the same barrier but minus the intermethyl contribution. In the absence of $\mathcal{H}_{D,inter}^c$ and coupled rotational polarizations, the relaxation should be bi-exponential as well as being slower. Until either the

dipolar relaxation or deuteration experiment is performed, the exponential relaxation of 1,4,5,8-tetramethylnaphthalene may be taken to be the combined result of strong steric coupling and intermethyl relaxation.

13.5.2 Intermediate Coupling

An interesting situation arises when cases of steric interaction intermediate to the above two are considered. Durene (1,2,4,5-tetramethylbenzene) and 2,3-dimethylmaleicanhydride have similar methyl-methyl geometries. When the T_1 relaxation of durene is measured near room temperature, it is found to be strictly exponential as shown in Figure II.34. On the other hand, 2,3-dimethylmaleicanhydride shows a non-exponential relaxation near room temperature (see Figure II.35). The measurements were performed using both single crystal (the durene used in the single crystal had one ring position deuterated) and powder samples, and the results were unchanged for both compounds. One possible explanation for the difference between the two compounds is as follows.

If the steric coupling is strongly dependent upon the fraction of time each methyl rotor is above the barrier in energy, then a small difference in the intermethyl barrier may cause a large difference in the observed relaxation at a given temperature. That is, ignoring the barrier to rotation from other molecules which is essentially stationary, the barrier which one methyl rotor sees is dependent upon the angular orientation of the

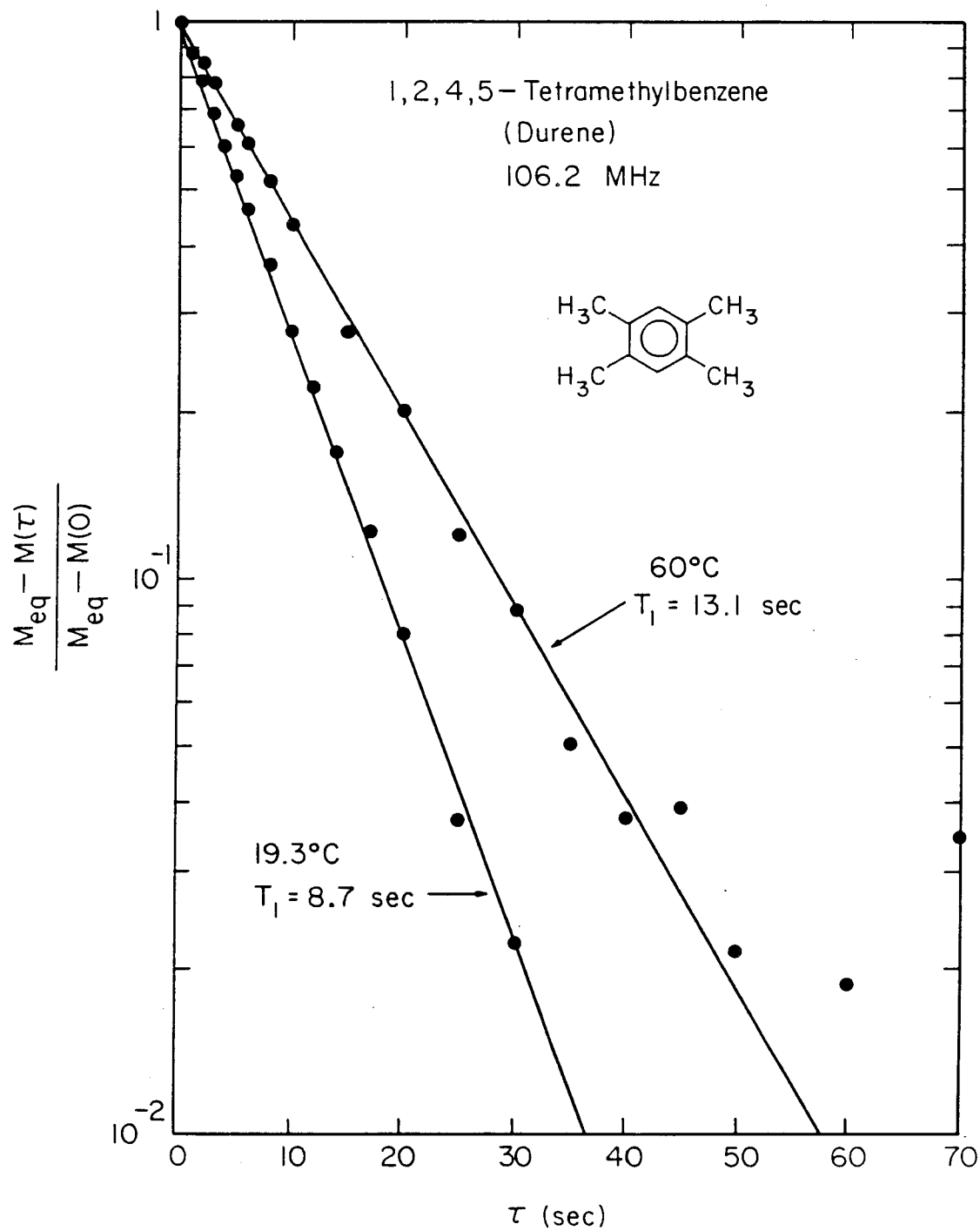
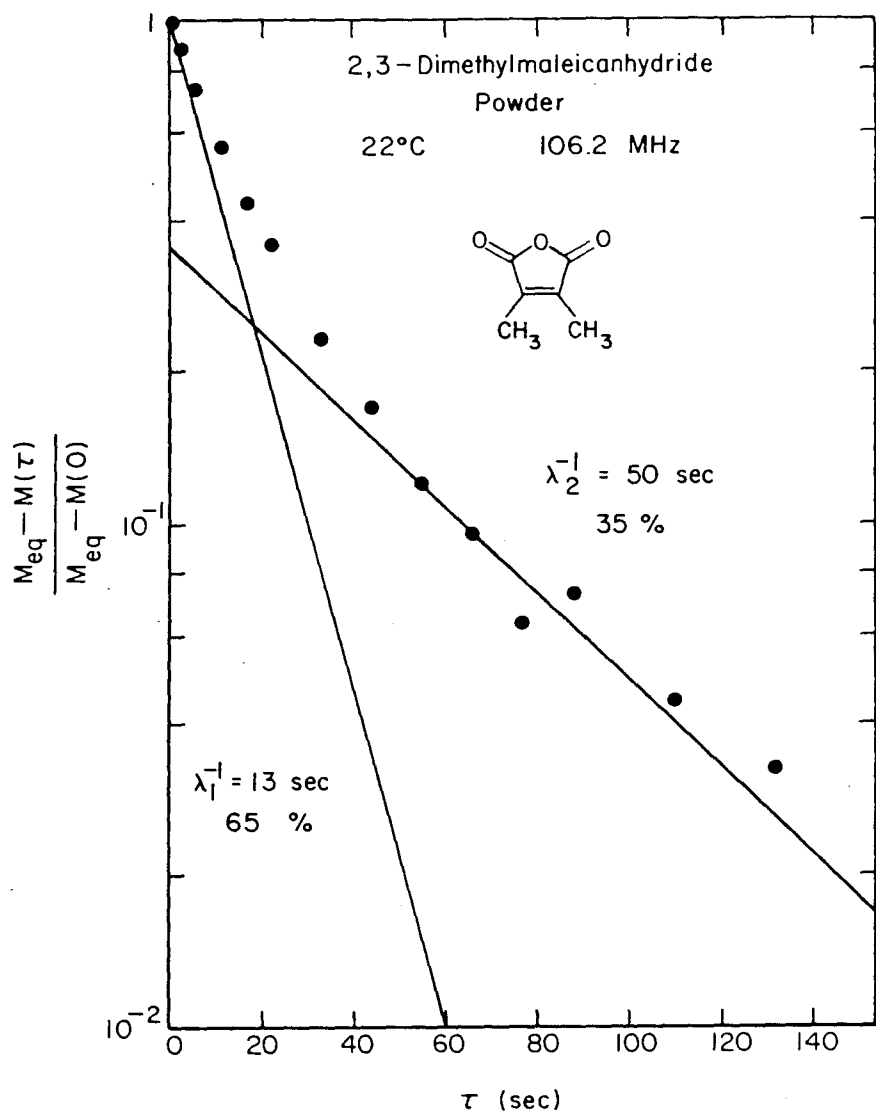


Figure II.34 Exponential T_1 relaxation observed for a polycrystalline sample of 1,2,4,5-tetramethylbenzene. The relaxation time at 19.3°C is accurate to within 1%, and the value at 60°C is accurate to within 2%.



XBL 812-8125

Figure II.35 Bi-exponential T_1 relaxation observed for a polycrystalline sample of 2,3-dimethylmaleicanhydride at 22°C. The short and long relaxation times are accurate to within 10% and 15%, respectively.

adjacent methyl rotor. Now if one methyl has sufficient energy to exceed the barrier height, then it may rotate freely without regard to the orientation of the adjacent methyl, and the motion of the two methyls is uncorrelated. If, on the other hand, the methyl rotors lie far below the barrier height in energy, then they must either tunnel, which is slow, or move in correlated fashion: as one methyl rotates, the barrier moves, and the other methyl must follow. If durene and 2,3-dimethylmaleicanhydride are in the region of marginal steric coupling, then it should be possible to detect the transition from weak to strong coupling. To test this hypothesis the temperature dependence of T_1 was studied.

The results for durene at 19° and 60°C are shown in Figure II.34. Except for some scatter in the smaller data points at 60°C there is no indication that the relaxation is becoming non-exponential at the higher temperature. The activation energy for the methyl reorientation is determined from the data to be 1.9 ± 0.1 kcal/mole. This energy has also been reported as 1.6 ± 0.1 kcal/mole by NMR T_1 measurements [43a] and 2.03 ± 0.16 kcal/mole by neutron scattering [43b]. The deviation of the 1.6 kcal/mole value from the other two may be an artifact of the data analysis which was used: T_1 data from 90 to 350 K was fitted assuming a single activation energy [43b], and it is now known that the T_1 of methyl groups may exhibit a smaller activation energy at low temperature than at high [44].

2,3-dimethylmaleicanhydride was studied extensively to see if the transition from weak to strong coupling could be detected.

In Figures II.36 to II.39 is shown the temperature dependence of the relaxation of a 2,3-dimethylmaleicanhydride single crystal at a fixed orientation. From the plots there is no trend to be discerned other than the increases of the rates as the correlation time becomes longer. Using the routine "VARPRO" to solve for C_1 ($C_1 + C_2$ are normalized to one), λ_1 and λ_2 , the single crystal data and that from powder experiments were analyzed; the results are plotted in Figures II.40 and II.41. The predominant feature of Figure II.40 is that the relaxation becomes more exponential (i.e., C_1 increases) as the temperature is increased. In fact, the relaxation for the powder was exponential at the highest temperature (i.e., 70°C which is well below the melting point of 93-96°C) measured as shown in Figure II.42. Unfortunately, the single crystal relaxation was not measured at 70°C also. Excluding the methyl-methyl steric interaction W and $\mathcal{K}_{D,inter}$, Eqs. (11.18a) and (11.27a) predict no temperature dependence for C_1 since this quantity involves a ratio of rates. Another peculiar feature of Figure II.40 is that the powder shows a much stronger temperature dependence than the single crystal. The temperature dependences of λ_1 and λ_2 are shown in Figure II.41.

From C_1 , λ_1 , λ_2 , and Eqs. (11.14), (11.18a) [or Eqs. (11.23), (11.27a)] were derived the rate constants S_{11} , S_{44} , and S_{14} . S_{11} and S_{44} are shown in Figures II.43a and II.43b as a function of temperature. The interesting feature of Figure II.43 is that S_{11} and S_{44} have slightly different temperature dependences; that is, they are relaxed by motions which have different activation

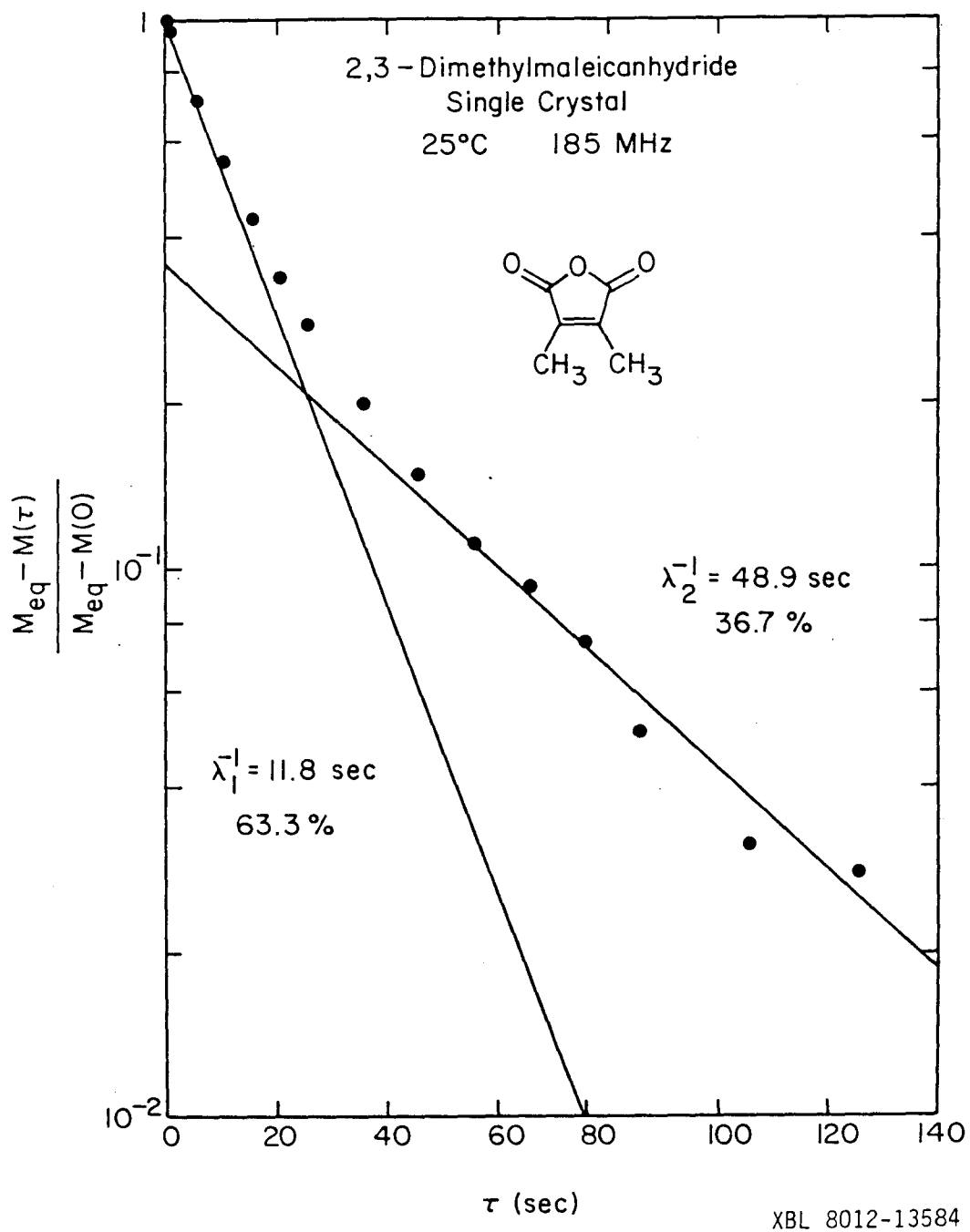


Figure II.36 Bi-exponential T_1 relaxation observed for a single crystal of 2,3-dimethylmaleicanhydride at 25°C. The short and long relaxation times are accurate to within 10% and 15%, respectively.

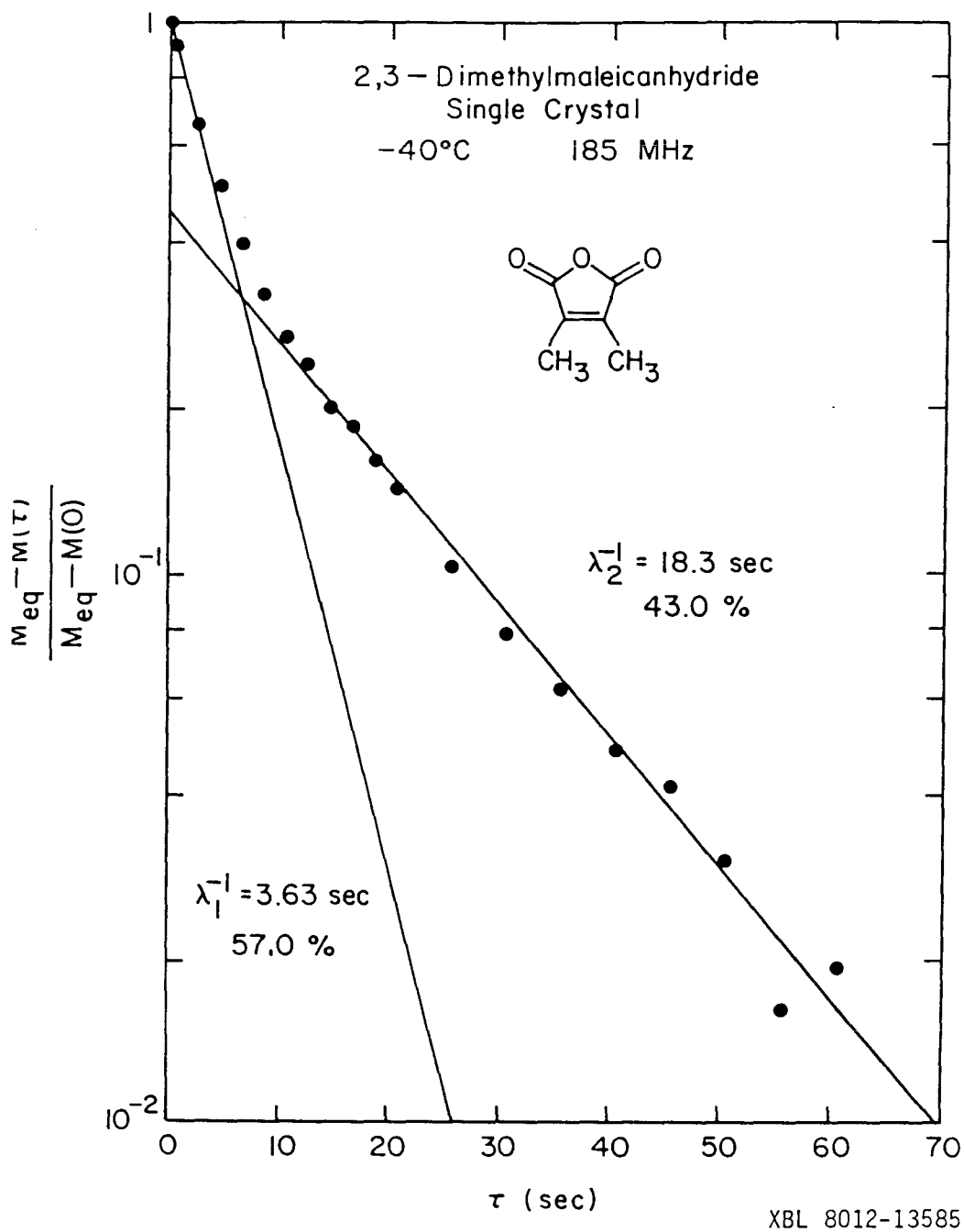


Figure II.37 Bi-exponential T_1 relaxation observed for a single crystal of 2,3-dimethylmaleicanhydride at -40°C . The relaxation times and percentages are accurate to within 10%.

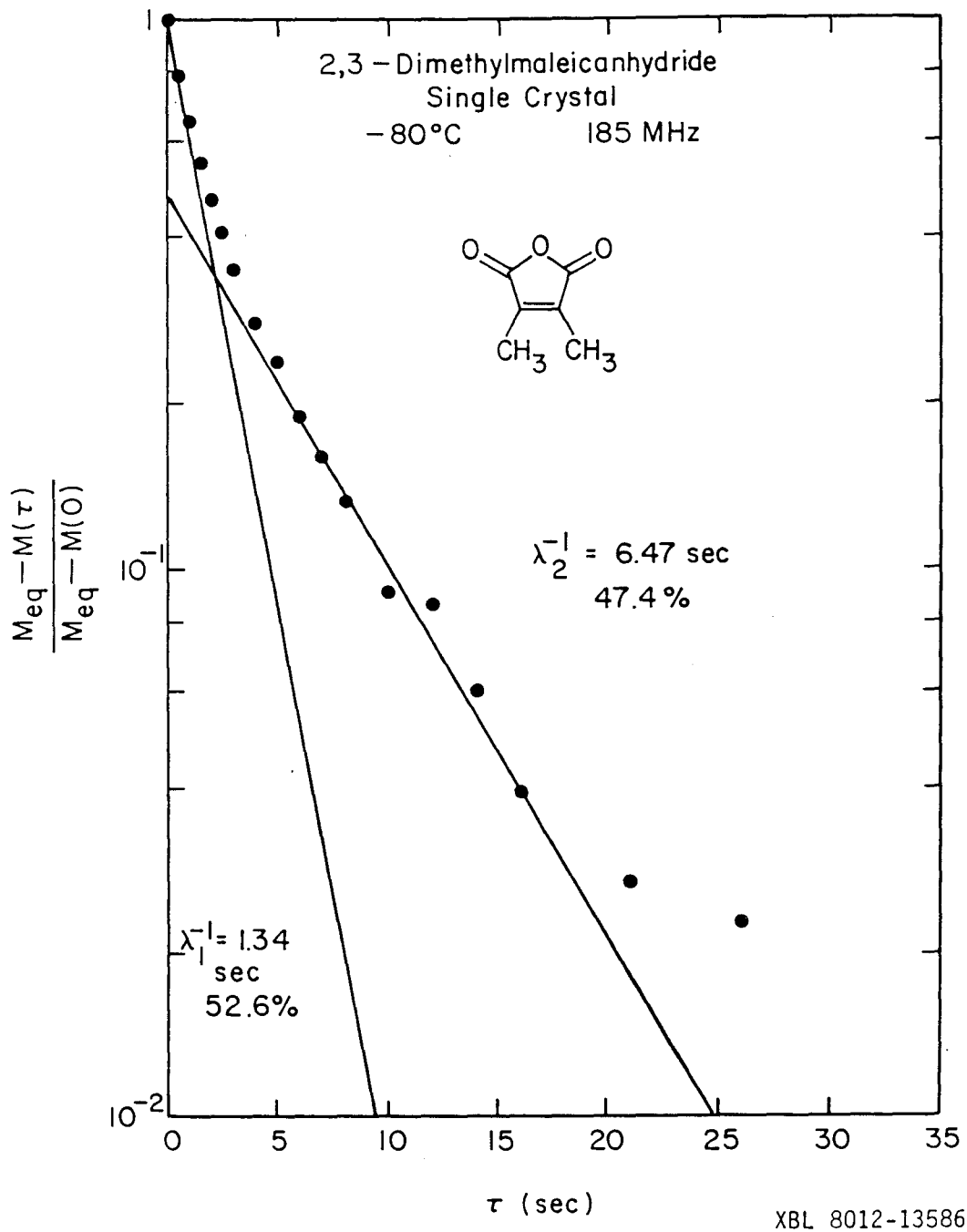


Figure II.38 Bi-exponential T_1 relaxation observed for a single crystal of 2,3-dimethylmaleicanhydride at -80°C . The relaxation times and percentages are accurate to within 10%.

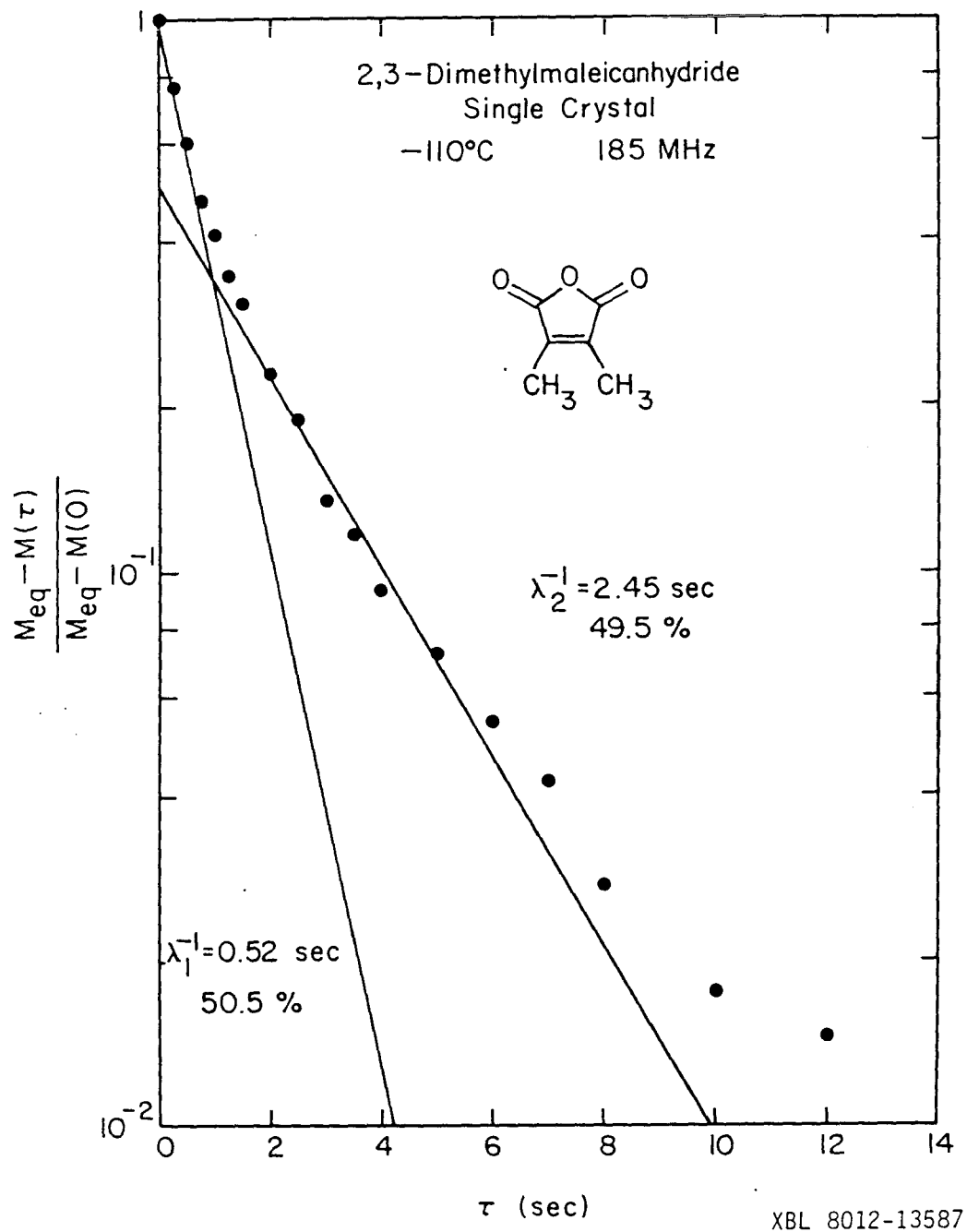
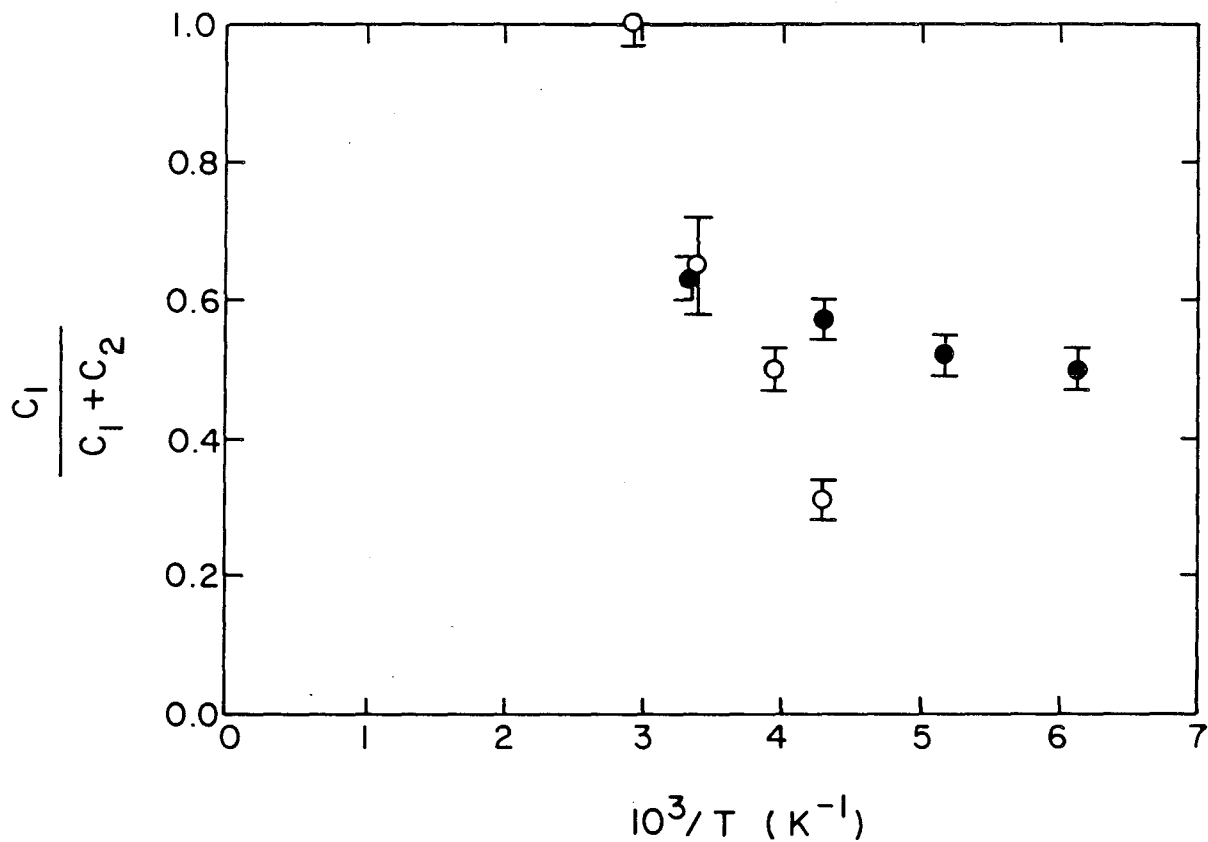
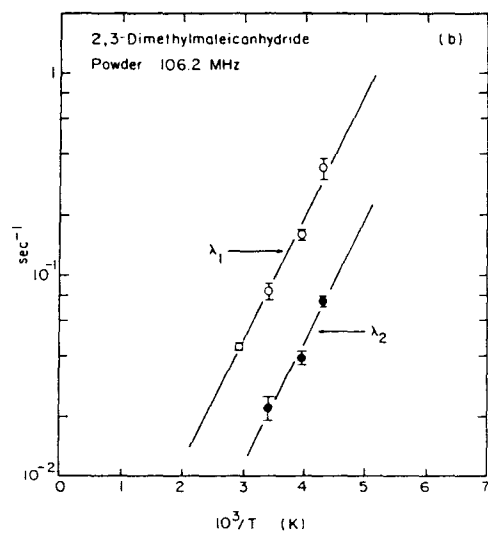
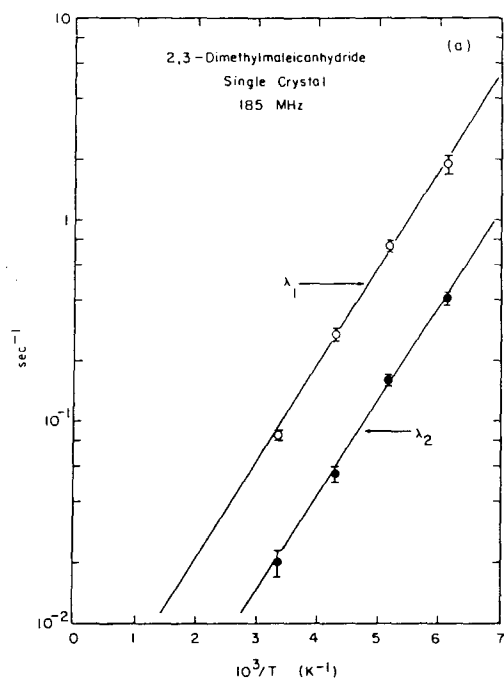


Figure II.39 Bi-exponential T_1 relaxation observed for a single crystal of 2,3-dimethylmaleicanhydride at -110°C . The relaxation times and percentages are accurate to within 10%.



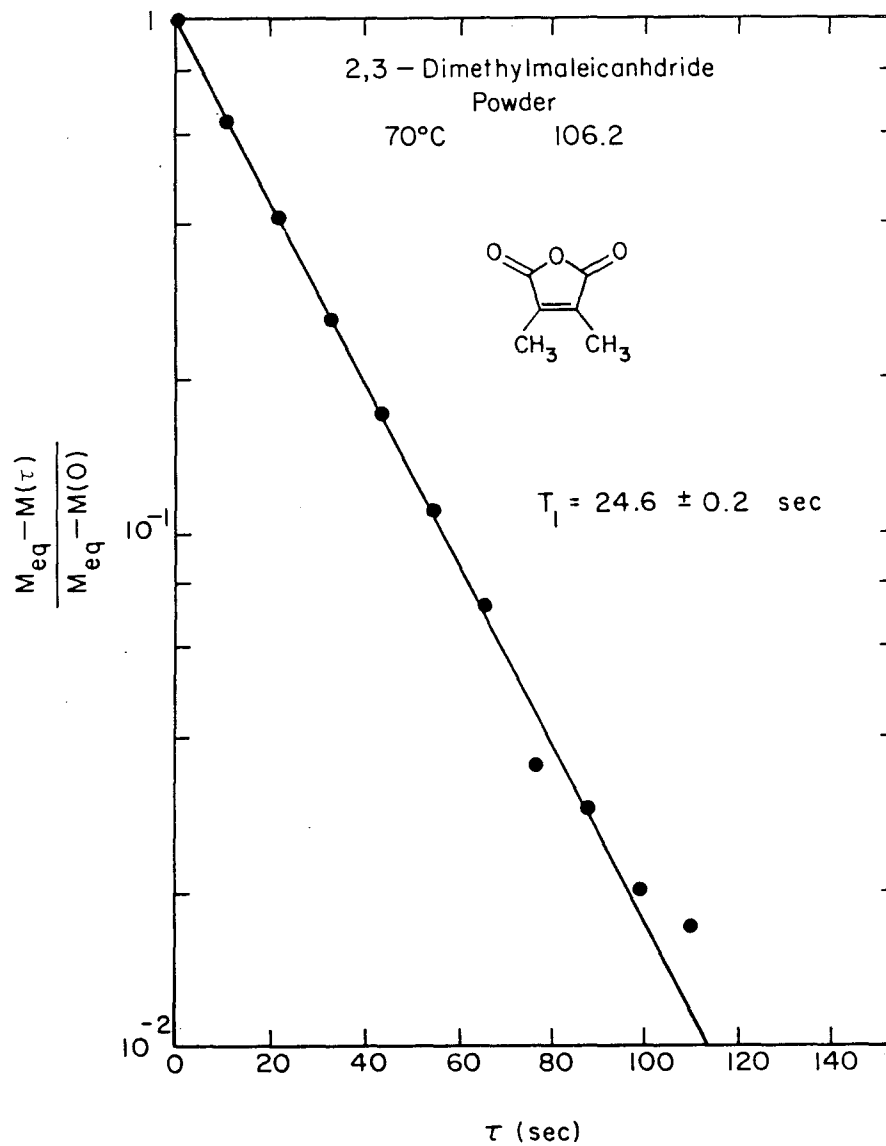
XBL 812-8060

Figure II.40 Temperature dependence of the degree of bi-exponentiality for 2,3-dimethylmaleicanhydride. Open circles are data for a polycrystalline sample, and the solid circles are data for a single crystal at a fixed orientation. The maximum deviation from exponential relaxation is for $C_1/(C_1+C_2)$ equal to 0.5. At the highest temperature used (70°C) the polycrystalline sample showed exponential relaxation (see Figure II.42).



NBL 812-8127

Figure II.41 Temperature dependence of λ_1 and λ_2 for 2,3-dimethylmaleicanhydride. (a) Single crystal at a fixed orientation. (b) Polycrystalline sample.



XBL 812-8129

Figure II.42 Exponential T_1 relaxation observed for a polycrystalline sample of 2,3-dimethylmaleicanhydride at 70°C.

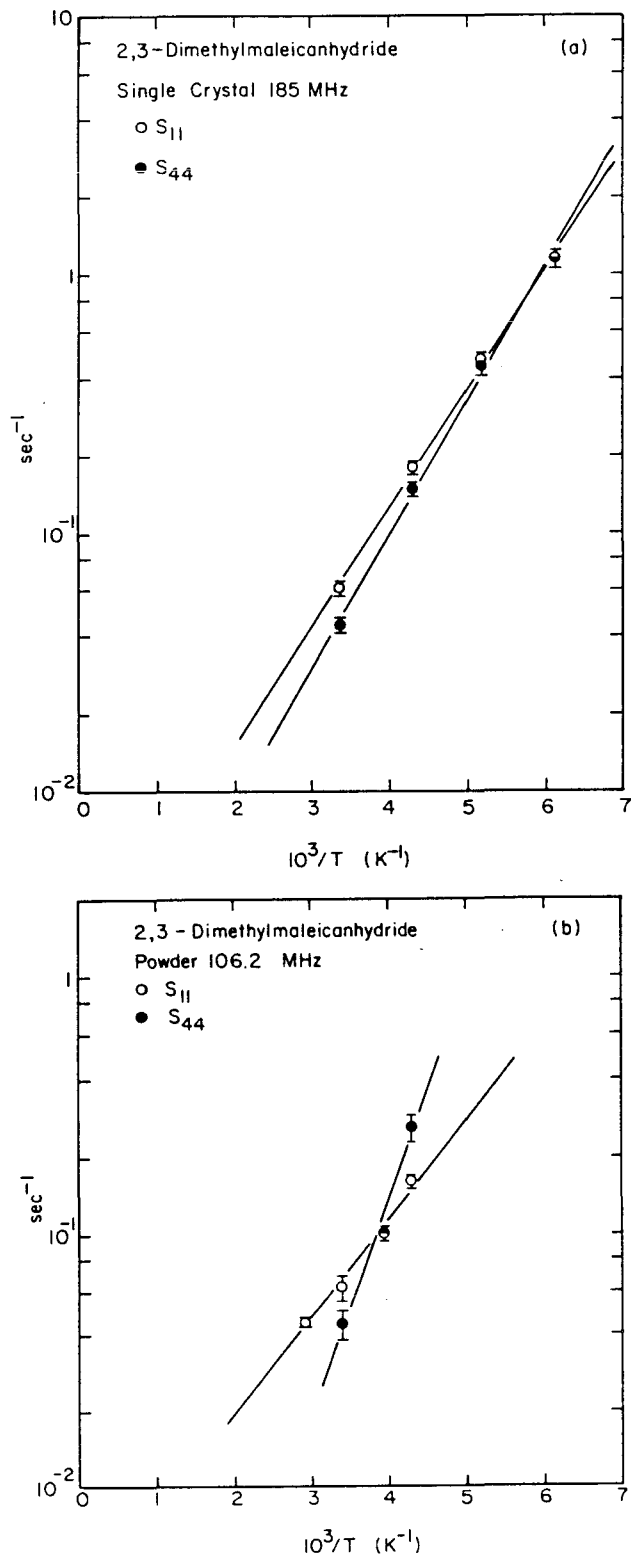


Figure II.43 Temperature dependence of S_{11} and S_{44} for 2,3-dimethylmaleicanhydride. (a) Single crystal at a fixed orientation. (b) Polycrystalline sample.

energies. This is not predicted by Eqs. (11.4a), (11.4c) which describe intramethyl relaxation. Thus, the discrepancy is probably due to intermethyl contributions to S_{11} and S_{44} . It is not unusual that they are affected differently since Zeeman and rotational polarizations may be relaxed by different transitions.

The temperature dependence of S_{14} is shown in Figure II.44. There is no sudden change as a function of temperature which would indicate a transition from independent [Eq. (11.15)] to coupled [Eq. (11.24)] methyl groups. The results on C_1 , however, indicate that if there is a transition it occurs at the highest temperature measured; S_{14} , of course, could not be determined for the exponential decay at 70°C.

The activation energies associated with each of the relaxation rates are compiled in Table II.4. Although the single crystal values are comparable to that measure for durene, the powder values are substantially different. The difference between the single crystal and powder results is not understood. Furthermore, the temperature dependence of T_1 did not reconcile the difference between durene and 2,3-dimethylmaleicanhydride. It may be that intermolecular couplings dominate the durene relaxation and therefore invalidate comparisons made on the basis of molecular structure.

A single crystal of 2,3-dimethylmaleicanhydride containing 10% perdeuterated material was grown in the hope that the crystal could be aligned via the angular dependence of the deuterium quadrupole splitting (see section 12.1). This was unsuccessful

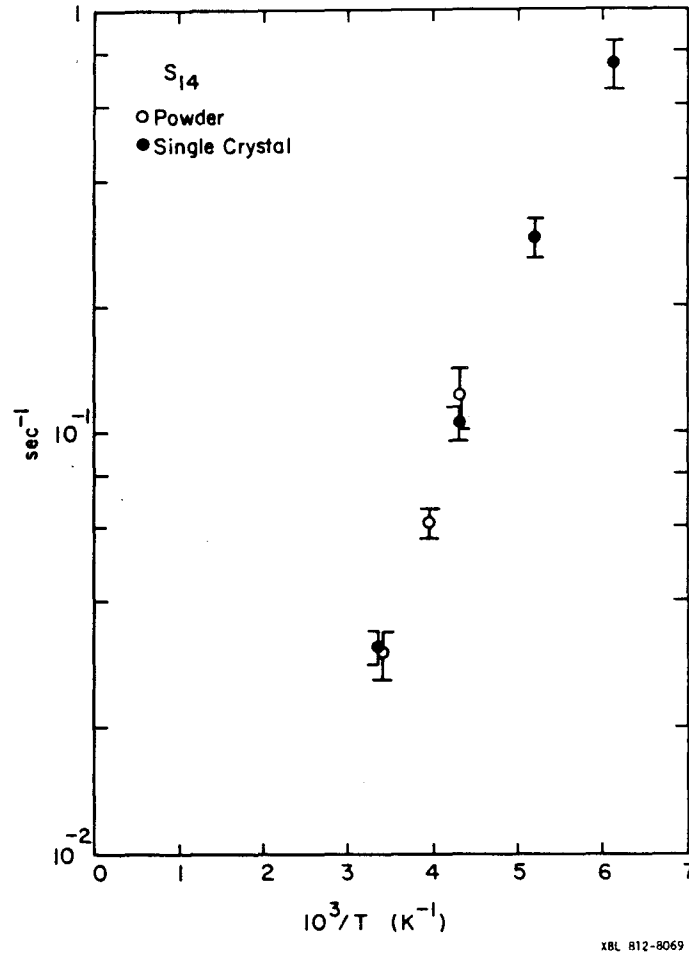


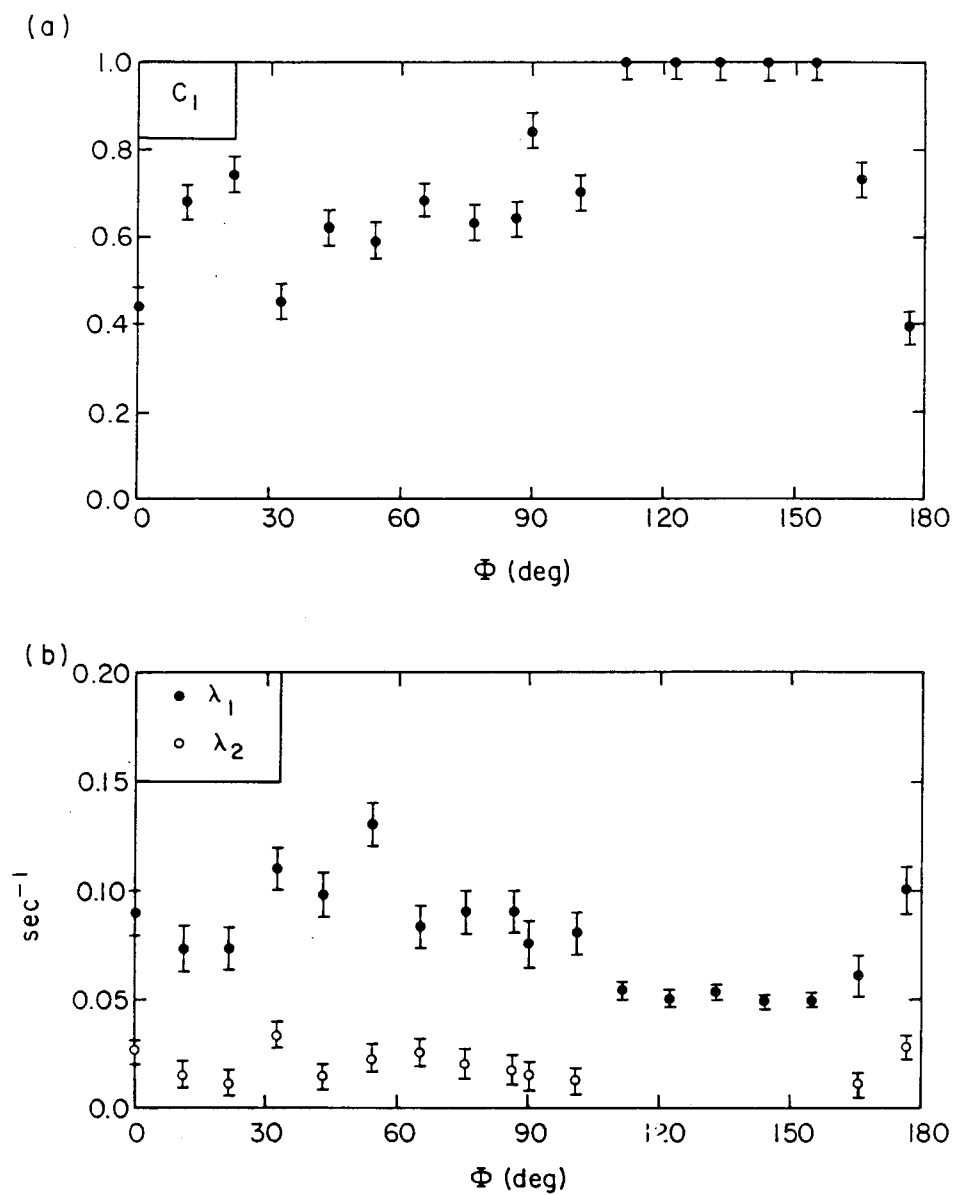
Figure II.44 Temperature dependence of S_{14} for single crystal and polycrystalline samples of 2,3-dimethylmaleicanhydride. The proton frequency is 185 MHz for the single crystal data and 106.2 MHz for the powder data.

due to the complexity of the deuterium NMR spectrum. The angular dependence of the relaxation was studied nevertheless, to see how great the anisotropy is. The angular dependence of C_1 , λ_1 , and λ_2 are recorded in Figures II.45a and II.45b, and the derived values of S_{11} , S_{44} , and S_{14} are shown in Figures II.46a and II.46b. There is a region where the relaxation becomes exponential (see Figure II.45a), but since the molecular orientations could not be identified, it is not possible to correlate the results with the predictions for either independent or coupled methyl groups. It would be very interesting to study the temperature dependence of the anisotropy, particularly with regard to understanding the difference between powder and single crystal (Table II.4).

Table II.4 Activation Energies^a for the Relaxation Rate Constants of 2,3-Dimethylmaleicanhydride at High Temperature

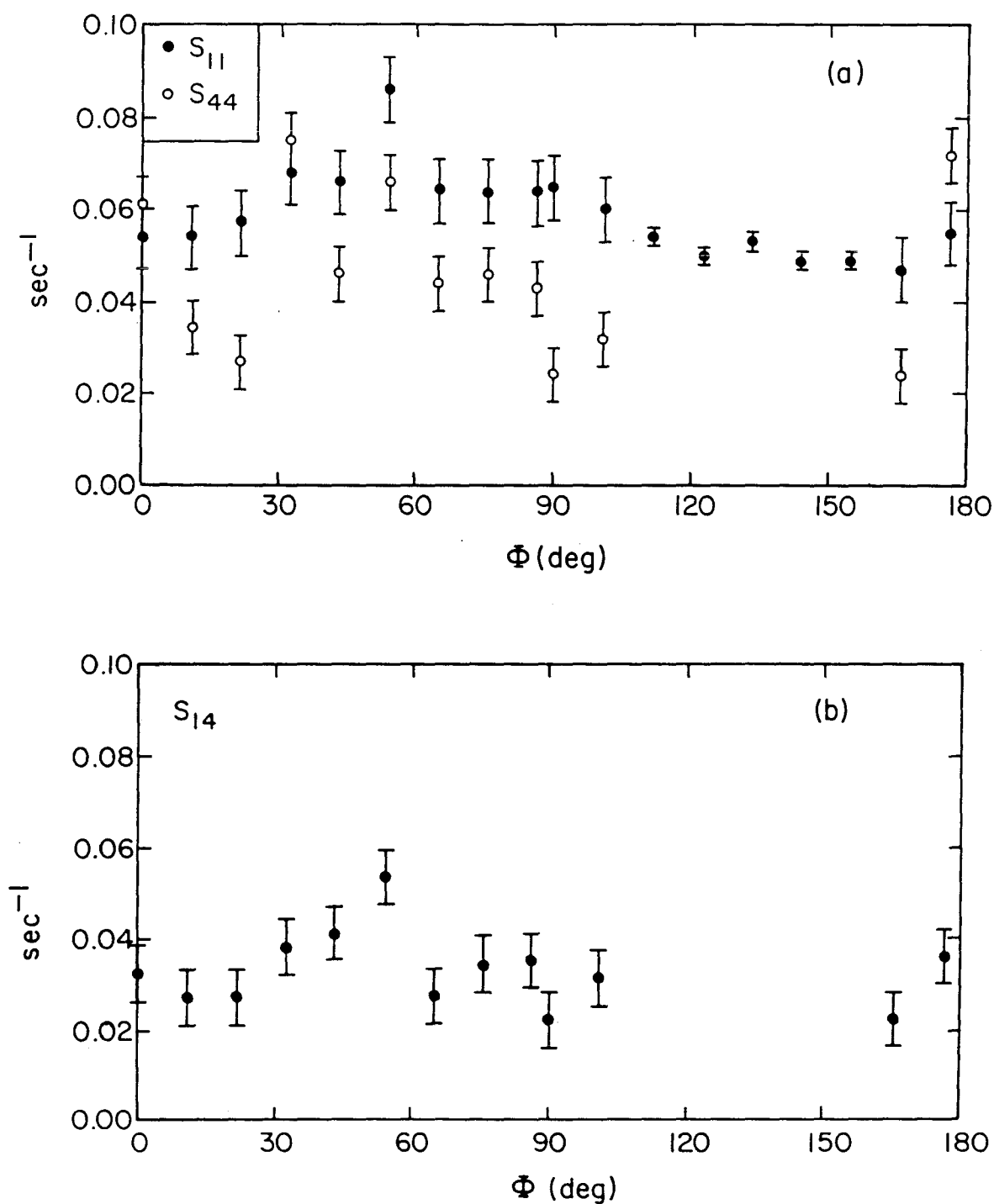
Relaxation Rate Constant	Powder E _a kcal/mole	Single Crystal E _a kcal/mole
S ₁₁	1.7 ± 0.1	2.1 ± 0.1
S ₄₄	3.8 ± 0.4	2.4 ± 0.1
S ₁₄	2.9 ± 0.4	2.3 ± 0.1

^aThe activation energies (E_a) are obtained from the data of Figures II.43 and II.44. An Arrhenius expression is assumed for the correlation time τ_c which is proportional to each of the relaxation rate constants through Eqs. (11.4a)-(11.4c) and (11.5).



XBL 812-8130

Figure II.45 Angular dependence of C_1 , λ_1 , and λ_2 for a single crystal of 2,3-dimethylmaleicanhydride. The proton frequency was 185 MHz, and the temperature was 25°C. (a) $C_1/(C_1+C_2)$ is plotted; the relaxation appears exponential from 112° to 155°. (b) λ_2 is undefined for the region of exponential relaxation.



XBL 812-8070

Figure II.46 Angular dependence of S_{11} , S_{44} , and S_{14} for a single crystal of 2,3-dimethylmaleicanhydride. The proton frequency was 185 MHz, and the temperature was 25°C . S_{44} and S_{14} are undefined for the region 112° to 155° where the relaxation is exponential.

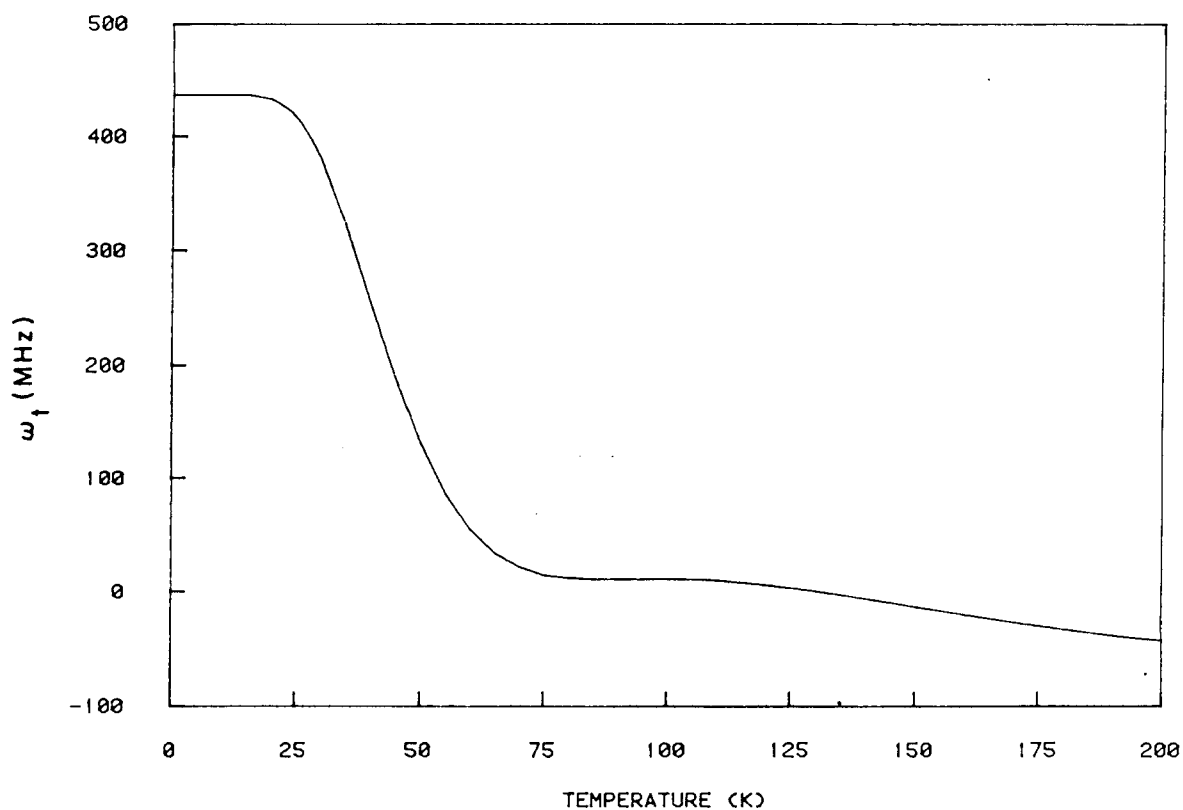
13.6 Temperature Dependent Tunneling Frequency

In section 10.1 the standard model (slightly modified from Reference 11) was presented for explaining the temperature dependence of the observable tunneling frequency ω_t . Calculations from the computer program "methyl" are now presented in order to point out some of the interesting features as well as precautions which are inherent in the use of Eq. (10.7) for ω_t .

In Figure II.47 the theoretical temperature dependence of ω_t is plotted for a barrier V_3 of 1 kcal/mole. The low temperature plateau value of ω_t is the ground state tunneling splitting Δ_0 . As the temperature increases from zero the tunneling splittings $\Delta_0, \Delta_1, \Delta_2, \dots$ of alternating sign average together so that ω_t falls rapidly around 50 K. This is the familiar behavior of ω_t as observed experimentally [12,13,45,46]. To be noted in Figure II.47 is the reappearance of a negative ω_t around 200 K. This author knows of no experiments in which a high temperature tunneling splitting of this sort has been observed. Of the experimental techniques available, Pintar's spin-locking experiments [46], which involve a resonant transfer of energy, are probably best suited for such a measurement. NMR lineshape and relaxation studies would be insensitive to ω_t since at high temperature both are dominated by fast stochastic methyl group reorientation.

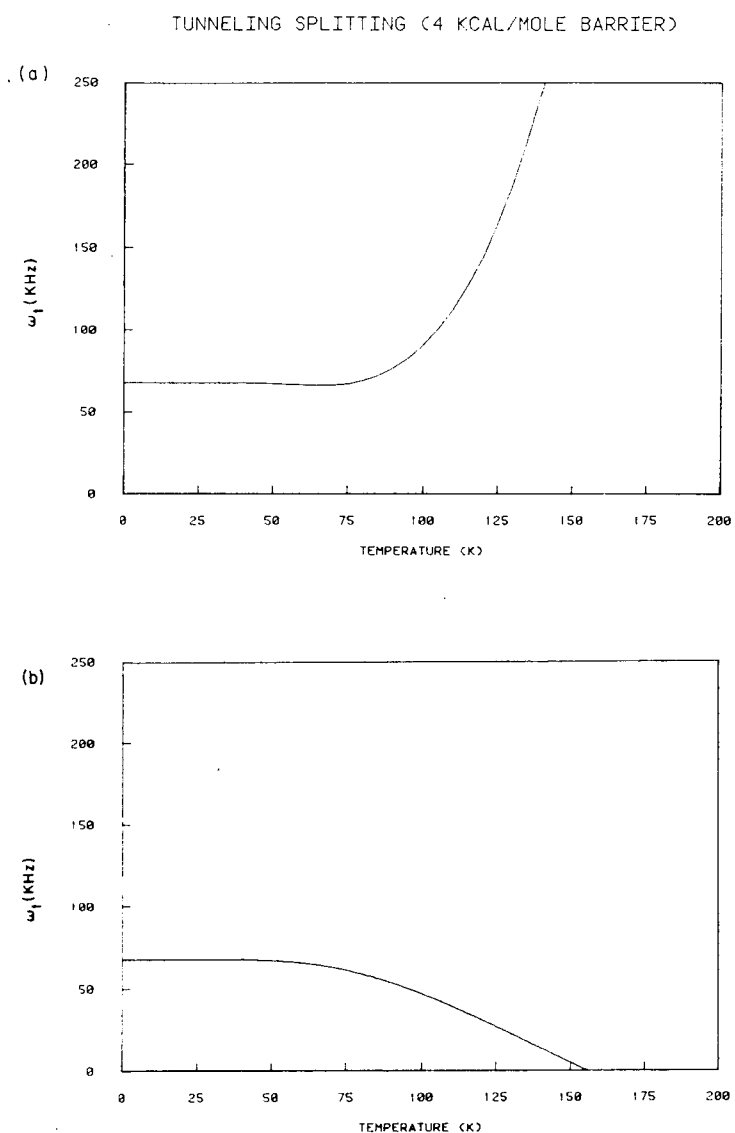
An anomalous case of the temperature dependence will serve to illustrate the limitations of Eq. (10.7). In Figure II.48a is shown the calculation of ω_t for a 4 kcal/mole barrier. Rather

TUNNELING SPLITTING (1 KCAL/MOLE BARRIER)



XBL 812-8115

Figure II.47 Theoretical temperature dependence of the average tunneling splitting ω_t for a C_3 rotor with a 1 kcal/mole rotation barrier. The torsional energies and tunneling splittings were calculated with the program "methyl.f4p", and ω_t was calculated with Eq. (10.7).



XBL 812-8123

Figure II.48 Theoretical temperature dependence of the average tunneling splitting ω_t for a C_3 rotor with a 4 kcal/mole rotation barrier. The torsional energies and tunneling splittings were calculated with the program "methyl.f4p." (a) ω_t was calculated with Eq. (10.7). (b) ω_t was calculated using only the two lowest torsional levels.

than falling, there is an almost monotonic increase of ω_t with increasing temperature. This is in marked contrast to the work of Johnson and Mottley [12] where a barrier of 4 kcal/mole is reported, and yet their data show a tunneling splitting which decreases from a low temperature value of 21 kHz to zero at 85 K. Pintar [46] studied the same compound ($\text{CH}_3\text{CD}_2\text{I}$), and although his experimental fitting parameters do not correspond to a 4 kcal/mole barrier, his data do show a drop in ω_t from 48 kHz at low temperature to near zero at 90 K. In both cases the authors were able to fit their data by using only the two lowest tunneling splittings, Δ_0 and Δ_1 , in calculating ω_t . They are right in assuming that the population of higher levels is quite small, but these levels still contribute significantly to the average since for a barrier of 4 kcal/mole:

$$|\Delta_i| \gg |\Delta_0|, |\Delta_1| \quad (13.21)$$

for $i > 1$.

The underlying assumption of the Boltzmann average of Eq. (10.7) is that the averaging process (i.e., the transitions between torsional states) takes place at a rate much higher than the tunneling frequencies being averaged. For a 4 kcal/mole barrier:

$$\Delta_0 = 6.8 \times 10^4 \text{ Hz}$$

$$\Delta_1 = -6.3 \times 10^5 \text{ Hz}$$

$$\Delta_2 = 6.6 \times 10^7 \text{ Hz} \quad ,$$

and the torsional splittings are

$$e_1 - e_0 = 690 \text{ cal/mole}$$

$$e_2 - e_1 = 652 \text{ cal/mole} \quad .$$

Since the energy differences between the torsional levels are comparable, it may be assumed that the phonon induced transitions between them all proceed at about the same rate Ω . If the phonon density is such that

$$|\Delta_2| > \Omega > |\Delta_1|, |\Delta_0| \quad , \quad (13.22)$$

then:

- 1) The condition of fast exchange [47] applies to Δ_0 and Δ_1 , and an average tunneling splitting appears which is weighted by the Boltzmann factors for e_0 and e_1 , and
- 2) slow exchange applies to Δ_2 so that Δ_2 does not contribute to the average, but rather appears as a distinct tunneling splitting with intensity given by the Boltzmann factor for e_2 .

If condition (13.22) holds at temperatures < 100 K, then it is correct to include only the two lowest levels in the averaging process. The results of such a calculation are shown in Figure II.48b.

It is interesting to note that Johnson and Mottley [12] reported that in some experiments their main observed spectrum for ω_t was superposed with a low intensity spectrum corresponding to a much larger tunneling splitting. Furthermore, Allen [14] used an exchange theory with the two lowest levels to fit Johnson

and Mottley's data; the derived exchange rate was $\Omega = 10 \Delta_0$. The result of these observations is that it is more appropriate to use an exchange theory [14,47] than the thermodynamic average Eq. (10.7) to treat ω_t at low temperature.

Along other lines, it is interesting to compare the classical rotation rate of the hindered methyl rotor with its tunneling frequency. Using the program "methyl" to calculate the expectation value $\langle m \rangle_i$ for the E^a state of the i^{th} torsional level, the rotation frequency $\langle v_R \rangle_i$ is:

$$\langle v_R \rangle_i = \langle m \rangle_i \hbar / (2\pi I) \quad (13.23)$$

where I is the methyl group moment of inertia, $5.5 \times 10^{-40} \text{ g cm}^2$ [10]. In Table II.5 are listed $\langle v_R \rangle_i$ and Δ_i for the first several torsional levels of a methyl rotor with a 1 kcal/mole barrier. Since $\langle m \rangle$ alternates in sign from level to level, this provides, perhaps, a more intuitive view of why coherent tunneling rotation stops at high temperature. That is, as a methyl group in a given torsional level begins to rotate in a clockwise direction, then it is excited to another level and rotates in a counter-clockwise direction, then it decays to a lower level and rotates again in a clockwise direction, etc., with the net effect being that if the transitions are fast enough, the methyl group essentially stands still. This kind of "tunneling blocking" has been referred to in other contexts as well [48,49].

The advantage of viewing the averaging as taking place over $\langle v_R \rangle_i$ rather than Δ_i is simply that the frequency of rotation can

be used to characterize the levels above and below the barrier in energy, whereas it is not evident that the tunneling splitting is a meaningful quantity to apply to the free-rotor-like wave functions above the barrier. In either case there is little quantitative difference as indicated by Table II.5.

Table II.5 Comparison of Classical Rotation Rate and Tunneling Frequency of a Methyl Rotor with a 1 kcal/mole Barrier.

Torsional Level	$\langle v_{R_i} \rangle \times 10^{-12} \text{ Hz}^a$	$\Delta_i \times 10^{-12} \text{ Hz}^b$
0	0.00052	0.00044
1	-0.0174	-0.0146
2	0.232	0.167
3	-0.722	-0.920
4	1.95	1.49
5	-2.33	-2.50
6	3.00	2.84
7	-3.32	-3.48
8	3.95	3.79
9	-4.26	-4.41

^a $\langle v_{R_i} \rangle$ is the classical rotation rate of the E^a state of the methyl rotor in the i^{th} torsional level.

^b Δ_i is the tunneling frequency of the i^{th} torsional level.

14. SUMMARY AND DISCUSSION

The experiments of the preceding chapter provide an overview of the possibilities and difficulties of using Zeeman spin-lattice relaxation to probe methyl group rotation and torsion. The mathematical framework for analyzing the experiments is presented in the sections on independent (11.3.1) and coupled (11.3.2) methyl groups. The treatment of independent methyl groups follows from the work of Emid [6,23,25], while the solution of the coupled methyl group problem is new to this work. At high temperature all of the spin thermodynamics can be viewed as relating solely to the spin states with the coupling between spin and rotor being a consequence of the Pauli exclusion principle. At low temperature the complexity of the treatment increases rapidly [11,50,51,52] as ω_t becomes comparable to the frequency of stochastic methyl group reorientation.

The experiments of sections 13.1, 13.2, and 13.3 illustrate the basic features of the coupling between Zeeman and rotational polarization and demonstrate the validity of the rotational polarization quasi-constant as written in Eq. (11.16). The experiments on equilibrium rotational polarization (section 13.4) are important, because they provide a crucial test of the coupling between spin and spatial wave functions via the Pauli principle; the existence of this coupling at high temperature has been called into question by a few authors [17,18,53]. Unfortunately, sufficient signal to noise was not achieved to conclude that $P_{r,eq}$ is definitely non-zero.

The study of methyl-methyl gearing (section 13.5) is perhaps the area where rotational polarization can play its most useful role. The results on 1,4,5,8-tetramethylanthracene and 1,4,5,8-tetramethylnaphthalene are entirely consistent with the expectations for independent and geared methyl groups, respectively. These measurements, however, are made questionable by the presence of $\mathcal{H}_{D,inter}$. This is not an irresolvable point though; using dipolar relaxation measurements to obtain S_{44} , the contribution of intermethyl relaxation is readily determined.

The differences between durene and 2,3-dimethylmaleicanhydride and between powder and single crystal samples of 2,3-dimethylmaleicanhydride are not understood. From molecular considerations any differences are expected to be slight. An especially interesting study would be to orient a single crystal of, for instance, 2,3-dimethylmaleicanhydride and compare directly the predictions for independent and geared methyl groups with experiment. The orientations where the relaxation is expected to change from non-exponential to exponential are quite different in the two coupling extremes, and trial calculations with the program "couple.c" (Appendix E) indicate large changes in λ_1 , λ_2 as well. This study in conjunction with dipolar relaxation measurements is required if definitive statements about rotational polarization and steric coupling are to be made. Once such a study is completed, then the foundation is laid for using rotational polarization to make general observations about the degree of methyl-methyl gearing in different molecules.

In conclusion, the comments on the temperature dependence of the tunneling frequency are intended as a warning regarding the use of the various expression for ω_t appearing in the literature. The remarks on the relationship between $\langle v_{R_i} \rangle$ and Δ_i are included for the purpose of demystifying the disappearance of tunneling at high temperature.

REFERENCES

1. J. Jeener, *Advances in Magnetic Resonance* (Academic, New York-London, 1968), Vol. 3, p. 205.
2. W. Th. Wenckebach, T. J. B. Swannenburg, and N. J. Poulis, *Phys. Rep.* 14, 181 (1974).
3. M. Goldman, *Spin Temperature and Nuclear Magnetic Resonance in Solids* (Oxford University Press, London, 1970), p. 52ff.
4. R. L. Hilt and P. S. Hubbard, *Phys. Rev.* 134, A392 (1964).
5. A. E. Zweers, Ph.D. dissertation, University of Leiden, The Netherlands (1976), pp. 93, 94, 98, 99.
6. S. Emid, R. J. Baarda, J. Smidt, and R. A. Wind, *Physica* 93B, 327 (1978).
7. C. P. Slichter, *Principles of Magnetic Resonance* (Springer, Berlin-Heidelberg-New York, 1978), p. 154ff.
8. A. Abragam and M. Goldman, *Nuclear Magnetism, Order and Disorder* (Oxford University Press, London, in press, 1981), Chapter 1, section C.
9. C. S. Johnson and L. G. Pedersen, *Problems and Solutions in Quantum Chemistry and Physics* (Addison-Wesley, Reading-Menlo Park-London-Amsterdam-Don Mills-Sydney, 1976), p. 329.
10. G. Herzberg, *Molecular Spectra and Molecular Structure II. Infrared and Raman Spectra of Polyatomic Molecules* (Van Nostrand-Reinhold, New York-Cincinnati-Toronto-London-Melbourne, 1945), p. 437.
11. S. Emid and R. A. Wind, *Chem. Phys. Lett.* 33, 269 (1975).
12. C. S. Johnson and C. Mottley, *Chem. Phys. Lett.* 22, 430 (1973).

13. S. Clough and J. W. Hennel, *J. Phys. C: Solid St. Phys.* 8, 3115 (1975).
14. P. S. Allen, *J. Phys. C: Solid St. Phys.* 7, L22 (1974).
15. W. Müller-Warmuth, R. Schüler, M. Prager, and A. Kollmar, *J. Chem. Phys.* 69, 2382 (1978).
16. D. Smith, *J. Chem. Phys.* 73, 3947 (1980).
17. Reference 5, pp. 65-71.
18. S. Emid, *Chem. Phys. Lett.* 72, 189 (1980).
19. S. Emid, R. A. Wind, and S. Clough, *Phys. Rev. Lett.* 33, 769 (1974).
20. R. A. Wind and S. Emid, *Phys. Rev. Lett.* 33, 1422 (1974).
21. Reference 7, pp. 138-143.
22. Reference 1, footnote 15.
23. R. A. Wind, S. Emid, and J. F. J. M. Pourquié, *Phys. Lett.* 53A, 310 (1975).
24. Reference 5, Appendix E.
25. R. A. Wind, S. Emid, J. F. J. M. Pourquié, and J. Smidt, *J. Phys. C: Solid St. Phys.* 9, 139 (1976).
26. J. H. Freed and G. K. Fraenkel, *J. Am. Chem. Soc.* 86, 3477 (1964).
27. E. E. Gurnell and P. Diehl, *Mol. Phys.* 24, 489 (1972).
28. N. Ya. Shteinshneider, *Teor. Eksp. Khim.* 11, 313 (1975).
29. J. Tang and A. Pines, *J. Chem. Phys.* 73, 2512 (1980).
30. *CRC Handbook of Chemistry and Physics* (CFC Press, Cleveland, 1977), 58th edition.
31. Reference 5, p. 81.
32. W. C-W. Shih, Ph.D. dissertation, University of California,

- Berkeley (Lawrence Berkeley Laboratory report LBL-10097, 1979), p. 243.
33. V. R. Cross, R. K. Hester, and J. S. Waugh, *Rev. Sci. Instrum.* 47, 1486 (1976).
 34. W. Gordy and R. L. Cook, *Microwave Molecular Spectra*, vol. 9 of *Technique of Organic Chemistry*, edited by W. West (Interscience, New York, 1970), Chapter 11.
 35. Reference 34, p. 375.
 36. R. L. Shoemaker and W. H. Flygare, *J. Am. Chem. Soc.* 91, 5417 (1969).
 37. (a) G. H. Golub, V. Pereyra, *Siam J. Numer. Anal.* 10, 413 (1973).
(b) G. H. Golub, V. Pereyra, Stanford C. S. Report 72-261, Feb. 1972.
(c) M. R. Osborne, in *Numerical Methods for Non-Linear Optimization*, edited by Lootsma (Academic, London, 1972).
 38. F. Krogh, *Comm. ACM* 17, 167 (March, 1974).
 39. L. Kaufman, *B.I.T.* 15, 49 (1975).
 40. J. U. von Schuetz and H. C. Wolf, *Z. Naturforsch.* 27a, 42 (1972).
 41. A. Kawamori and R. Takagi, *J. Mag. Res.* 7, 324 (1972).
 42. J. Jeener and P. Broekaert, *Phys. Rev.* 157, 232 (1967).
 43. (a) P. S. Allen and A. Cowking, *J. Chem. Phys.* 49, 789 (1968).
(b) J. J. Rush, *J. Chem. Phys.* 47, 3936 (1967).
 44. J. Haupt, *Z. Naturforsch.* 26a, 1578 (1971).
 45. S. Clough and J. R. Hill, *J. Phys. C: Solid St. Phys.* 7, L20 (1974).

46. D. W. Nicoll and M. M. Pintar, Phys. Rev. Lett. 41, 1496 (1978).
47. A. Carrington and A. D. McLaughlan, Introduction to Magnetic Resonance (Harper and Row, New York-Evanston-London, 1967), Chapter 12.
48. R. A. Harris and L. Stodolsky, Phys. Lett. 78B, 313 (1978).
49. M. Simonius, Phys. Rev. Lett. 40, 980 (1978).
50. S. Emid, R. A. Wind, A. E. Zweers, and H. B. Brom, Physica 81B, 140 (1976).
51. A. E. Zweers, Ph.D. dissertation, University of Leiden, The Netherlands (1976).
52. S. Emid and R. A. Wind, Physica 93B, 344 (1978).
53. S. Clough, J. Phys. C: Solid St. Phys. 5, L204 (1972).

APPENDIX A: Program "sing5.f4p"


```

      program sing5
c
c sing5 calculates the singlet character as a function of time for the
c two electrons of a radical pair. up to 4 hyperfines can be input
c for each radical. other input consists of the two g-factors, the
c magnetic field, and time values for the calculation. the singlet
c character is output (along with "time" and "delta-time") into the
c file "sing.val" for further processing to determine the
c recombination yield.
c
      common/blk1/mat(5,32),mtv(32),mpick(10)
      common/blk4/nblk1(32),nev1(6),inblk1(6),inev1(6),loc1(32)
      common/blk5/nblk2(32),nev2(6),inblk2(6),inev2(6),loc2(32)
      common/blk6/p1,p2
      common/blk7/c1(252),ev1(32),c2(252),ev2(32)
      common/blk8/nsinds,nblks1,nblks2
      dimension mats(4,256),hmat(10,10),u(10,10),a1(4),a2(4)
      dimension s(1000),t(1000),dt(1000)
      equivalence (mat(1,1),mats(1,1)),(p1(1),hmat(1,1))
      equivalence (p2(1),u(1,1))
      complex p1(252),p2(252)
c
c input routine
c
      call into5(ni1,a1,g1,ni2,a2,g2,h,loop1,loop2,loop3,loop4,loop5)
c
c calculations for radical 1
c 1. construct spin configurations
c
      call setup(ni1,nuc1,nrow1,ncol1)
      mt=nrow1
      nblks1=mt+1
      inc=1
      ine=1
c
c 2. pick all configurations of a given angular momentum
c 3. construct hamiltonian matrix for these configurations
c 4. diagonalize the hamiltonian matrix
c 5. repeat the procedure for each possible angular momentum
c
      do 100 i=1,nblks1
      call pick(mt,ncol1,nfns,nblk1,loc1,i)
      call hamil(nrow1,nfns,a1,a1,h,hmat)
      call hdiag(hmat,nfns,c1(inc),ev1(ine),u)
      nev1(i)=nfns
      inev1(i)=ine
      inblk1(i)=inc
      ine=ine+nfns
      inc=inc+nfns*nfns
      mt=mt-2
100 continue
c
c the above 5-step procedure is repeated for the second radical
c
      call setup(ni2,nuc2,nrow2,ncol2)
      mt=nrow2
      nblks2=mt+1
      inc=1
      ine=1
      do 200 i=1,nblks2

```

```

      call pick(mt,ncol2,nfns,nblk2,loc2,i)
      call hamil(nrow2,nfns,a2,q2,h,hmat)
      call hdiag(hmat,nfns,c2(inc),ev2(ine),u)
      nev2(i)=nfns
      inev2(i)=ine
      inblk2(i)=inc
      ine=ine+nfns
      inc=inc+nfns*nfns
      mt=mt-2
200   continue
      write(6,205)
205   format(1x,"diagonalization completed - begin time
c development")
c
c   construct the matrix of all singlet configurations
c
      call sing(nuc1,nuc2,mats,nsings)
c
c   calculate the evolution of singlet character with time
c
      ti=0.
      loop=0
      if(loop1.gt.0) call stime5(ti,1.e-11,loop1,loop,s,t,dt,mats)
      if(loop2.gt.0) call stime5(ti,1.e-10,loop2,loop,s,t,dt,mats)
      if(loop3.gt.0) call stime5(ti,1.e-09,loop3,loop,s,t,dt,mats)
      if(loop4.gt.0) call stime5(ti,1.e-08,loop4,loop,s,t,dt,mats)
      if(loop5.gt.0) call stime5(ti,1.e-07,loop5,loop,s,t,dt,mats)
c
c   output section
c
      open(unit=01,name='sing.val',type='new')
      write(1,300)
300   format(1x,"sing.val" - output file for "sing5")
      write(1,400) nil
400   format(/,1x,i1," hyperfines on radical 1:")
      if(nil1.gt.0) write(1,500) (a1(i), i=1,nil1)
500   format(5x,f8.3," gauss")
      write(1,600) g1
600   format(/,5x,f6.4" = g-value")
      write(1,700) ni2
700   format(/,1x,i1," hyperfines on radical 2:")
      if(ni2.gt.0) write(1,500) (a2(i), i=1,ni2)
      write(1,800) q2
      write(1,800) n
800   format(/,1x,e11.3," gauss external magnetic field")
      write(1,900) nsings
900   format(/,1x,i5," singlets calculated")
      write(1,1000) loop
1000  format(/,1x,i5," different time values calculated:")
      write(1,1100) loop1
1100  format(5x,i5," x 1.0e-11 sec")
      write(1,1200) loop2
1200  format(5x,i5," x 1.0e-10 sec")
      write(1,1300) loop3
1300  format(5x,i5," x 1.0e-9 sec")
      write(1,1400) loop4
1400  format(5x,i5," x 1.0e-8 sec")
      write(1,1500) loop5
1500  format(5x,i5," x 1.0e-7 sec")
      write(1,1500)

```

```
1600   format('/',1x,'      time          s(t)          dt(t)  ')
1700   write(1,1700) (t(i),s(i),dt(i),i=1,loop)
1700   format(1x,3e15.5)
1700   close(unit=01)
1700   end
```

```

c
c  subroutine into5 follows.
c
      subroutine into5(ni1,a1,g1,ni2,a2,g2,h,loop1,loop2,loop3,
c loop4,loop5)
c
c  input routine written for program "sing5"
c
      dimension a1(4),a2(4)
      write(o,100)
100     format(1x,"program sing5...",&1x,
c "cidnp singlet calculation",&1x,
c "enter number of spins on each radical (up to 4 for each):",&3)
      read(5,150) ni1,ni2
150     format(2i2)
      write(o,200)
200     format(/,1x,"note: hyperfine constants and magnetic field",&1x,
c/x,"must have the same units (gauss)",&1x,
      if(ni1.eq.0) go to 350
      write(o,300) ni1
300     format(1x,"enter the",&1x," hyperfine constants for radical 1")
      read(5,305) (a1(i),i=1,ni1)
305     format(10f4.0)
350     if(ni2.eq.0) go to 450
      write(o,400) ni2
400     format(1x,"enter the",&1x," hyperfine constants for radical 2")
      read(5,305) (a2(i),i=1,ni2)
450     write(o,500)
500     format(/,1x,"enter the g-factor for radical 1:",&3)
      read(5,305) g1
      write(o,600)
600     format(1x,"enter the g-factor for radical 2:",&3)
      read(5,305) g2
      write(o,700)
700     format(/,1x,"enter the magnetic field strength:",&3)
      read(5,305) h
      write(o,800)
800     format(/,1x,"time increment information - enter the number of"
c/x," iterations (1000 total) for each of the following times.")
      write(o,815)
815     format(1x,"1.0e-11 sec :",&3)
      read(5,865) loop1
      write(o,825)
825     format(1x,"1.0e-10 sec :",&3)
      read(5,865) loop2
      write(o,835)
835     format(1x,"1.0e-09 sec :",&3)
      read(5,865) loop3
      write(o,845)
845     format(1x,"1.0e-08 sec :",&3)
      read(5,865) loop4
      write(o,855)
855     format(1x,"1.0e-07 sec :",&3)
      read(5,865) loop5
865     format(14)
      write(o,900)
900     format(/,1x,"thank-you and may you have a good calculation",&1x)
      return
      end
c

```

```

c  subroutine setup follows.
c
      subroutine setup(ni,nuc,nrow,ncol)
c
c  sets up the matrix of all possible spin configurations
c  for a given radical - uses binary counting for generating
c  all of the permutations of up and down spins
c
      common/lblk1/mat(5,32),mtv(32),mpick(10)
      nuc=2**ni
      nrow=ni+1
      ncol=nuc+nuc
      do 600 nca=1,nuc
      ncb=nca+nuc
      mat(1,nca)=1
      mat(1,ncb)=-1
      mi=0
      if(nrow.eq.1) go to 550
      num=nca-1
      jbin=nuc
      do 450 j=2,nrow
      jbin=jbin/2
      k=num-jbin
      if(k) 50,150,350
50      mat(j,nca)=-1
      mat(j,ncb)=-1
      mi=mi-1
      go to 450
150     mat(j,nca)=1
      mat(j,ncb)=1
      mi=mi+1
      if(j.eq.nrow) go to 550
      j1=j+1
      do 250 nr=j1,nrow
      mat(nr,nca)=-1
      mat(nr,ncb)=-1
      mi=mi-1
250     continue
      go to 550
350     mat(j,nca)=1
      mat(j,ncb)=1
      mi=mi+1
      num=k
      continue
450     mtv(nca)=mi+1
550     mtv(ncb)=mi-1
600     continue
      return
      end

c  subroutine pick follows.
c
      subroutine pick(mt,ncol,nfns,nblk,loc,i)
c
c  picks out all basis functions of a given total
c  angular momentum
c
      common/lblk1/mat(5,32),mtv(32),mpick(10)
      dimension nblk(1),loc(1)
      nfns=0

```

```

do 100 j=1,ncol
  if(mtv(j).ne.mt) go to 100
  nfns=nfns+1
  mpick(nfns)=j
  nblk(j)=i
  loc(j)=nfns
100  continue
     return
     end

c
c  subroutine hamil follows.
c
c      subroutine hamil(nrow,nfns,a,g,h,hmat)
c
c  constructs the hamiltonian matrix for a group of
c  spin states
c
c      common/iblk1/mat(5,32),mtv(32),mpick(10)
c      dimension hmat(nfns,nfns),a(1),mcol(5),hvec(10)
c      gfree=2.002522
c      do 1000 i=1,nfns
c        nbf=mpick(i)
c        ms=mat(1,nbf)
c        mcol(1)=ms
c        sec=0.
c        if(nrow.eq.1) go to 150
c        do 50 igo=2,nrow
c          mi=mat(igo,nbf)
c          mcol(igo)=mi
c          nhyp=igo-1
c          sec=sec+a(nhyp)*mi
50      continue
150     hmat(i,1)=ms*(g*n/gfree+sec*.5)*.5
c          if(i.eq.nfns) go to 1100
c          ioff=i+1
c          do 250 igo=ioff,nfns
c            hvec(igo)=0.
250         continue
c          if(ms.eq.-1) go to 550
c          mcol(1)=-1
c          do 450 igo=2,nrow
c            nhyp=igo-1
c            if(mcol(igo).eq.1) go to 450
c            mcol(igo)=1
c            do 350 irun=ioff,nfns
c              nbf2=mpick(irun)
c              if(1check(mcol,mat(1,nbf2),nrow).eq.0) go to 350
c              hvec(irun)=a(nhyp)*.5
350         continue
c          mcol(igo)=-1
c          continue
c          go to 850
450         mcol(1)=1
550         do 750 igo=2,nrow
c           nhyp=igo-1
c           if(mcol(igo).eq.-1) go to 750
c           mcol(igo)=-1
c           do 650 irun=ioff,nfns
c             nbf2=mpick(irun)
c             if(1check(mcol,mat(1,nbf2),nrow).eq.0) go to 650

```

```

        hvec(irun)=a(nhyp)*.5
650      continue
        mcol(igo)=1
750      continue
850      do 950 igo=ioff,nfns
          hmat(i,igo)=hvec(igo)
          hmat(igo,i)=hvec(igo)
950      continue
1000     continue
1100     return
        end

c
c function icode follows.
c
c       function icode(ivec,jvec,nrow)
c
c if two vectors are not identical the function returns zero
c otherwise it returns 1
c
c       dimension ivec(1),jvec(1)
c       icode=0
c       do 100 i=1,nrow
100      if(ivec(i).ne.jvec(i)) go to 200
c       continue
c       icode=1
200      return
c       end

c
c subroutine hdiag follows.
c
c       subroutine hdiag(h,n,cv,ev,u)
c
c diagonalization routine
c based on the method of jacobi, it diagonalizes a real
c symmetric matrix by performing a rotation whenever the
c angle is greater than a given threshold. this process
c continues with the threshold angle being decreased until
c some minimum angle criterion is met.
c
c       dimension h(n,n),u(n,n),cv(1),ev(1)
c       do 100 i=1,n
c       do 50 j=i,n
c       u(i,j)=0.
c       u(j,i)=0.
50      continue
c       u(i,i)=1.
100     continue
c       nr=0
c       if(n.eq.1) go to 700
c       angmin=0.017
c       ang=0.1745
c       istop=n-1
200     test=tan(ang)*.5
300     do 400 i=1,istop
c       ip=i
c       hi=h(i,i)
c       jgo=i+1
c       do 350 j=jgo,n
c       jp=j
c       hij=h(i,j)

```

```

      hjj=h(j,j)
      adj=hi-hjj
      if(abs(hij).gt.test*abs(adj)) go to 500
350   continue
400   continue
      if(ang.lt.angmin) go to 700
      ang=ang*.33333
      go to 200
500   nr=nr+1
      opp=2.*hij
      theta=arctan(opp,adj)*.5
      c=cos(theta)
      s=sin(theta)
      do 600 k=1,n
      if(k.lt.ip) hik=h(k,ip)
      if(k.gt.ip) hik=h(ip,k)
      if(k.lt.jp) hjk=h(k,jp)
      if(k.gt.jp) hjk=h(jp,k)
      if(k.lt.ip.and.k.ne.jp) h(k,ip)=hik*c+hjk*s
      if(k.gt.ip.and.k.ne.jp) h(ip,k)=hik*c+hjk*s
      if(k.lt.jp.and.k.ne.ip) h(k,jp)=-hik*s+hjk*c
      if(k.gt.jp.and.k.ne.ip) h(jp,k)=-hik*s+hjk*c
      uki=u(k,ip)
      ukj=u(k,jp)
      u(k,ip)=uki*c+ukj*s
      u(k,jp)=-uki*s+ukj*c
600   continue
      cos2=c*c
      sin2=s*s
      cross=2.*hij*c*s
      h(ip,jp)=0.
      h(ip,ip)=hi*cos2+cross+hjj*sin2
      h(jp,jp)=hi*sin2-cross+hjj*cos2
      go to 500
700   ind=0
      do 800 j=1,n
      ev(j)=h(j,j)
      do 750 i=1,n
      ind=ind+1
      cv(ind)=u(i,j)
750   continue
800   continue
      return
      end

c
c  function arctan follows.
c
c      function arctan(opp,adj)
c
c  computes the arc-tangent of opp/adj
c
c      arctan=1.570796327
c      if(adj.eq.0.) go to 100
c      if(abs(adj).lt.abs(opp)*1.e-20) go to 100
c      arg=opp/adj
c      arctan=atan(arg)
100   return
      end

c
c  subroutine sing follows.

```



```

C
C   subroutine sing(nuc1,nuc2,mats,nsings)
C
C   sets up the matrix of all possible singlet configurations
C
C       dimension mats(4,256)
C       nsings=nuc1*nuc2
C       icol=0
C       do 100 i=1,nuc1
C       do 50 j=1,nuc2
C       icol=icol+1
C       mats(1,icol)=i
C       mats(2,icol)=j+nuc2
C       mats(3,icol)=i+nuc1
C       mats(4,icol)=j
50      continue
100     continue
        return
        end

C
C   subroutine prod follows.
C
C       subroutine prod(c,ev,t,nblks,inblk,inev,nev,p)
C
C   computes the product of the eigenvector matrix
C   (in vector form) with the phase vector and with the
C   transpose of the eigenvector matrix. gives the
C   time development of the wave functions.
C
C       dimension c(1),ev(1),inblk(1),inev(1),nev(1)
C       complex p(1)
C
C   tig is 'time in inverse gauss', i.e. the conversion from gauss to
C   radians.
C
C       tig=t*1.759e07
C       do 100 i=1,nblks
C       inc=inblk(i)
C       ine=inev(i)
C       call psub(c(inc),ev(ine),tig,nev(i),p(inc))
100     continue
        return
        end

C
C   subroutine psub follows.
C
C       subroutine psub(c,ev,t,nev,p)
C
C   multiplies diagonal block matrices for routine prod
C
C       dimension c(1),ev(1)
C       complex p(1),phase(10),phold
C       do 100 k=1,nev
C       arg=ev(k)*t
C       if(abs(arg).gt.100.) arg=argue(ev(k),t)
C       phase(k)=cmplx(cos(arg),-sin(arg))
100     continue
        do 500 i=1,nev
        ipart=(i-1)*nev
        do 250 j=i,nev

```

```

      jpart=(j-1)*nev
      ij=jpart+i
      ji=ipart+j
      phold=cmplx(0.,0.)
      do 150 k=1,nev
      kpart=(k-1)*nev
      ik=kpart+i
      jk=kpart+j
      phold=phold+c(ik)*phase(k)*c(jk)
150    continue
      p(ij)=phold
      p(ji)=phold
250    continue
300    continue
      return
      end

c
c  function argue follows.
c
c      function argue(ev,t)
c
c  reduces a large trigonometric argument (the product
c  of ev and t) to a small one
c
c      twopi=6.283185308
c      w=ev/twopi
c      iw=w
c      rw=w-iw
c      it=t
c      rt=t-it
c      a1=iw*rt
c      i1=a1
c      r1=a1-i1
c      a2=it*rw
c      i2=a2
c      r2=a2-i2
c      argue=(r1+r2+rw*rt)*twopi
c      return
c      end

c
c  subroutine sfind follows.
c
c      subroutine sfind(mats,schar)
c
c  routine to project the singlet character out of
c  those states originating in the singlet manifold.
c
c      common/iblk4/nblk1(32),nev1(6),inblk1(6),inev1(6),loc1(32)
c      common/iblk5/nblk2(32),nev2(6),inblk2(6),inev2(6),loc2(32)
c      common/iblk6/p1,p2
c      common/iblk8/nsings,nblks1,nblks2
c      dimension mats(4,256)
c      complex p1(252),p2(252),scoef
c      schar=0.
c      do 400 i=1,nsings
c      is1=mats(1,i)
c      is2=mats(2,i)
c      is3=mats(3,i)
c      is4=mats(4,i)
c      ib1=nblk1(is1)

```

```

      ib2=nb1k2(is2)
      ib3=nb1k1(is3)
      ib4=nb1k2(is4)
      do 350 j=i,nsings
      js1=mats(1,j)
      js2=mats(2,j)
      js3=mats(3,j)
      js4=mats(4,j)
      jb1=nb1k1(js1)
      jb2=nb1k2(js2)
      jb3=nb1k1(js3)
      jb4=nb1k2(js4)
      if(ib1.ne.jb1) go to 50
      if(ib2.ne.jb2) go to 350
      ind1a=ind(inb1k1(ib1),nev1(ib1),loc1(js1),loc1(is1))
      ind2b=ind(inb1k2(ib2),nev2(ib2),loc2(js2),loc2(is2))
      ind1b=ind(inb1k1(ib3),nev1(ib3),loc1(js3),loc1(is3))
      ind2a=ind(inb1k2(ib4),nev2(ib4),loc2(js4),loc2(is4))
      scoef=p1(ind1a)*p2(ind2b)+p1(ind1b)*p2(ind2a)
      s=real(scoef*conjg(scoef))
      go to 250
50    if(ib1.ne.jb3) go to 150
      if(ib2.ne.jb4) go to 350
      ind1=ind(inb1k1(ib1),nev1(ib1),loc1(js3),loc1(is1))
      ind2=ind(inb1k2(ib2),nev2(ib2),loc2(js4),loc2(is2))
      scoef=p1(ind1)*p2(ind2)
      s=real(scoef*conjg(scoef))
      go to 250
150   if(ib3.ne.jb1) go to 350
      if(ib4.ne.jb2) go to 350
      ind1=ind(inb1k1(ib3),nev1(ib3),loc1(js1),loc1(is3))
      ind2=ind(inb1k2(ib4),nev2(ib4),loc2(js2),loc2(is4))
      scoef=p1(ind1)*p2(ind2)
      s=real(scoef*conjg(scoef))
250   if(.gt.i) s=s*2.
      schar=schar+s
350   continue
400   continue
      schar=schar*.25
      return
      end

c
c function ind follows.
c
c      function ind(inblk,nev,i,j)
c
c computes index for vector entry
c
c      ind=(j-1)*nev+i+inblk-1
c      return
c      end

c
c subroutine stime5 follows.
c
c      subroutine stime5(ti,del,ntimes,loop,s,t,dt,mats)
c
c calculate the evolution of singlet character with time
c
c      common/ib1k4/nb1k1(32),nev1(6),inb1k1(6),inev1(6),loc1(32)
c      common/ib1k5/nb1k2(32),nev2(6),inb1k2(6),inev2(6),loc2(32)

```

```

common/blk6/p1,p2
common/blk7/c1(252),ev1(32),c2(252),ev2(32)
common/blk8/nsings,nblks1,nblks2
dimension s(1000),t(1000),dt(1000),mats(4,256)
complex p1(252),p2(252)
ndel=0
do 100 i=loop+1,loop+ntimes
  ti=ti+del
  t(i)=ti
  dt(i)=del
  ndel=ndel+1
  call prod(c1,ev1,ti,nblks1,inblk1,inev1,nev1,p1)
  call prod(c2,ev2,ti,nblks2,inblk2,inev2,nev2,p2)
c
c project the singlet character out of each of the developing states
c
  call sfind(mats,schar)
  s(i)=schar/nsings
100 continue
  loop=loop+ndel
  return
end

```

APPENDIX B: Program "diffus.f4p"

```

      program diffus
c
c  program written to accompany "sing5".  "sing5" calculates the
c  singlet character of a given radical pair system as a
c  function of time.  "diffus" accepts s(t) data for c-12 and c-13
c  radical pairs from the files "c12.dat" and "c13.dat", respectively.
c  diffusion and reaction parameters are input from the file
c  "diffus.dat".
c
      real s12(1000), t12(1000), dt12(1000)
      real s13(1000), t13(1000), dt13(1000)
      common rcol, rzero, lamda, fs, ncol
      real kloss, lamda
      data pi/3.14159/
c
c  input section
c  input general parameters for radicals and solvent
c
      open( unit=01, name='diffus.dat', type='old', readonly )
      read(1, 50)
      read(1, 50)
50      format(1x)
      read(1,150) rcol
      rcol = rcol * 1.0e-8
150      format(f7.0)
      read(1, 50)
      read(1,150) rzero
      rzero = rzero * 1.0e-8
      read(1, 50)
      read(1,250) kloss
250      format(e15.5)
      read(1, 50)
      read(1,150) fs
      read(1, 50)
      read(1,250) pmin
      read(1,250) pmax
      read(1, 50)
      read(1,350) num
350      format(i5)
      read(1, 50)
      read(1,150) lamda
      read(1, 50)
      read(1,350) ncol
      close( unit=01 )
c
c  input t, s(t), and dt for c-12 radical pairs
c
      open( unit=01, name='c12.dat', type='old', readonly )
      read(1, 50)
      read(1, 50)
      read(1,400) ni
400      format(i1)
      do 450 i = 1, ni+3
450          read(1, 50)
      read(1,400) ni
      do 550 i = 1, ni+7
550          read(1, 50)
      read(1,350) lp12
      do 650 i = 1, 7
650          read(1, 50)

```

```

      read(1,750) ( t12(i), s12(i), dt12(i), i = 1, lp12 )
750   format(3e15.5)
      close( unit=01 )
c
c   input t, s(t), and dt for c=13 radical pairs
c
      open( unit=01, name='c13.dat', type='old', readonly )
      read(1, 50)
      read(1, 50)
      read(1,400) ni
      do 850 i = 1, ni+3
850   read(1, 50)
      read(1,400) ni
      do 950 i = 1, ni+7
950   read(1, 50)
      read(1,350) lp13
      do 1050 i = 1, 7
1050  read(1, 50)
      read(1,750) ( t13(i), s13(i), dt13(i), i = 1, lp13 )
      close( unit=01 )
c
c   output the input parameters
c
      write( 6, 1100 )
1100  format( /,1x,"output from "diffus.f4b"")
      write( 6, 1110 ) ncol
1110  format(/,1x,"radical-radical collision radius           :",e11.3)
      write( 6, 1120 ) rzero
1120  format(1x,"initial radical separation radius           :",e10.3)
      write( 6, 1130 ) kloss
1130  format(/,1x,"chemical loss rate constant (hz):",e10.3)
      write( 6, 1140 ) fs
1140  format(1x,"initial fraction of singlet:           ",f5.3)
      write( 6, 1150 ) lamda
1150  format(1x,"singlet reactivity per collision: ",f5.3)
      write( 6, 1160 ) ncol
1160  format(/,1x,"number of collisions in calculation:",i2)
      write( 6, 1170 ) lp12
1170  format(1x,"number of c-12 time values:",i5)
      write( 6, 1180 ) lp13
1180  format(1x,"number of c-13 time values:",i5)
      write( 6, 1190 )
1190  format(/,1x,"self-diffusion",6x,"c-12",6x,"c-13",3 )
      write( 6, 1200 )
1200  format( 6x,"enrichment",5x,"enhancement")
      write( 6, 1250 )
1250  format( 1x," coefficient ",6x,"yield",5x,"yield",3)
      write( 6, 1300 )
1300  format( 5x," factor ",5x,"factor=1.0")
c
c   set up parameters needed for the calculations.
c
      trp = 1.0 / kloss
      pmul = exp( alog( pmax / pmin ) / num )
      dself = pmin
c
c   loop to perform calculation as a function of diffusion coefficient.
c
      num = num + 1
      do 1000 idif = 1,num

```

```
      drel = 2.0 * dself
c
c calculation of recombination yield for c-12 radical pairs
c
      r12 = recom( s12, t12, dt12, trp, drel, lp12 )
c
c calculation of recombination yield for c-13 radical pairs
c
      r13 = recom( s13, t13, dt13, trp, drel, lp13 )
c
c calculate the enrichment factor "enr" and the enhancement
c factor "q".
c
      enr = ( r13 - r12 ) / ( 1.0 - r12 )
      q   = r13 / r12
c
c output section
c
      write( 6, 1350 ) dself, r12, r13, enr, q - 1.0
1350   format( 1x,e12.4,8x,f6.4,4x,f6.4,5x,f5.3,10x,f5.3)
      dself = dself * pmul
1000   continue
c
c end diffusion coefficient loop.
c
      end
```



```

C
C functions for the program "diffus": recom(), pl()
C
C the function "recom()" follows.
C
C     function recom( s, t, dt, trp, drel, loop )
C
C function written to accompany "diffus.f4p". "recom()" calculates
C the recombination yield for the radical pair.
C
C     common rcol, rzero, lamda, fs1, ncol
C     real s(1000), t(1000), dt(1000)
C     real lamda
C     data pi/3.14159/
C
C set up parameters needed for the calculations.
C
C     tdecay = -trp * alog(.999)
C     tmax = 7.0 * trp
C     c1 = (rcol / rzero) * (rzero - rcol) / sqrt(4.0 * pi * drel)
C     c2 = -( rzero - rcol )**2 / ( 4.0 * drel )
C     r1=0.
C     r2=0.
C     r3=0.
C     a1 = - ( 1.0 - 4.0 * fs1 ) / 3.0
C     b1 = ( 1.0 - fs1 ) / 3.0
C
C calculation of the recombination yield "recom"
C
C iteration loop for the first re-encounter fraction "r1"
C
C     do 500 i1=1, loop
C       if( t(i1) .gt. tmax ) go to 600
C
C calculate the re-encounter probability for the first collision.
C
C     prob1 = pl( t(i1), c1, c2 ) * dt(i1)
C     if( t(i1) .gt. tdecay ) prob1 = prob1 * exp(-t(i1) / trp )
C
C calculate the singlet character of the radical pair.
C
C     s1 = a1 * s(i1) + b1
C
C calculate the integrated yield.
C
C     r1 = r1 + prob1 * s1
C     if( ncol .lt. 2 ) go to 500
C
C iteration loop for the second re-encounter fraction "r2"
C
C     fs2 = ( 1.0 - lamda ) * s1 / ( 1.0 - lamda * s1 )
C     a2 = - ( 1.0 - 4.0 * fs2 ) / 3.0
C     b2 = ( 1.0 - fs2 ) / 3.0
C     col2 = 0.0
C     do 300 i2=1, loop
C       time = t(i1) + t(i2)
C       if( time .gt. tmax .or. time .gt. t(loop) ) go to 400
C       prob2 = pl( t(i2), c1, c2 ) * dt(i2)
C       if( t(i2) .gt. tdecay ) prob2 = prob2 * exp( -t(i2) / trp )
C       s2 = a2 * s(i2) + b2

```

```

col2 = col2 + prob2 * s2
if( ncol .lt. 3 ) go to 300
c
c iteration loop for the third re-encounter fraction "r2"
c
fs3 = ( 1.0 - lamda ) * s2 / ( 1.0 - lamda * s2 )
a3 = - ( 1.0 - 4.0 * fs3 ) / 3.0
b3 = ( 1.0 - fs3 ) / 3.0
col3 = 0.0
do 100 i3=1, loop
time = t(i1) + t(i2) + t(i3)
if( time .gt. tmax .or. time .gt. t(loop) ) go to 200
prob3 = p1( t(i3), c1, c2 ) * at(i3)
if(t(i3).gt.tdecay) prob3 = prob3 * exp( -t(i3) / trp )
s3 = a3 * s(i3) + b3
col3 = col3 + prob3 * s3
100 continue
200 r3 = r3 + ( col3 * prob1*(1.0-lamda*s1) * prob2*(1.0-lamda*s2) )
c
c end third re-encounter loop.
c
300 continue
400 r2 = r2 + ( col2 * prob1 * ( 1.0 - lamda * s1 ) )
c
c end second re-encounter loop.
c
500 continue
c
c end first re-encounter loop.
c
600 recom = lamda * ( r1 + r2 + r3 )
return
end

c
c function "p1()" follows.
c
function p1( t, c1, c2 )
p1 = c1 / t**1.5
arg = c2 / t
if ( arg .le. -75.0 ) p1 = 0.0
if ( arg .gt. -75.0 .and. arg .lt. -0.001 ) p1 = p1 * exp( arg )
return
end

```

APPENDIX C: Program "methyl.f4p"

```

      program methyl
c
c program to calculate the energy levels of a c3-rotor in a cos(3x)
c type potential. the levels consist of three types corresponding
c to the symmetries (a,ea, and eb) of the three irreducible
c representations of a c3-system (i.e. a methyl group).
c because of the magnetic moment of the rotating
c methyl group, the degeneracy between "ea" and "eb" states of the
c same energy level is broken in the presence of a magnetic field.
c this magnetic interaction is included in the calculation. the
c purpose of the program is to calculate p(ea)-p(eb) relative to the
c proton magnetization and p(a)=(p(ea)+p(eb)) as a function of
c temperature for a given barrier height where p( ) indicates
c population.
c written by larry l. sterna - november 1979.
c
      implicit double precision (a-h,o-z)
      dimension e(15), a(15), h(15,15), ev(15), u(15,15), effm(15)
      dimension effma(15), effme(15), t(35), rp(35), wt(35)
      integer nval(15)
      write(6,100)
100  format(/,1x,"program methyl...",/,1x,
c"program to calculate the level populations of a methyl-rotor",/,
c1x,"as a function of temperature for a given barrier height",/,/,
c1x,"enter the number of temperatures: ",$)
      read(5,150) ntemps
150  format(i2)
      write(6,200) ntemps
200  format(1x,"enter the ",i2," temperatures (kelvin):")
      do 400 i = 1,ntemps
      write(6,300) i
300  format(6x,i2," temperature = ",$)
      read(5,350) t(i)
350  format(f7.0)
400  continue
      write(6,450)
450  format(1x,"output eigenvectors? enter 1 for yes, 0 for no: ",$)
      read ( 5, 150 ) igen
      write(6,500)
500  format(1x,"enter the barrier height (kcal/mole): ",$)
      read(5,350) v3
c
c set up constants needed in the calculation.
c hbar = hbar x 1.e+20
c ergs = conversion from kcal/mole to ergs/molecule
c bcon = boltzmann's constant
c pi = pi
c gch3 = methyl group g-factor
c gpro = proton g-factor
c ch3i = methyl group moment of inertia x 1.e+40
c hamiltonian terms
c ekin = kinetic energy term
c epot0 = secular potential energy term
c epot3 = non-secular potential energy term
c
      hbar = 1.05443e-07
      ergs = 6.94980e-14
      bcon = 1.38044e-16
      pi = 3.14159
      gch3 = 0.3

```

```

      qpro = 5.585486
      ch3i = 5.5
      ekin = (hbar**2)/(2. * ch3i )
      epot0 = (v3 * eras)/2.
      epot3 = -(v3 * erqs)/4.
c
c calculate the energies of the "a" and "ea" states in the absence of
c a magnetic field.
c
      if ( iden .eq. 1 ) open( unit=01,name='eigen.val',type='new' )
      do 1350 i = 1,2
c
c do the "a" states first.
c
      nval(1) = -21
c
c do the "ea" states second.
c
      if(1.eq.2) nval(1) = -20
      do 700 j = 2,15
      nval(j) = nval(j-1) + 3
700   continue
c
c set up the hamiltonian matrix.
c
      do 900 i = 1,15
      h(i,i) = ( ekin * nval(i)**2 ) + epot0
      do 800 j = i,15
      if((j-i).eq.1) h(i,j) = epot3
      if((j-i).gt.1) h(i,j) = 0.
      h(j,i) = h(i,j)
800   continue
900   continue
c
c diagonalize the hamiltonian matrix
c
      call diaqub(h,15,ev,u)
c
c calculate the "effective" m-value (i.e. angular momentum) of
c each eigenstate.
c
      do 1100 j = 1,15
      effm(j) = 0.0
      do 1000 i = 1,15
      effm(j) = effm(j) + (u(i,j)**2) * nval(i)
1000   continue
1100   continue
c
c if specified (i.e., iden = 1), output the eigenvectors, etc.
c into the file "eigen.val".
c
      if ( iden .ne. 1 ) go to 1170
      if(1.eq.1) write(1,1105) v3
1105   format(1x,"a-eigenstates for barrier height = ",f5.3,
      c" kcal/mole",/)
      if(1.eq.2) write(1,1110) v3
1110   format(1x,"ea-eigenstates for barrier height = ",f5.3,
      c" kcal/mole",/)
      do 1160 i = 1,15
      write(1,1120) i,ev(j),effm(j),nval(1),u(1,j)

```

```

1120   format(1x,i2,5x,e12.5,5x,f9.4,5x,i3,5x,f9.6)
      write(1,1140) (nval(i),u(i,j),i=2,15)
1140   format(39x,i3,5x,f9.6)
      write(1,1150)
1150   format(/)
1160   continue
1170   continue
c
c   order the eigenvalues and m-values.
c
      do 1300 i = 1,15
        inew = i
        enew = ev(i)
        eold = ev(i)
        do 1200 j = i,15
          if(ev(j).lt.enew) inew = j
          if(ev(j).lt.enew) enew = ev(j)
1200        continue
          ev(i) = enew
          ev(inew) = eold
          if(l.eq.1) a(i) = ev(i)
          if(l.eq.2) e(i) = ev(i)
          oldm = effm(i)
          effm(i) = effm(inew)
          effm(inew) = oldm
          if(l.eq.1) effma(i) = effm(i)
          if(l.eq.2) effme(i) = effm(i)
1300        continue
1350        continue
          if ( iden .eq. 1 ) close( unit=01 )
c
c   calculate the level populations, rotational polarization,
c   tunnelling frequency, and average rotation rate (hertz)
c   as a function of temperature.
c
      do 1500 n = 1,ntemps
        bt = bcon * t(n)
c
c   avqwt = average tunnelling splitting (wt)
c   avqma (avame) = average m-value of the a(e)-states
c                   avqma should be zero - nonzero value indicates
c                   round-off error in diagonalization.
c   za(e) = partition function for the a(e)-torsional levels.
c
        avqma = 0.0
        avame = 0.0
        avqwt = 0.0
        za = 0.0
        ze = 0.0
        do 1400 i = 1, 15
c
c   a(1) is the lowest possible energy for the rotor.
c
          bfa = fexpdp( - ( a(i) - a(1) ) / bt )
          bfe = fexpdp( - ( e(i) - a(1) ) / bt )
          avqwt = avqwt + ( e(i) - a(i) ) * ( bfa + bfe )
          za = za + bfa
          ze = ze + bfe
          avqma = avqma + effma(i) * bfa
          avame = avame + effme(i) * bfe

```

```

1400   continue
      avama = avama / za
      avame = avame / ze
c
c   the rotational polarization "rp" is defined in terms of the
c   percent of the proton zeeman magnetization.
c
      rp(n) = 2.0 * avame * 100. * gch3/qpro
c
c   "wt" is the tunnelling splitting, i.e. the average energy
c   difference between the a- and e-states.
c
      wt(n) = avawt / ( za + ze )
      wt(n) = wt(n) / ( 2.0 * pi * hbar * 1.0e-20 )
1500   continue
c
c   output the results.
c
      open( unit=01,name='rotor.val',type='new' )
      write(1,1900) v3
1900   format(1x,"rotor.val" = output from "methvl",//,
c6x,"barrier height = ",f5.3," kcal/mole",//,16x,"e-energy",
c8x,"effective",8x,"a-energy",8x,"effective",/,5x,"level",5x,
c"(kcal/mole)",5x,"ea" m-value",5x,"(kcal/mole)",5x,
c"a" m-value")
      write(1,2000) (i,e(i)/erqs,effme(i),a(i)/erqs,effma(i), i=1,15)
2000   format( 6x, i2, 7x, f8.3, 10x, f8.4, 7x, f8.3, 9x, f8.4 )
      write( 1, 2020 )
2020   format(/,15x,"tunnelling splitting",5x,"tunnelling splitting",
c/,5x,"level",9x,"(kcal/mole)",16x,"(hertz)")
      do 2060 i = 1,15
          tunnel = e(i) - a(i)
          write(1,2040) i, tunnel / erqs, tunnel*1.0e+20 / (2.*pi*hbar)
2040   format( 6x, i2, 12x, f8.5, 16x, e12.5 )
2060   continue
      write(1,2100)
2100   format(/,5x,"temperature",6x,"rotational",9x,"tunnelling",
c/,6x,"(kelvin)",7x,"polarization",4x,"splitting (hz)")
      write( 1, 2200 ) ( i, t(i), rp(i), wt(i), i = 1, ntemps )
2200   format( 2x, i2, ' ', f7.2, 9x, f6.4, 11x, e10.3 )
      write( 1, 2300 )
2300   format(/,1x,"*",/,2x,"rotational polarization is percent of
c proton zeeman magnetization.")
      close( unit=01 )
      write( 6, 2400 )
2400   format( /, 1x, "*** output in the file "rotor.val" ***",/)
      stop
      end

```

```

c
c  subroutine diagdb follows - double precision version.
c
      subroutine ddiagb(h,n,ev,u)
c  diagonalization routine written for anymag..version 1
c  based on the method of Jacobi, it diagonalizes a real
c  symmetric matrix by performing a rotation whenever the
c  angle is greater than a given threshold. this process
c  continues with the threshold angle being decreased until
c  some minimum angle criterion is met.
c  modified for program "methyl".
c  "hdiag" uses the function "arctan".
c  written by Larry L. Starna
      implicit double precision (a-h,o-z)
      dimension h(n,n),u(n,n),ev(1)
      do 100 i=1,n
      do 50 j=i,n
      u(i,j)=0.
      u(j,i)=0.
50      continue
      u(i,i)=1.
100     continue
      nr=0
      if(n.eq.1) go to 700
      anqmin = 0.000017
      anq=0.1745
      istop=n-1
200     test=dtan(anq)*.5
300     do 400 i=1,istop
      ip=i
      hij=h(i,i)
      jgo=i+1
      do 350 j=jgo,n
      jp=j
      hij=h(i,j)
      hjj=h(j,j)
      adj=hij-hjj
      if(dabs(hij).gt.test*dabs(adj)) go to 500
350     continue
400     continue
      if(ang.lt.anqmin) go to 700
      anq=anq*.33333
      go to 200
500     nr=nr+1
      opp=2.*hij
      theta=darctn(opp,adj)*.5
      c=dcos(theta)
      s=dsin(theta)
      do 600 k=1,n
      if(k.lt.ip) hik=h(k,ip)
      if(k.gt.ip) hik=h(ip,k)
      if(k.lt.jp) hjk=h(k,jp)
      if(k.gt.jp) hjk=h(jp,k)
      if(k.lt.ip.and.k.ne.jp) h(k,ip)=hik*c+hjk*s
      if(k.gt.ip.and.k.ne.jp) h(ip,k)=hik*c+hjk*s
      if(k.lt.jp.and.k.ne.ip) h(k,jp)=-hik*s+hjk*c
      if(k.gt.jp.and.k.ne.ip) h(jp,k)=-hik*s+hjk*c
      uki=u(k,ip)
      ukj=u(k,jp)
      u(k,ip)=uki*c+ukj*s

```



```

        u(k,jp)=-uki*s+ukj*c
600    continue
        cos2=c*c
        sin2=s*s
        cross=2.*hij*c*s
        h(ip,jp)=0.
        h(ip,ip)=hii*cos2+cross+hjj*sin2
        h(jp,jp)=hii*sin2-cross+hjj*cos2
        go to 300
700    do 800 j=1,n
        ev(j)=h(i,j)
800    continue
        return
        end

c
c  function darctn follows.
c
c      function darctn(opp,adj)
c
c  function written for anymag...version 1
c  computes the arc-tangent of opp/adj
c
c      implicit double precision (a-h,o-z)
        darctn=1.570796327
        if(adj.eq.0.) go to 100
        if(abs(adj).lt.abs(opp)*1.e-20) go to 100
        arg=opp/adj
        darctn=datan(arg)
100    return
        end

c
c  function fexdpd follows.
c
c      function fexdpd(arg)
c
c  function computes the real exponential of "arg".  if "arg"
c  is smaller than -75, "fexp" returns the value 0.  the
c  purpose of this function is to prevent the "unix" system
c  from returning a "floating overflow message" which occurs
c  when the minimum storage size of the machine is approached.
c
c      implicit double precision (a-h,o-z)
        fexdpd = 0.
        if(arg.gt.-75.) fexdpd = dexp(arg)
        return
        end

```

APPENDIX D: Reduction of (N+1) x (N+1) Set of Relaxation Equations
to 2 x 2 System

The relaxation eigenvectors for the system of N methyl groups are obtained from the characteristic equation of the relaxation matrix:

$$\det(S-\lambda I) = \begin{vmatrix} S_{11}^{-\lambda} & S_{14}(\theta_1) & S_{14}(\theta_2) & S_{14}(\theta_3) & \dots \\ S_{14}(\theta_1)/N & S_{44}^{-\lambda} & 0 & 0 & \dots \\ S_{14}(\theta_2)/N & 0 & S_{44}^{-\lambda} & 0 & \dots \\ S_{14}(\theta_3)/N & 0 & 0 & S_{44}^{-\lambda} & \dots \\ \vdots & \vdots & \vdots & \vdots & \dots \\ \vdots & \vdots & \vdots & \vdots & \dots \end{vmatrix} = 0 \quad (D.1)$$

To reduce this equation to the 2 x 2 system of equations which describe the Zeeman relaxation, it is only necessary to consider the eigenvalues. These may be obtained by induction from the solution of a 4 x 4 relaxation matrix (i.e., three methyl groups). The analogy between the (N+1) x (N+1) case and the 4 x 4 case is made by writing the characteristic equation for each and then expanding the determinant of each into its second row minors. By comparison of the corresponding minors the solution of the 4 x 4 case is straightforwardly generalized. It follows that for N methyl groups there are N-1 eigenvalues λ_i equal to S_{44} and two eigenvalues λ_1, λ_2 which are given by [1]

$$\lambda_{1,2} = (S_{11} + S_{44})/2 \pm \frac{1}{2} [(S_{11} - S_{44})^2 + 4 S_{14}^2]^{1/2} \quad (\text{D.2})$$

where

$$S_{14}^2 = \sum_i^N S_{14}^2(\theta_i)/N \quad . \quad (\text{D.3})$$

It follows very simply from the equation

$$(S - \lambda_i) \psi_i = 0 \quad (\text{D.4})$$

that the $N-1$ eigenvectors ψ_i with $\lambda_i = S_{44}$ are all uncoupled from the Zeeman system. Consequently, the Zeeman system is a linear combination of only two eigenvectors, ψ_1 and ψ_2 :

$$\tilde{M}(t)/M_{\text{eq}} = C_1 \exp(-\lambda_1 t) + C_2 \exp(-\lambda_2 t) \quad . \quad (\text{D.5})$$

It follows that

$$\dot{M}(t)/M_{\text{eq}} = -\lambda_1 C_1 \exp(-\lambda_1 t) - \lambda_2 C_2 \exp(-\lambda_2 t) \quad (\text{D.6})$$

and from the relaxation equation

$$\dot{M}(t)/M_{\text{eq}} = [-S_{11} M(t) - \sum_i^N S_{14}(\theta_i) R_i(t)]/M_{\text{eq}} \quad . \quad (\text{D.7})$$

The following parameter is defined [2,3]:

$$P_r(t) = \sum_i^N S_{14}(\theta_i) R_i(t)/(2\sqrt{6} K) = \sum_i^N \cos(\theta_i) R_i(t) \quad (\text{D.8})$$

making $P_r(t)$ the net projection of rotational polarization along the magnetic field. Since both $M(t)$ and $P_r(t)$ are sums over all of the methyl groups, division by M_{eq} normalizes both. For

treatment of experimental data, sums such as Eqs. (D.3) and (D.8) must be replaced by single crystal or powder averages.

It now follows that from Eqs. (D.5)-(D.8) that

$$2\sqrt{6} K P_r(t)/M_{eq} = (\lambda_1 - S_{11})C_1 \exp(-\lambda_1 t) + (\lambda_2 - S_{11})C_2 \exp(-\lambda_2 t) \quad (D.9)$$

By taking the values of Eqs. (D.5)-(D.8) at $t=0$, the coefficients C_1 and C_2 are found to be:

$$C_1 = [(S_{11} - \lambda_2)\tilde{M}(0) - 2\sqrt{6} K P_r(0)] / [(\lambda_1 - \lambda_2)M_{eq}] \quad (D.10a)$$

and

$$C_2 = [\tilde{M}(0) - C_1] / M_{eq} \quad (D.10b)$$

The crucial element in simplifying the relaxation equations into a 2 x 2 set is that all of the individual rotational polarizations have the same auto-relaxation rate constant S_{44} . At low temperature when S_{44} becomes angular dependent, the relaxation of the Zeeman system becomes multi-exponential, and no simplification is possible [3].

APPENDIX E: Program "couple.c"

```

#include <stdio.h>
#define pi 3.14159
#define r 1.8e-08
#define hbar 1.05443e-27
#define gamma 26753.0
main()
    /* Program couple... */
    /* This program calculates the relaxation of two */
    /* methyl groups which are sterically coupled so as */
    /* to rotate in a geared fashion. The two methyl */
    /* groups are assumed to be attached to a rigid */
    /* molecular frame and separated by a fixed angle. */
    /* The calculation is an extension of the SRSO model */
    /* developed Emd and Mind. */
    /* The program uses the subroutine "diag" and the */
    /* function "arctan." */
    /* Written by Larry L. Stern */
    /* Department of Chemistry */
    /* University of California, Berkeley */
    /* June 1980 */

    double phiA, phiB, del, alpha, s1a, s1b, s1a, s1b, s1a, s1b, s1a, s1b;
    double tau, w, cosa, cosb, sinb;
    double r0, s[20][20], c[20][20], r0[3][3], av[3], b0[3];
    double pow(), cos(), sin(), sqrt(), arctan();
    int i, j;
    FILE *fopen(), *fp;

/* Input section */
    printf ( " Program couple...\n" );
    printf ( " Program to calculate the coupled relaxation behavior " );
    printf ( " of two methyl groups with\n steric interaction which " );
    printf ( " couples the two rotational polarizations.\n\n" );
    printf ( " Enter the angle (degrees) of the first methyl group: " );
    scanf ( "%f", &phiA );
    printf ( " Enter the angle (degrees) separating the two methyl " );
    printf ( " groups\n in the molecular frames " );
    scanf ( "%f", &del );
    printf ( " Enter the azimuthal angle (degrees) of the second methyl: " );
    scanf ( "%f", &alpha );
    printf ( " Enter the correlation time for methyl motion: " );
    scanf ( "%f", &tau );
    printf ( " Enter the strength (Hz) of the steric couplings: " );
    scanf ( "%f", &w );
    printf ( "\n Enter the initial conditions..." );
    printf ( "\n      (Z - Zeq) / Zeq = " );
    scanf ( "%f", &b0[0] );
    printf ( "      R1 + R2 = " );
    scanf ( "%f", &b0[1] );
    printf ( "      -R1 + R2 = " );
    scanf ( "%f", &b0[2] );

/* Spew back the input parameters. */
    fp = fopen ( "couple.val", "w" );
    fprintf ( fp, " Output from \"couple...\n" );
    fprintf ( fp, "\n Angle of first methyl group = %.1f degrees.", phiA );
    fprintf ( fp, "\n Methyl-methyl separation angle = %.1f degrees.", del );
    fprintf ( fp, "\n Azimuthal angle of second methyl group = " );
    fprintf ( fp, " %.1f degrees.", alpha );
    fprintf ( fp, "\n Methyl group correlation time = %.3e seconds.", tau );
    fprintf ( fp, "\n Methyl-methyl steric coupling strength = %.2f Hz.", w );
    fprintf ( fp, "\n\n Initial conditions..." );
    fprintf ( fp, "\n      Quantity      Value" );
    fprintf ( fp, "\n      (Z - Zeq) / Zeq      %.5f", b0[0] );
    fprintf ( fp, "\n      R1 + R2              %.5f", b0[1] );
    fprintf ( fp, "\n      -R1 + R2            %.5f", b0[2] );

/* Set up parameters, matrices, etc. for calculation. */
    r0 = hbar / pow ( r, 3.0 );

```

```

r0 = r0 * r0 * pow( gamma, 4.0 ) * tau * 27.0 / 128.0 ;
phia = 2.0 * pi * phia / 360.0 ;
del = 2.0 * pi * del / 360.0 ;
alpha = 2.0 * pi * alpha / 360.0 ;
cosa = cos( phia ) ;
cosb = cos( del ) * cos( phia ) - sin( del ) * cos( alpha ) * sin( phia ) ;
sinb = sqrt( 1.0 - cosb * cosb ) ;
phia = phia * 360.0 / ( 2.0 * pi ) ;
phib = arctan( sinb, cosb ) * 360.0 / ( 2.0 * pi ) ;
w = w / ( 2.0 * pi ) ;
/* Parameters of the relaxation matrix s. */
s11a = 16.0 * r0 * ( 1.0 + 3.0 * cosa * cosa ) / 3.0 ;
s11b = 16.0 * r0 * ( 1.0 + 3.0 * cosb * cosb ) / 3.0 ;
s14a = 16.0 * sqrt( 6.0 ) * r0 * cosa / 3.0 ;
s14b = 16.0 * sqrt( 6.0 ) * r0 * cosb / 3.0 ;
s44 = 8.0 * r0 ;
s[0][0] = ( s11a + s11b ) / 2.0 ;
s[0][1] = ( s14a + s14b ) / 2.0 ;
s[0][2] = (-s14a + s14b ) / 2.0 ;
s[1][1] = s44 + 2.0 * w ;
s[1][2] = 0.0 ;
s[2][2] = s44 ;
for ( i = 0 ; i <= 2 ; ++i )
  for ( j = 0 ; j <= 1 ; ++j )
    s[i][j] = s[j][i] ;
fprintf ( fp, "\n\n Initial Relaxation Matrix..." ) ;
for ( i = 0 ; i <= 2 ; ++i )
  (
    fprintf ( fp, "\n" ) ;
    for ( j = 0 ; j <= 2 ; ++j )
      fprintf ( fp, "X13.4f", s[i][j] ) ;
  )
/* Diagonalize the relaxation matrix. */
diag ( 3, s, c, ev ) ;
/* Construct the relaxation equations for the system defined by the initial */
/* conditions. */
for ( i = 0 ; i <= 2 ; ++i )
  (
    psi0 = 0.0 ;
    for ( j = 0 ; j <= 2 ; ++j )
      psi0 = psi0 + c[j][i] * b0[j] ;
    for ( j = 0 ; j <= 2 ; ++j )
      c0[j][i] = psi0 * c[j][i] ;
  )
/* Output section. */
fprintf ( fp, "\n\n Eigenvector Matrix...\n" ) ;
for ( i = 0 ; i <= 2 ; ++i )
  fprintf ( fp, "      Psi-Xd", i, j ) ;
fprintf ( fp, "\n (Z - Zeq)/Zeq" ) ;
for ( j = 0 ; j <= 2 ; ++j )
  fprintf ( fp, "X12.5f", c[0][j] ) ;
fprintf ( fp, "\n      R1 + R2      " ) ;
for ( j = 0 ; j <= 2 ; ++j )
  fprintf ( fp, "X12.5f", c[1][j] ) ;
fprintf ( fp, "\n      -R1 + R2      " ) ;
for ( j = 0 ; j <= 2 ; ++j )
  fprintf ( fp, "X12.5f", c[2][j] ) ;
fprintf ( fp, "\n\n Eigenstate      Relaxation Rate      Relaxation Time" ) ;
for ( i = 0 ; i <= 2 ; ++i )
  fprintf ( fp, "\n X5j X18.4f X18.3f", i, ev[i], 1.0 / ev[i] ) ;
fprintf ( fp, "\n\n Field angle of first methyl = X.1f degrees.", phia ) ;
fprintf ( fp, "\n Field angle of second methyl = X.1f degrees.", phib ) ;
fprintf ( fp, "\n\n Relaxation Coefficient Matrix...\n" ) ;
for ( i = 0 ; i <= 2 ; ++i )
  fprintf ( fp, "      Psi-Xd", i ) ;
fprintf ( fp, "\n (Z - Zeq)/Zeq" ) ;

```

```
for ( j = 0 ; j <= 2 ; ++j )
    fprintf ( fp, "%12.5f", c0[0][j] ) ;
fprintf ( fp, "\n  R1 + R2  " ) ;
for ( j = 0 ; j <= 2 ; ++j )
    fprintf ( fp, "%12.5f", c0[1][j] ) ;
fprintf ( fp, "\n -R1 + R2  " ) ;
for ( j = 0 ; j <= 2 ; ++j )
    fprintf ( fp, "%12.5f", c0[2][j] ) ;
fprintf ( fp, "\n" ) ;
```

}


```

else
  h1k = h[i] [k] ;
  if ( k < j )
    hjk = h[k] [j] ;
  else
    hjk = h[j] [k] ;
  if ( k < i )
    hki [i] = h1k * c + hjk * s ;
  else
    hki [k] = h1k * c + hjk * s ;
  if ( k < j )
    hkj [j] = -h1k * s + hjk * c ;
  else
    hkj [k] = -h1k * s + hjk * c ;
}
ukl = u[k] [l] ;
ukj = u[k] [j] ;
u[k] [i] = -ukl * c + ukj * s ;
u[k] [j] = -ukl * s + ukj * c ;
} /* end "for" loop over k */
cos2 = c * c ;
sin2 = s * s ;
cross = 2.0 * h11 * c * s ;
h[i] [i] = 0.8 ;
h11 [i] = h11 * cos2 + cross + h11 * sin2 ;
h11 [j] = h11 * sin2 - cross + h11 * cos2 ;
nr = nr + 1 ;
} /* end "if" condition for rotation */
} /* end "for" loop over j ( and i ) */
} /* end "while" for nr > nrad */
} /* end "for" loop over ang */
/* Fill the vector of eigenvalues with the diagonal elements of h. */
for ( i = 0 ; i <= n-1 ; ++i )
  ev[i] = h[i] [i] ;
}

double arctan ( opp, adj )
/* Function written for "diag.c". */
/* Calculates the arc-tangent of opp/adj even if the */
/* argument is infinite. */
double opp, adj ;
{
  double val, fabs(), atan() ;
  if ( fabs ( adj ) < fabs ( opp ) * 1.0e-20 )
    val = 1.570796327 ;
  else
    val = atan ( opp / adj ) ;
  if ( adj < 0.0 )
    val = val + 3.14159 ;
  return ( val ) ;
}

```

APPENDIX F: Synthesis and Crystal Growing

The syntheses of compounds used in this work are described below unless they are commercially available. Zone refining and crystal growing are discussed at the end.

^{13}C -dibenzylketone (1,3-diphenyl-2-propanone-2- ^{13}C) was prepared by pyrolysis of phenylacetic acid-1- ^{13}C calcium salt in a procedure similar to that of H. Apitzsch [4].

α - ^{13}C -toluene was prepared from benzoic acid-1- ^{13}C by lithium aluminum hydride reduction followed by bromination with PBr_3 and again reduction by lithium aluminum hydride.

2,3-dimethylmaleicanhydride- d_6 which is a previously unknown compound was prepared as follows. In a stainless steel bomb of 150 ml capacity was placed 4g of 2,3-dimethylmaleicanhydride, 80 ml D_2O (99.8% D), and 0.42 g of anhydrous potassium carbonate. The bomb was heated in an oven at 155-159°C with the temperature controlled by a thermostatic thermometer touching the outside of the bomb. Temperature control was very critical. After \sim 20 hours the bomb was opened, and the contents were acidified with dilute HCl and extracted with methylene chloride after saturating the aqueous phase with NaCl. The organic phase was dried with MgSO_4 , evaporated, and distilled on a bulb-to-bulb apparatus at 20 torr. 2.35 g of material was obtained which was found by mass spectroscopy to be 95% deuterated. 4 g of the 95% deuterated material was prepared and then re-exchanged as above to obtain 1.74 g of material after recrystallization in petroleum ether. The 2,3-dimethylmaleicanhydride- d_6 had a melting point of 93-94° and was 99.3%

deuterated as determined by mass spectroscopy.

Durene-d₁ (1,2,4,5-tetramethylbenzene-3-d₁) was synthesized by metallation of bromodurene with butyllithium followed by quenching with D₂O.

1,4,5,8-tetramethylantracene was synthesized according to the procedure of Ellison and Hey [5].

1,4,5,8-tetramethylnaphthalene was synthesized according to the procedure of Mosby [6].

The durene and all of the compounds used for single crystal preparation were zone refined. The zone refiner has 22 zones, 10 of which were used; 50 passes were typically run.

Single crystals are grown from a melt using the Bridgman technique [7,8]. A vertical growth technique is used where an evacuated pyrex tube containing the zone refined material is lowered through a heating solenoid. The pyrex tubes are conical with a moulded constriction at one end to facilitate seed growth. Typically, 1.5 g of material is used, and the conical single crystals obtained are 4 cm long and have a 12 mm diameter at the larger end. The growth rate for a 2,3-dimethylmaleicanhydride crystal is about one week.

REFERENCES

1. R. A. Wind, S. Emid, and J. F. J. M. Pourquié, *Phys. Lett.* 53A, 310 (1975).
2. S. Emid, R. J. Baarda, J. Smidt, and R. A. Wind, *Physica* 93B, 327 (1978).
3. R. A. Wind, S. Emid, J. F. J. M. Pourquié, and J. Smidt, *J. Phys. C: Solid St. Phys.* 9, 139 (1976).
4. H. Apitzsch, *Ber.* 37, 1428 (1904).
5. H. Ellison and D. H. Hey, *J. Chem. Soc. London*, 1847 (1938).
6. W. L. Mosby, *J. Am. Chem. Soc.* 74, 2564 (1952).
7. P. W. Bridgman, *Proc. Amer. Acad. Arts Sci.* 60, 305 (1925).
8. D. W. Jones, in *Crystal Growth Theory and Techniques*, edited by C. H. L. Goodman (Plenum, London-New York, 1974), Vol. 1, p. 238ff.